

Mapping and Investigation of Atrial  
Electrogram Fractionation in Patients with  
Persistent Atrial Fibrillation

Thesis submitted for the degree of  
Doctor of Philosophy  
at the University of Leicester

by

Tiago Paggi de Almeida  
Department of Engineering  
University of Leicester

2016

# Mapping and Investigation of Atrial Electrogram Fractionation in Patients with Persistent Atrial Fibrillation

**Tiago Paggi de Almeida**

## **Abstract**

Atrial fibrillation (AF) is the most common sustained cardiac arrhythmia found in clinical practice, and it is a leading cause of stroke. It has been shown that triggers in the pulmonary veins (PVs) are important in the initiation and perpetuation of paroxysmal AF. PV isolation (PVI) by radiofrequency catheter ablation has been proved effective in treating patients with paroxysmal AF. However, the identification of critical areas for successful ablation in patients with persistent AF (persAF) remains a challenge due to an incomplete understanding of the mechanistic interaction between relevant atrial substrate and the initiation and maintenance of AF. Complex fractionated atrial electrograms (CFAEs) are believed to represent remodelled atrial substrate and, therefore, potential targets for persAF ablation. Since its introduction in 2004, CFAEs have been accepted and incorporated as an additional therapy to PV isolation (PVI) to treat patients with persAF by many laboratories. Inconsistent CFAE-guided ablation outcomes have, however, cast doubt on the efficacy of this approach. The majority of the electrophysiological studies rely on automated CFAE detection algorithms embedded in electro-anatomical mapping (EAM) systems to identify CFAEs during persAF ablation. Different companies have developed algorithms based on different aspects of the atrial electrogram (AEG). Differences in these algorithms could lead to discordant CFAE classifications by the available EAM systems, giving rise to potential disparities in CFAE-guided ablation. Additionally, previous studies support the existence of fractionated AEGs not related to AF perpetuation, and fractionated AEGs that represent sources responsible for AF maintenance. Those investigations relied on few AEG descriptors, which can be a limiting factor when describing a complex phenomenon such as AF. Discerning the different types of CFAEs is crucial for AF ablation therapy. Finally, the spatio-temporal behaviour of AEGs collected during persAF remains poorly explored. This study encloses contributions towards the minimization of discordances in automated classification of CFAEs, the characterization of AEGs before and after PVI, and the investigation of the temporal behaviour of consecutive AEGs and the consistency of CFAEs using different AEG segment lengths.

## **Acknowledgements**

Many people contributed directly and indirectly to the completion of this work. First, I would like to express my sincere gratitude to my supervisors, Dr. Fernando S. Schlindwein and Prof. G. André Ng, for their trust, guidance, insights, constant support and critical analysis throughout this work. I learned a lot from the unique atmosphere of collaboration between engineers and clinicians established by you. It allowed me to have a deep immersion on both clinical and technical perspectives of the research, which I always will remember in my scientific career. I truly hope we can continue to collaborate.

My acknowledgement to Dr. Peter Stafford, Dr. Jiun Tuan, Dr. Will Nicholson, Dr. Alistair Sandilands, Dr. Riyaz Somani and Dr. Alexandre Lobo for their rich contributions to the work. I have also benefited from many discussions, friendship and support from my colleagues: Dr. João Loures Salinet Jr., Dr. Frederique J. Vanheusden, Xin Li, Nawshin Dastagir and Dr. Taher Biala. Our discussions always helped me to look deeper and forward in our research. Thanks to Kusimo Habeeb, Xiong Cong and Michael Bell for their dedication and help during the development of their final year projects.

Many thanks to my first supervisor, Dr. Daniel S. S. Sampaio, from the Sao Paulo State University (UNESP), Brazil. Your motivation and enthusiasm are contagious, and you have a big share of responsibility for me to have started my academic career. Also I would like to thank Prof. Eduardo T. Costa, from the University of Campinas (UNICAMP), Brazil, for believing in my potential and encouraging the realization of my PhD at the University of Leicester. Thank you for your constant support, tutoring and encouragement. Our talks have a profound effect on me.

My gratitude to my sponsor, the National Council for Scientific and Technological Development (CNPq) of Brazil, Ministry of Science and Technology, process number 200251/2012-0, for providing such an excellent support during my studies in Leicester.

Thanks to Ursula Maciel, Fernando Ragonette, Sérgio Cruz, Fernando Kublai, Fernando Faria and Gerson Montenegro, from whom I learned many valuable lessons that I continue to use to date.

Thanks to all my friends in Brazil and in the UK. In such vibrant places, I had the privilege to meet amazing people that I will always remember and cherish all the great moments

we shared. Thanks for being so supportive. My special thanks to Gavin Chu, Vartika Kumar, Guilherme Pimentel and Darya Krasilnikov for your invaluable friendship. After so many talks and discussions, I think you know more about my work than I do. We will be waiting for you in Brazil. Thanks to Walkiria Schlindwein and Alex Schlindwein, for all the wonderful moments and for being so kind to us, all the time.

Finally I would like to thank my family. My mother, Fátima, and my father, Paulo, for being constantly present in my life, despite being physically an ocean of distance away. You are my source of inspiration, and will always have my love and admiration for being such an example of integrity, respect and loving family. My sister, Carol, for being the best sister one could ask for. For the three of you: I love you very much! Thanks also to my ‘new’ family, Mr. Luiz and Mrs. Luiza, Paulinho and Dudu, and Fubá, for your absolute trust and for always looking after us when we need the most.

At last, we have been together for amazing sixteen years, and it feels like we are just starting. Thanks, my beloved wife, Karina, for your love, tenderness, friendship, patience and motivation. You make all challenges worth fighting for. I am looking forward to our next adventures.

To all of you: thank you!

# Contents

Abstract.....	i
Acknowledgements.....	ii
List of Figures.....	ix
List of Tables.....	xv
List of Abbreviations.....	xvi
<b>1 Introduction</b>	<b>1</b>
1.1 Structure of the work.....	3
1.1.1 Aims.....	3
1.1.2 Structure of the thesis.....	4
<b>2 Medical Background</b>	<b>5</b>
2.1 The heart.....	5
2.1.1 Cardiac electrophysiology.....	5
2.1.2 Measuring the cardiac electric activity.....	9
2.1.3 Intracardiac AEG recording techniques.....	10
2.1.3.1 The unipolar recording configuration.....	11
2.1.3.2 The bipolar recording configuration.....	13
2.1.3.3 The local atrial cycle length.....	13
2.2 Atrial fibrillation.....	14
2.2.1 Epidemiology and prognosis.....	15
2.2.2 Mechanisms of atrial fibrillation.....	16
2.2.2.1 The atrial substrate.....	16
2.2.2.2 Multiple rapid ectopic activity.....	18
2.2.2.3 Multiple wavelet hypothesis.....	19
2.2.2.4 Multiple-circuit re-entry theory.....	20
2.2.3 Clinical management of atrial fibrillation.....	21
2.2.3.1 Pharmacological therapy.....	21
2.2.3.2 Non-pharmacological therapies.....	22
2.2.4 Catheter ablation of atrial fibrillation.....	22

2.2.4.1	Electro-anatomical mapping (EAM) systems.....	23
2.2.4.2	Ablation of paroxysmal atrial fibrillation.....	24
2.2.4.3	Ablation of persistent atrial fibrillation .....	25
2.2.5	Complex fractionated atrial electrograms .....	27
2.2.5.1	Brief historical notes on fractionated AEGs.....	29
2.2.5.2	Visual classification of atrial electrograms during atrial fibrillation.....	31
2.2.5.3	Automated algorithms for CFAE classification .....	33
2.2.5.4	Other indices of fractionation .....	34
2.2.5.5	CFAE's spatio-temporal behaviour .....	35
2.2.5.6	The outcomes of CFAE-guided ablation in persAF .....	36
<b>3</b>	<b>Mathematical &amp; Signal Processing Tools</b>	<b>39</b>
3.1	Statistical measures.....	39
3.1.1	Central moments .....	40
3.1.2	Median and interquartile range.....	41
3.1.3	Covariance and correlation.....	42
3.1.4	Kernel density estimator.....	42
3.2	Indices of fractionation .....	43
3.2.1	Indices of fractionation computed by commercial mapping systems .....	44
3.2.2	Information theory indices .....	44
3.2.2.1	Shannon entropy (ShEn).....	44
3.2.2.2	Approximate entropy.....	44
3.2.2.3	Sample entropy .....	45
3.2.2.4	Kullback-Leibler divergence (or relative entropy) .....	46
3.2.3	Amplitude based indices .....	46
3.2.4	Frequency based indices.....	47
3.2.4.1	Fourier transform.....	47
3.2.4.2	Continuous Fourier transform.....	47
3.2.4.3	Discrete Fourier transform & Fast Fourier transform.....	47
3.2.4.4	Anti-leaking window .....	48
3.2.4.5	Zero padding.....	48
3.2.4.6	The DF and OI.....	48
3.3	Digital filters .....	50

3.4	Wavelet transform.....	50
3.4.1	The wavelet filter banks .....	52
3.4.2	SWT filter.....	53
3.5	Classification and pattern recognition.....	55
3.5.1	Receiver operating characteristic curves.....	55
3.5.2	Multivariate analyses.....	56
3.5.2.1	Multivariate analysis of variance (MANOVA) .....	56
3.5.2.2	Linear discriminant analysis (LDA) .....	57
3.6	Offline reconstruction of 3D atrial maps .....	58
<b>4</b>	<b>Minimizing discordances in automated classification of fractionated electrograms in human persistent atrial fibrillation</b>	<b>61</b>
4.1	Introduction.....	61
4.2	Methods .....	63
4.2.1	Automated CFAE detection .....	63
4.2.1.1	The NavX algorithm (EnSite System version 8.0 software, 2008) .....	64
4.2.1.2	The CARTO algorithm (CARTO 3 system, 2008-2014, version 4.3).....	64
4.2.2	Study population .....	65
4.2.3	Electrophysiological study .....	66
4.2.4	Comparing CFAE definitions between EAM systems.....	66
4.2.4.1	Signal analysis .....	66
4.2.4.2	Influence of EGM settings on CFAE classification.....	66
4.2.4.3	CFAE detection thresholds for CFE-Mean and ICL .....	67
4.2.4.4	CFAE detection thresholds for CFE-StdDev, ACI and SCI.....	67
4.2.4.5	Validation of the revised thresholds for CFAE detection performed by NavX and CARTO .....	68
4.2.5	Statistical analysis .....	69
4.3	Results.....	69
4.3.1	Influence of EGM settings on CFAE classification .....	69
4.3.2	CFAE detection thresholds for CFE-Mean and ICL .....	71
4.3.3	CFAE detection thresholds for CFE-StdDev, ACI and SCI.....	74
4.3.4	Validation of the revised thresholds for CFAE detection performed by NavX and CARTO .....	76
4.4	Discussion.....	78

4.4.1 Atrial substrate characterized by CFAE.....	78
4.4.2 The lack of a gold standard for CFAE definition.....	79
4.4.3 CFAE detection performed by NavX and CARTO algorithms.....	79
4.4.4 Study limitations .....	80
4.5 Conclusions.....	80
<b>5 Characterization of atrial electrogram fractionation before and after pulmonary vein isolation in human persistent atrial fibrillation</b>	<b>82</b>
5.1 Introduction.....	82
5.2 Methods .....	83
5.2.1 Study population .....	83
5.2.2 Electrophysiological study .....	83
5.2.3 Signal analysis.....	84
5.2.4 Indices of fractionation.....	86
5.2.5 Statistical analysis .....	86
5.3 Results.....	87
5.3.1 Effect of PVI+RL on the distribution of CFAEs.....	87
5.3.2 Correlation between indices of fractionation .....	90
5.3.3 Effect of PVI+RL on the indices of fractionation .....	90
5.3.4 Characterization of AEGs before and after PVI+RL .....	90
5.4 Discussion.....	95
5.4.1 AEG fractionation as surrogate for AF drivers .....	95
5.4.2 Multivariate analysis for atrial substrate characterization.....	96
5.4.3 Substrate-based ablation for persAF .....	98
5.4.4 Study limitations .....	98
5.5 Conclusions.....	98
<b>6 The spatio-temporal consistency of atrial electrograms in persistent atrial fibrillation</b>	<b>100</b>
6.1 Introduction.....	100
6.2 Methods .....	101
6.2.1 Study population .....	101
6.2.2 Electrophysiological study .....	102
6.2.3 Signal analysis.....	102

6.2.4	Temporal consistency of AEG fractionation with different segment lengths .....	102
6.2.5	Temporal behaviour of consecutive AEGs .....	104
6.2.6	Statistical analysis .....	104
6.3	Results.....	105
6.3.1	Temporal behaviour of consecutive AEGs .....	105
6.3.2	Temporal consistency of AEG fractionation with different segment lengths .....	109
6.4	Discussion.....	112
6.4.1	Patient-specific atrial substrate in persAF .....	112
6.4.2	The temporal behaviour of AEGs during persAF .....	112
6.4.3	The AEG duration for atrial substrate assessment .....	113
6.4.4	Limitations .....	114
6.5	Conclusions.....	114
<b>7</b>	<b>Main findings and future investigations</b>	<b>115</b>
7.1	Main Findings .....	115
7.2	Future Investigations.....	117
7.2.1	CFAE ESTimation imPRovement based on the agreement between EnSite NavX and BioSense CARTO (CFAE ESPRESSO).....	117
7.2.2	Multivariate characterization of atrial substrate in persAF patients.....	119
7.2.3	DF-guided persAF ablation.....	121
7.2.4	Phase analysis and rotor-guided persAF ablation .....	123
7.2.5	Multi-mechanism integrative tool for online AF mapping.....	124
7.3	Publications, conferences and supervisions .....	126
7.3.1	Journal publications.....	126
7.3.2	Journal publications in submission .....	126
7.3.3	Journal publications in preparation .....	126
7.3.4	Conference papers .....	127
7.3.5	Conference abstracts .....	128
7.3.6	Supervisions and Co-supervisions .....	131
7.3.6.1	Master’s degree.....	131
7.3.6.2	B.Eng. Final Year Project.....	131
	Appendices.....	132
	References.....	166

## List of Figures

Figure 2-1 Structure of the heart and the course of blood flow through the heart chambers and heart valves. RA = right atrium; RV = right ventricles; LA = left atrium; LV = left ventricle. ....	6
Figure 2-2 Cardiac (ventricular) muscle cell action potential with the four phases (explanation in the text). ....	8
Figure 2-3 SA node and the specialized conductive system in the heart.....	8
Figure 2-4 Illustration of an ECG segment collected from a subject during SR, highlighting the atrial and ventricular activations (P wave and QRS complex, respectively), followed by the ventricular repolarization (T wave).....	10
Figure 2-5 Illustration of the genesis of extracellular potentials ( $\Phi_o$ ) modified from (Malmivuo and Plonsey, 1995). The depolarization of myocytes' transmembrane potential ( $V_m$ ) propagation (A) generates inwards and outwards transmembrane currents ( $i_m$ ) that operate as a propagating dipole, creating extracellular potentials. These extracellular potentials can be captured by catheters with electrodes in their tips, and the resulting signal is referred to as an AEG.....	11
Figure 2-6 Illustration of both unipolar and bipolar recordings generated by an activation wave traveling along a myocardial bundle from the left to the right. The unipolar configuration captures the global electric activity of the area surrounding the electrode. Conversely, the bipolar finds the difference between the two electrodes, minimizing the common-mode noise influence, leaving mostly the local signal. Modified from (Kusumoto, 1999). ....	12
Figure 2-7 Example of bipolar AEG recorded during AF with respective cycle lengths between subsequent local activations. The mean CL in this example is 262 ms. ..	14
Figure 2-8 A. ECG in SR showing consistent P waves and regular ventricular response (RR intervals). B. ECG in AF showing fibrillatory <i>f</i> -waves and irregular ventricular response. ....	15
Figure 2-9 Possible mechanisms of atrial remodelling during AF. Reproduced with permission from (Allessie <i>et al.</i> , 2002). APD = action potential duration; AFCL = atrial fibrillation cycle length; $\theta$ = conduction velocity.....	17
Figure 2-10 Graphical representation of the different theories regarding mechanisms underlying AF initiation and maintenance. AF initiation and perpetuation requires both triggers for its onset and a substrate for its maintenance, but these mechanisms are likely to co-exist at various times. ....	18
Figure 2-11 Illustration of a re-entry circuit. A. Activation wave front in ideal conditions. B. Continuous activation due to alterations in the conduction velocity or in the refractory period, sustaining a continuous re-entry circuit. The white regions represent non-activated state; the black regions represent activated state; the dotted regions represent refractory state. Adapted from (Mines, 1913).....	21

Figure 2-12 Illustration of bipolar AEGs collected during AF. A. Bipolar AEG with small amplitude, continuous fractionated atrial activity (CFAE). B. Bipolar AEG with discrete organised activations (non-CFAE).....	28
Figure 2-13 Graphical representation of the possible mechanisms involved in the genesis of CFAEs. A. Wave break. B. Wave collision. C. Anisotropic conduction. D. Leading circle re-entry. E. Spiral wave re-entry.....	29
Figure 2-14 Illustration bipolar AEGs collected during AF according the classification suggested by Wells and colleagues (Wells <i>et al.</i> , 1978). A. AEG of type I showing discrete depolarisation activities separated by an isoelectric baseline free of perturbation. B. AEG of type II with identifiable depolarisation activity but with perturbations of the baseline between atrial complexes. C. AEG of type III which failed to demonstrate either depolarisation events or isoelectric intervals. ....	32
Figure 3-1 Illustration of a Gaussian distribution, the median and the IQR. Modified from (Schilling, 2012). ....	41
Figure 3-2 Illustration of the estimation of the pdfs from a white noise (A) and an AEG (B) using the KDE the Epanechnikov kernel smoothing function and the default bandwidth defined by MATLAB.....	43
Figure 3-3 Illustration of signal processing steps on a bipolar AEG collected during AF. A: Segment of a bipolar AEG showing 3 discrete activations with a CL of approximately 260 ms. B: Rectified bipolar AEG. C: AEG after low-pass filtering at 20 Hz. D. corresponding power spectrum of the bipolar AEG with DF = 3.92 Hz (corresponding to a CL of 255 ms) and OI = 0.935.....	49
Figure 3-4 Illustration of a bipolar AEG collected at 1200 Hz before (A) and after (B) a 50 Hz notch filter, and their respective frequency spectra (C). ....	51
Figure 3-5 Illustration of two mother wavelets used in the present work. A. The Haar wavelet and B. The Daubechies D11.....	51
Figure 3-6 Illustration of a filter bank using SWT. A. Three filter bank levels showing high (H) and low (L) pass filters, the details (D) and approximations (A) computed at each level. B. The frequency components present at each level of the filter bank. $f_N$ = Nyquist frequency.....	52
Figure 3-7 Illustration of the same bipolar AEG shown in Figure 3-4 (after the 50 Hz notch filter), before and after SWT filtering. A. AEG before SWT filter. B. Filtered AEG. C. Resulting noise removed from the AEG.....	54
Figure 3-8 Illustration of a ROC curve construction process. A threshold is used to discriminate two distributions. Since there is overlap between them, some will be correctly marked (TP - true positive; TN – true negative) and some will be incorrectly marked (FP - false positive; FN – false negative).....	55
Figure 3-9 Illustration of a A. confusion matrix and B. a ROC curve.....	56
Figure 3-10 Illustration of the content of the XML files exported from NavX containing all the vertices and triangles (or polygons) that constitute the 3D LA mesh that were	

assessed by a MATLAB script. The vertices (A) account for the XYZ location of all points distributed in the 3D geometry, while the triangles (B) define how those points are connected one to another to create a closed 3D geometry..... 58

Figure 3-11 Illustration of the offline 3D atrial geometry. A. The triangulated mesh grid reconstructed in MATLAB based on exported vertices and triangles exported from NavX. B. The final 3D LA geometry. C. NavX CFAE map calculated using its threshold for fractionation. D. CARTO CFAE map calculated using its threshold for fractionation. .... 59

Figure 4-1 NavX (left) and CARTO (right) 3D atrial geometry representation for the same patient, with their respective automated CFAE detection algorithms. On the bottom part of the figure, the top traces refer to a segment of fractionated bipolar AEG (AEG 1), and bottom traces refer to a non-fractionated segment of bipolar AEG (AEG 2), both recorded from the LA endocardium. The AEG 1 has CFE-Mean = 50.42 ms and ICL = 6. The AEG 2 has CFE-Mean = 123 ms and ICL = 1. Explanation regarding the algorithms is provided in the text. AEG = atrial electrogram; CFE-Mean = index used by NavX to quantify AEG fractionation; FI = fractionated interval; ICL = Interval Confidence Level: index used by CARTO to quantify AEG; LPV = left pulmonary veins; MV = mitral valve; RPV = right pulmonary veins. These abbreviations were used in the subsequent figures. .... 62

Figure 4-2 Illustration of the method for training the ROC curves and validating the proposed revised thresholds. A. Thirty datasets – with 679 randomly selected AEGs each – were used to train and create the ROC curves. B. For each of the thirty datasets, the remaining 118 AEGs were used to validate the thresholds found in the ROC curves..... 68

Figure 4-3 3D CFAE map showing the anterior (upper) and posterior (bottom) view of the LA from one patient according to CFE-Mean (left hand side) and ICL (right hand side), using different EGM settings. NavX EGM settings identify more regions of the LA as CFAE than CARTO’s when applied to either CFE-Mean or ICL. .... 70

Figure 4-4 Comparison between CFE-Mean and ICL measured for all 797 AEGs, as determined by default NavX and CARTO EGM settings, respectively. Their respective default thresholds are highlighted ( $CFE-Mean \leq 120$  ms;  $ICL \geq 7$ ). Four quadrants were delimited: two quadrants where ICL and CFE-Mean agreed in terms of categorization, i.e., whether an AEG is fractionated or not fractionated; and two quadrants in which they disagreed. Examples of AEGs for each of the quadrants are shown, to illustrate the characteristics of each group. 230 (out of 797) AEGs with organized activations were found in the non-fractionated agreement zone (green). When looking at the AEGs corresponding to the disagreement quadrants (grey), one notices that they are less organized, still with distinguishable activations. In one grey region (bottom left), 282 AEGs have been classified as CFAEs by NavX but not by CARTO. In the other grey region (top right) 12 AEGs have been classified as CFAEs by CARTO, but not by NavX. Finally, 273 highly fractionated AEGs were found in the CFAE agreement zone (red). .... 72

Figure 4-5 The distributions for the AEGs classified as non-CFAEs or CFAEs by both systems, as well as AEGs that had different classifications for each system, are

shown according to CFE-Mean (A), ICL (B), CFE-StdDev (C), ACI (D) and SCI (E). **** P<0.0001.....	73
Figure 4-6 Mean (black lines) and individual (grey lines) receiver operating characteristic (ROC) curves used to adjust CFAE classification. ROC curve of A. ICL based classification using CFE-Mean $\leq 120$ ms as the reference classification and; B. CFE-Mean based classification using ICL $\geq 7$ as the reference classification. The CFAE classification in agreement by CFE-Mean and ICL using their revised thresholds (CFE-Mean $\leq 84.1 \pm 0.4$ ms; ICL $\geq 3.8 \pm 0.4$ ) was used to create ROC curves of C, D and E. C. CFE-StdDev; D. ACI and; E. SCI. The AUROC and optimum sensitivity and specificity for each measure are listed in Table 4-3 and Table 4-4. Explanations are provided in the text. ....	74
Figure 4-7 Illustration of CFAE classification performed by NavX and CARTO in the LA from one patient using their default (left) and revised (right) thresholds. Explanations are provided in the text. ....	77
Figure 5-1 NavX (upper left) and CARTO (upper right) 3D LA geometry representation for the same patient, with their respective automated CFAE detection algorithms (Almeida <i>et al.</i> , 2016). The illustrated AEG has CFE-Mean = 50.42 ms and ICL = 6. LA regions hosting AEGs with both CFE-Mean $\leq 120$ ms and ICL $\geq 4$ were considered CFAEs (bottom map). ....	85
Figure 5-2 Illustration of the different types of AEGs found in this study. A. 207 AEGs before ablation were compared with 207 AEGs after ablation, collected in corresponding LA region. Four groups of AEGs were identified in terms of CFAE, before and after ablation: CFAE before and after ablation (group 1); CFAE before, non-CFAE after ablation (group 2); non-CFAE before, CFAE after ablation (group 3); and non-CFAE before and after ablation (group 4). B. Illustration of AEGs found in each group. Highly fractionated AEGs were found in group 1 before and after ablation; fractionated AEGs before ablation with increased organization after ablation in group 2; organized activation before ablation with increased fractionation after ablation in group 3; organized activation before and after ablation in group 4. ....	88
Figure 5-3 Effect of PVI on the AF behaviour. A. 45% of the AEGs classified as CFAEs before ablation remained fractionated after ablation, while the remainder became non-CFAE. 71% of the AEGs classified as non-CFAEs before ablation remained not fractionated after ablation, while the remainder became CFAE. B. Incidence of different types of AEGs (group 1, 2, 3 and 4) in the different LA regions, namely: roof, anterior wall, septum, PVs, posterior wall and lateral. The number of paired points – before and after ablation – collected per regions is also provided.....	89
Figure 5-4 Correlations between different indices of fractionation measured from the same AEG database. Confounding indices had high correlation among each other: CFE-Mean vs. CFE-StdDev, ACI vs. SCI, ShEn vs. SampEn, ShEn vs. K-L, SampEn vs. K-L and PP vs. RMS. The remaining indices had moderate or poor correlation with each other. **** P<0.0001; *** P<0.001; ** P<0.01; * P<0.05; ns = not significant. ....	91

- Figure 5-5 Effect of PVI and roof line creation on the indices of fractionation. Effect of PVI and roof line creation on: A. CFE-Mean; B. ICL; C. CFE-StdDev; D. ACI; E. SCI; F. ShEn; G. SampEn; H. K-L; I. PP; J. RMS; K. DF; L. OI. All indices, except OI, were significantly affected by ablation. \*\*\*\* P<0.0001; \*\*\* P<0.001; \*\* P<0.01. .... 92
- Figure 5-6 The characterization of AEGs in the different groups (1, 2, 3 and 4) at baseline according different indices of fractionation: A. CFE-Mean; B. ICL; C. CFE-StdDev; D. ACI; E. SCI; F. ShEn; G. SampEn; H. K-L; I. PP; J. RMS; K. DF; L. OI..... 93
- Figure 5-7 The characterization of AEGs in the different groups (1, 2, 3 and 4) at baseline according different indices of fractionation: A. CFE-Mean; B. ICL; C. CFE-StdDev; D. ACI; E. SCI; F. ShEn; G. SampEn; H. K-L; I. PP; J. RMS; K. DF; L. OI..... 94
- Figure 6-1 A. Different segment lengths exported from NavX to investigate the temporal consistency of AEG fractionation. The maximum AEG length that can be exported from NavX is 8 s, and smaller segments are exported as portions of the original 8 s. B. The 8 s segments were divided in three consecutive 2.5 s segments, as illustrated in Figure 1B, accordingly: 0 to 2.5 s; 2.5 s to 5 s; 5 s to 7.5 s..... 103
- Figure 6-2 Illustration of the different types of AEGs found when analysing the consecutive AEG segments. Stable CFAEs (upper trace) are AEGs with  $ICL \geq 4$  in all assessed segments (upper trace). Stable non-CFAEs (middle trace) are AEGs with  $ICL < 4$  in all assessed segments. Unstable AEG (lower trace) are AEGs with  $ICL$  varying from  $ICL \geq 4$  to  $ICL < 4$  within the assessed segments. .... 106
- Figure 6-3 The resultant LA maps based on the three consecutive AEG segments with 2.5 s duration each for one patient as measured by ICL (upper), ACI (middle) and SCI (bottom). The location of the AEGs classified as stable CFAE, stable non-CFAE and unstable shown in Figure 6-2 are marked in the ICL map..... 107
- Figure 6-4 The temporal behaviour of three consecutive AEG segments with 2.5 s duration each. The 8 s segments were divided in three consecutive 2.5 s length segments. The ICL was measured in each segment and classified whether as fractionated or non-fractionated. The AEGs that remained fractionated, remained non-fractionated and changed classification were assessed between segments. .. 107
- Figure 6-5 A. All AEG segments were mutually compared. The percentage of ‘stable CFAE’; ‘stable non CFAE’ and ‘unstable AEG’ in each segment was calculated. B. The temporal decay of stable AEGs was assessed. In the first 2.5 s segment, all AEGs were considered stable. On segment 2, a total of 151 AEGs were classified as unstable. On the last segment, additional 62 AEGs changed their classification. The exponential best fit with a temporal decay with time constant ( $\tau$ ) of 2.8 s. C. The regional occurrence of the different types of AEGs normalized by the number of collected points per region. .... 108
- Figure 6-6 A. The ICL, ACI and SCI measured with 2.5 s, 5 s and 8 s. B. Bland-Altman plots for ICL, ACI and SCI measured with 2.5 s, 5 s and 8-s. \*\*\*\* P<0.0001; \*\*\* P<0.001..... 110

Figure 6-7 The resultant LA maps based on the different segment lengths (2.5 s, 5 s and 8 s) for one patient as measured by ICL (upper), ACI (middle) and SCI (bottom). .....	111
Figure 7-1 The CFAE ESPRESSO protocol for NavX. ....	118
Figure 7-2 The CFAE ESPRESSO protocol for CARTO. ....	120
Figure 7-3 Representation of the cumulative HDF clouds stacked on the 3D LA (left-hand side) and 2D spatial map of LA (right-hand side). Modified from (Dastagir <i>et al.</i> , 2014). ....	122
Figure 7-4 Illustration of recurrent patterns with the 2D HDF maps involved in each pattern and the corresponding time windows numbers. Color-coded 3D geometry shows the overlap of all the pattern windows. Modified from (Li <i>et al.</i> , 2015)...	123
Figure 7-5 Consecutives 2D phase mapping with PS drifting point dislocating across the LA area at different short time steps. The paired PS point had their trajectory starting near the roof (left-hand side) and move through the LA endocardium area (A); (B) an analogous lack of spatio-temporal PS stability behaviour is observed now with a set of two paired PS points. ....	124
Figure 7-6 Representation of the cumulative rotor occurrence stacked on the 3D LA.	124
Figure 7-7 A. DF with fixed colour map B.DF with adaptive colour map. C. OI with adaptive colour map D. RI with adaptive colour map E. Phase maps with slider to play, pause, forward and backward. ....	125

## List of Tables

Table 4-1 Review of CFAE mapping systems, EGM settings and success rate in different clinical studies. Previous studies conducted either additional or lone CFAE-guided ablation using different mapping systems and varying operator-defined settings, resulting in conflicting outcomes.....	63
Table 4-2 Clinical characteristics of study population (N = 18).....	65
Table 4-3 Sensitivity and specificity for A. ICL based classification using CFE-Mean $\leq$ 120 ms as the reference classification and; B. CFE-Mean based classification using ICL $\geq$ 7 as the reference classification.....	75
Table 4-4 Sensitivity and specificity for CFE-StdDev, ACI and SCI according to CFAE classification agreement between CFE-Mean and ICL. ....	76
Table 5-1 Clinical characteristics of study population (N = 18).....	84
Table 6-1 Clinical characteristics of study population (N = 18).....	101
Table 6-2 Spearman's correlation and Kappa score for ICL, ACI and SCI measured from the consecutive 2.5 s AEG segments. ....	106
Table 6-3 Spearman's correlation and Kappa score for ICL, ACI and SCI measured from the different segment lengths (2.5 s, 5 s and 8 s).....	111

## List of Abbreviations

3D	3-dimensional
ACI	Average Complex Interval
AEG	Atrial Electrogram
AD	Amplitude Distribution
AF	Atrial Fibrillation
AP	Action Potential
ApEn	Approximate Entropy
AUROC	Area Under the Receiver Operating Characteristic curve
AV	Atrioventricular (node)
CFAE	Complex Fractionated Atrial Electrogram
CL	Cycle Length
CS	Coronary Sinus
DF	Dominant Frequency
DWT	Discrete Wavelet Transform
EAM	Electro-anatomical mapping (system)
ECG	Electrocardiogram
EP	Electrophysiology
FFT	Fast Fourier Transform
FI	Fractionation Interval
FIRM	Focal Impulse and Rotor Modulation
HDF	Highest Dominant Frequency
ICL	Interval Confidence Level
IQR	Interquartile Range
IVC	Inferior Vena Cava
KDE	Kernel Density Estimator
LA	Left Atrium
LDA	Linear Discriminant Analysis
LOOCV	Leave-one-out cross-validation
LV	Left Ventricle
MANOVA	Multivariate analysis of variance

MRI	Magnetic resonance imaging
MV	Mitral Valve
OI	Organization Index
Pdf	Probability density function
PV	Pulmonary Veins
PVI	Pulmonary Veins Isolation
RA	Right Atrium
RF	Radiofrequency
ROC	Receiver Operating Characteristic
RV	Right Ventricle
SA	Sinoatrial (node)
SD, $\sigma$	Standard Deviation
SampEn	Sample Entropy
SCI	Shortest Complex Interval
ShEn	Shannon Entropy
SVC	Superior Vena Cava
SR	Sinus Rhythm
WACA	Wider Continuous Circumferential Ablation
WT	Wavelet Transform

# Chapter 1

## Introduction

Atrial fibrillation (AF) is the most common sustained cardiac arrhythmia found in clinical practice, and its prevalence increases with age. The loss of effective atrial contraction usually induces haemodynamic disorders, resulting in significant increase in morbidity and mortality. Approximately 33.5 million people are affected by AF in the world as per 2010 (0.5% to 1% of the world population), with more than 0.5 million of people in the UK affected in 1995, and about 200 thousand new cases each year (Chugh *et al.*, 2014, Stewart *et al.*, 2004). AF accounts for approximately one-third of hospitalizations for cardiac rhythm disturbances. The cost of clinical care of AF includes hospital costs, medication, follow-up, disability and emergency measures, adding up to 1% of the National Health Service budget in the United Kingdom and around US\$ 20 billion of annual expenses in the United States of America (Chugh *et al.*, 2014). The pursuit of efficient and successful treatment for AF is, therefore, important.

Pharmacological therapy is typically preferred as the first line of treatment for ventricular rate control and to avoid clot formation in most patients with AF, but it is usually followed by strong side effects, such as increasing the probability of heart failure, bradycardia or heart block (Calkins *et al.*, 2009). Currently, radiofrequency (RF) catheter ablation is regarded as the most accepted interventional procedure for AF treatment. Triggers in the pulmonary veins (PVs) have been proven important in the initiation and perpetuation of the arrhythmia in early stages (Haissaguerre *et al.*, 1998). Consequently, PV isolation (PVI) performed by RF ablation became the standard treatment for paroxysmal AF (pAF), with success rates as high as 80% of the cases (Oral *et al.*, 2002). However, PVI is less effective in patients with persistent AF (persAF), with success rate varying from 20% to 90% of the cases using different ablation strategies (Lim *et al.*, 2015). This inconsistency in persAF ablation outcomes is possibly due to extensive atrial substrate remodelling induced by long-term AF and little knowledge of the mechanistic perpetuation of AF in such conditions (Oral *et al.*, 2002).

Sustained AF causes changes in the cardiac tissue characteristics, inducing structural and electric remodelling (de Bakker and Wittkampf, 2010). Atrial electrograms (AEGs) acquired from such regions demonstrate low amplitude, multiple deflections activations that characterize ‘fractionated’ activity as a consequence of slow or inhomogeneous conduction. These regions – also referred to as the atrial substrate – are believed to be important in triggering and perpetuating atrial arrhythmias (Ashihara *et al.*, 2012). Complex fractionated atrial electrograms (CFAEs) are believed to represent such remodelled atrial substrates during AF (Nademanee *et al.*, 2004). CFAE-guided ablation quickly became a consolidated therapy for persAF adjunctive to PVI due to positive effects reported in early data (Deisenhofer *et al.*, 2009, Elayi *et al.*, 2008, Lin *et al.*, 2009a, Verma *et al.*, 2007, Verma *et al.*, 2008a, Verma *et al.*, 2010). Conflicting ablation outcomes have, however, cast doubt on the efficacy of this approach, and CFAEs have been criticized as an alternative for AF therapy (Dixit *et al.*, 2012, Oral *et al.*, 2009, Verma *et al.*, 2015, Wong *et al.*, 2015). Understanding possible reasons for disparities in CFAE-guided ablation outcomes, as well as better characterization of AEGs related to atrial substrate, may contribute towards better outcomes in persAF ablation.

A potential contributing factor concerning the low reproducibility of CFAE-guided ablation outcomes involves the current lack of consensus on the definition of a CFAE. Different medical equipment companies have developed 3D electro-anatomical mapping (EAM) systems with embedded automated CFAE detection algorithms to assist CFAE-guided ablation during electrophysiological (EP) studies (Monir and Pollak, 2008, Verma *et al.*, 2008a). However, different companies developed CFAE detection algorithms that evaluate different aspects of the AEG, creating their own CFAE definition. Differences in these algorithms could lead to discordant CFAE classifications by the available mapping systems, giving rise to potential disparities in CFAE-guided ablation.

A second contributing factor for inconsistent CFAE-guided outcomes in persAF ablation is that not all fractionated AEG might be related with atrial substrate. Conceptually, all CFAEs are thought to represent remodelled atrial substrate (de Bakker and Wittkampf, 2010). However, previous works have shown that a large proportion of CFAEs are a result of remote AF drivers and, therefore, a passive phenomenon not important to the maintenance of AF (Jadidi *et al.*, 2012a, Rostock *et al.*, 2006, Roux *et al.*, 2009, Tuan *et*

*et al.*, 2011). Conversely, other studies have suggested that some CFAEs represent active sources responsible for the perpetuation of AF (Takahashi *et al.*, 2008, Verma *et al.*, 2014, Yamabe *et al.*, 2009). Discerning different types of AEG fractionation might help in the characterization of atrial substrate in persAF studies. Additionally, most of those works have relied on few, if not only one, descriptors measured from the AEGs, which can be a limiting factor when describing a complex phenomenon such as persAF. Using multiple indices of fractionation is, therefore, crucial for investigating different features of the AEGs during AF (Schilling *et al.*, 2015).

Finally, the unstable temporal behaviour of atrial electrical activity during persAF might influence ablation target identification, and that could be another factor to explain the conflicting persAF ablation outcomes in previous studies. CFAEs are thought to represent remodelled tissues that are anchored in the atrium. While some studies have suggested that AEG fractionation has a high degree of spatial and temporal stability (Redfearn *et al.*, 2009, Roux *et al.*, 2008, Scherr *et al.*, 2009, Verma *et al.*, 2008b), others have suggested that the assessment of AEG fractionation requires a recording duration of at least 5 s at each site to obtain a consistent fractionation (Lin *et al.*, 2008, Stiles *et al.*, 2008, Tsai *et al.*, 2012). However, algorithms embedded in some EAM systems rely on 2.5 s AEG duration for automated CFAE classification, which could affect the ablation strategy and contribute to the conflicting outcomes in AEG-guided ablation in persAF.

## **1.1 Structure of the work**

### **1.1.1 Aims**

The main objective of this work is to investigate current methods for AEG fractionation classification during persAF and its relationship with the underlying mechanisms for AF maintenance and perpetuation. This objective was pursued through investigations regarding (i) the differences in CFAE algorithms embedded in EAMs that are currently used in EP studies using the same AEG data; (ii) the prevalence of CFAEs before and after PVI in patients with persAF; and (iii) the spatio-temporal behaviour of AEGs during persAF.

The results presented in this thesis are fruits of the collaboration between the Bioengineering Group, led by Dr. Fernando S. Schlindwein, and the Cardiovascular

Research Group, led by Prof. G. André Ng, both from the University of Leicester. Prof. Ng is also a consultant cardiologist at Glenfield Hospital, in Leicester UK, where the data used in this thesis were collected. Glenfield Hospital is one of 3 hospitals within the University Hospitals of Leicester that have strong collaboration with the University of Leicester.

### **1.1.2 Structure of the thesis**

Chapters 2 and 3 of the thesis briefly introduce some of the medical, mathematical and signal processing background material used in this work.

Chapter 4 describes a direct, head-to-head, quantitative comparison of CFAE categorization according to different automated algorithms embedded in two widely used commercial systems, using the same bipolar AEG data. In this chapter, different settings are investigated on CFAE quantification performed by different commercial algorithms, fractionation characterization as performed by these CFAE algorithms are assessed, and revised thresholds for those systems are proposed to minimize the differences in CFAE classification performed by either system.

Chapter 5 investigates the presence and characteristics of AEG fractionation before and after PVI and roof line ablation (PVI+RL) in patients with persAF using multiple indices of fractionation. This chapter suggests co-existence of AEGs that are responsive and AEGs that are unresponsive to PVI+RL. Current methods for AEG classification are imperfect, but the multiple combinations between them were able to significantly discriminate the different types of AEGs.

Chapter 6 investigates the spatio-temporal behaviour of AEGs and the consistency of AEG fractionation using different AEG segment lengths. This chapter shows that the ablation target identification using AEGs with 2.5 s duration – as defined by some EAM systems – is dependent on the time instant that the AEGs are collected. Consecutive 2.5 s AEGs produced different classification maps, which would affect the ablation strategy and contribute to the conflicting outcomes in AEG-guided ablation in persAF. AEGs with 5 s or longer should be considered for consistent AEG classification.

Chapter 7 summarizes the main findings from this thesis and highlights potential future investigations.

## Chapter 2

# Medical Background

### 2.1 The heart

The primary function of the heart is to circulate blood through the body by acting as a mechanical pump (Downey and Heusch, 2001). The human heart rests on the diaphragm, between the lower part of the two lungs and occupies a small region between the third and sixth ribs in the central portion of the thoracic cavity of the body (Schneck, 2000). It is composed of four chambers, two atria and two ventricles (Figure 2-1). The atria receive blood either from the body or from the lungs and fill the ventricles, while the ventricles pump blood either to the lungs or to the body. Functionally, the heart consists of two parts which are separated by the cardiac septum. The right heart (right atrium, RA; right ventricle, RV) collects blood with waste products and CO<sub>2</sub> from the body and pumps it to the lungs, where CO<sub>2</sub> is exchanged for O<sub>2</sub>. The left heart (left atrium, LA; left ventricle, LV) collects blood rich in oxygen from the lungs and pumps it through the body (Shoucri, 1991). Figure 2-1 illustrates the heart's structure and the blood flow through the chambers.

The wall of the heart consists of three layers. The endocardium is the inner layer which covers the whole interior. The outer layer is called epicardium and is also the inner layer of the pericardium. The myocardium is located between the endocardium and the epicardium and is the muscle responsible for the contraction of the heart (Schilling, 2012).

#### 2.1.1 Cardiac electrophysiology

Electrical potentials exist across the membranes of virtually all cells of the body. Cardiac muscle cells are capable of generating rapidly changing electrochemical impulses at their membranes, and these impulses are used to transmit signals along the myocyte's membranes (Guyton and Hall, 2006). The origin of this electrical potential – also known as membrane potential – lies in the maintainance of different ionic concentrations through

the cell semipermeable membrane (Plonsey and Barr, 2007). In cardiac cells,  $\text{Na}^+$ ,  $\text{Ca}^{2+}$ ,  $\text{K}^+$  and  $\text{Cl}^-$  ions are important in defining the membrane potential. The electrochemical potential of a particular ion is the potential which the cell membrane would have if the membrane were permeable to that ion alone. Consequently, the membrane potential is defined by a combination of the concentration differences of each ion through the cell membrane and on the selective permeability of the membrane in relation to each of the ions. In cardiac myocytes, the membrane potential at rest is about -100 mV, following the equilibrium potential of the  $\text{K}^+$  ion (Guyton and Hall, 2006).

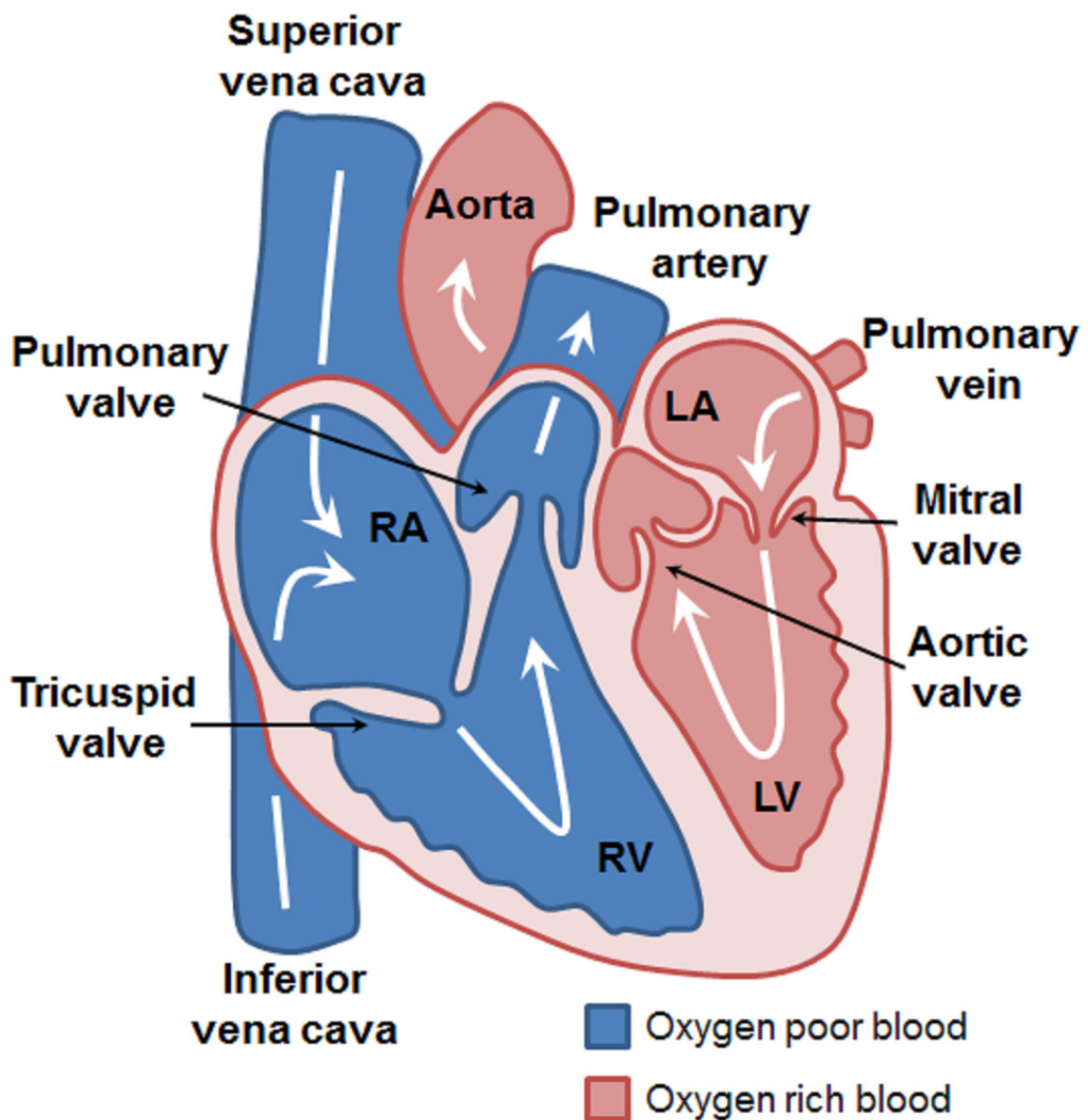


Figure 2-1 Structure of the heart and the course of blood flow through the heart chambers and heart valves. RA = right atrium; RV = right ventricles; LA = left atrium; LV = left ventricle.

In excitable cells, the membrane potential might vary due to a stimulus. When this stimulus minimizes the the membrane potential, i.e., the interior of the cell becomes less negative, the cell membrane is said to be depolarised. Depolarisations might cause the cell membrane to reach a certain potential threshold and trigger a fast depolarisation event that causes the membrane potential do become positive (close to +30 mV), following the equilibrium potential for the  $\text{Na}^+$ , returning to resting potential after 200–300 ms in cardiac myocytes (Guyton and Hall, 2006). This quick transient variation in the membrane potential is called action potential (AP). The AP is the electrical signal that is propagated throughout the cardiac myocytes triggering contraction. The cardiac AP relates with cardiac muscle contraction by excitation-contraction coupling, in which the AP induces an increase of cytosolic concentraion of  $\text{Ca}^{2+}$ , and the  $\text{Ca}^{2+}$  participates in muscular contraction (Guyton and Hall, 2006).

A general cardiac AP is illustrated in Figure 2-2. The rapid phase of depolarisation termed phase 0 is the result of opening of fast  $\text{Na}^+$  membrane channels and the simultaneous closure of  $\text{K}^+$  membrane channels. This causes the cell to approach the equilibrium potential for  $\text{Na}^+$ . Phase 1 is an initial repolarisation caused by an outward current from  $\text{K}^+$  channels opening (transient outward current). Phase 1 is followed by a plateau (phase 2), during which the membrane remains depolarised mainly due to the opening of  $\text{Ca}^{2+}$  channels, which is balanced by an outward current of  $\text{K}^+$  ions (delayed rectifier  $\text{K}^+$  channels). The repolarization phase (phase 3) results from the reopening of  $\text{K}^+$  channels in which the membrane potential returns to its resting level. The resting potential between beats is referred to as phase 4, and at that time the membrane potential of the cell is near the equilibrium potential for  $\text{K}^+$  (Plonsey and Barr, 2007). During phases 0 to 2, it is not possible to induce another AP and this is referred to as the ‘refractory period’ of the cell. During phase 3, it is possible to induce another AP if the stimulation is considerably strong. The cell is normally excitable from phase 4 onwards.

A particular group of cells in the heart can generate their own AP cyclically and are known as the sinoatrial (SA) node (Figure 2-3). SA myocytes generate spontaneous APs and act as the natural pacemaker of the heart (Downey and Heusch, 2001).

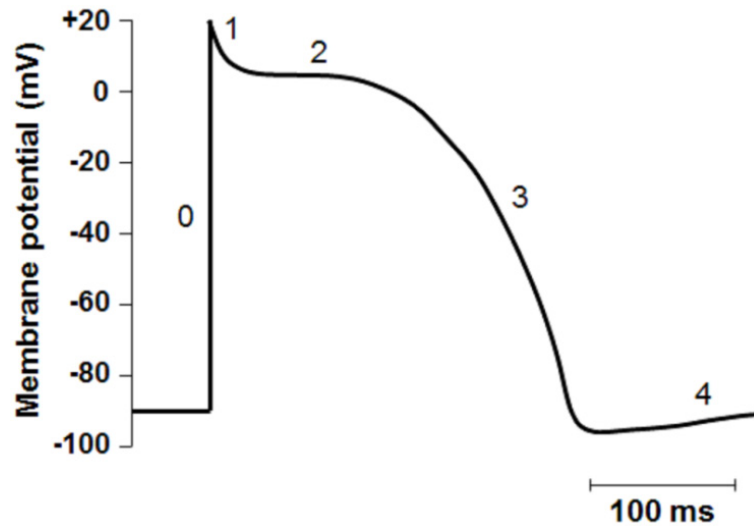


Figure 2-2 Cardiac (ventricular) muscle cell action potential with the four phases (explanation in the text).

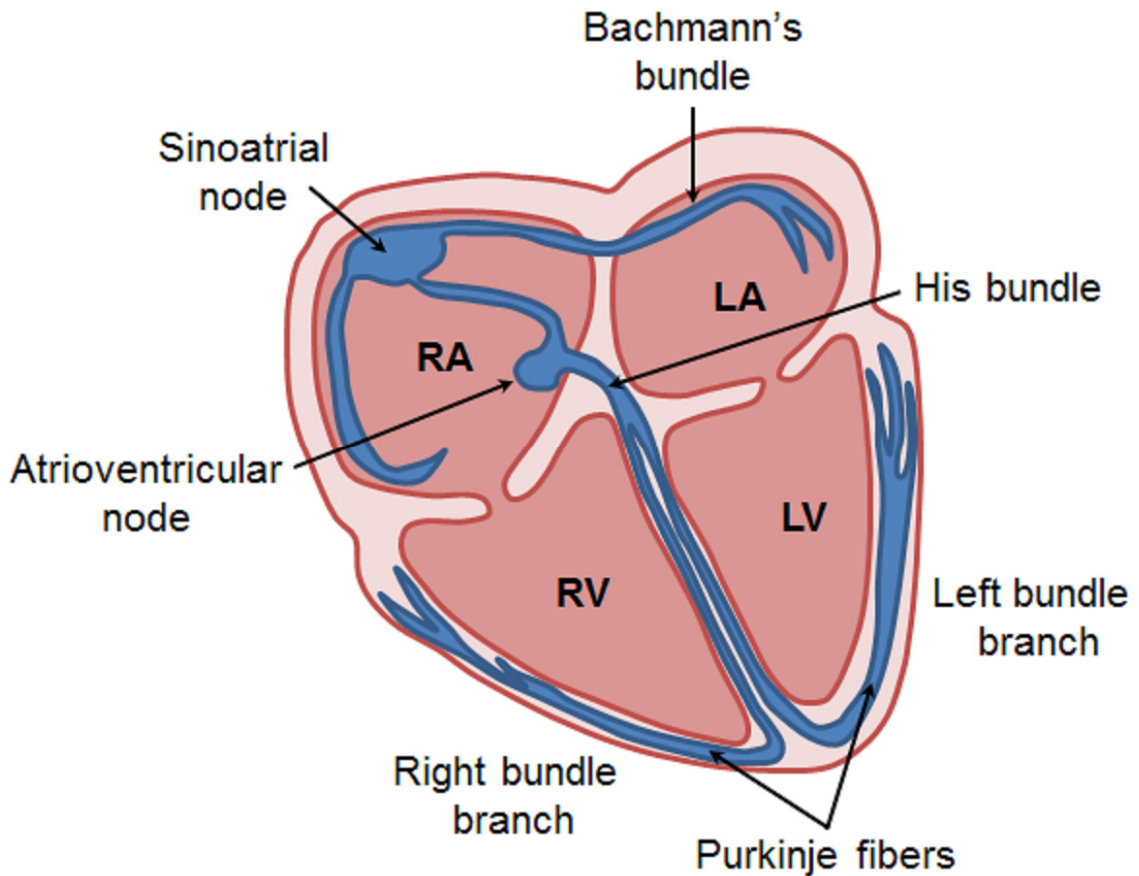


Figure 2-3 SA node and the specialized conductive system in the heart.

Cardiac muscle fibers are made up of many individual myocytes that are mutually connected. The cell membranes fuse with one another in such a way that they form permeable junctions (gap junctions) that allow almost totally free diffusion of ions.

Therefore, ions move with ease in the intracellular fluid along the longitudinal axes of the cardiac muscle fibers so that, under normal conditions, APs travel easily from one myocyte to the next, past the intercalated discs. Thus, the heart is seen as a functional syncytium in which the myocytes are so interconnected that when one of these cells becomes excited, the AP can spread from cell to cell through the gap junctions to all of them (Guyton and Hall, 2006). Therefore, the SA node ordinarily controls the beat rate of the entire heart. APs from the SA are propagated throughout both atria and specialised conduction cells, and reach the atrioventricular (AV) node. The AV node directs the activation wave front to the heart apice, triggering APs along the ventricles. In the healthy heart, the cyclic activity in the SA is regulated at 60 and 90 beats per minute, but these frequencies can be increased or decreased by the sympathetic or parasympathetic branches of the autonomic nervous system (Guyton and Hall, 2006).

Changes in the automaticity of the SA node and other myocytes – as well as remodelling of the heart’s conduction system – can lead to heart arrhythmias, which can deteriorate the ability of the heart to pump blood effectively (Guyton and Hall, 2006).

### **2.1.2 Measuring the cardiac electric activity**

The study of the electrical activity of the heart is important because it is directly related to the contraction behaviour of the cardiac muscle. Consequently, irregular electrical activity might be an indicative of structural heart alteration, such as myocardial infarction. The easier and most popular method for assessing the resultant electrical activity of the heart is the electrocardiogram (ECG), whose concepts have been introduced by Willem Einthoven in 1906 (Einthoven, 1906), and much explored since then (Geselowitz, 1989). The ECG is a non-invasive diagnostic method for analysing the electrical activity of the entire heart, providing information about the overall behaviour of the heart. For instance, in an ECG signal collected during sinus rhythm (SR) – as in the ECG segment shown in Figure 2-4 – it is possible to visualize the resulting electrical activation from the atria (P wave), followed by the ventricular activation (QRS complex), and the ventricular repolarization (T wave). The atrial repolarization occurs somewhere in the middle of the QRS complex but, since its amplitude is small compared to it, it is not possible to visualize.

Despite the fact that roughly any cardiac arrhythmia can be diagnosed with the ECG, it fails in providing further details of the cardiac disorder. In such cases, an EP study might be recommended. That consists in the recording of electrical activity from numerous intracardiac electrodes in order to characterise details of the cardiac substrate and the propagation of arrhythmias throughout both endocardium and myocardium (Eckardt and Breithardt, 2009). Following the inception of cardiac catheterization in the 1940s, catheter-based techniques were developed to record intracardiac electrical activity using catheters with electrodes in their tips (Borggreffe *et al.*, 1990).

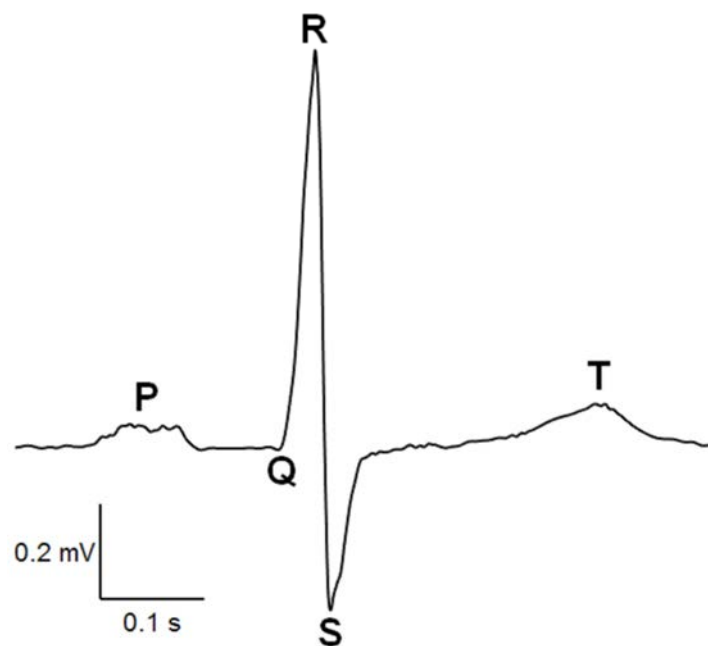


Figure 2-4 Illustration of an ECG segment collected from a subject during SR, highlighting the atrial and ventricular activations (P wave and QRS complex, respectively), followed by the ventricular repolarization (T wave).

### 2.1.3 Intracardiac AEG recording techniques

The AEG provides information about the electric behaviour of the underlying cardiac tissue. Therefore, the interpretation of the recorded AEG is fundamental during clinical investigations of arrhythmias during EP studies (Stevenson and Soejima, 2005).

A wavefront activation propagating throughout the cardiac syncytium depolarizes the membrane of the cardiac myocytes ( $V_m$ ), generating transmembrane currents ( $i_m$ ) that operate as a current dipole. The transmembrane currents produce extracellular potential ( $\Phi_o$ ) that can be captured by intracardiac catheters in the form of AEGs (Malmivuo and Plonsey, 1995). The genesis of extracellular potentials is illustrated in Figure 2-5.

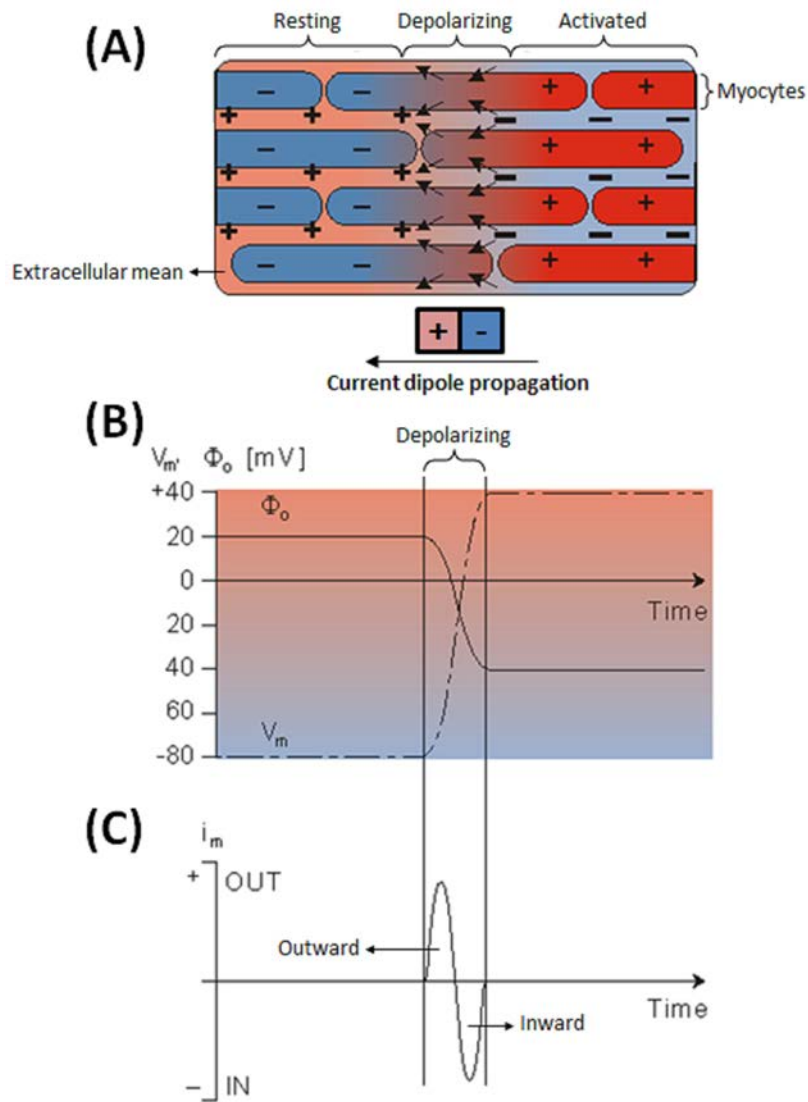


Figure 2-5 Illustration of the genesis of extracellular potentials ( $\Phi_o$ ) modified from (Malmivuo and Plonsey, 1995). The depolarization of myocytes' transmembrane potential ( $V_m$ ) propagation (A) generates inwards and outwards transmembrane currents ( $i_m$ ) that operate as a propagating dipole, creating extracellular potentials. These extracellular potentials can be captured by catheters with electrodes in their tips, and the resulting signal is referred to as an AEG.

There are two different recording configurations for AEG collection, as illustrated in Figure 2-6: unipolar or bipolar (Segal *et al.*, 2011). Each configuration perceives the propagating current dipole differently, providing different clinical information.

### 2.1.3.1 The unipolar recording configuration

Unipolar AEGs are obtained by positioning the exploring electrode – usually located at a catheter's tip – in the atrium and the reference electrode distant from the heart such that

it has little or no cardiac signal (Eckardt and Breithardt, 2009). The unipolar configuration records the global electric activity of the area surrounding the electrode, including the electric activity from the population of cells surrounding it (Figure 2-6). The major disadvantage of unipolar recordings is that they contain substantial far-field signal generated by depolarisation of tissue remote from the recording electrode, as well as noise from alternating current power supply (Segal *et al.*, 2011).

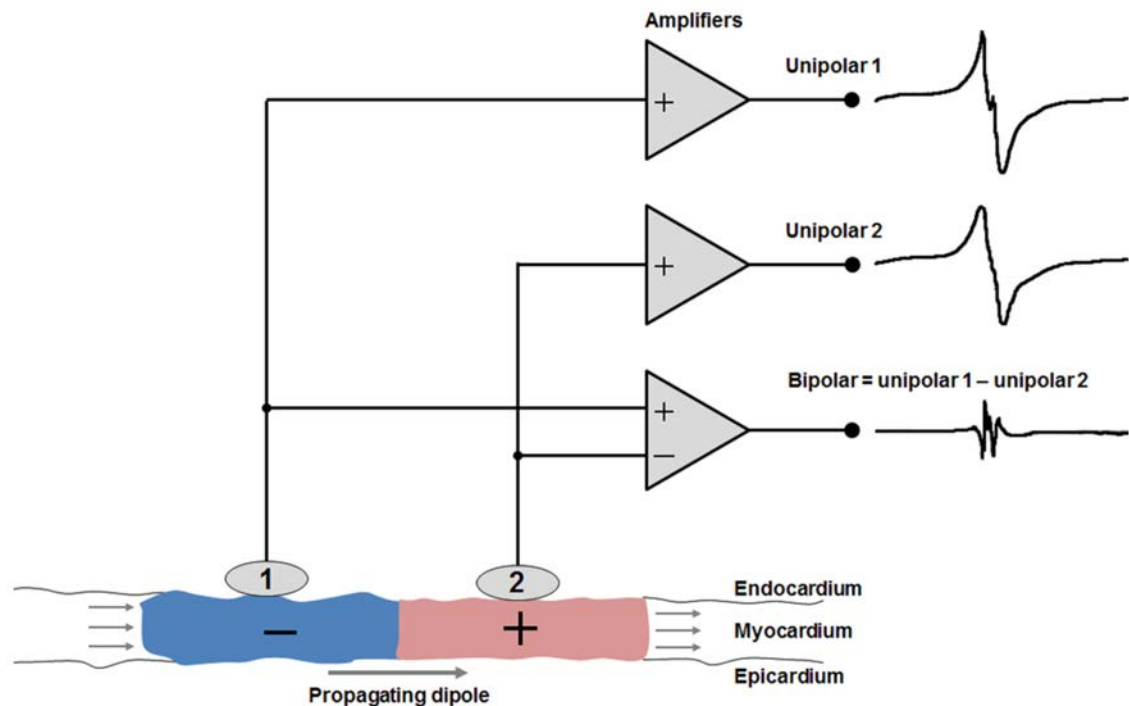


Figure 2-6 Illustration of both unipolar and bipolar recordings generated by an activation wave traveling along a myocardial bundle from the left to the right. The unipolar configuration captures the global electric activity of the area surrounding the electrode. Conversely, the bipolar finds the difference between the two electrodes, minimizing the common-mode noise influence, leaving mostly the local signal. Modified from (Kusumoto, 1999).

The unipolar AEG collected where the activation front starts will be negative because the electrode is located in the negative part of the potential field. A unipolar AEG collected in the middle of the activation will present a biphasic shape, whereas it is positive if the unipolar AEG is collected where the activation comes to an end (de Bakker and Wittkamp, 2010). Additionally, previous works have shown that the negative down stroke deflection of the unipolar AEG coincides with the AP depolarization of the group of cells surrounding the electrode (Spach *et al.*, 1979, Steinhaus, 1989). Therefore, the unipolar configuration is useful in activation mapping procedures (Eckardt and

Breithardt, 2009). Unipolar AEGs usually require a band-pass filter (in the range of 0.1 Hz – 300 Hz) after being collected (Stevenson and Soejima, 2005).

### *2.1.3.2 The bipolar recording configuration*

Bipolar recordings are obtained by positioning two closely spaced exploring electrodes in the area of interest (Eckardt and Breithardt, 2009). The resultant AEG is the voltage difference between the two electrodes (Figure 2-6). The bipolar configuration is able to substantially suppress far-field signal generated by depolarisation of tissue remote from the recording electrode, as well as common-mode noise from alternating current power supply.

The main advantage of the bipolar mode lies in the detection of local low amplitude potentials important in understanding the mechanisms of arrhythmias that may have been undetectable using the unipolar configuration (Kimber *et al.*, 1996). The bipolar configuration is the most common technique used in EP studies during AF treatment. The main disadvantage of this configuration is that the resulting bipolar AEG is dependent on the relative orientation of the electrodes in relation to the wave front propagation (Segal *et al.*, 2011). Bipolar AEGs are also subject to band-pass filtering (in the range of 30 Hz – 300 Hz) after being collected to remove components generated by the repolarisation of the cells and high noise frequency influence (Stevenson and Soejima, 2005).

### *2.1.3.3 The local atrial cycle length*

The local activation time of a group of cardiac cells can be inferred from either unipolar or bipolar AEGs. The time elapsed between consecutive local activation times in an AEG is an important feature in EP studies during AF, defined as the ‘cycle length’ (CL). The CL represents the rate of activation of the underlying atrial tissue (Figure 2-7), providing important direct information about the local AF organization, atrial conduction and activation pattern. For instance, CL increase is often noticed before AF termination during ablation (Kim *et al.*, 1996).

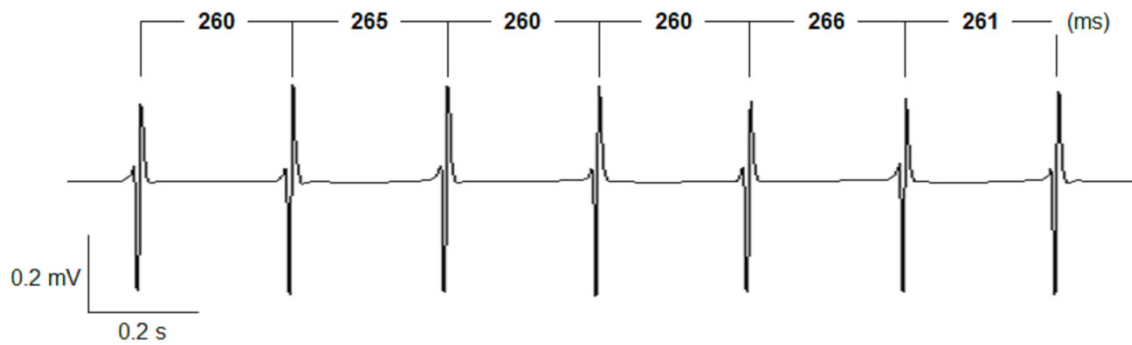


Figure 2-7 Example of bipolar AEG recorded during AF with respective cycle lengths between subsequent local activations. The mean CL in this example is 262 ms.

## 2.2 Atrial fibrillation

According to the ACC/AHA/ESC Practice Guidelines (American College of Cardiology Foundation – ACCF; American Heart Association – AHA; European Society of Cardiology – ESC), AF is defined as “a supraventricular tachyarrhythmia characterized by uncoordinated atrial activation with consequent deterioration of atrial mechanical function. On the ECG, AF is characterized by the replacement of consistent P waves by rapid oscillations or fibrillatory waves (*f*-waves) that vary in amplitude, shape, and timing, associated with an irregular, frequently rapid ventricular response” (Fuster *et al.*, 2006). The atria might be depolarised with a frequency of 350 – 600 beats per minute during AF. Figure 2-8 illustrates an ECG during SR and an ECG during AF.

AF can be classified by its clinical relevance and temporal patterns. When AF is diagnosed in a patient without clinically detectable heart disease, it is referred to as lone AF (Fenelon and de Paola, 2000). A first-detected episode of AF considers the possibility of previous undetected episode. When a patient has had 2 or more detected episodes, AF is considered to be recurrent (Fuster *et al.*, 2006). Despite current debate, the most accepted classification for recurrent AF was proposed by Gallagher and Camm (Gallagher and Camm, 1998):

- Paroxysmal: AF that terminates spontaneously or with intervention within 7 days of onset. The episodes may recur with variable frequency;
- Persistent: AF sustained longer than 7 days or requires cardioversion regardless of the duration of the episode. If AF is sustained for longer than a year, it can be referred to a longstanding persAF);

- Permanent: when there has been a joint decision by the patient and clinician to cease further attempts to restore and/or maintain SR, AF is referred to as permanent AF. Acceptance of AF represents a therapeutic attitude on the part of the patient and clinician rather than an inherent pathophysiological attribute of the AF. Acceptance of AF may change as symptoms, the efficacy of therapeutic interventions, and patient and clinician preferences evolve.

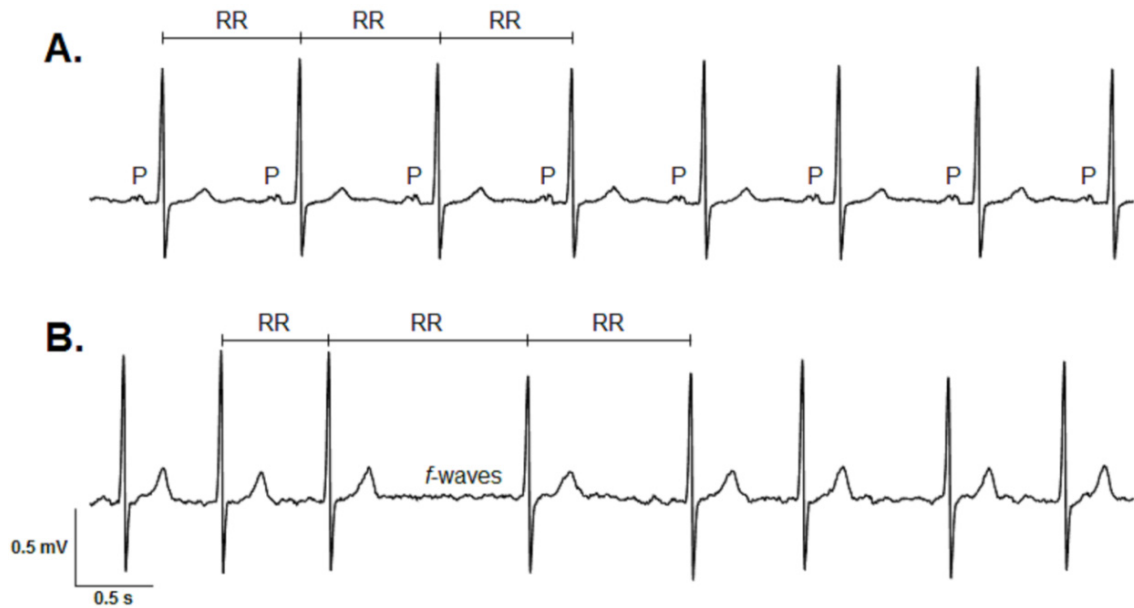


Figure 2-8 A. ECG in SR showing consistent P waves and regular ventricular response (RR intervals). B. ECG in AF showing fibrillatory *f*-waves and irregular ventricular response.

### 2.2.1 Epidemiology and prognosis

AF is the most common cardiac arrhythmia found in clinical practice, affecting approximately 33.5 million people around the world as per 2010 (0.5% to 1% of the world population) (Chugh *et al.*, 2014). The prevalence of AF increases with age, from  $\leq 0.5\%$  at 40–50 years, to 5–15% at 80 years, with men more often affected than women (Camm *et al.*, 2010). AF affects about 2 million people in the United States (Fuster *et al.*, 2006), and more than 0.5 million of people in the UK had AF in 1995, with 200 thousand new cases each year (Stewart *et al.*, 2004). The loss of effective atrial contraction might cause blood clot formation in the atria and, consequently, the occurrence of thromboemboli. These thromboemboli tend to propagate and might find their way into the brain, with the occurrence of stroke increasing fivefold in patients with AF (Oral, 2009). AF accounts for approximately one-third of hospitalizations for cardiac rhythm disturbances. The costs

of clinical care of AF sum up of hospital costs (52%), costs of medication (23%), follow up (9%), follow-up examinations (8%), disability (6%) and emergency measures (2%) (Fuster *et al.*, 2006), summing up to 1% of the National Health Service budget in the United Kingdom (approximately £2.5 thousand per patient per year) and around US\$ 20 billion of annual expenses in the United States of America (Chugh *et al.*, 2014).

## **2.2.2 Mechanisms of atrial fibrillation**

AF initiation and perpetuation requires both triggers for its onset and a substrate for its perpetuation (Fuster *et al.*, 2006). In general, patients with pAF are likely to have a predominance of factors that trigger AF, whereas patients with persAF are more likely to have a predominance of perpetuating factors due to atrial remodelling (Nattel *et al.*, 2009). There is, however, overlap between these mechanisms in a sense that patients with pAF might not present identifiable triggers, as well as triggers can be found as the main cause for maintenance of AF in patients with persAF (Ziad *et al.*, 2013). Nevertheless, previous work introduced the idea that “AF begets AF”, suggesting that ectopic activities would induce pAF and, in a long term perspective, promote the remodelling of the atrium tissue to a self-sustained arrhythmia (Wijffels *et al.*, 1995).

### *2.2.2.1 The atrial substrate*

Atrial substrate is a term commonly used referring to the remodelled atrial tissue that might participate in the perpetuation of AF. Previous work has shown that atrial remodelling might be induced by electrical, contractile and structural changes caused by sustained AF (Allessie *et al.*, 2002). Figure 2-9 shows the multiple pathways in which atrial remodelling might occur during AF.

- Electrical remodelling: previous work has shown that sustained AF reduces the expression of Ca<sup>2+</sup> channels in cardiac cell membranes, which shortens the AP and the local atrial CL (Yue *et al.*, 1997). A reduction in the conduction velocity has also been observed in AF (Gaspo *et al.*, 1997). Reductions in both refractory period and conduction velocity affect the wavelength – defined as distance travelled by the activation wave front during an activation period (Lewis, 1925). Therefore, the wavelength is defined as the product of the conduction velocity and

the refractory period of the underlying cardiac tissue. Small wavelengths might induce small circuits of activations, which would support AF perpetuation.

- Contractile remodelling: the reduction of the expression of  $\text{Ca}^{2+}$  channels reduces the cytosolic concentration of  $\text{Ca}^{2+}$ , which affects the contractility of atrial tissue, increasing the compliance, dilatation and consequently, the stretch of the atrial tissue. Stretch of atrial myocardium is hypothesized to act as a stimulus for structural remodelling of the atria (Allessie *et al.*, 2002).
- Structural remodelling: AF might also induce structural changes in the atrial tissue, such as increase in cell size, alterations in connexins' expression, myocardial infarction, increased collagen deposition, among others (Ausma *et al.*, 1997, de Bakker *et al.*, 1993, van der Velden *et al.*, 2000). These structural alterations would produce a complex network of intermingled collagen and myocardial fibres, which could create regions of block (or slow conduction) and anisotropic means for the wave front propagation, inducing random propagation of atrial activations, contributing for AF perpetuation.

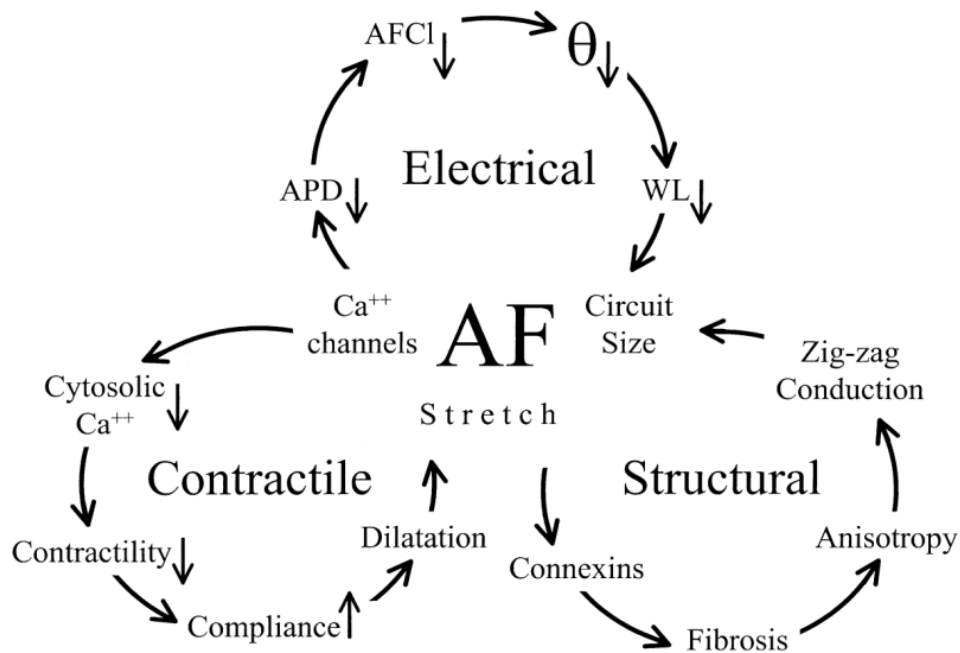


Figure 2-9 Possible mechanisms of atrial remodelling during AF. Reproduced with permission from (Allessie *et al.*, 2002). APD = action potential duration; AFCL = atrial fibrillation cycle length;  $\theta$  = conduction velocity.

Despite many advances and extensive research to understand possible mechanisms of atrial remodelling, the mechanisms of AF initiation and perpetuation are still debated.

There are currently three theories explaining the EP mechanisms of AF (Figure 2-10): (i) multiple rapid ectopic activity; (ii) multiple wavelet hypothesis and; (iii) multiple-circuit re-entry theory (Ziad *et al.*, 2013).

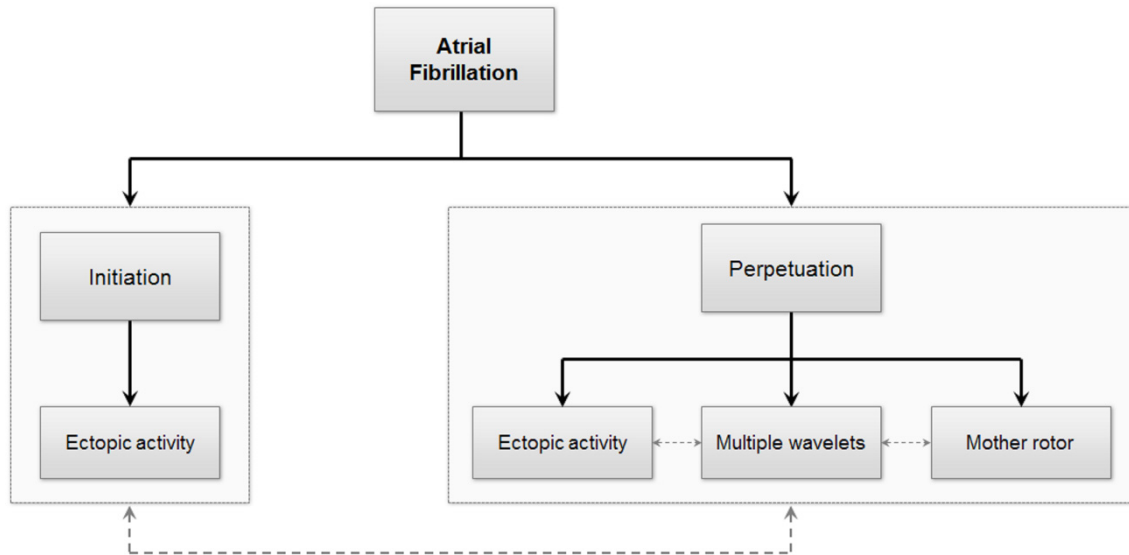


Figure 2-10 Graphical representation of the different theories regarding mechanisms underlying AF initiation and maintenance. AF initiation and perpetuation requires both triggers for its onset and a substrate for its maintenance, but these mechanisms are likely to co-exist at various times.

### 2.2.2.2 Multiple rapid ectopic activity

Ectopic activity accounts for rapidly firing focus and it can be responsible for either triggering or perpetuating AF. The concept of ectopic activities has been introduced in the early 20<sup>th</sup> century (Winterberg, 1907), and further verified experimentally in 1940 (Scherf, 1947). In both works, vagal nerve stimulation in humans accelerated and sustained the arrhythmia, suggesting the existence of ectopic activities from those sites. Further observations from EP studies supported the idea that AF is related to focal mechanisms (Haissaguerre *et al.*, 1994, Jais *et al.*, 1997). More specifically, triggers originating from the myocardial sleeves of the PVs have been proven important in the initiation and perpetuation of the arrhythmia in early stages in humans (Haissaguerre *et al.*, 1998). The work from Haissaguerre and colleagues is considered a cornerstone in cardiac EP (Haissaguerre *et al.*, 1998), with a great influence on current AF treatment. Ectopic activities from the PVs have been shown to be responsible to about 90% of AF initiation in patients with pAF (Oral *et al.*, 2002).

Previous works have shown that autonomic nervous system stimulation, bradycardia and acute atrial stretch are factors that can generate ectopic activity for triggering AF (Chen *et al.*, 2006). It is believed that the junction between the PVs and the LA has discontinuous myocardial fibres separated by fibrotic tissues, and the PV muscle sleeve is highly anisotropic, which can explain the high incidence of ectopic activity in this region. Schotten and colleagues (Schotten *et al.*, 2011) reviewed the electrophysiological basis of PV ectopic activity, listing the morphology and EP of PV myocytes, the tissue structure and the conduction patterns in myocardial sleeves as potential causes for ectopic activities.

Recent works suggest that these ectopic focal discharges are indeed focal fibrillation waves originated from endo-epicardial breakthroughs (de Groot *et al.*, 2010). Accordingly, whenever an activation wave front fades away during AF in one cardiac layer, the wave front propagation in the other layer would conduct transmurally and replace the extinguished wave by one or more focal-breakthrough waves, which would explain the self-sustaining nature of AF and ectopic activities (de Groot *et al.*, 2010).

### 2.2.2.3 Multiple wavelet hypothesis

The multiple wavelet hypothesis states that AF is fundamentally a turbulent and self-sustaining process, which takes place in an inhomogeneous excitable medium. The concept that self-sustaining multiple wavelets propagate randomly through the atria without the existence of a focal trigger was firstly introduced by Moe and Abildskov in 1959 (Moe and Abildskov, 1959), and further explored using their computer model (Moe *et al.*, 1964). They have shown that, in cases where atrial remodelling was evidenced, irregular activation wave front becomes fractionated as it divides about islets or strands of refractory tissue and each of the daughter wavelets would be considered as an independent offspring (Moe *et al.*, 1964).

Allessie and colleagues provided the first demonstrations of multiple propagating wavelets giving rise to turbulent atrial activation in a dog model of AF (Allessie *et al.*, 1985, Kirchhof *et al.*, 1993). Pharmacological experiments showed that AF termination was preceded by a decrease in the number of wavelets after administration of antiarrhythmic drugs (Wang *et al.*, 1992, Wang *et al.*, 1993). The presence of multiple wavelets meandering in human atria has been reported later in EP studies during AF

(Allessie *et al.*, 2010, Konings *et al.*, 1994). More importantly, these works have shown that the multiple wavelets are sustained by functional conduction blocks present in the atria during AF. These conduction blocks represent alterations in the wavelength in the atrial substrate, and might induce wave break, wave collision and anisotropic conduction, perpetuating the wavelets and AF.

The multiple wavelet hypothesis has been acknowledged as the most accepted theory by clinical electrophysiologists in the last 50 years. However, recent investigations reporting the existence of multiple-circuit re-entries in the atria during AF have increased the debate about the underlying AF mechanisms and about the validity of the multiple wavelet hypothesis (Jalife *et al.*, 2002).

#### *2.2.2.4 Multiple-circuit re-entry theory*

Multiple-circuit re-entry theory considers that one or several re-entries behave as a cyclic periodic activation wave front, from which multiple wavelets might emanate into the atrial tissue, uncoordinatedly spreading in various directions. Although the re-entry theory is being currently revisited, it was firstly introduced by Mines around 1910 (Mines, 1913). As later explained by Allessie and colleagues (Allessie *et al.*, 1973), the propagating circuit is defined by the EP properties of the fibres composing the circuit – i.e. the conduction velocity and refractory period – in which the head of the circulating wave front is continuously biting in its own tail of refractoriness, as illustrated in Figure 2-11.

A study with segmented turtle hearts provided the first experimental evidence of the concept that fibrillatory conduction might be perpetuated by circus movement (Garrey, 1914). More, it has shown that a minimum tissue mass is needed to perpetuate AF. Re-entry activations were later observed in rabbit (Allessie *et al.*, 1973), dog (Schuessler *et al.*, 1992) and sheep hearts (Mandapati *et al.*, 2000, Skanes *et al.*, 1998), either from optical or electrical recordings. More recently, studies have reported the identification of re-entry activations in isolated myocardium cells and in human heart (Pertsov *et al.*, 1993). Nevertheless, there is debate about the participation of re-entry circuits in the perpetuation of AF. Allessie and de Groot, for instance, stated that they have failed to find re-entry circuits in human heart during fibrillation (Allessie and de Groot, 2014).

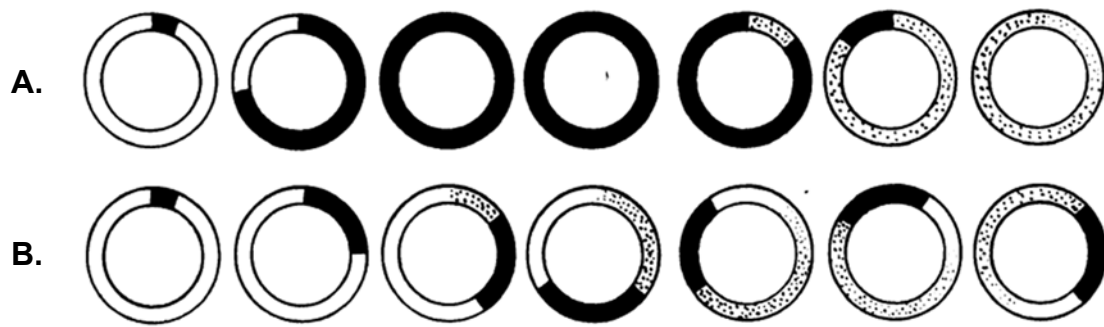


Figure 2-11 Illustration of a re-entry circuit. A. Activation wave front in ideal conditions. B. Continuous activation due to alterations in the conduction velocity or in the refractory period, sustaining a continuous re-entry circuit. The white regions represent non-activated state; the black regions represent activated state; the dotted regions represent refractory state. Adapted from (Mines, 1913).

The mechanisms that drive AF have been under discussion for a long time, as it can be inferred from Sir Thomas Lewis comments: “fibrillation is not purely a circus movement. My view is that if atrial flutter proves to be a circus movement, then a circus movement is readily converted into fibrillation. More than this I am not prepared to concede at present” (Lewis, 1925). AF is a complex, dynamic arrhythmia, and it is very likely that multiple mechanisms, such as those above mentioned, concurrently contribute in the initiation and perpetuation of AF.

### 2.2.3 Clinical management of atrial fibrillation

Management of patients with AF involves three main objectives (Bollmann and Lombardi, 2006, Fuster *et al.*, 2006): i) ventricular rate control; ii) thromboemboli prevention; iii) restoration of sinus rhythm. Two clinical approaches are considered for AF treatment: pharmacological and non-pharmacological.

#### 2.2.3.1 Pharmacological therapy

Pharmacological therapy is the first line of treatment for asymptomatic AF, and considers the administration of antiarrhythmic drugs for ventricular rate control and to avoid clot formation in most patients with AF. The ventricular rate control is crucial for the maintenance of proper hemodynamic function, while anti-clotting drugs help to avoid the formation of thromboemboli. However, antiarrhythmic drugs have strong side effects, such as increasing the probability of heart failure, bradycardia or heart block (Calkins *et al.*, 2009). Nevertheless, anti-clotting and antiarrhythmic drugs – such as flecainide,

amiodarone, beta blockers or channel blockers – are usually administered to patients undergoing non-pharmacological treatment in order to minimize the risk of thromboembolism and to control the ventricular rate.

#### 2.2.3.2 *Non-pharmacological therapies*

Non-pharmacological therapies are the first line of treatment in symptomatic AF, and can be divided in three procedures: i) cardioversion; ii) surgical ablation and; iii) RF catheter ablation.

Electrical cardioversion therapy is usually performed in an attempt to restore SR, especially in patients with persAF duration longer than 48 hours (Bollmann and Lombardi, 2006). Implantable pacemakers can also be used for long-term rate control (Nattel, 2002). Ablation therapy – either surgical or catheter-based – is recommended when electrical cardioversion fails to restore SR.

Surgical ablation (or maze) is an open chest procedure, consisting of cardiac transmural incisions made in the left and right atria, dividing the atria into small, electrically isolated compartments, creating electrical barriers (Cox *et al.*, 1991). The maze procedure relies on the hypothesis that the main mechanism responsible for the initiation and maintenance of AF is the existence of multiple wavelets randomly meandering in the atria. The electrical barriers created in the atria during the procedure form regions of functional block, reducing the atrial tissue mass needed to propagate the wavelets and, consequently, the AF (Cox *et al.*, 1991, Garrey, 1914, Yamazaki and Jalife, 2012). The maze procedure has been highly effective in eliminating AF, with reported success rate as high as 98% (Cox *et al.*, 1996). However, the technically challenging nature of the surgery, high rate of post-procedure permanent pacemaker implantation and loss of atrial mechanical function limited the widespread acceptance of the maze technique.

#### **2.2.4 Catheter ablation of atrial fibrillation**

The positive AF termination outcomes of the maze procedure motivated the use of a less aggressive technique for modifying atrial substrate, the RF catheter ablation (Fuster *et al.*, 2006). Scheinman and colleagues reported the first RF catheter ablation procedure targeting the AV junction to control refractory supraventricular arrhythmias (Scheinman *et al.*, 1982). Their work showed the safeness of catheter ablation, suggesting that it could

supplant the need for open heart surgical procedures in such cases. During the procedure, catheters with electrodes in their tips are inserted in the patient's heart. RF energy is applied to the electrodes, heating the catheter's tip targeting the arrhythmia-related tissue, burning and destroying the atrial substrate responsible for initiating or perpetuating arrhythmia, or simply creating myocardial lesions to block the AF electrical wave front propagation (Nattel, 2002).

#### 2.2.4.1 *Electro-anatomical mapping (EAM) systems*

When catheter ablation was introduced in EP studies (Scheinman *et al.*, 1982), the procedures were guided with fluoroscopy, in which a continuous X-ray beam is used to investigate the patient's heart, with evident impact to the patient and the clinical team. In the late 1990s, EAM systems were introduced into clinical practice to support EP studies (Wittkamp *et al.*, 1999). These commercial solutions use non-fluoroscopic methods for endocardial mapping to generate a 3D anatomical map of the heart's chambers, reducing fluoroscopic exposure and radiation dose during EP procedures (Rolf *et al.*, 2015). Among the data provided by EAM are chamber reconstruction, tagging of important anatomic landmarks and ablation lesions, display of diagnostic and mapping catheters with reduced fluoroscopy dosage, activation and voltage mapping. During arrhythmia mapping, EAMs allow operators to record intracardiac electrical activation in relation to anatomic location in a cardiac chamber of interest (Gepstein *et al.*, 1997, Schilling *et al.*, 1998, Wu *et al.*, 2008).

Currently, there are two widely accepted systems in clinical use for EP studies: the EnSite NavX® system (St Jude Medical, St. Paul, MN, USA) and the CARTO® system (Biosense Webster, Baldwin Park, CA, USA) (Aizer *et al.*, 2008, Scherr *et al.*, 2007). NavX uses impedance changes to define the catheter localisation, while CARTO uses magnetic field (Segal *et al.*, 2011). Both NavX and CARTO are usually used with point-by-point, sequential AEG collection. EAM technologies that provide simultaneous AEG collection have been introduced in the clinical practice to overcome the limitations imposed by sequential point-by-point mapping.

St Jude Medical has presented a noncontact high density balloon mapping (EnSite 3000 or EnSite Velocity, St Jude Medical, St. Paul, MN, USA) that allows simultaneous recording electrical activity of the inner surface of the atrium without the contact between

the electrodes from the balloon and endocardium wall of the atrium (Schilling *et al.*, 1998). The balloon contains a multielectrode array (64 unipolar electrodes) that is placed in the middle of the atrial cavity. Far-field atrial activity is simultaneously collected by the 64 electrodes mounted in the balloon, and an inverse solution calculates and interpolates up to 2048 unipolar AEGs that are projected to the atrial wall of the 3D anatomical model. High density simultaneous recordings of the electrical activity of the inner surface of the atrium with contact between the electrodes from the balloon and endocardium wall of the atrium has been introduced by Topera (RhythmView®, Menlo Park, CA, USA), in which 64 electrodes distributed in a basket are in contact with the endocardial surface allowing the system to record up to 64 simultaneous unipolar AEGs or 32 simultaneous bipolar AEGs (Rolf *et al.*, 2015).

Although those technologies provide an alternative to sequential point-by-point mapping, they also have some limitations. The inverse solution used by the noncontact balloon mapping might add undesired distortion to the resultant reconstructed AEGs, especially in cases where the distance between the atrial wall and the balloon is higher than 4 cm (Schilling *et al.*, 1998). Similarly, the contact basket still suffers from low spatial resolution and poor contact with the atrial wall, which affects the quality of the measured atrial electrical activity (Walters and Kalman, 2015). Those methods, however, remain promising tools for mapping and investigating the underlying mechanisms of persAF perpetuation.

#### *2.2.4.2 Ablation of paroxysmal atrial fibrillation*

In 1998, Haïssaguerre and colleagues (Haïssaguerre *et al.*, 1998) have shown that the electrical isolation of the PV, performed by RF catheter ablation, would terminate AF in such patients. The PVI by RF ablation is usually performed by the creation of segmented lesions around the PV ostia, or by wider continuous circumferential ablation (WACA) lesions created to surround the PVs. Irrespective of the method, these lesions create barriers that electrically disconnect the PVs from the rest of the atria, preventing triggers originating in the PVs to perpetuate in the LA and initiate or sustain the arrhythmia (Calkins *et al.*, 2012c). Non-PV triggers initiating AF have also been reported during pAF occurring in the posterior wall of the LA, the superior and inferior vena cava (SVC, IVC), the coronary sinus (CS), among other regions (Calkins *et al.*, 2012c).

Haïssaguerre's study consolidated RF catheter ablation as the most accepted procedure for AF treatment, supported by the fact that catheter ablation is less life-threatening than the maze procedure (Oral, 2009). Since then, catheter ablation has evolved from being an experimental method to the most common practice performed in EP procedures for AF therapy (Bollmann and Lombardi, 2006, Natale *et al.*, 2007). Further studies in PVI performed by catheter ablation resulted in termination of pAF in about 80% of the cases, in which between 30% and 40% needed a second procedure (Oral *et al.*, 2002, Stevenson and Albert, 2012, Terasawa *et al.*, 2009, Wright *et al.*, 2008).

#### 2.2.4.3 Ablation of persistent atrial fibrillation

PVI is consistently less effective in patients with persAF due to an incomplete understanding of the mechanistic interaction between relevant atrial substrate and the initiation and maintenance of AF (Haïssaguerre *et al.*, 2005a, Oral *et al.*, 2002). The creation of ablation lines aimed at mimicking the lines of the surgical maze is currently one of the most accepted procedures additional to PVI in persAF therapy (Calkins *et al.*, 2012c). Accordingly, PVI is commonly followed by the creation of lines of block in the LA, usually targeting the roof (connecting the superior lines of the left and right upper PVI lesions); the region between the mitral valve (MV) and the left inferior PV; and anteriorly between the roof line near the left or right circumferential lesion and the mitral annulus. As a consequence, extensive ablation and repeated procedures are often required in persAF ablation, which increases the chances for clinical complications and resources to be allocated.

Haïssaguerre and colleagues (Haïssaguerre *et al.*, 2005b) have shown that AF is more likely to terminate after a gradual or sudden increase in CL as a result of catheter ablation. The same study has showed that the probability of AF termination is directly proportional to the amount of lesions performed by ablation. A review recently published by Lim *et al.* (Lim *et al.*, 2015) has shown that AF termination in persAF ablation ranges 20% to 90% of the cases using different ablation strategies. The same study also concluded that AF termination during AF ablation confers improved long-term freedom from atrial arrhythmias (Lim *et al.*, 2015, Zhou *et al.*, 2013). Therefore, additional strategies to improve AF termination rates during persAF ablation with minimum amount of ablation are of great interest. In particular, the identification of patient-specific AF drivers gained

evidence to design tailored ablation strategies. AEG-guided ablation has become an important strategy in patient-specific persAF treatment since the AEG provides further details about the underlying cardiac substrate for each particular patient.

For instance, the analysis of AEGs in the frequency domain has emerged with great expectation and is becoming a complementary tool to study the pathophysiology and mechanisms of AF (Skanes *et al.*, 1998). It is believed that the dominant frequency (DF) – defined as the biggest peak in the frequency spectrum of the AEG within a physiological range (usually between 3 Hz and 20 Hz) – represents the main activation wave front of an atrial region, and therefore would correlate with the local atrial CL during AF (Ng *et al.*, 2006). It has been suggested that areas harbouring high DF may represent sites with high periodic activation, driven by either ectopic activity or re-entry circuits that perpetuates the arrhythmia (Jalife *et al.*, 2002). Moreover, it has been suggested that ablation at these sites could be an effective strategy to terminate AF (Sanders *et al.*, 2005). An additional index to frequency spectrum analysis is the organization index (OI). The OI is derived by dividing the area under the DF and its harmonics by the total power of the frequency spectrum, and it measures the variability of the DF. Therefore, high OI represents less variability of DF and, consequently, higher AEG organization (Takahashi *et al.*, 2006). Termination of pAF has been reported after RF ablation of sites with high frequency activity in different locations of the atrium (Sanders *et al.*, 2005). Elimination of LA-to-RA frequency gradients by ablation has been shown to contribute to long-term SR maintenance in AF patients (Atienza *et al.*, 2009). Additionally, it has been reported that an increase of OI measured from AEGs precedes termination of AF during ablation and that overall atrial OI increases after PVI (Takahashi *et al.*, 2006). Our group has shown, however, that the DF might not be spatio-temporally stable, suggesting that targeting sites of high DF from a single time frame is unlikely to be a reliable ablation strategy (Salinet *et al.*, 2013). We have also shown the existence of atrial regions more prone to host a high DF patterns, despite the lack of DF spatio-temporal stability. Such regions could be markers of AF drivers in persAF patients (Dastagir *et al.*, 2014, Li *et al.*, 2015).

More recently, EP studies have reported that targeting re-entries – in these investigations referred to as ‘rotors’ – during AF ablation terminated the arrhythmia (Narayan *et al.*,

2012). This strategy uses panoramic sampling of the atria and computational spatio-temporal mapping to identify regions of recurrent organized rotational activity (Benharash *et al.*, 2015, Gray *et al.*, 1998). These organized rotational activities are identified from the analytical signal of the AEG computed using the Hilbert Transform. This analytical signal is used to compute the instantaneous phase of the AEG, from which regions in the atria hosting phase discontinuities are identified as points of singularity (PS) (Rodrigo *et al.*, 2014). Finally, these PSs are marked and targeted for catheter ablation. The relationship with the multiple re-entry theory – which has intense support from optical mapping studies (Mandapati *et al.*, 2000) – as well as the high termination rate for persAF ablation reported in early data have facilitated the acceptance of rotor-guided ablation (Haissaguerre *et al.*, 2014, Narayan *et al.*, 2012). However, there is currently intense debate on rotor-guided ablation as these works differ in terms of the spatio-temporal stability of the rotors in the atria during AF, and that rotor-guided ablation might not be as effective in treating persAF as initially reported (Benharash *et al.*, 2015, Buch *et al.*, 2016, Mohanty *et al.*, 2016). Recent investigation on the relationship between atrial regions hosting high DF and rotors suggest that PSs are localized mainly around high DF regions, and that rotors of opposite chirality would induce the transit of high DF clouds between them (Dastagir *et al.*, 2015a).

Investigations in both frequency domain and phase of the AEGs have contributed significantly to improving the understanding of patient-specific mechanisms of the arrhythmia. However, there is an ablation strategy that has been in evidence and under intense debate in the last decade: patient-specific substrate modification guided by fractionated AEGs.

### **2.2.5 Complex fractionated atrial electrograms**

In 2004, Nademanee and colleagues (Nademanee *et al.*, 2004) reported 96% of success rate of AF termination only ablating areas with AEGs with complex activations. Nademanee's findings were received with great enthusiasm – as well as scepticism – by the scientific community. CFAEs were initially described as being i) AEGs composed of two deflections or more, and/or perturbation of the baseline with continuous deflection of a prolonged activation complex over a 10-s recording period; ii) AEGs with a very short CL ( $\leq 120$  ms) averaged over a 10-s recording period (Nademanee *et al.*, 2004). EP

studies targeting CFAEs during ablation usually consider bipolar AEGs since this recording configuration allows for the collection of local electrical activation. Figure 2-12 shows a bipolar AEG with small amplitude, continuous fractionated activity (CFAE), and a bipolar AEG with discrete organised activations (non-CFAE).



Figure 2-12 Illustration of bipolar AEGs collected during AF. A. Bipolar AEG with small amplitude, continuous fractionated atrial activity (CFAE). B. Bipolar AEG with discrete organised activations (non-CFAE).

Ultimately, areas with fractionated electrical activity during AF are believed to represent areas of slow conduction and/or at pivot points where the wavelets turn around at the end of the arcs of functional blocks. Therefore, the rationale supporting CFAEs relies on the hypothesis that AF is a self-sustaining arrhythmia where multiple wavelets meander in the atria, as suggested by Moe and Abildskov (Moe and Abildskov, 1959). Despite intense debate, previous works have shown that these areas of functional block might induce wave break or wave collision in the presence of fibrotic tissue (Allessie *et al.*, 2010, Konings *et al.*, 1994), anisotropic conduction (de Bakker *et al.*, 1993), leading circle re-entry (Lee *et al.*, 2014) and spiral wave re-entry (Heijman *et al.*, 2015). In all these cases, as illustrated by Figure 2-13, areas of the atria presenting such fractionated activation are believed to be important sites for AF perpetuation and, therefore, targets for ablation (Ganesan *et al.*, 2013, Knecht *et al.*, 2009, Nademanee *et al.*, 2004).

CFAEs have been reported to be found most frequently at the proximal fraction of the CS; the junction between the SVC and the RA; the septal wall anterior to the right superior and inferior PVs; the anterior wall medial to the LA appendage; the area between the LA

appendage and left superior PV; the posterosuperior wall medial to the left superior PV (Nademanee, 2011).

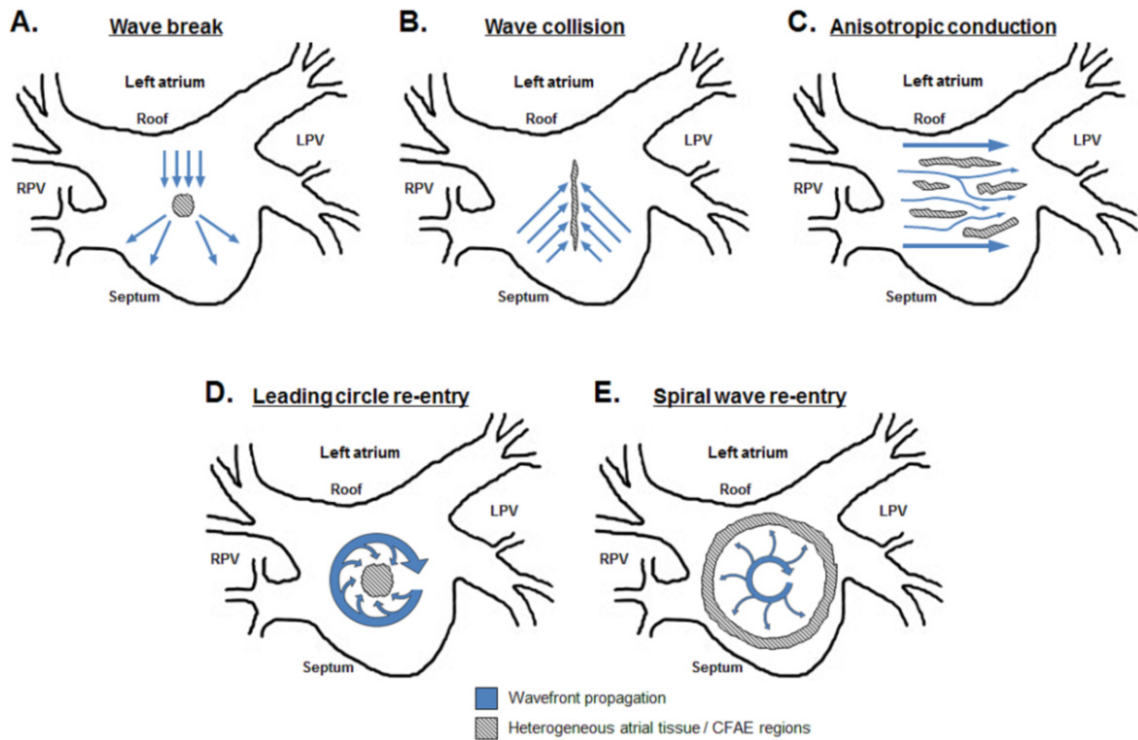


Figure 2-13 Graphical representation of the possible mechanisms involved in the genesis of CFAEs. A. Wave break. B. Wave collision. C. Anisotropic conduction. D. Leading circle re-entry. E. Spiral wave re-entry.

### 2.2.5.1 Brief historical notes on fractionated AEGs

Although studies relating CFAEs and AF gained more relevance in 2004 with Nademanee's seminal work (Nademanee *et al.*, 2004), fractionated electrograms were first reported in 1961 by Durrer and colleagues (Durrer *et al.*, 1961). They reported fractionation as a stable phenomenon in epicardial infarcted regions with both unipolar and bipolar AEGs.

Cosio and collaborators (Cosio *et al.*, 1983) were the first to relate fractionated AEGs and AF, suggesting that fractionation is related with areas of slow conduction and shorter effective refractory periods, supporting the existence of re-entries in such areas.

Gallagher (Gallagher *et al.*, 1982) and Gardner (Gardner *et al.*, 1985) argued whether or not fractionation was caused by noise artifacts. On the one hand, Gallagher and colleagues supported that fractionated AEGs might occur due to electrodes artifacts, and mentioned

that fractionation has been captured in a ‘Jell-o brain’. On the other hand, Gardner and collaborators performed an extensive EP and anatomical study on fractionated AEGs and its relation with artifacts. The authors reported fractionation during SR, tachycardia and in infarcted regions and concluded that fractionation is not caused by artifacts. They also suggested fractionation might be caused by slow and inhomogeneous conduction and the spatial-time summation of extracellular currents, which could indicate the presence of multiple wavelets or re-entrant circuits. Gardner’s work helped to consolidate bipolar AEGs as the gold standard for measuring fractionation, and also showed that the direction of the bipolar electrodes affects fractionation as collected by the AEGs – this latter reinforced by Correa de Sa and colleagues (Correa de Sa *et al.*, 2011).

In 1993, de Bakker and colleagues have reported that slow conduction in the infarcted myocardial tissue is caused by a "zigzag" course of activation. In such cases, the recording electrodes positioned in the tissue will not only record activity in the bundle underneath the electrode, but also the activity of wave fronts propagating in distant bundles. Because of asynchronous activation in the various bundles, multiple deflections will arise, which results in fractionated AEGs (de Bakker *et al.*, 1993, de Bakker and Wittkamp, 2010).

Konings and colleagues (Konings *et al.*, 1997) related the morphology of unipolar AEGs during AF with the occurrence of specific patterns of conduction. More specifically, they related fractionated activity with local asynchronous activations that may occur due to: spatial dispersion of refractory periods; tissue inhomogeneity, resulting in uncoordinated conduction patterns; the presence of insulating collagenous septa between atrial muscle bundles.

In 2006, Rostock and colleagues (Rostock *et al.*, 2006) showed that CL is a major determinant of fractionation occurrence during AF, suggesting that shortening of CL precedes the development of CFAE.

Kalifa and collaborators (Kalifa *et al.*, 2006) reported that the area surrounding the region hosting the DF during AF has high propagation pattern variability and fractionated activity. These findings were later reinforced by Nademanee (Nademanee, 2011).

More recently, Jadidi and collaborators (Jadidi *et al.*, 2012b) have shown that CFAE’s distribution in the atria is highly variable, depending on direction and rate of activation.

The same group has later suggested that CFAEs are inversely related to atrial regions with fibrosis (Jadidi *et al.*, 2013).

De Bakker and Wittkamp (de Bakker and Wittkamp, 2010) revisited possible causes of fractionation. They reported that CFAEs can be caused by:

- Electrodes' movement;
- Signal filtering might add unwanted deflection, affecting fractionation outcome;
- Remote atrial far-field activity may affect the local AEG and lead to an apparently fractionated signal (Narayan *et al.*, 2011). Unipolar recordings are more sensitive to remote activity than bipolar;
- The direction of bipolar electrodes can induce fractionation due to the heart inhomogeneity, which supports the theory of electrical dissociation and atrial substrate remodelling AF;
- Heart structures with different activation patterns. AEGs captured near two structures will often show multiple deflections because of activation in the two different structures;
- Fractionation might be induced by alterations in conduction velocity, which in turn can be altered by contractile, electrical and structural remodelling.

#### 2.2.5.2 Visual classification of atrial electrograms during atrial fibrillation

In 1978, Wells and colleagues (Wells *et al.*, 1978) classified bipolar AEGs into four different types according to the morphological characteristics of the signals:

- Type I – highly organised – characterised by discrete depolarisation activities separated by an isoelectric baseline free of perturbation;
- Type II – moderately organised – identifiable depolarisation activity but with perturbations of the baseline between atrial complexes;
- Type III – low organised – AEG which failed to demonstrate either depolarisation events or isoelectric intervals;
- Type IV – characterized by alternation between type III and the other types.

The authors have also noticed that AEGs during AF were not stable in most of the reported cases, changing from one type to any other arbitrarily. Wells' classification for AEGs during AF has become widely used in AEG classification investigations using

visual inspection of AEGs performed by specialists. The visual inspection of AEGs has been adopted as the “gold reference” for many years, and many works relied on it in the investigation of methods for substrate characterisation. Figure 2-14 illustrates the classification suggested by Wells and colleagues in three bipolar AEGs collected during AF (Wells *et al.*, 1978).

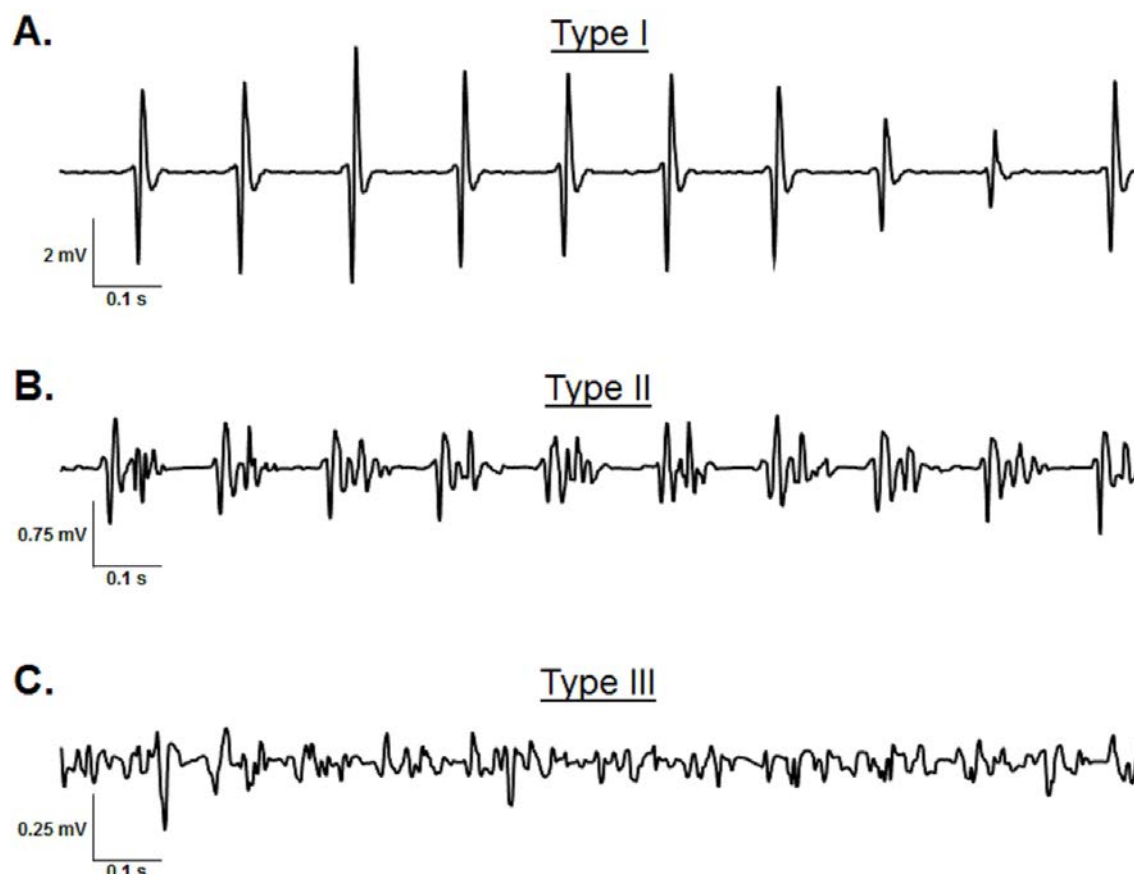


Figure 2-14 Illustration bipolar AEGs collected during AF according the classification suggested by Wells and colleagues (Wells *et al.*, 1978). A. AEG of type I showing discrete depolarisation activities separated by an isoelectric baseline free of perturbation. B. AEG of type II with identifiable depolarisation activity but with perturbations of the baseline between atrial complexes. C. AEG of type III which failed to demonstrate either depolarisation events or isoelectric intervals.

Hoekstra *et al.* (Hoekstra *et al.*, 1995) categorized AEGs during AF using nonlinear techniques, supporting the AEG classification defined by Wells and colleagues (Wells *et al.*, 1978).

Barbaro and colleagues were the first to consider multiple indices measured from bipolar AEGs during AF, also following visual AEGs classification (Barbaro *et al.*, 2000). These indices were used to design a multidimensional classification based on minimum-distance

features (Barbaro *et al.*, 2000, Barbaro *et al.*, 2001). The authors have shown that AF type I has a baseline free of perturbation and thus the amplitude distribution (AD) is dominated by a large peak in the central mean value; the baseline in AF type II is disturbed, hence the AD presents significant bins around the mean value; in AF type III, the baseline is barely detectable, and the bins in the AD are spread out and widely distributed over an extensive range around the mean value.

Mainardi and colleagues (Mainardi *et al.*, 2001) used linear (cross-correlation) and nonlinear (mutual corrected conditional entropy) methods to characterise AEGs dynamics during AF based on visual analysis of the AEGs. More recently, Orozco-Duque and colleagues have used multifractal analysis for grading CFAEs also based on visual classification (Orozco-Duque *et al.*, 2015), and Schilling and collaborators (Schilling *et al.*, 2015) have classified different ranks of fractionation using multiple indices of fractionation.

Despite the valuable contribution of those investigations, the visual assessment of fractionation introduces subjectivity to the method as each specialist has his/her own perception of what defines fractionation, even supported by Wells' AEG classification. Additionally, the visual identification of AEG fractionation might not correspond with the true atrial substrate. These factors induce inconsistencies to the methods, and would make the reproducibility of the CFAE classification difficult.

#### *2.2.5.3 Automated algorithms for CFAE classification*

The reproducible high curative success rates initially reported by Nademanee and colleagues when targeting CFAEs during ablation (Nademanee *et al.*, 2004) has been challenging. One of the reasons for such low reproducibility of outcomes could be due to the fact that the authors performed CFAE classification visually by the operator. With the objective of minimizing inconsistencies in CFAE classification, medical equipment companies have developed 3D EAM systems with embedded automated CFAE detection algorithms to optimize substrate mapping, and assist CFAE-guided ablation during EP procedures.

The two EAM systems broadly used in clinical practice – NavX and CARTO – have modules integrated in their software for automated CFAE mapping (Aizer *et al.*, 2008,

Scherr *et al.*, 2007). The algorithms embedded in those systems incorporate CFAE characteristics as initially described by Nademanee and colleagues (Nademanee *et al.*, 2004). For both systems, sequential bipolar AEGs are captured throughout the atrium guided by the 3D anatomical map generated by the system. The algorithms for automated CFAE detection will be described and discussed in detail on *Chapter 4, Minimizing discordances in automated classification of fractionated electrograms in human persistent atrial fibrillation*.

The time duration of each recorded AEG depends on the system – and algorithm – that has been used. The AEGs are band-pass filtered as defined by the operator. Once the indices provided by the algorithms embedded on both systems are calculated for each point in the 3D EAM, the operator can visualize the resultant CFAE map (colour-coded) according to each respective index.

Nevertheless, individual commercial systems developed CFAE detection algorithms that evaluate different aspects of the AEG. As a consequence, there is currently no consensus on CFAEs definition. Additionally, commercial systems allow for operator-defined settings, which also affect CFAE identification (Almeida *et al.*, 2016).

#### *2.2.5.4 Other indices of fractionation*

Many indices of fractionation – additional to those measured by the automated algorithms embedded in commercial systems – have been introduced in AF investigations. Nonlinear similarity index was developed and used to address AEG morphology and consistency over time (Faes *et al.*, 2002, Lin *et al.*, 2013). The authors reported that CFAE sites tagged by automated CFAE classification with high similarity index are important for AF maintenance and, consequently, are important sites for ablation.

Shannon Entropy (ShEn) has been used to measure the complexity of AEGs (Chen *et al.*, 2009). Ng and colleagues (Ng *et al.*, 2010) have shown that ShEn assumes small values for AEGs with organized activation and high values for CFAEs. Recent studies have shown the relationship between multiple wavelets hypothesis and the multiple re-entry theory (Ganesan *et al.*, 2013, Lee *et al.*, 2014). The authors reported fractionated activity in the pivot of the rotor using ShEn. ShEn and other descriptors will be briefly introduced on *Chapter 3, Mathematical & Signal Processing Tools*.

Recent work has suggested that LA atrial structural remodelling can be detected by late enhancement magnetic resonance imaging (MRI) and correlated with reduced AEG amplitudes (Mahnkopf *et al.*, 2010). Low peak-to-peak amplitude (PP) of AEGs has been introduced as a marker for atrial structural remodelling during AF and, therefore, targets for ablation (Oakes *et al.*, 2009, Rolf *et al.*, 2014). It has been suggested that ablation of low PP regions might have compensatory effects in addition to PVI in persAF therapy (Rolf *et al.*, 2014).

As stated previously in section 2.2.4.3 *Ablation of PersAF*, DF and OI calculated from AEGs have been used to identify areas within the atria that may be responsible for driving AF (Salinet *et al.*, 2013).

Each of the above mentioned indices measures one feature of the AEG and the underlying atrial tissue. Most of the investigations on CFAEs have relied on few – if not only one – indices of fractionation, which can be a limiting factor when describing a complex phenomenon such as persAF. Investigating different features from the AEGs might improve our understanding of the arrhythmia and our capability to successfully identify areas that are critical to the maintenance of AF (Schilling *et al.*, 2015).

#### 2.2.5.5 CFAE's spatio-temporal behaviour

The reliability of the CFAE spatio-temporal behaviour is an important factor for the application of clinical CFAE mapping (Tsai *et al.*, 2012), and it has been under discussion since its introduction as an additional ablative therapy for AF. According to Nademanee and collaborators (Nademanee *et al.*, 2006), “CFAEs are surprisingly stationary, exhibiting relative spatial and temporal stability”. As a consequence, this temporal stability would allow sequential point-to-point AEG measurement to capture CFAEs, as a region showing fractionated activation would consistently show fractionated activation, as well as regions without fractionation would always be free of fractionation. Accordingly, CFAEs mapping systems, such as CARTO and NavX, perform the mapping sequentially, point-by-point.

CFAEs spatio-temporal behaviour has been assessed by two main methods (Lau *et al.*, 2012): i) sequential 3D CFAE maps. In this approach, CFAE stability is assessed by comparing two or more sequential 3D maps for the presence of CFAE or the degree of

AEG fractionation at similar atrial regions. Some researchers reported high CFAEs temporal-stability when comparing two sequential 3D maps (Roux *et al.*, 2008, Scherr *et al.*, 2009, Verma *et al.*, 2008a). However, Habel and collaborators (Habel *et al.*, 2010) reported low CFAEs spatio-temporal stability when comparing more than two sequential 3D maps; ii) in short-term continuous recordings. In this approach, the AEG of a single site is divided in windows with same time duration. CFAEs temporal behaviour is assessed by comparing the presence of CFAE or the degree of AEG fractionation between time windows. Lau and colleagues reported 75% of stable CFAEs in continuous recordings of mean 1.25 minutes based on a review of five studies (Lau *et al.*, 2012).

The choice of recording duration to consistently measure AEG fractionation remains contentious. Each automated CFAEs mapping system considers different AEG duration for CFAEs measurement. For instance, CARTO uses AEG recording with fixed duration of 2.5 s for CFAEs mapping (Monir and Pollak, 2008, Porter *et al.*, 2008, Scherr *et al.*, 2009). More recently, however, Tsai and colleagues (Tsai *et al.*, 2012) suggested that AEG recording duration of 5 s would provide more consistent CFAE identification using CARTO criteria.

Roux and colleagues (Roux *et al.*, 2008) have shown that CFAEs have high spatio-temporal stability using a 2 s AEG time window with NavX criteria. Lin and collaborators (Lin *et al.*, 2008) and Stiles and colleagues (Stiles *et al.*, 2008) independently reported that the segment length does affect the fractionation outcome. Both studies suggested that mapping CFAEs with NavX system requires a recording duration of  $\geq 5$  s at each site to identify fractionation consistently.

#### *2.2.5.6 The outcomes of CFAE-guided ablation in persAF*

CFAE-guided ablation remains one of the most controversial topics in AF therapy. The role of CFAE mapping has significantly reduced since its adoption as an ablation strategy for persAF adjunct to PVI and anatomical lines creation due to disparities in CFAE-guided ablation outcomes (Sohal *et al.*, 2015). While some researchers reported persAF termination rates superior to 50% of the cases (Elayi *et al.*, 2008, Lin *et al.*, 2009a, Nademanee *et al.*, 2004, Verma *et al.*, 2010), other studies have reported much lower success rates after CFAE-guided ablation (Oral *et al.*, 2007, Oral *et al.*, 2009, Porter *et al.*, 2008, Verma *et al.*, 2011). Nevertheless, ablation targeting atrial regions hosting

fractionated activity in addition to standard PVI and anatomical lines ablation as an attempt to improve outcomes in patients with persAF is still broadly performed in many clinical centres around the world.

Recent investigations increased even more the controversy surrounding CFAE-guided ablation. Multicentre studies have reported no incremental benefit of CFAE ablation when performed in addition to PVI and linear ablation (Verma *et al.*, 2015, Wong *et al.*, 2015). A recent meta-analysis also reported that additional atrial ablation targeting CFAEs resulted in no improvement in mid-term procedural outcome or freedom from AF (Providência *et al.*, 2015). Although the authors also reported no increase in procedural-related adverse events, CFAE ablation is related with longer procedures time, which increases both costs and potential complications associated with the procedure.

It is clear from these studies that a majority of CFAEs are not active participants in the AF process and as such are poor targets for ablation (Sohal *et al.*, 2015) and that current methods for identifying CFAEs have failed to provide a definite solution for persAF therapy. A recent review by Sohal and colleagues, however, suggest that some CFAEs are indeed critical sites for AF maintenance and better identification of these may result in better outcomes in persAF ablation (Sohal *et al.*, 2015).

There are some possible reasons for the low reproducibility of CFAE-guided ablation outcomes, as already mentioned above, that will be covered in the present thesis. Firstly, recent works have reported a low correlation between different indices of fractionation (Almeida *et al.*, 2016, Lau *et al.*, 2015). Differences in automated algorithms to classify CFAEs could lead to discordant CFAE classifications by the available mapping systems, giving rise to potential disparities in CFAE-guided ablation. Minimizing the differences in CFAE classification as performed by different methods may help to clarify the significance of CFAE as a driver of persAF.

Secondly, previous works have shown that a large proportion of CFAEs are a result of remote AF drivers and, therefore, a passive phenomenon not important to the maintenance of AF (Rostock *et al.*, 2006, Roux *et al.*, 2009, Tuan *et al.*, 2011, Jadidi *et al.*, 2012a). Conversely, other studies have suggested that some CFAEs represent active sources responsible for the perpetuation of AF (Takahashi *et al.*, 2008, Yamabe *et al.*, 2009,

Verma *et al.*, 2014). The characterisation of different types of AEG fractionation might help to detect regions critical to the maintenance of AF (Lin *et al.*, 2009b).

Finally, successful CFAE ablation is based on the assumption that the fractionated AEGs represent anchored anatomic areas that are critical to the maintenance of AF. If a healthy atrial tissue is incorrectly classified as CFAEs – and this could happen due to limitations in the CFAE algorithm or because the region under analysis is prone to passive wave collision – and targeted for ablation, areas of slow conduction could result from the ablation, thereby creating more pro-arrhythmogenic areas, which would perpetuate the arrhythmia instead of terminating it (Wong *et al.*, 2015, Zaman and Narayan, 2015). The temporal behaviour of AEGs should be considered in order to improve atrial substrate identification.

## Chapter 3

# Mathematical & Signal Processing Tools

To date there is no agreement on the definition of a CFAE. Previous studies relied either on visual inspection or on automated algorithms embedded in commercial systems (Calo *et al.*, 2008, Hunter *et al.*, 2009, Monir and Pollak, 2008, Scherr *et al.*, 2007, Scherr *et al.*, 2009, Verma *et al.*, 2008a). A clinician visual assessment of fractionation might introduce subjectivity in CFAE classification, which would difficult reproducibility of the results. Similarly, the outcomes of CFAE-guided ablation in persAF using commercial systems have demonstrated diversified successes. Automated algorithms embedded in commercial systems have been independently validated, and have never been directly compared. Finally, the majority of the works on CFAEs have relied on few – if not only one – indices of fractionation, which can be a limiting factor. Investigating different features from the AEGs might improve our understanding of the areas that are critical to the maintenance of AF. In this chapter some mathematical and signal processing techniques that have been used in this work are briefly described.

### 3.1 Statistical measures

The probabilistic properties of a continuous random variable can be defined through a function  $p(x)$ , known as the probability density function (pdf) (Hayter, 2012). The probability that the random variable lies between two values  $a$  and  $b$  is obtained by integrating the pdf between these two values:

$$P(a \leq X \leq b) = \int_a^b p(x)dx \quad (3.1)$$

A valid pdf  $p(x)$  cannot take negative values and must integrate to one over the whole sample space, so that the total probability is equal to 1. The pdf provides complete information about the probabilistic properties of a random variable but, since the pdf can be difficult to be estimated, random variables are often described by summary measures.

### 3.1.1 Central moments

A random variable  $X$  taking the values  $x_i$  with probability values  $p_i$  has an expected value of

$$E\{X\} = \int_{-\infty}^{\infty} x \cdot p(x) dx = \mu_X \quad (3.2)$$

$E\{X\}$  provides a summary measure of the average value taken by the random variable and is also known as the mean of the random variable. Higher order statistics referred to the mean, known as central moments, are used to describe the spread, asymmetry, and curvature of a pdf. In general, the  $k^{\text{th}}$  central moment is defined as

$$E\{[X - E\{X\}]^k\} = \int_{-\infty}^{\infty} [x - E\{X\}]^k p(x) dx = \mu_X^k \quad (3.3)$$

The second central moment, the variance, measures the spread or variability in the values taken by the random variable. Larger values of the variance indicate that the distribution is more spread out.

$$\text{Var}(X) = E\{[X - E\{X\}]^2\} = \sigma_X^2 \quad (3.4)$$

The square root of the variance,  $\sigma_X$ , is known as the standard deviation (SD) of the distribution of the random variable and is often used in place of the variance to describe the spread of the distribution.

The third central moment, the skewness, is a measure of the asymmetry of a distribution. A negative skewness indicates that the tail on the left side of the pdf is longer than the tail on the right side. A positive skewness indicates that the tail on the right side is longer than the one on the left side. If the values are symmetrically distributed on both sides of the mean, the skewness is zero.

$$\text{Skew}(X) = E\left\{\left[\frac{X - E\{X\}}{\sigma}\right]^3\right\} = \frac{\mu_X^3}{\sigma_X^3} \quad (3.5)$$

The fourth central moment, the kurtosis, is a measure of the concentration of probabilities in a pdf.

$$Kurt(X) = E \left\{ \left[ \frac{X - E\{X\}}{\sigma} \right]^4 \right\} = \frac{\mu_X^4}{\sigma_X^4} \quad (3.6)$$

The kurtosis of an arbitrary Gaussian distribution is always 3. The excess is defined as

$$Excess(X) = Kurt(x) - 3 \quad (3.7)$$

Therefore, the excess is zero in a Gaussian pdf, negative in pdfs with rounded peak (known as sub-Gaussian), and positive in pdfs with sharper peak (referred to as super-Gaussian) (Schilling, 2012).

### 3.1.2 Median and interquartile range

In this work, all continuous non-normally distributed variables are expressed as median  $\pm$  interquartile range (IQR). The median provides information about the middle value of the pdf of a random variable. The random variable is equally likely to be either smaller or larger than the median (Hayter, 2012).

Quantiles of random variables also provide information about the spread or variability of the distribution of the random variable. They are often written as a percentage, referred to as percentiles. The lower quartile of a distribution (Q1) is defined to be the 25<sup>th</sup> percentile of the distribution, and the upper quartile (Q3) of a distribution is defined to be the 75<sup>th</sup> percentile. Therefore, two quartiles, together with the median, partition the state space of a random variable into four quarters, each of which has a probability of 0.25 (Figure 3-1).

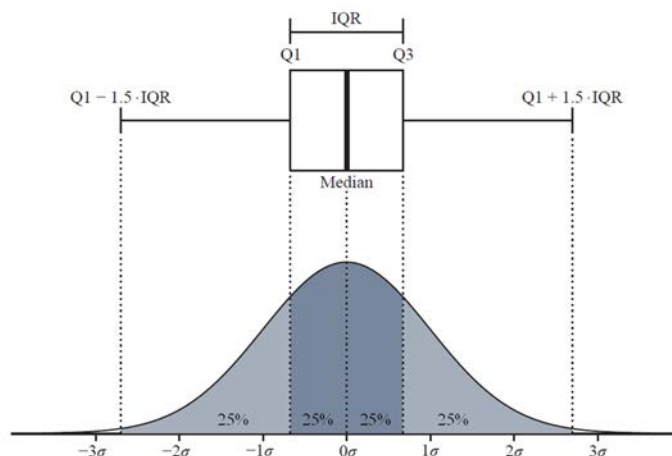


Figure 3-1 Illustration of a Gaussian distribution, the median and the IQR. Modified from (Schilling, 2012).

The IQR, defined as the distance between the two quartiles, can be used similar to the variance to provide an indication of the spread of a distribution. Larger values of the IQR indicate that a random variable has a pdf with larger range (Hayter, 2012).

### 3.1.3 Covariance and correlation

The strength of the dependence of two random variables on each other is indicated by their covariance. Since the covariance is not normalized, it can assume any positive or negative number, and independent random variables have a covariance of 0 (Hayter, 2012).

$$Cov(X, Y) = E\{[X - E\{X}][Y - E\{Y}]\} = E\{XY\} - E\{X\}E\{Y\} \quad (3.8)$$

In practice, the dependence between two random variables is usually assessed through their correlation. The correlation is found by normalizing the covariance between two random variables by their SD. Consequently, the correlation is constrained to values between  $-1$  and  $1$ , and independent random variables have a correlation of  $0$ .

$$Corr(X, Y) = \frac{Cov(X, Y)}{\sqrt{Var(X)Var(Y)}} \quad (3.9)$$

### 3.1.4 Kernel density estimator

Pdf estimates are closely related to the histogram, but can be endowed with properties such as smoothness or continuity. According to Izenman (Izenman, 2008), pdf estimates can be effective in decision making, such as nonparametric discrimination and classification analysis. The kernel density estimator (KDE) is believed to be the most popular nonparametric pdf estimation method. A pdf pattern (known as the kernel function) is summed at over  $N$  points centred at each data point  $x_n$ . Hence, the summation of kernel functions centralized at each data point  $x_n$  provides an estimative of the pdf of a random variable, accordingly:

$$\hat{p}(x) = \frac{1}{Nh} \sum_{n=1}^N K\left(\frac{x - x_n}{h}\right) \quad (3.10)$$

where  $N$  is the total number of data points,  $K$  is the kernel smoothing function and  $h > 0$  is a bandwidth factor. Common kernel functions are Epanechnikov, Gaussian, triangular

or box (Izenman, 2008). The choice of the bandwidth factor  $h$  is crucial in density estimation. In case a Gaussian kernel is chosen, the  $h$  represents the SD of the Gaussian components. Therefore,  $h$  is a smoothing parameter, with trade-off between sensitivity to noise at small  $h$  and over-smoothing at large  $h$  (Bishop, 2006). In the present work, the Epanechnikov kernel smoothing function was chosen (Lake, 2009), with default bandwidth defined by MATLAB. Figure 3-2 illustrates the pdf of a white noise generated on MATLAB and a bipolar AEG collected during AF using the above mentioned method. The area under the curve of all pdfs calculated in this work were equal to 1, as expected.

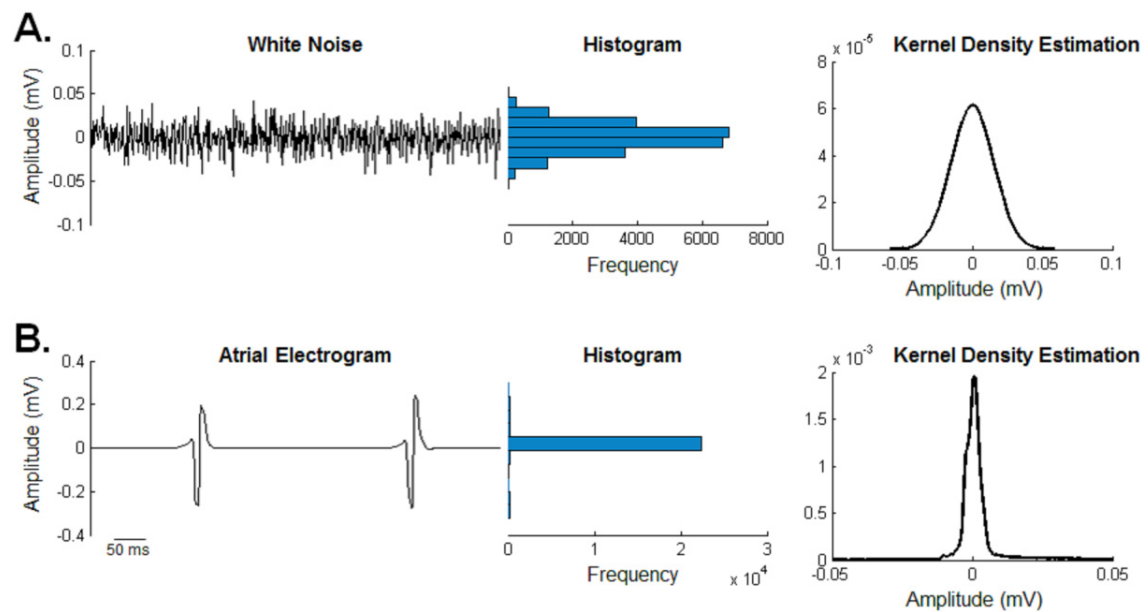


Figure 3-2 Illustration of the estimation of the pdfs from a white noise (A) and an AEG (B) using the KDE the Epanechnikov kernel smoothing function and the default bandwidth defined by MATLAB.

### 3.2 Indices of fractionation

The electric behaviour of the underlying cardiac tissue can be assessed by the AEG. Different features can be extracted from the AEG, and each feature provides different information regarding the underlying cardiac tissue. In many cases, these features are concealed in the intracardiac signal, and some signal processing techniques might be necessary to disclose the feature of interest. The investigation of multiple features extracted from the AEGs provides, therefore, a multidimensional perspective of the cardiac tissue integrity. In this work, twelve features have been extracted from the bipolar AEGs to improve our understanding of the AF and CFAEs. As such, they are referred to as indices of fractionation, and have been divided in: i) indices of fractionation computed

by commercial mapping systems; ii) information theory indices; iii) amplitude based indices and; iv) frequency based indices. These indices are briefly introduced below.

### 3.2.1 Indices of fractionation computed by commercial mapping systems

The indices of fractionation computed by NavX and CARTO that are usually used in EP studies to guide AF ablation are described in detail on *Chapter 4, Minimizing discordances in automated classification of fractionated electrograms in human persistent atrial fibrillation*. An offline MATLAB algorithm used to compute the indices of fractionation defined by CARTO is described in *Appendix A, Validation of an Offline Algorithm to reproduce CARTO CFAE definition for CFAE Identification*.

### 3.2.2 Information theory indices

#### 3.2.2.1 Shannon entropy (ShEn)

The concept of entropy was first introduced by Shannon on his work about information theory as a measure of information, choice and uncertainty (Shannon, 1948). The entropy of a random variable gives us a notion of how much information is contained in the variable. Cover and Thomas have described entropy as a measure of uncertainty of a random variable (Cover and Thomas, 1991). The entropy  $H$  of a set of possible events ( $X = x_1, x_2, \dots, x_n$ ) whose probabilities of occurrence are  $p_1, p_2, \dots, p_n$ , is defined by:

$$H = - \sum_{i=1}^n p_i \log p_i \quad (3.11)$$

The largest value of  $H$  occurs when the pdf has a uniform distribution. It assumes small values for distributions that are concentrated on certain values, or has a pdf with a sharp peak (Hyvarinen and Oja, 2000). ShEn is used as a measure of the degree of organization of a signal. In the present work, the probabilities of occurrences found by the KDE were used to compute the ShEn. Nevertheless, some approximations have been proposed to calculate entropy.

#### 3.2.2.2 Approximate entropy

The Approximate Entropy (ApEn), as suggested by Pincus, is the negative natural logarithm of the conditional probability that a variable ( $X$ ) of length  $N$  repeat itself for  $m+1$  points after being repeated itself for  $m$  points, within a tolerance  $r$  (Pincus, 1991).

The similarity criterion  $r$  is commonly expressed as a fraction of the  $\sigma$  of the data, making the ApEn a scale-invariant measure. Low ApEn values indicate low complexity in the time series.

For  $m$  or  $m + 1$  points, two subsets are considered similar if

$$|X_{i+k} - X_{j+k}| < r, \text{ for } 0 < k < m \text{ (or } m + 1) \quad (3.12)$$

Consider  $P_m$  as the set of all patterns from  $X_N$  with length  $m$  ( $p_m(1), p_m(2), \dots, p_m(N-m+1)$ ). The fraction of patterns ( $C_{i,m}(r)$ ) of length  $m$  that resemble the pattern of the same length that begins at interval  $i$  can be defined by

$$C_{i,m} = \frac{n_{i,m}(r)}{N - m + 1} \quad (3.13)$$

where  $n_{i,m}(r)$  is the number of patterns in  $P_m$  that are similar to  $p_m(i)$ , given the similarity criterion of  $r$ .  $C_m(r)$  is defined as the average of all the  $C_{i,m}(r)$  values, which express the prevalence of repetitive patterns of length  $m$  in  $X_N$ . The same step is repeated for  $m+1$ , with the constraint that  $C_{m+1}(r)$  is a subset of  $C_m(r)$  that also matches for length  $m+1$ . Finally,  $\text{ApEn}(X_N, m, r)$  is given as

$$\text{ApEn}(X_N, m, r) = -\ln \frac{C_m(r)}{C_{m+1}(r)} \quad (3.14)$$

One major limitation of this method is that a correction is needed to avoid  $[\ln(0)]$ , which has been shown as being the same as allowing templates to match themselves, which is a strong source of bias toward  $\text{ApEn} = 0$  when there are few matches and when  $C_m(r)$  and  $C_{m+1}(r)$  are small (Lake *et al.*, 2002).

### 3.2.2.3 Sample entropy

The Sample entropy (SampEn) is the negative natural logarithm of the conditional probability that a variable ( $X$ ) of length  $N$  repeat itself for  $m+1$  points after being repeated itself for  $m$  points, within a tolerance  $r$ , without allowing self-matches (Lake *et al.*, 2002). It has been shown that SampEn displays the property of relative consistency in situations where ApEn does not, being more robust with smaller datasets and when there are only a few matches of patterns (Richman and Moorman, 2000). For all EGM signals, the SampEn measurements were calculated using the  $r = 0.2$  and  $m = 3$  (Alcaraz *et al.*, 2010).

### 3.2.2.4 Kullback-Leibler divergence (or relative entropy)

Kullback-Leibler divergence, also known as relative entropy, is a measure of the distance between two distributions (Cover and Thomas, 1991). For instance, considering that  $q(x)$  is an estimated distribution from an unknown distribution  $p(x)$ , the relative entropy  $D(p||q)$  is a measure of the inefficiency of assuming that the distribution is  $q$  when the true distribution is  $p$ :

$$D(p||q) = - \sum_{i=1}^n p_i \log q_i - \left( - \sum_{i=1}^n p_i \log p_i \right) \quad (3.15)$$

$$D(p||q) = \sum_{i=1}^n p_i \log \frac{p_i}{q_i} \quad (3.16)$$

The relative entropy is always non-negative and is zero if and only if  $p = q$ . In the present work, we will compare standardized AEGs with a standardized Gaussian white noise, following the rationale proposed by Wells classifications for AEGs (Wells *et al.*, 1978).

Similar to the calculation of ShEn, K-L was calculated using the probabilities of occurrences found by the KDE.

### 3.2.3 Amplitude based indices

Low peak-to-peak (PP) amplitude of AEGs has been introduced as a marker for atrial scar during AF and, therefore, targets for ablation (Rolf *et al.*, 2014). However, the PP currently assessed by commercial systems refers to only one atrial activation within a time window, which might not be a good representation of the entire AEG segment. Therefore, the root mean square (RMS) of the AEG amplitude was measured considering the entire AEG segment. The RMS is the squared quadratic sum of the amplitude values in a signal  $x$ , i.e.:

$$x(RMS) = \frac{1}{n} \sum_{i=1}^n \sqrt{x_i^2} \quad (3.17)$$

Similarly, small values of RMS would suggest more fractionation.

### 3.2.4 Frequency based indices

The frequency domain representation of a waveform can provide more useful information than the time domain representation. Determining the frequency content of a waveform is termed spectral analysis, in which a waveform is decomposed into its constituent frequencies (Semmlow, 2009).

#### 3.2.4.1 Fourier transform

The Fourier Transform (FT) is the most popular technique for spectral analysis. It decomposes the waveform into a series of sinusoids that are at the same frequency as, or multiples of, the waveform frequency. This family of sinusoids can be expressed either as sines and cosines, each of appropriate amplitude.

#### 3.2.4.2 Continuous Fourier transform

The continuous notation for the FT considers infinite cycle duration. Considering that

$$e^{-j\frac{2\pi t}{T}} = \cos\left(\frac{2\pi t}{T}\right) - j\sin\left(\frac{2\pi t}{T}\right) \quad (3.18)$$

the Continuous Fourier Transform (CFT) of  $x(t)$  can be expressed as

$$X(f) = \int_{-\infty}^{\infty} x(t)e^{-j\frac{2\pi t}{T}} dt \quad (3.19)$$

which is the convolution between the original waveform and sines and cosines components. The absolute value of the FT  $|X(f)|$  is denoted as frequency spectrum of  $x(t)$ . The spectrum components correspond to the energy of the particular frequency component in the signal.

#### 3.2.4.3 Discrete Fourier transform & Fast Fourier transform

The equations for computing Fourier series analysis of digitized data are the same as for continuous data except the integration is replaced by summation. The waveform  $x(t)$  is discretized with sampling frequency  $f_s$ , with all of the information contained in the frequency range of 0 to  $f_s/2$  ( $f_s/2$  being the Nyquist frequency). The discrete waveform is represented as  $x_k$ , where

$$x(t) = x\left(\frac{k}{f_s}\right) = x_k \quad (3.20)$$

$k$  is assessed in the range of  $0 < k < N-1$ , where  $N$  is the total number of samples. The discrete Fourier transform (DFT) is defined as

$$X(m) = \sum_{k=0}^{N-1} x_k e^{-j\frac{2\pi km}{N}} \quad (3.21)$$

where  $m$  indicates the harmonic number. The Fast Fourier Transform (FFT) is a fast algorithm approach for spectral estimation based on the DFT. The computational cost required for computing the DFT of an  $N$ -samples waveform is proportional to  $N^2$ . For a segment where  $N$  is an integer power of 2, the FFT algorithm reduces the computational cost to  $N \log_2(N)$  number of operations (Cooley *et al.*, 1969).

#### 3.2.4.4 Anti-leaking window

The absence of an anti-leaking window function is, by default, a rectangular window, which might induce undesirable effects in the frequency spectrum domain due to abrupt discontinuities in the beginning or in the end of the segment (Harris, 1978). The edges of the waveform can induce singularity points of abrupt discontinuities that can be minimized by anti-leakage windows. The Hanning (or Hamming) anti-leakage window was used in the present work for presenting small weighting peak amplitude values of side lobes with narrow width of the main lobe peak amplitude.

#### 3.2.4.5 Zero padding

Zero-padding refers to increasing the number of samples with zero elements to improve spectral estimation representation. The zero-padding does not improve the spectral resolution, but it does improve the representation of the spectral estimation as the extra values are interpolations of the original waveform, reducing the  $f_{\text{step}}$  in the frequency domain.

#### 3.2.4.6 The DF and OI

As previously described in *Chapter 2, Medical Background*, DF is defined as the biggest peak in the frequency spectrum of an AEG, and it is believed that atrial regions harbouring

high DF may represent sites with fast periodic activation, driven by either ectopic activity or re-entry circuits (Jalife *et al.*, 2002).

Although the DF calculation from unipolar AEGs is straightforward, some pre-processing is needed for bipolar AEGs, accordingly: i) rectification; ii) low-pass filter at 20 Hz; iii) Anti-leaking Hanning window; iv) zero-padding; v) FFT, where the DF is found (Ng *et al.*, 2006). In the present work, DF was defined as the frequency with highest amplitude within the physiologically relevant range (3.5 to 20 Hz) (Salinet *et al.*, 2013).

The OI measures the variability of the frequency spectrum of an AEG. The OI is derived by dividing the area under the DF and its harmonics by the total power of the frequency spectrum. High OI represents less variability of frequency and, consequently, higher AEG organization (Takahashi *et al.*, 2006):

$$OI = \frac{\text{Area (DF + harmonics)}}{\text{Area below frequency spectrum}} \quad (3.22)$$

Figure 3-3 illustrates the signal processing steps to calculate the DF and OI in a bipolar AEG.

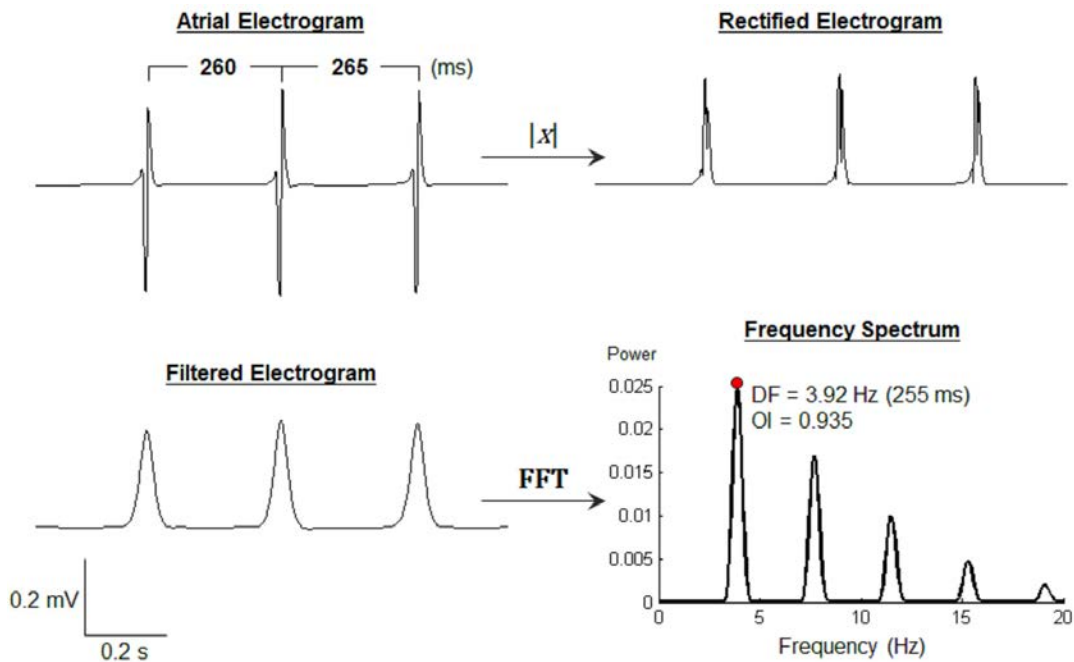


Figure 3-3 Illustration of signal processing steps on a bipolar AEG collected during AF. A: Segment of a bipolar AEG showing 3 discrete activations with a CL of approximately 260 ms. B: Rectified bipolar AEG. C: AEG after low-pass filtering at 20 Hz. D. corresponding power spectrum of the bipolar AEG with DF = 3.92 Hz (corresponding to a CL of 255 ms) and OI = 0.935.

### 3.3 Digital filters

Filtering is a technique used to attenuate or suppress undesired frequencies in a waveform. It can be used to remove noise and improve the signal-to-noise ratio of a signal. Digital filters are filters designed to attenuate frequency components after the waveform has been discretized. They can be easily designed in computing software, such as MATLAB® (The Mathworks Inc., Natick, MA, USA). The general output from a recursive filter, i.e., filter that considers previous values from both output and input states to define the current output, is given as (Semmlow, 2009):

$$y(n) = \sum_{k=0}^K b(k)x(n-k) - \sum_{l=1}^L a(l)y(n-l) \quad (3.23)$$

where  $x(\cdot)$  is the input signal,  $b(k)$  are the feedforward filter coefficients,  $K$  is the feedforward filter order,  $y(\cdot)$  is the output signal,  $a(k)$  are the feedback filter coefficients and  $L$  is the feedback filter order.

There are countless filter configurations and designs depending on its application. This work used an infinite impulse response notch filter centred on 50 Hz to remove power line noise, as provided by MATLAB as the function *iircomb*, which allows for the suppression of the centred frequency and its harmonics, e.g., 50 Hz, 100 Hz, 150 Hz, and so on. An example of one AEG used in this work with and without the notch filter is given on Figure 3-4.

### 3.4 Wavelet transform

While the FFT decomposes the waveform into a series of sinusoids that are at the same frequency as, or multiples of, the waveform frequency, the Wavelet Transform (WT) decomposes the waveform into a series of a predefined probing function (or wavelets) (Daubechies, 1992). A variety of wavelets may be used, but the family of wavelets always consists of enlarged or compressed versions of the basic function, as well as translations, which allows the WT to give information about the frequency content of a signal and at which time segment a frequency occurs. This concept leads to the defining equation for the stationary wavelet transform (SWT):

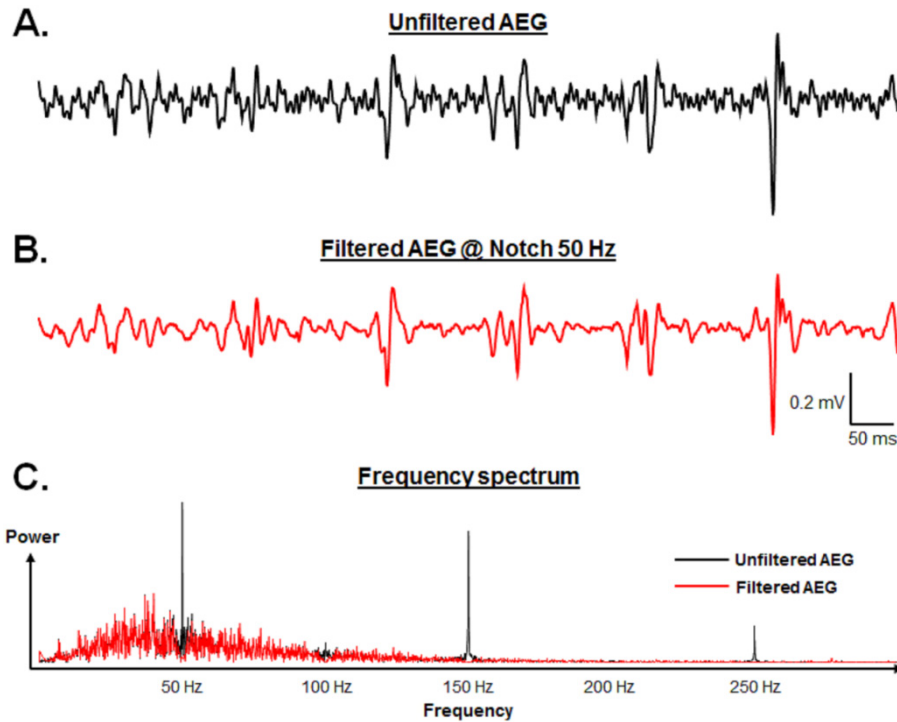


Figure 3-4 Illustration of a bipolar AEG collected at 1200 Hz before (A) and after (B) a 50 Hz notch filter, and their respective frequency spectra (C).

$$W(a, b) = \int_{-\infty}^{\infty} x(t) \frac{1}{\sqrt{|a|}} \varphi\left(\frac{t-b}{a}\right) dt \quad (3.24)$$

where  $b$  time shifts and  $a$  scales the wavelet,  $\varphi$ , across  $x(t)$ .  $\varphi$  might also be referred to as the mother wavelet, which is the wavelet is in its natural form. Figure 3.5 shows two often used wavelets. The Haar wavelet is often used to remove high frequencies noise, and the wavelet Daubechies D11 is used to remove baseline wander from a signal.

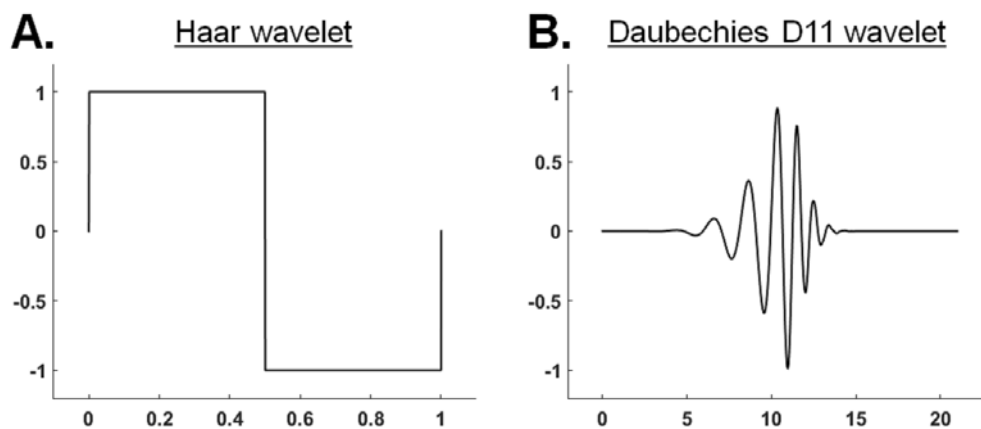


Figure 3-5 Illustration of two mother wavelets used in the present work. A. The Haar wavelet and B. The Daubechies D11.

### 3.4.1 The wavelet filter banks

Signal filtering using WT can be performed by filter banks. In such case, the wave form passes through a pair of low-pass and high-pass filters, resulting in low frequency contents – referred to as approximations – and high frequency contents – referred to as details – of the signal. The approximations are then referred to another pair of low-pass and high-pass filters to be decomposed on the next level. Figure 3-6 illustrates a filter bank using SWT.

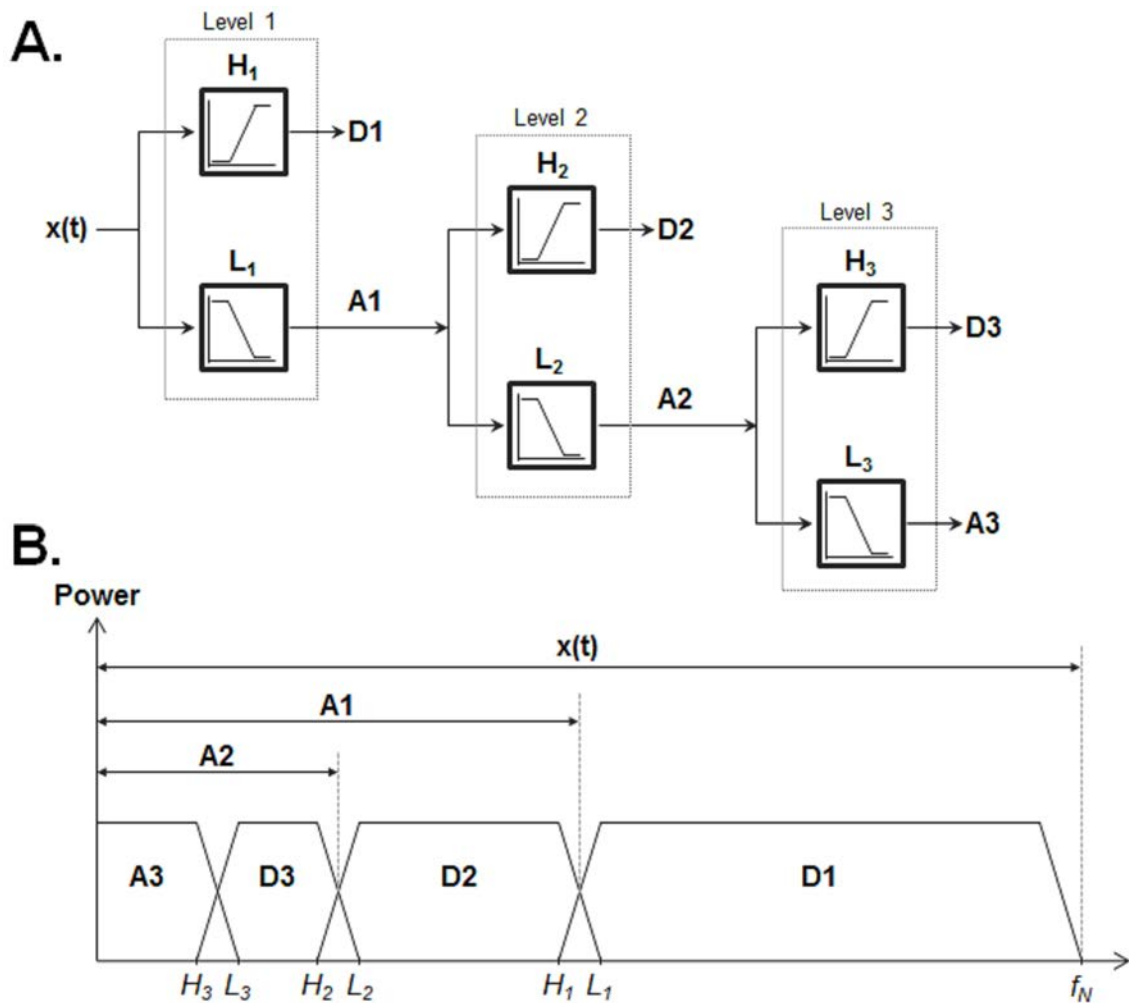


Figure 3-6 Illustration of a filter bank using SWT. A. Three filter bank levels showing high (H) and low (L) pass filters, the details (D) and approximations (A) computed at each level. B. The frequency components present at each level of the filter bank.  $f_N$  = Nyquist frequency.

At each level, the maximum frequency component present in the signal is half of the maximum frequency of the previous level. Therefore, the maximum frequency component of the original signal  $x(t)$  is the Nyquist frequency  $f_N$ . After the filtering

performed on Level 1, the approximation A1 referred to the next level comprises maximum frequency components limited by  $\frac{f_N}{2}$ . Therefore, assuming that  $x(t)$  has been collected with sample frequency  $f_s$  at 1200 Hz (i.e.  $f_N = 600$  Hz), D1 represents the frequency band between 300 – 600 Hz; D2: 150 – 300 Hz; D3: 75 – 150 Hz; and A3: 0 – 75 Hz.

Although the discrete form of the wavelet transform is usually considered for filter banks analyses, recent work has shown that SWT should be preferred for filtering in the presence of white noise due to time-invariance properties of the SWT which helps to preserve the wave shape (Zhou *et al.*, 2006). In the discrete WT (DWT), a fundamental computational step is downsampling, which could result in information loss. The SWT, on the contrary, is implemented without downsampling, keeping all the elements in the coefficients across all the decomposition levels (Zhou *et al.*, 2006).

### 3.4.2 SWT filter

The AEGs investigated in this work have been filtered in EAM systems within the frequency band between 30 – 300 Hz. Baseline oscillations caused by low frequency components and high frequency noise might distort the AEG and induce errors on the descriptors from the AEGs. Therefore, removing those undesired frequencies components is crucial for the correct analysis of the AEGs. For this purpose, an algorithm was developed based on previous method (Schilling, 2012). Considering the AEGs of the present work have been collected with  $f_s$  at 1200 Hz, the AEGs were decomposed with wavelet Daubechies D11 into details 8. The approximation at level 8 corresponds to frequency band between 0 – 2.34 Hz. The approximations of this level were set to zero for baseline oscillation reduction.

For high frequency noise reduction, the AEGs were decomposed with wavelet Haar into details 7. The level 1 corresponds to frequency band between 300 – 600 Hz, which have no EP relevance. Hence, it is possible to assume that in the presence of a white noise – that affects the frequency spectrum homogeneously – would be evident in the frequency band with variance  $\sigma_w^2$ . An adaptive threshold was calculated for each AEG, accordingly:

$$T_r = \sigma_w^2 \sqrt{2 \cdot \ln N} \quad (3.25)$$

where  $N$  is the length of the AEG. The threshold  $T_i$  represents the amplitude level of the white noise distributed in the AEG. This threshold is applied in all the levels of the filter bank. At each level, the amplitudes higher than the threshold are conserved, while amplitudes below the threshold are suppressed. The resulting filtered AEGs were computed with the levels after thresholding with the inverse WT.

Figure 3-7 shows the same bipolar AEG shown in Figure 3-4, collected at 1200 Hz. Figure 3-7 shows the AEG after the 50 Hz notch filter, before and after a baseline wander removal with wavelet Daubechies D11 up to level 8, and high frequency denoising with wavelet Haar up to level 7 (Schilling, 2012).

Zhou and colleagues have shown that SWT is not efficient in removing sinusoidal components, as those found in power line noise (Zhou *et al.*, 2006). Therefore, both Notch filter and SWT should be considered for proper AEG denoising.

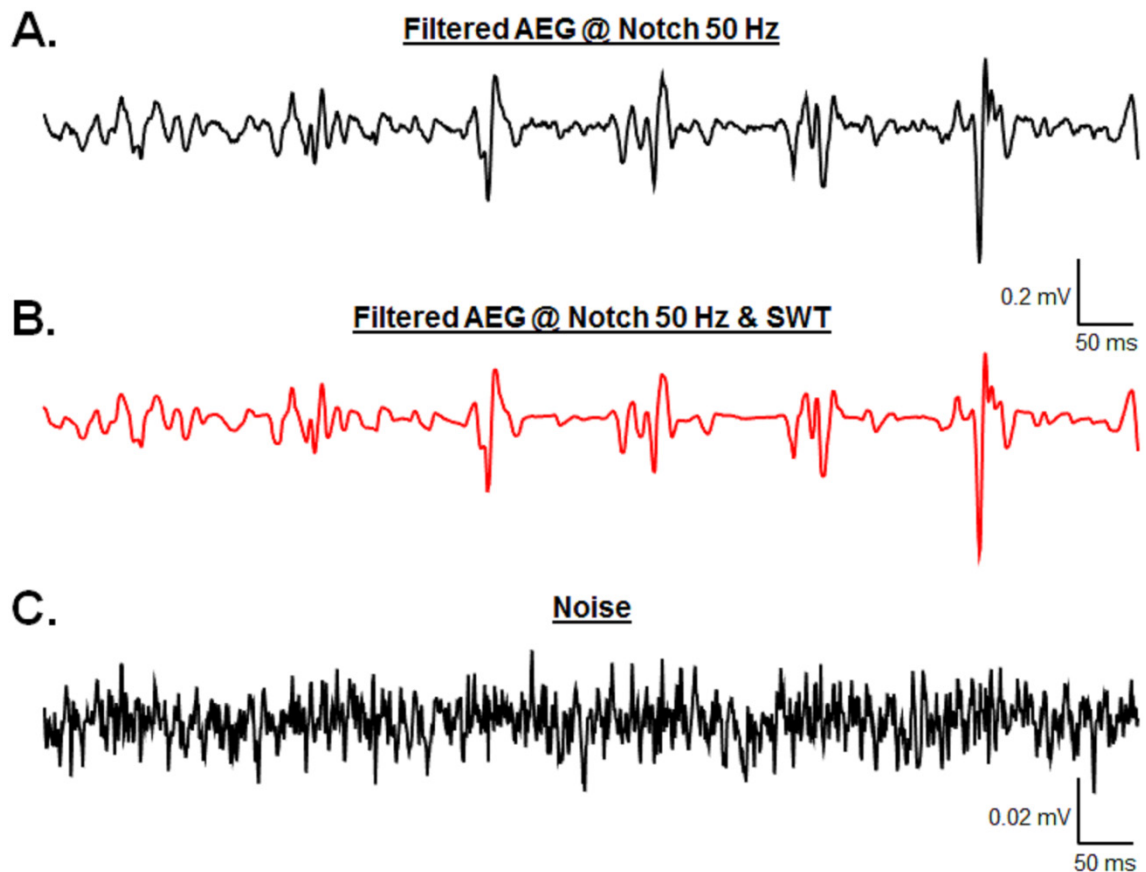


Figure 3-7 Illustration of the same bipolar AEG shown in Figure 3-4 (after the 50 Hz notch filter), before and after SWT filtering. A. AEG before SWT filter. B. Filtered AEG. C. Resulting noise removed from the AEG.

### 3.5 Classification and pattern recognition

#### 3.5.1 Receiver operating characteristic curves

Originally developed for radar-signal detection methodology (signal-to-noise), Receiver Operating Characteristic (ROC) curves are extensively used for visualizing, organizing and selecting classifiers based on their performance (Fawcett, 2006). In the present work, ROC curves have been used as a classifier to assess the ability of a metric to distinguish two classes of either CFAE or non-CFAE. For instance, let us assume that we have two groups of AEGs classified as either CFAEs or non-CFAEs. Then we assess a feature extracted from the AEGs, creating two distributions, as per Figure 3-8. Given the classification and a threshold, the instance of each AEG is assessed, with four possible outcomes: i) if the instance is positive and it is classified as positive, it is counted as a true positive (TP); ii) if the instance is positive and it is classified as negative, it is counted as a false negative (FN); iii) if the instance is negative and it is classified as negative, it is counted as a true negative (TN); iv) if the instance is negative and it is classified as positive, it is counted as a false positive (FP) (Fawcett, 2006).

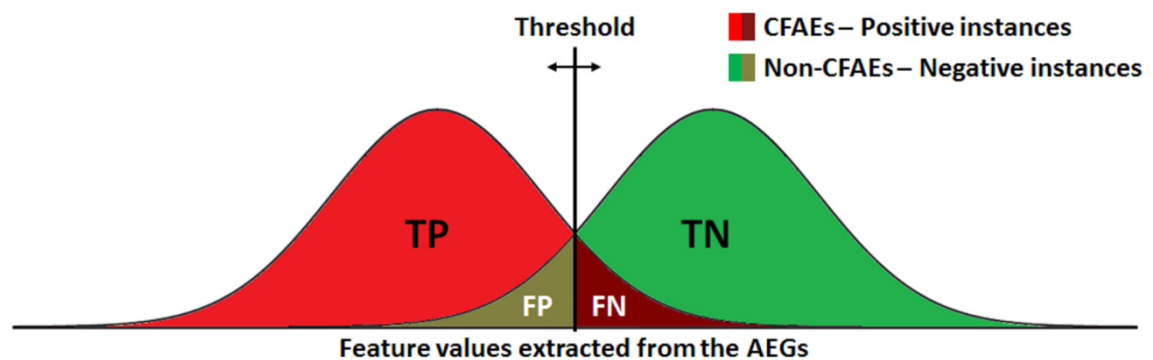


Figure 3-8 Illustration of a ROC curve construction process. A threshold is used to discriminate two distributions. Since there is overlap between them, some will be correctly marked (TP - true positive; TN – true negative) and some will be incorrectly marked (FP - false positive; FN – false negative)

For each threshold, a two-by-two confusion matrix can be constructed representing the dispositions of the set of instances (Figure 3-9A), from which originates the common performance metrics:

$$sensitivity = \frac{TP}{TP + FN} \quad (3.26)$$

$$specificity = \frac{TN}{FP + TN} \quad (3.27)$$

Consequently, each threshold creates a pair (*sensitivity*, *1-specificity*) that are coordinates in the ROC curve. Figure 3-9B shows an example of a ROC curve. The area under the ROC curve (AUROC) is an important measure of the quality of the feature as a classifier. The software IBM SPSS Statistics Version 20 was used in this work to generate the ROC analyses.

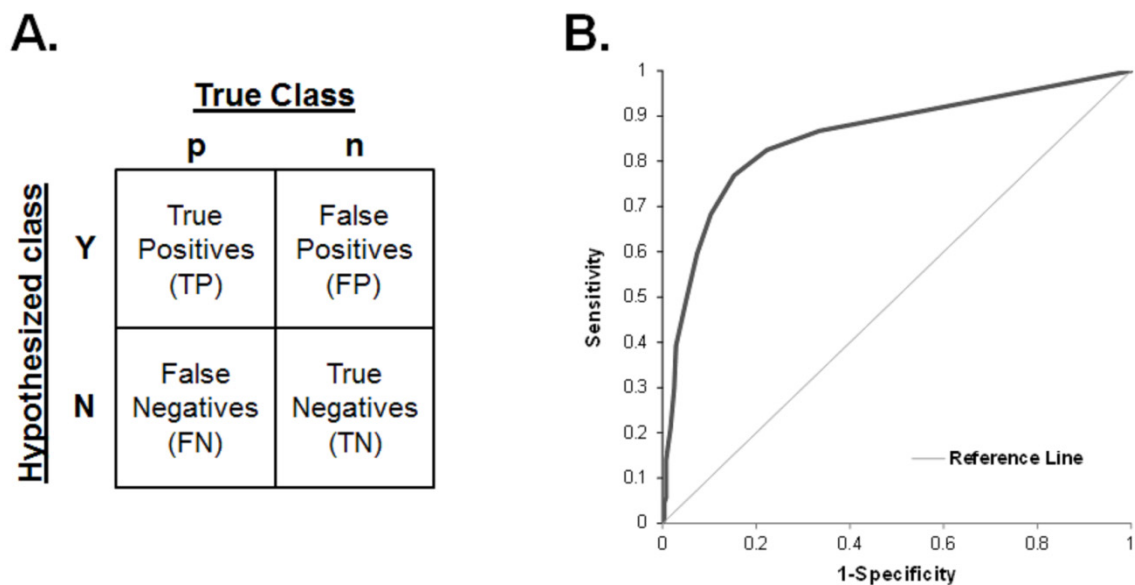


Figure 3-9 Illustration of a A. confusion matrix and B. a ROC curve.

### 3.5.2 Multivariate analyses

#### 3.5.2.1 Multivariate analysis of variance (MANOVA)

The main purpose of analysis of variance (ANOVA) is to test for significant differences between means. While the *t-test* is the preferred method to investigate differences between two groups, ANOVA is the preferred method to investigate differences in the presence of more than two groups. However, both the *t-test* and ANOVA consider different groups from one dependent variable. In cases with several dependent variables, the generalized version of ANOVA, or the multivariate ANOVA (MANOVA), can be used to look at interactions between independent variables. While the ANOVA shows whether groups differ along a single dimension defined by the single dependent variable, the MANOVA has the power to detect whether groups differ along a combination of dimensions defined by the several dependent variables. As a consequence, MANOVA

can be used to test the difference between groups across several dependent variables simultaneously. MANOVA incorporates information about several outcome measures and informs whether different groups can be distinguished by a combination of scores on several dependent measures. The ANOVA calculates how much variance can be explained by an experimental manipulation. The MANOVA also takes into account several dependent variables simultaneously and it does this by using a matrix that contains information about the variance accounted for by each dependent variable. The MANOVA compares the ratio of systematic to unsystematic variance for several dependent variables. This comparison is made by using the ratio of a matrix representing the systematic variance of all dependent variables to a matrix representing the unsystematic variance of all dependent variables. Therefore, the test statistic in both ANOVA and MANOVA represents the ratio of the effect of the systematic variance to the unsystematic variance: in ANOVA these variances are single values, but in MANOVA each is a matrix containing many variances and covariances. A comprehensive mathematical review behind both ANOVA and MANOVA can be found in the work by Bray and Maxwell (Bray and Maxwell, 1985).

MANOVA assumes multivariate normality and homogeneity of covariance matrices. A robust MANOVA has to be performed if those assumptions are broken, as described by Field and colleagues (Field *et al.*, 2012). In the present work, a robust MANOVA using Munzel and Brunner's method has been used to test the difference between groups across the different indices of fractionation (Munzel and Brunner, 2000). Further details can be found on *Chapter 5, the effect of pulmonary vein isolation on electrogram fractionation prevalence in human persistent atrial fibrillation*.

### 3.5.2.2 Linear discriminant analysis (LDA)

Usually, MANOVA is followed by the Linear Discriminant Analysis (LDA) to see how the dependent variables discriminate the groups (Field *et al.*, 2012). LDA can be used to determine whether groups differ with regard to the mean of a variable, and then use that variable to predict group membership.

The LDA identifies variates, defined as linear combinations of the dependent variables. These variates represent the combination of underlying dimensions of the dependent variables, and are used to explain the group differences found by the MANOVA. Once

the significant variates have been identified, it is possible to identify how the dependent variables contribute to the variates by looking LDA coefficients. High scores indicate that a dependent variable is important for a variate, and variables with positive and negative coefficients are contributing to the variate in opposite ways. Finally, the groups discriminated by a variate can be investigated. In the present work, the LDA has been used to investigate how the different indices of fractionation discriminated the different groups. Further details can also be found on *Chapter 5, the effect of pulmonary vein isolation on electrogram fractionation prevalence in human persistent atrial fibrillation*.

### 3.6 Offline reconstruction of 3D atrial maps

The 3D EAM systems create anatomical maps of the LA during EP studies to facilitate the investigation of the rhythm disturbances and to reduce the amount of fluoroscopy. These systems display the LA as a mesh of triangles. This triangulated mesh can be exported for offline studies. In the present work, the 3D mesh representation of the LA for each patient was exported directly from NavX.

XML files containing all the *vertices* and *triangles* (or *polygons*) that constitute the 3D LA mesh have been exported from NavX and assessed by a MATLAB script (Figure 3-10).

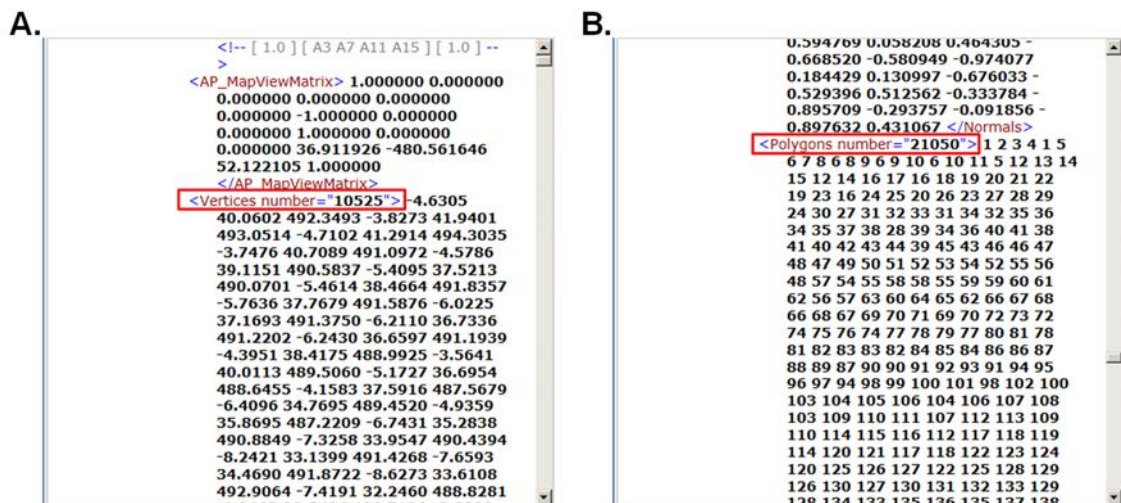


Figure 3-10 Illustration of the content of the XML files exported from NavX containing all the vertices and triangles (or polygons) that constitute the 3D LA mesh that were assessed by a MATLAB script. The vertices (A) account for the XYZ location of all points distributed in the 3D geometry, while the triangles (B) define how those points are connected one to another to create a closed 3D geometry.

The *vertices* account for the XYZ location of all points distributed in the 3D geometry, while the *triangles* define how those points are connected one to another to create a closed 3D geometry. This allowed an offline representation of the LA structure as illustrated in Figure 3-11A and 3-11B.

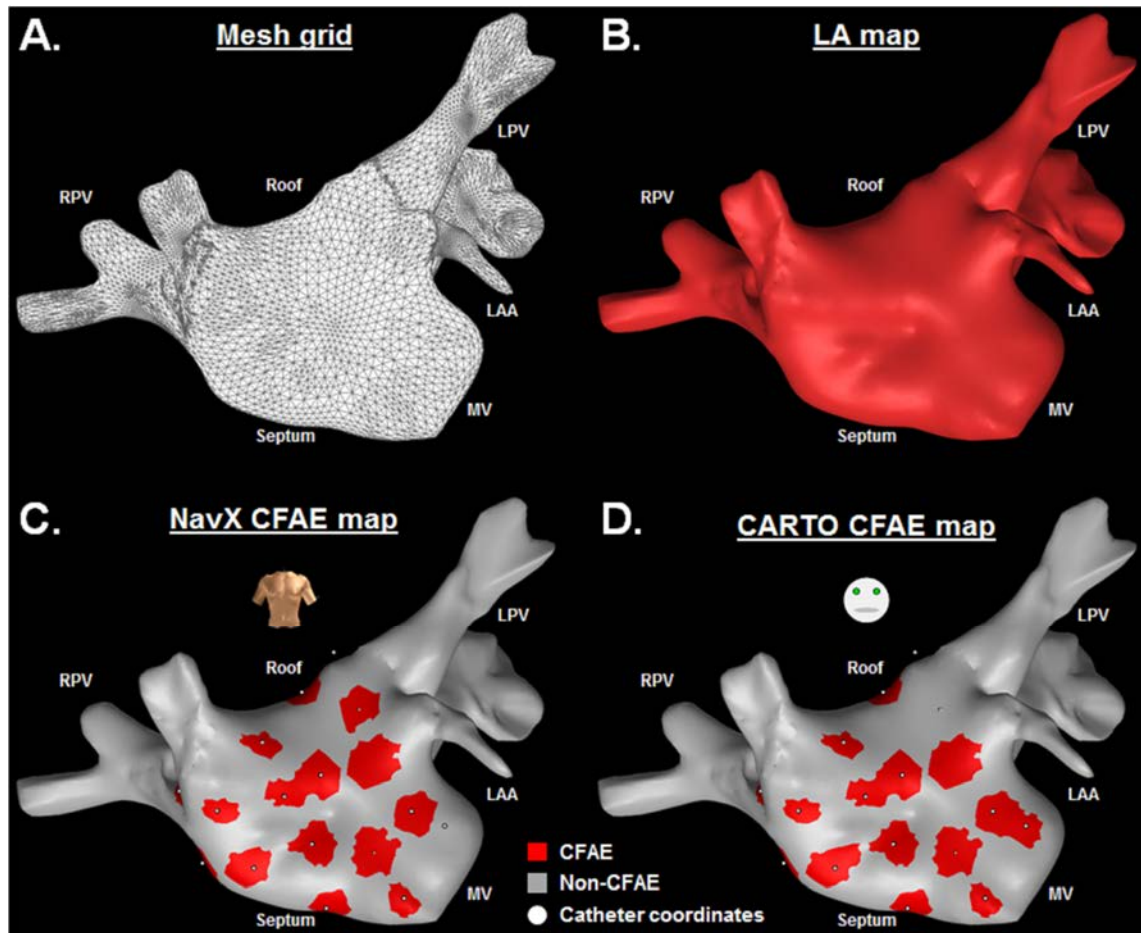


Figure 3-11 Illustration of the offline 3D atrial geometry. A. The triangulated mesh grid reconstructed in MATLAB based on exported vertices and triangles exported from NavX. B. The final 3D LA geometry. C. NavX CFAE map calculated using its threshold for fractionation. D. CARTO CFAE map calculated using its threshold for fractionation.

Once the 3D LA geometry was reconstructed in MATLAB, the adjusted XYZ coordinates of the catheter electrodes – as exported from NavX – for each measurement point could be referred in the geometry. Hence, the information of each index of fractionation could be projected onto the vertex pointed by the catheter coordinates. In particular, the indices calculated by the commercial systems along with their limits that define fractionation were used to highlight the atrial regions that are fractionated. The indices of fractionation computed by NavX and CARTO that are normally used in EP studies to guide AF ablation

are described in detail on *Chapter 4, Minimizing discordances in automated classification of fractionated electrograms in human persistent atrial fibrillation*.

The vertex pointed by the catheter coordinates was painted in red in case the index calculated by the systems resulted in CFAE. Figure 3-11C shows the resulting CFAE map calculated by NavX, and the Figure 3-11D illustrates the CFAE map calculated by CARTO, along with the original measuring vertex from the catheter coordinates. In order to improve the spatial perception of the index distribution on the LA, two neighbouring vertices were considered as part of the original measuring vertex. This approach would also take into consideration the catheter displacement that usually occurs during AEG collection (Chu *et al.*, 2014).

## Chapter 4

# Minimizing discordances in automated classification of fractionated electrograms in human persistent atrial fibrillation

### 4.1 Introduction

Catheter ablation has been consolidated as the most accepted percutaneous procedure for AF treatment, achieving success rate as high as 90% in patients with pAF (Calkins *et al.*, 2012b, Haissaguerre *et al.*, 1998). Ablation is still suboptimal in patients with persAF due to an incomplete understanding of the mechanistic interaction between relevant atrial substrate and the initiation and maintenance of AF.

Sustained AF causes changes in the cardiac tissue characteristics, inducing structural and electric remodelling (de Bakker and Wittkamp, 2010). These regions can potentially host tissue with slow or inhomogeneous conduction, inducing re-entry circuits, resulting in fractionated fibrillatory conduction (Ashihara *et al.*, 2012), and are important in triggering and perpetuating atrial arrhythmias. AEGs acquired from such atrial substrate regions demonstrate the low amplitude, multiple deflections activations that characterize fractionated activity (Figure 4-1). The ablation of atrial substrate hosting CFAEs has been accepted by many as a useful additional therapy for persAF treatment (Calkins *et al.*, 2012b). Disparities in CFAE-guided ablation outcomes have, however, cast doubt on the efficacy of this approach (Table 4-1) (Elayi *et al.*, 2008, Lin *et al.*, 2009a, Nademanee *et al.*, 2004, Oral *et al.*, 2007, Oral *et al.*, 2009, Porter *et al.*, 2008, Verma *et al.*, 2010, Verma *et al.*, 2011).

Automated CFAE detection can be performed during electrophysiologic studies by algorithms embedded in commercial 3D EAM systems (Monir and Pollak, 2008, Verma *et al.*, 2010). The two EAM systems being used in clinical practice for CFAE mapping

are the NavX and the CARTO (Figure 4-1) (Aizer *et al.*, 2008, Scherr *et al.*, 2007). The algorithms embedded in those systems incorporate CFAE characteristics as initially described by Nademanee *et al.* (Nademanee *et al.*, 2004). Each algorithm, however, considers different premises to quantify fractionation and the classification by the different systems do not always agree (Lau *et al.*, 2015). Details about the algorithms and the indices of fractionation computed by NavX and CARTO are provided on *Section 4.2.1 Automated CFAE detection*. We hypothesized that the discordances between systems might result in different ablation target identification and generate discordant clinical results. In this chapter we report a direct comparison of the automated CFAE classification performed by the algorithms embedded in NavX and CARTO. We also propose new thresholds for both primary and complementary indices to minimize the differences in CFAE classification performed by either system.

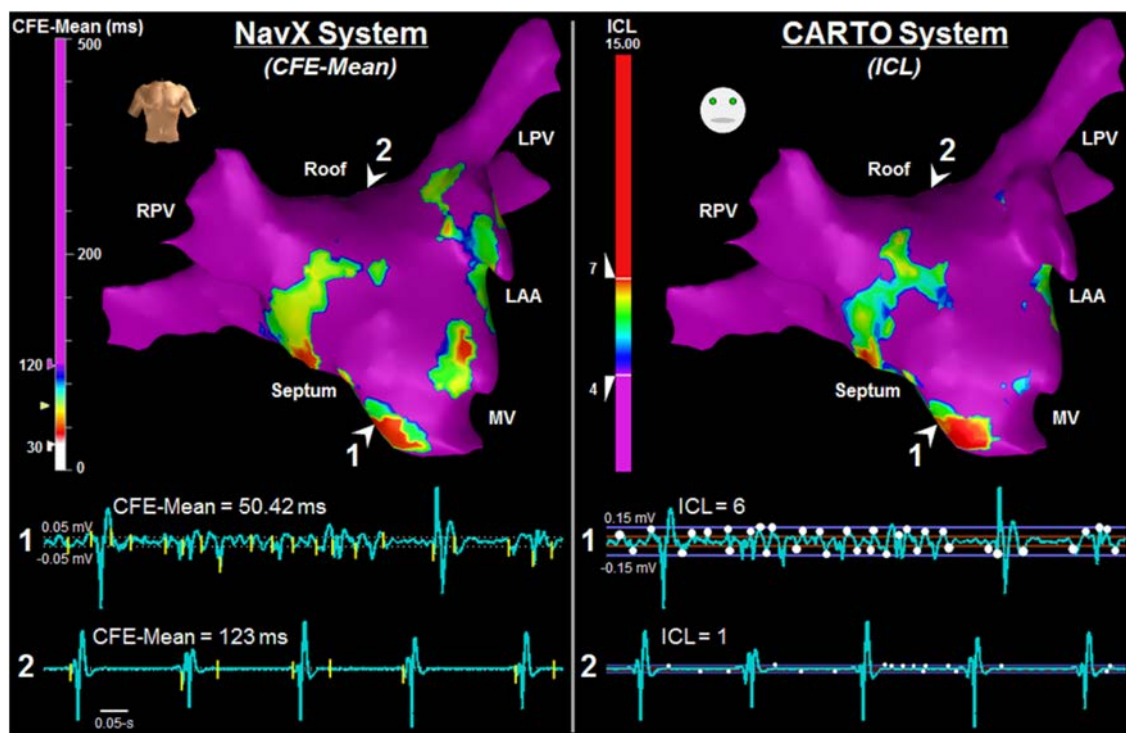


Figure 4-1 NavX (left) and CARTO (right) 3D atrial geometry representation for the same patient, with their respective automated CFAE detection algorithms. On the bottom part of the figure, the top traces refer to a segment of fractionated bipolar AEG (AEG 1), and bottom traces refer to a non-fractionated segment of bipolar AEG (AEG 2), both recorded from the LA endocardium. The AEG 1 has CFE-Mean = 50.42 ms and ICL = 6. The AEG 2 has CFE-Mean = 123 ms and ICL = 1. Explanation regarding the algorithms is provided in the text. AEG = atrial electrogram; CFE-Mean = index used by NavX to quantify AEG fractionation; FI = fractionated interval; ICL = Interval Confidence Level: index used by CARTO to quantify AEG; LPV = left pulmonary veins; MV = mitral valve; RPV = right pulmonary veins. These abbreviations were used in the subsequent figures.

Table 4-1 Review of CFAE mapping systems, EGM settings and success rate in different clinical studies. Previous studies conducted either additional or lone CFAE-guided ablation using different mapping systems and varying operator-defined settings, resulting in conflicting outcomes.

Study	EGM settings		Mapping system	# patients	Success rate (%)
	Amplitude (mV)	Time (ms)			
(Elayi <i>et al.</i> , 2008)	-	$\leq 120$	NavX	49	61
(Lin <i>et al.</i> , 2009a)	-	$\leq 50$	NavX	30	53
(Nademanee <i>et al.</i> , 2004)	$\leq 0.15$	$\leq 120$	CARTO	121	95
(Oral <i>et al.</i> , 2007)	-	$\leq 120$	CARTO	100	16
(Oral <i>et al.</i> , 2009)	-	$\leq 120$	CARTO	50	18
(Porter <i>et al.</i> , 2008)	0.05 – 0.15	60 – 120	CARTO	67	20
(Verma <i>et al.</i> , 2011)	-	40 – 120	NavX	30	14
(Verma <i>et al.</i> , 2010)	0.05 $\leq$	30 – 120	NavX	35	54

## 4.2 Methods

### 4.2.1 Automated CFAE detection

NavX and CARTO provide primary indices to assess CFAE objectively, and complementary indices to further inform the electrophysiological study. Previous works have attempted to optimize CFAE detection using only the primary indices provided by the EAM systems (Aizer *et al.*, 2008). There are currently no defined thresholds for the complementary indices to characterize CFAEs. Additionally, both systems allow for operator-defined settings – in this work referred to as ‘EGM settings’ – to tune CFAE detection. Previous studies had attempted to optimize CFAE detection using these algorithms by varying EGM settings with different ablation outcomes (Table 1) (Elayi *et al.*, 2008, Lin *et al.*, 2009a, Nademanee *et al.*, 2004, Oral *et al.*, 2007, Oral *et al.*, 2009, Porter *et al.*, 2008, Verma *et al.*, 2010, Verma *et al.*, 2011).

#### 4.2.1.1 The NavX algorithm (*EnSite System version 8.0 software, 2008*)

NavX provides 3D EAM (Figure 4-1 left) and online automated CFAE detection based on CFE-Mean. CFE-Mean is defined as the average FI between consecutive negative deflections ( $-dV/dt$ ) inside a time window set by the user (from 1 to 8 s) of sequentially recorded bipolar AEGs (Figure 4-1 bottom left) (Aizer *et al.*, 2008). The negative deflections must meet three criteria in order to be marked: (1) exceed a peak-to-peak threshold greater than baseline noise; (2) have time duration within a threshold to avoid detection of ventricular far-field events; and (3) exceed a refractory period after the previous marked deflection to minimize multiple detections on a single deflection. NavX's default EGM settings include a peak-to-peak sensitivity of 0.05 mV, deflection duration of less than 10 ms and refractory period of 30 ms. AEGs with CFE-Mean within the range of 30 – 120 ms are considered to be fractionated. These settings can be changed by the user (Table 4-1) (Aizer *et al.*, 2008). NavX also computes the standard deviation of FI distribution inside a pre-defined time window as a complementary index, known as CFE-StdDev.

#### 4.2.1.2 The CARTO algorithm (*CARTO 3 system, 2008-2014, version 4.3*)

CARTO provides 3D EAM (Figure 4-1 right) and online automated CFAE detection based on complex intervals occurring inside a 2.5 s window of sequentially recorded bipolar AEGs (Scherr *et al.*, 2007). The algorithm identifies voltage peaks and troughs of bipolar AEGs that exceed a lower voltage threshold – to exclude noise – but do not exceed an upper voltage threshold. Similar to the NavX algorithm, the user can alter these CARTO thresholds (Table 4-1). The time intervals between successive peaks and troughs occurring within the voltage window are automatically marked by the system. The complex intervals marked within a time interval duration – defined by the operator – are identified during a 2.5 s time window (Figure 4-1 bottom right). The number of identified complex intervals is referred to as the Interval Confidence Level (ICL), and characterizes the repetitiveness of the CFAE complexes. CARTO's default EGM settings consider a voltage window of 0.05 – 0.15 mV and a programmable time interval of 50 – 110 ms. Typically,  $ICL < 4$  represents low fractionation,  $4 \leq ICL < 7$  refers to moderate fractionation and  $ICL \geq 7$  indicates high fractionation (Scherr *et al.*, 2007). CARTO software also finds, as complementary indices, the average of the identified interval,

referred to as the average complex interval (ACI), and the shortest identified interval, referred to as the shortest complex interval (SCI).

#### 4.2.2 Study population

The study population consisted of 18 persAF patients (16 male; mean age  $56.1 \pm 9.3$  years; history of AF  $67.2 \pm 45.6$  months) referred to our institution for first time catheter ablation. Details of the clinical characteristics of the study subjects have been provided elsewhere (Tuan *et al.*, 2011). Study approval was obtained from the local ethics committee and all procedures were performed with full informed consent. Table 4-2 summarizes the clinical characteristics of the study subjects.

Table 4-2 Clinical characteristics of study population (N = 18).

Age, yrs	$56.1 \pm 9.3$
Male/Female	16/2
History of AF, months	$67.2 \pm 45.6$
Ejection Fraction,%	$48 \pm 1$
Left Atrial Diameter, mm	$47 \pm 1$
History of coronary artery disease	4
Medication* (number of patients on)	
ACE inhibitor / ARB	11
Amiodarone	10
Beta-blockers	8
Calcium channel blockers	2
Digoxin	1
Sotalol	5

\* All anti-arrhythmic and rate-controlling drugs were stopped for at least five half-lives before the procedure, with the exception of amiodarone. ACE = angiotensin-converting-enzyme; AF = atrial fibrillation; ARB = angiotensin receptor blockers. Values are in mean  $\pm$  SD or n.

All patients were in AF at the start of the procedure. Patients were treated in the Glenfield Hospital by doctors from the Cardiovascular Department led by Prof. G. André Ng.

### 4.2.3 Electrophysiological study

Details of the electrophysiologic study and mapping procedure have been described elsewhere (Tuan *et al.*, 2011). Briefly, 3D LA geometry was created within [Ensite] NavX using a deflectable, variable loop circular PV mapping catheter (Inquiry Optima, St. Jude Medical). PVI was performed, followed by the creation of a single roof line (Cool Path Duo irrigated RF catheter, St. Jude Medical). No additional ablation targeting CFAE was performed in this study. Sequential point-by-point bipolar AEGs were collected from 15 pre-determined atrial regions before and after LA ablation with the ablation catheter (Tuan *et al.*, 2011). A total of 797 AEGs were recorded from the LA, with a sampling frequency of 1.2 kHz, and band-pass filtered within 30–300 Hz. When an improvement of signal-to-noise ratio was necessary, a 50 Hz Notch filter was applied.

### 4.2.4 Comparing CFAE definitions between EAM systems

#### 4.2.4.1 Signal analysis

Each AEG, its corresponding CFE-Mean and CFE-StdDev, were exported from NavX with three time window lengths (2.5 s, 5 s and 8 s). A validated offline MATLAB algorithm was used to compute the ICL, ACI and SCI of each exported AEG for CFAE identification as defined by CARTO – see *Appendix A, Validation of an Offline Algorithm to reproduce CARTO CFAE definition for CFAE identification* (Almeida *et al.*, 2016).

Currently, the CARTO system considers only 2.5 s AEGs for CFAE detection. Hence, there is no validated ICL threshold for CFAE classification using time windows longer than 2.5 s. Nevertheless, the effects of different time windows – 2.5 s, 5 s, 8 s – were assessed on ICL and CFE-Mean for the completeness of the investigation – see *Appendix B, Influence of AEG duration on ICL and CFE-Mean*. Little influence on overall CFE-Mean was found when using different time windows. Therefore, for the remaining parts of the study, NavX and CARTO indices were measured using fixed 2.5 s AEG duration to allow a like-for-like comparison (Monir and Pollak, 2008, Verma *et al.*, 2010).

#### 4.2.4.2 Influence of EGM settings on CFAE classification

CFE-Mean and ICL were individually assessed, exploring the effects of varying EGM settings: NavX EGM settings (30-120 ms) and CARTO EGM settings (50-110 ms). Hence, the threshold for CFAE classification was 30-120 ms if CFE-Mean was measured

using NavX EGM settings, and 50-110 ms for CARTO EGM settings (Monir and Pollak, 2008, Verma *et al.*, 2010).  $ICL \geq 7$  was used as the default threshold for CARTO CFAE categorization to assess the impact of both NavX and CARTO EGM settings (Porter *et al.*, 2008).

#### *4.2.4.3 CFAE detection thresholds for CFE-Mean and ICL*

CFAE detection and classification were performed on 697 randomly sampled AEGs (out of the total 797), first using CFE-Mean and then ICL. This dataset was used to create ROC curves and hence obtain the optimum sensitivity and specificity thresholds for both indices, using the counterpart index as the comparator (Figure 4-2A) (Fawcett, 2006). The ICL based classification was assessed by creating a ROC curve, using CFE-Mean and the NavX EGM settings ( $CFE-Mean \leq 120$  ms) as the reference classification (CFAE / non-CFAE) (Verma *et al.*, 2010). The revised threshold for ICL was identified based on the optimum sensitivity and specificity on the ROC curve – defined as the point on the curve with the shortest distance to the top left corner of the graph. Similarly, the CFE-Mean based classification was assessed by creating a ROC curve, using ICL and the CARTO EGM settings ( $ICL \geq 7$ ) as the reference classification (CFAE / non-CFAE) (Porter *et al.*, 2008). The revised threshold for CFE-Mean was identified based on the optimum sensitivity and specificity on the ROC curve. The AUROC and the P-value were also calculated.

This process was iterated thirty times, each time with a different dataset of randomly sampled AEGs for ROC curve construction (697 AEGs), giving a total of thirty ROC curves for ICL and thirty for CFE-Mean in order to minimize data sampling and selection biasing.

#### *4.2.4.4 CFAE detection thresholds for CFE-StdDev, ACI and SCI*

The revised thresholds for both CFE-Mean and ICL found in the ROC curves were used to perform a new CFAE classification on the thirty sets of 697 randomly sampled AEGs. In this new classification, an AEG was classified as CFAE only if both CFE-Mean and ICL agreed with the classification using their revised thresholds. These classifications were used to create ROC curves and hence obtain the optimum sensitivity and specificity thresholds for the complementary indices – CFE-StdDev, ACI and SCI.

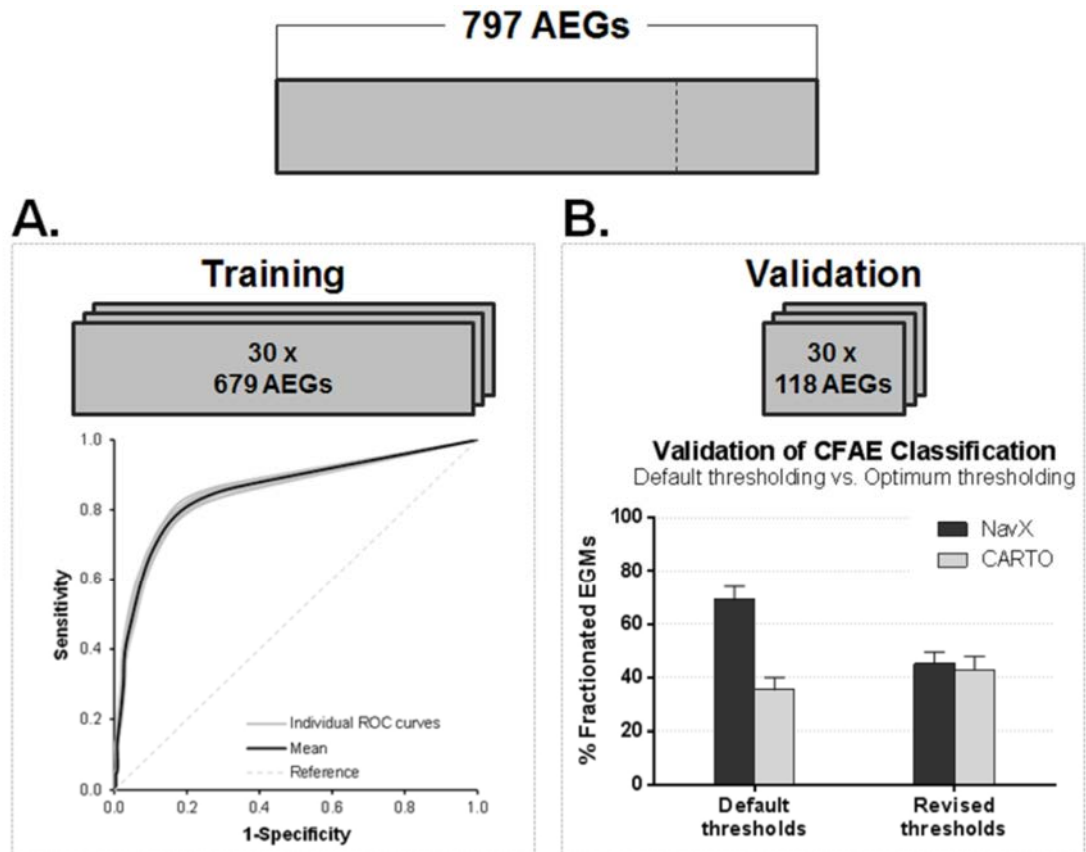


Figure 4-2 Illustration of the method for training the ROC curves and validating the proposed revised thresholds. A. Thirty datasets – with 679 randomly selected AEGs each – were used to train and create the ROC curves. B. For each of the thirty datasets, the remaining 118 AEGs were used to validate the thresholds found in the ROC curves.

#### 4.2.4.5 Validation of the revised thresholds for CFAE detection performed by NavX and CARTO

The revised thresholds found in the ROC curves for both NavX – CFE-Mean and CFE-StdDev – and CARTO – ICL, ACI and SCI – were validated using the remaining 118 AEGs (thirty sets of 118 AEGs randomly selected) (Figure 4-2B).

For each of the thirty datasets, CFAE classification was performed using the combined assessment of both primary and complementary indices. Explicitly, an AEG was classified as CFAE if it complied with both CFE-Mean and CFE-StdDev for NavX classification. Similarly, an AEG was classified as CFAE if it complied with ICL, ACI and SCI for CARTO classification.

### 4.2.5 Statistical analysis

All continuous normally distributed variables are expressed as mean  $\pm$  SD. Continuous non-normally distributed variables are expressed as median  $\pm$  IQR. Nonparametric paired multiple data were analysed using the Friedman test with Dunn's correction, while nonparametric unpaired data were analysed using the Mann–Whitney test. Categorical data were expressed as percentages and analysed using the two-sided Yates-corrected Chi-square test. The quantification of the agreement between the rankings made by CFE-Mean and ICL – as measured using their default settings – was assessed by the Spearman's correlation between both indices. The level of agreement in the CFAE classification performed by the two systems was assessed by the Cohen's kappa ( $\kappa$ ) score (Cohen, 1968). Kappa score within range  $0 \leq \kappa < 0.4$  suggests marginal agreement between two indices;  $0.4 \leq \kappa \leq 0.75$  good agreement and;  $\kappa > 0.75$  excellent agreement (Landis and Koch, 1977). P-values less than 0.05 were considered statistically significant.

## 4.3 Results

### 4.3.1 Influence of EGM settings on CFAE classification

CFAE classification differed as performed by CFE-Mean and ICL using their respective default EGM settings. CFE-Mean classified 70% of the AEGs as CFAEs using NavX EGM settings, while ICL classified 36% using CARTO EGM settings ( $P < 0.0001$ ).

Changing the EGM settings alters CFAE classification. Figure 4-3 demonstrates the importance of EGM settings for CFAE classification. It illustrates the 3D CFAE map (anterior and posterior views) of one of the patients according to CFE-Mean and ICL, using different EGM settings. CFE-Mean measured using NavX's settings identified more atrial regions as CFAEs, while ICL measured using CARTO's settings showed fewer regions as fractionated. When analysing the entire database, the NavX EGM settings consistently categorized more AEGs as fractionated than the CARTO EGM settings (70% vs. 54%,  $P < 0.0001$  for CFE-Mean; 62% vs. 36%,  $P < 0.0001$  for ICL).

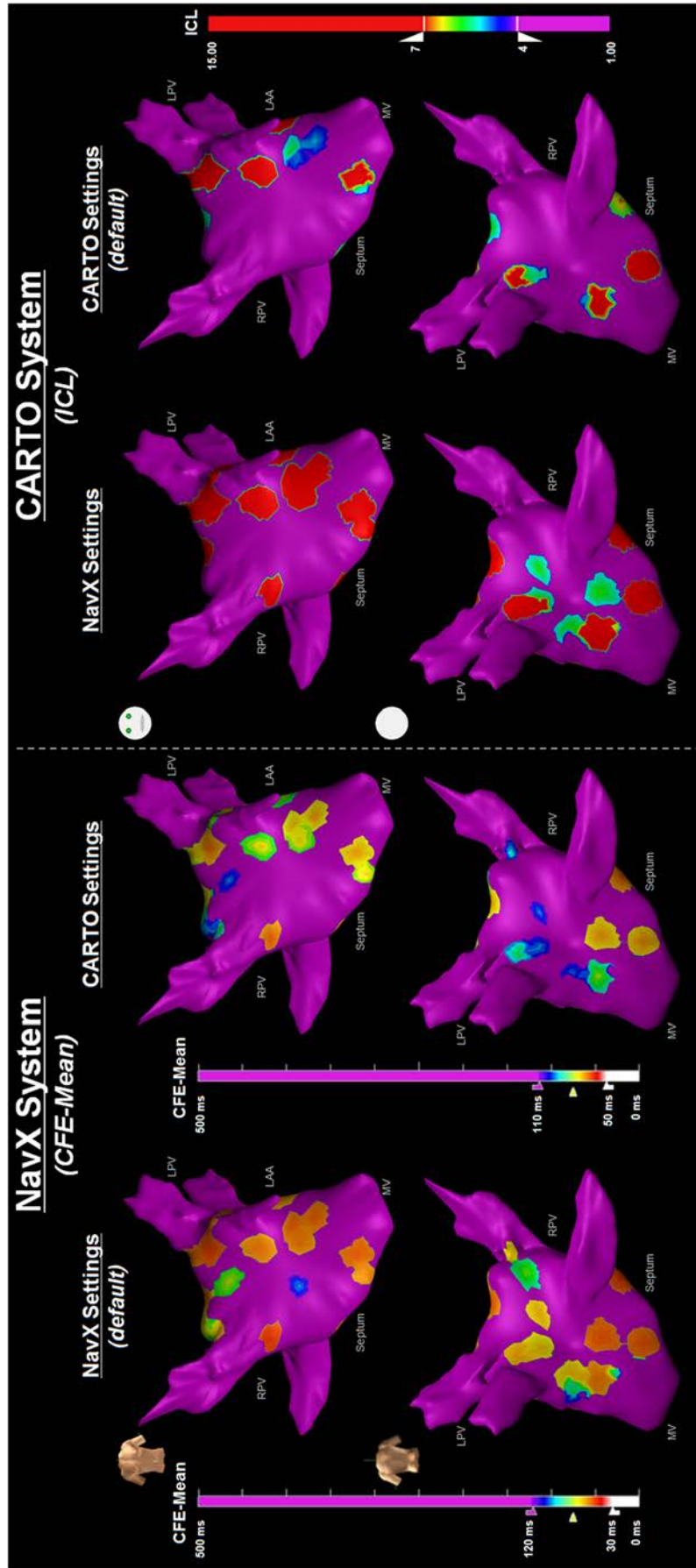


Figure 4-3 3D CFAE map showing the anterior (upper) and posterior (bottom) view of the LA from one patient according to CFE-Mean (left hand side) and ICL (right hand side), using different EGM settings. NavX EGM settings identify more regions of the LA as CFAE than CARTO's when applied to either CFE-Mean or ICL.

### 4.3.2 CFAE detection thresholds for CFE-Mean and ICL

The comparison between CFE-Mean and ICL (measured using their default settings) for each of the 797 AEGs is illustrated in Figure 4-4. The respective default thresholds for both CFAE detection techniques are highlighted. The four quadrants delimited by the thresholds illustrate the zones of agreement and disagreement between CFE-Mean and ICL. Spearman's correlation between the classifications by the two indices was  $\rho=-0.563$  ( $P<0.0001$ ). 230 (out of 797) AEGs with organized activations were found in the non-fractionated agreement zone (green). When looking at the AEGs corresponding to the disagreement quadrants (grey), 282 AEGs have been classified as CFAEs by NavX but not by CARTO in one grey region (bottom left). In the other grey region (top right), 12 AEGs have been classified as CFAEs by CARTO, but not by NavX. Finally, 273 highly fractionated AEGs were found in the CFAE agreement zone (red).

Quantitative results are provided in Figures 4-5A to 4-5E to characterize the AEGs after the objective comparison between CFE-Mean and ICL. The results show the distributions for primary and complementary indices (CFE-Mean, ICL, CFE-StdDev, ACI and SCI, respectively) for the AEGs classified as non-CFAEs or CFAEs by both systems, as well as AEGs that had different classifications for each system. For all indices, the distributions for the AEGs classified as CFAE (red) were significantly different ( $P>0.0001$ ) than the combined distributions of non-CFAEs together with those AEGs with different classifications for each system (green + grey).

Figure 4-6A and 4-6B show the ROC curves according to the CFAE classification performed by CFE-Mean and ICL. Table 4-3 provides the sensitivity, specificity and AUROC values for each case. The details of the ROC curves from the thirty datasets are provided in the *Appendix C, CFAE detection thresholds for CFE-Mean and ICL*.

The ICL based classification suggests that the default threshold for CARTO ( $ICL \geq 7$ ) provides high specificity but poor sensitivity for CFAE detection (Figure 4-6A, Table 4-3A). The revised threshold found from the ROC curves ( $ICL \geq 3.8 \pm 0.4$ ) provides optimum sensitivity and specificity for CFAE detection and classification using CFE-Mean  $\leq 120$  ms as the reference classification.

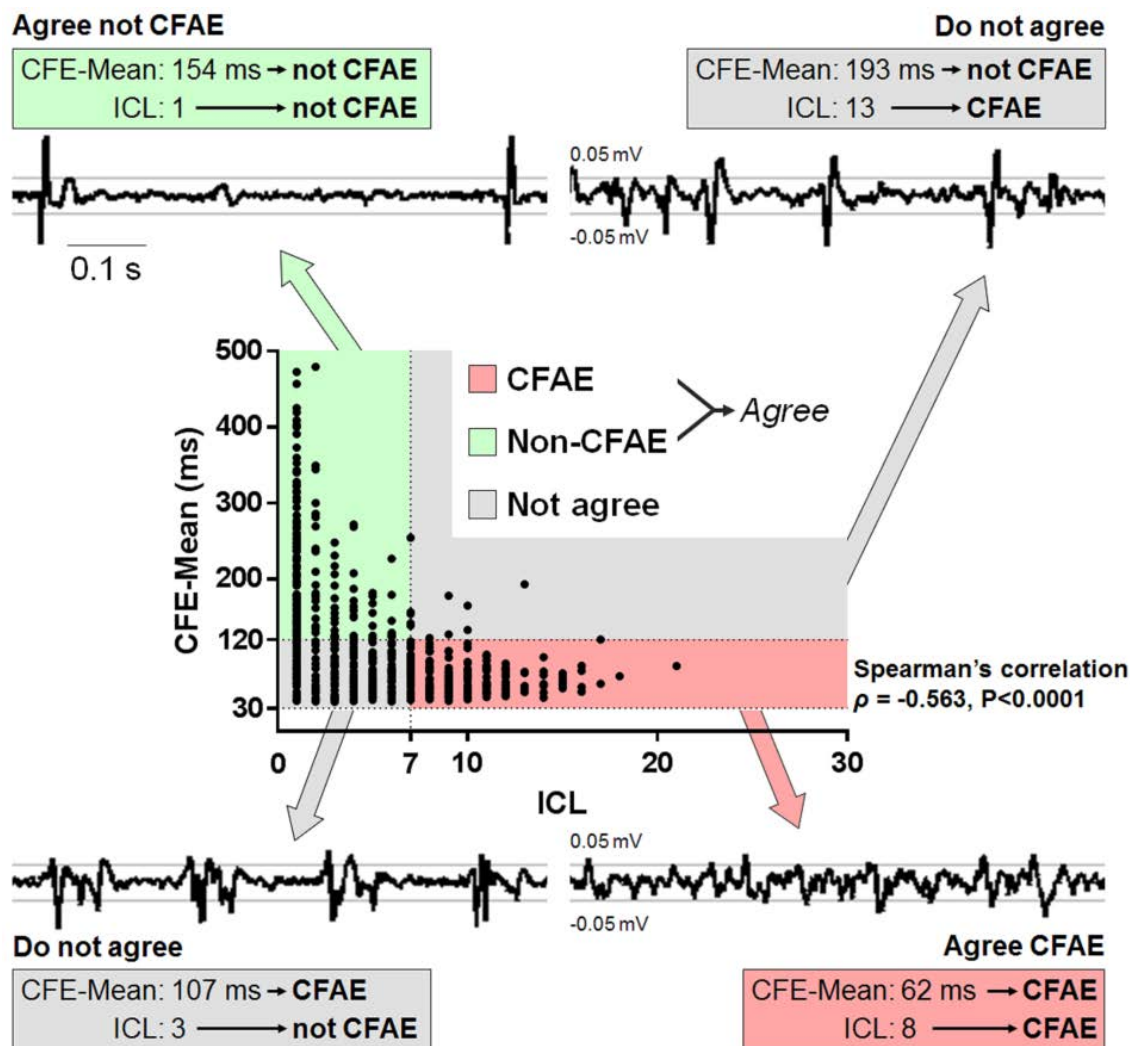


Figure 4-4 Comparison between CFE-Mean and ICL measured for all 797 AEGs, as determined by default NavX and CARTO EGM settings, respectively. Their respective default thresholds are highlighted (CFE-Mean  $\leq 120$  ms; ICL  $\geq 7$ ). Four quadrants were delimited: two quadrants where ICL and CFE-Mean agreed in terms of categorization, i.e., whether an AEG is fractionated or not fractionated; and two quadrants in which they disagreed. Examples of AEGs for each of the quadrants are shown, to illustrate the characteristics of each group. 230 (out of 797) AEGs with organized activations were found in the non-fractionated agreement zone (green). When looking at the AEGs corresponding to the disagreement quadrants (grey), one notices that they are less organized, still with distinguishable activations. In one grey region (bottom left), 282 AEGs have been classified as CFAEs by NavX but not by CARTO. In the other grey region (top right) 12 AEGs have been classified as CFAEs by CARTO, but not by NavX. Finally, 273 highly fractionated AEGs were found in the CFAE agreement zone (red).

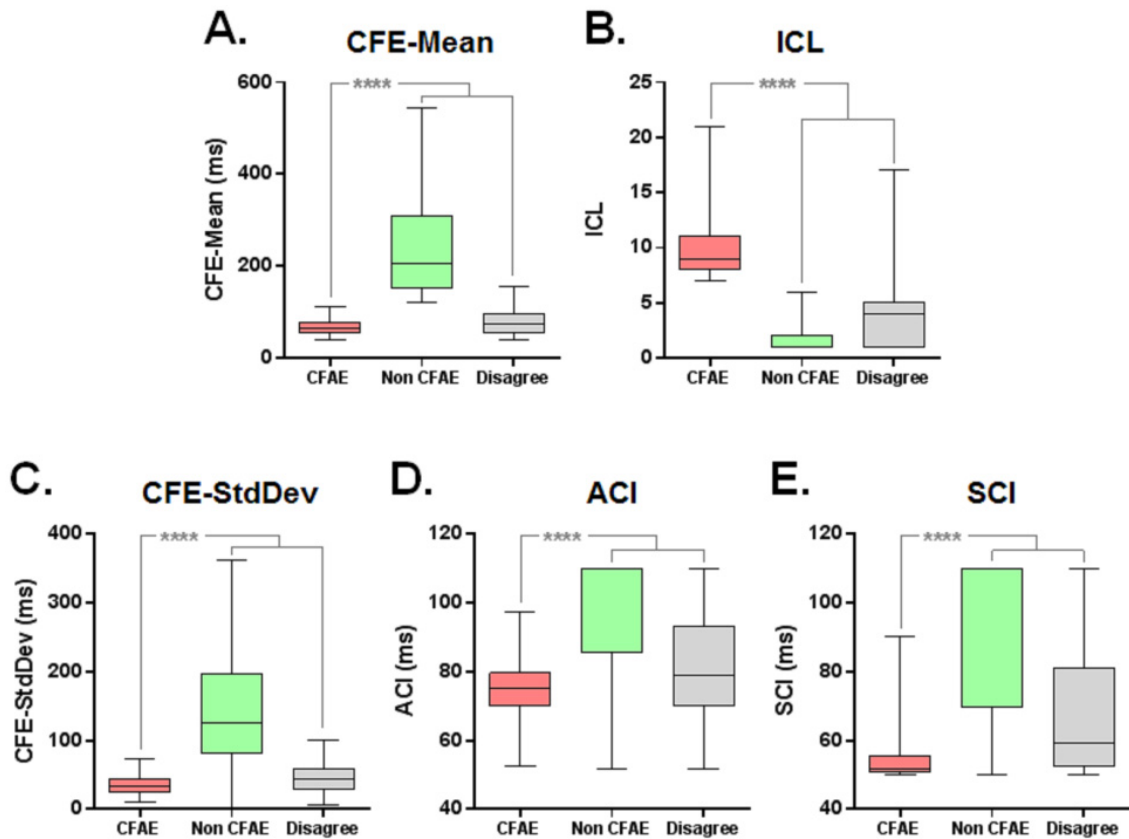


Figure 4-5 The distributions for the AEGs classified as non-CFAEs or CFAEs by both systems, as well as AEGs that had different classifications for each system, are shown according to CFE-Mean (A), ICL (B), CFE-StdDev (C), ACI (D) and SCI (E). \*\*\*\* P<0.0001.

The CFE-Mean based classification suggests that the default threshold for NavX (CFE-Mean  $\leq 120$  ms) provides high sensitivity but poor specificity for CFAE detection (Figure 4-6B, Table 4-3B). The revised threshold found from the ROC curves (CFE-Mean  $\leq 84 \pm 0.4$  ms) provides optimum sensitivity and specificity for CFAE detection and classification using ICL  $\geq 7$  as the reference classification.

Other thresholds for CFE-Mean and ICL based classification have been explored and support the present findings. Details are provided in the *Appendix C, CFAE detection thresholds for CFE-Mean and ICL*.

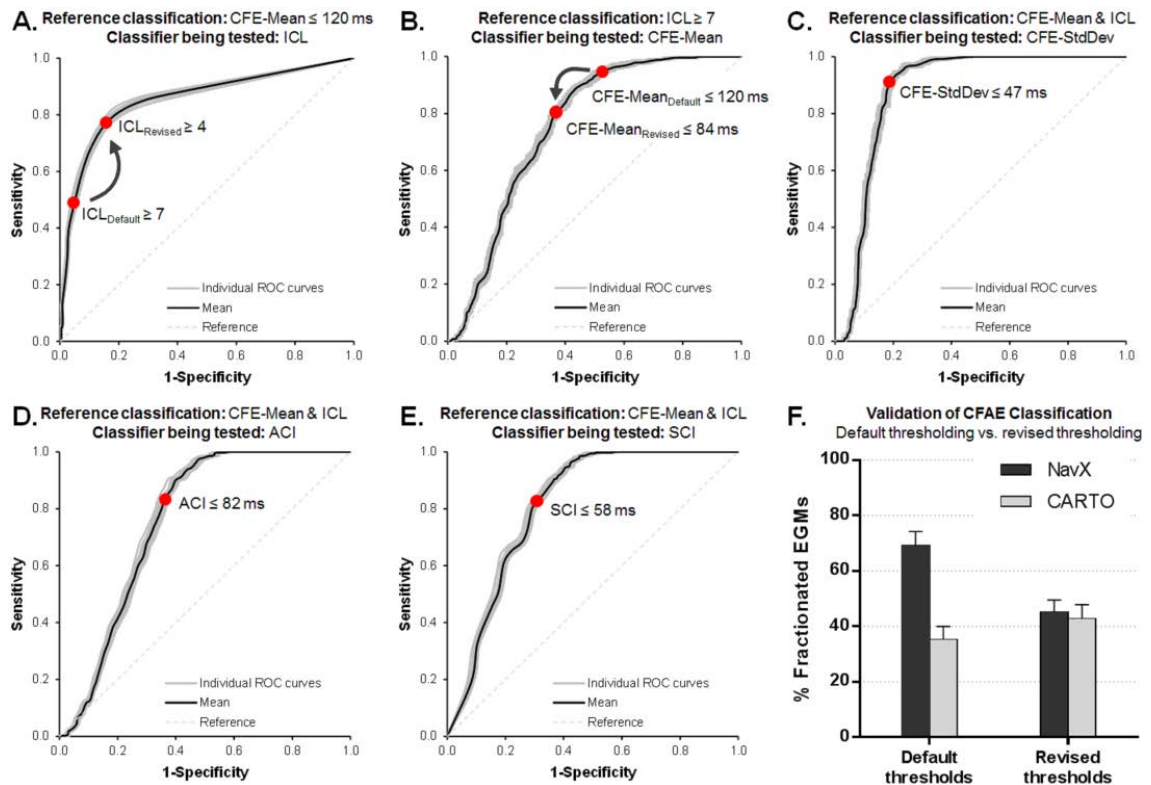


Figure 4-6 Mean (black lines) and individual (grey lines) receiver operating characteristic (ROC) curves used to adjust CFAE classification. ROC curve of A. ICL based classification using CFE-Mean  $\leq 120$  ms as the reference classification and; B. CFE-Mean based classification using ICL  $\geq 7$  as the reference classification. The CFAE classification in agreement by CFE-Mean and ICL using their revised thresholds (CFE-Mean  $\leq 84.1 \pm 0.4$  ms; ICL  $\geq 3.8 \pm 0.4$ ) was used to create ROC curves of C, D and E. C. CFE-StdDev; D. ACI and; E. SCI. The AUROC and optimum sensitivity and specificity for each measure are listed in Table 4-3 and Table 4-4. Explanations are provided in the text.

### 4.3.3 CFAE detection thresholds for CFE-StdDev, ACI and SCI

Figure 4-6C to 4-6E show the ROC curves for CFE-StdDev, ACI and SCI according to the CFAE classification performed by both CFE-Mean and ICL, using their revised thresholds. Table 4-4 provides the sensitivity, specificity and AUROC values. The details of the ROC curves from the thirty datasets are also provided in the *Appendix D, CFAE detection thresholds for CFE-StdDev, ACI and SCI*.

The ROC curves suggest that CFE-StdDev  $\leq 46.6 \pm 0.8$  ms (Figure 4-6C), ACI  $\leq 82.2 \pm 0.3$  ms (Figure 4-6D) and SCI  $\leq 58.6 \pm 0.4$  ms (Figure 4-6E) provide optimum sensitivity and specificity for CFAE detection, when considering the agreement between CFE-Mean and ICL for CFAE classification.

Table 4-3 Sensitivity and specificity for A. ICL based classification using CFE-Mean  $\leq 120$  ms as the reference classification and; B. CFE-Mean based classification using ICL  $\geq 7$  as the reference classification.

Reference classifier	Classifier being tested	Sensitivity	1-Specificity	AUROC	P-Value
<b>A.</b> CFE-Mean $\leq 120$ ms	ICL <sub>Default</sub> $\geq 7$	0.492 $\pm$ 0.008	0.050 $\pm$ 0.005	0.852 $\pm$ 0.005	****
	ICL <sub>Revised</sub> $\geq 3.8 \pm 0.4$	0.777 $\pm$ 0.022	0.162 $\pm$ 0.022		
<b>B.</b> ICL $\geq 7$	CFE-Mean <sub>Default</sub> $\leq 120$ ms	0.958 $\pm$ 0.005	0.552 $\pm$ 0.009	0.755 $\pm$ 0.005	****
	CFE-Mean <sub>Revised</sub> $\leq 84.1 \pm 0.4$ ms	0.807 $\pm$ 0.010	0.362 $\pm$ 0.006		

AUROC = Area under receiver operating characteristic curve; ICL = Interval confidence level.

Mean ( $\pm$  SD) of each sensitivity/specificity point from the thirty receiver operating characteristic (ROC) curves according to the CFAE classification performed by CFE-Mean and ICL. The mean ( $\pm$  SD) area under the ROC curve (AUROC) and optimum sensitivity and specificity for each measure are listed. \*\*\*\* P<0.0001.

Table 4-4 Sensitivity and specificity for CFE-StdDev, ACI and SCI according to CFAE classification agreement between CFE-Mean and ICL.

Thresholds	Sensitivity	1-Specificity	AUROC	P-value
CFE-StdDev $\leq 46.6 \pm 0.8$ ms	0.905 $\pm$ 0.012	0.185 $\pm$ 0.008	0.877 $\pm$ 0.014	****
ACI $\leq 82.2 \pm 0.3$ ms	0.827 $\pm$ 0.010	0.360 $\pm$ 0.009	0.759 $\pm$ 0.006	****
SCI $\leq 58.6 \pm 0.4$ ms	0.816 $\pm$ 0.012	0.300 $\pm$ 0.009	0.812 $\pm$ 0.005	****

Mean ( $\pm$  SD) of each sensitivity/specificity point from the thirty receiver operating characteristic (ROC) curves according to the CFAE classification performed concurrently by both CFE-Mean and ICL. The mean ( $\pm$  SD) area under the ROC curve (AUROC) and optimum sensitivity and specificity for each measure are listed. \*\*\*\* P<0.0001.

#### 4.3.4 Validation of the revised thresholds for CFAE detection performed by NavX and CARTO

Using the default thresholds (NavX: CFE-Mean  $\leq 120$  ms; CARTO: ICL  $\geq 7$ ) NavX classified 69  $\pm$  5% of the AEGs from the internal validation datasets as CFAEs, while CARTO detected 35  $\pm$  5% (P<0.0001). With the revised thresholds (NavX: CFE-Mean  $\leq 84.1 \pm 0.4$  ms and CFE-StdDev  $\leq 46.6 \pm 0.8$  ms; CARTO: ICL  $\geq 3.8 \pm 0.4$ , ACI  $\leq 82.2 \pm 0.3$  ms and SCI  $\leq 58.6 \pm 0.4$  ms) NavX classified 45  $\pm$  4%, while CARTO detected 42  $\pm$  5% (P<0.0001). These results are illustrated in Figure 4-6F.

Figure 4-7 illustrates CFAE classification performed by NavX and CARTO using the default (left hand side) and revised (right hand side) thresholds for the same patient. The CFAE maps produced by both systems using their default thresholds are very discordant, and these differences were minimized when each system used their revised thresholds. The CFAE maps created by both systems using their revised thresholds identified more similar atrial regions as target for ablation. The Kappa score between the CFAE categorization performed by NavX and CARTO significantly increased (P<0.0001) from  $\kappa = 0.34 \pm 0.07$  (marginal agreement, P<0.0001) using their default thresholds to  $\kappa = 0.45 \pm 0.10$  (good agreement, P<0.0001) with the proposed revised thresholds.

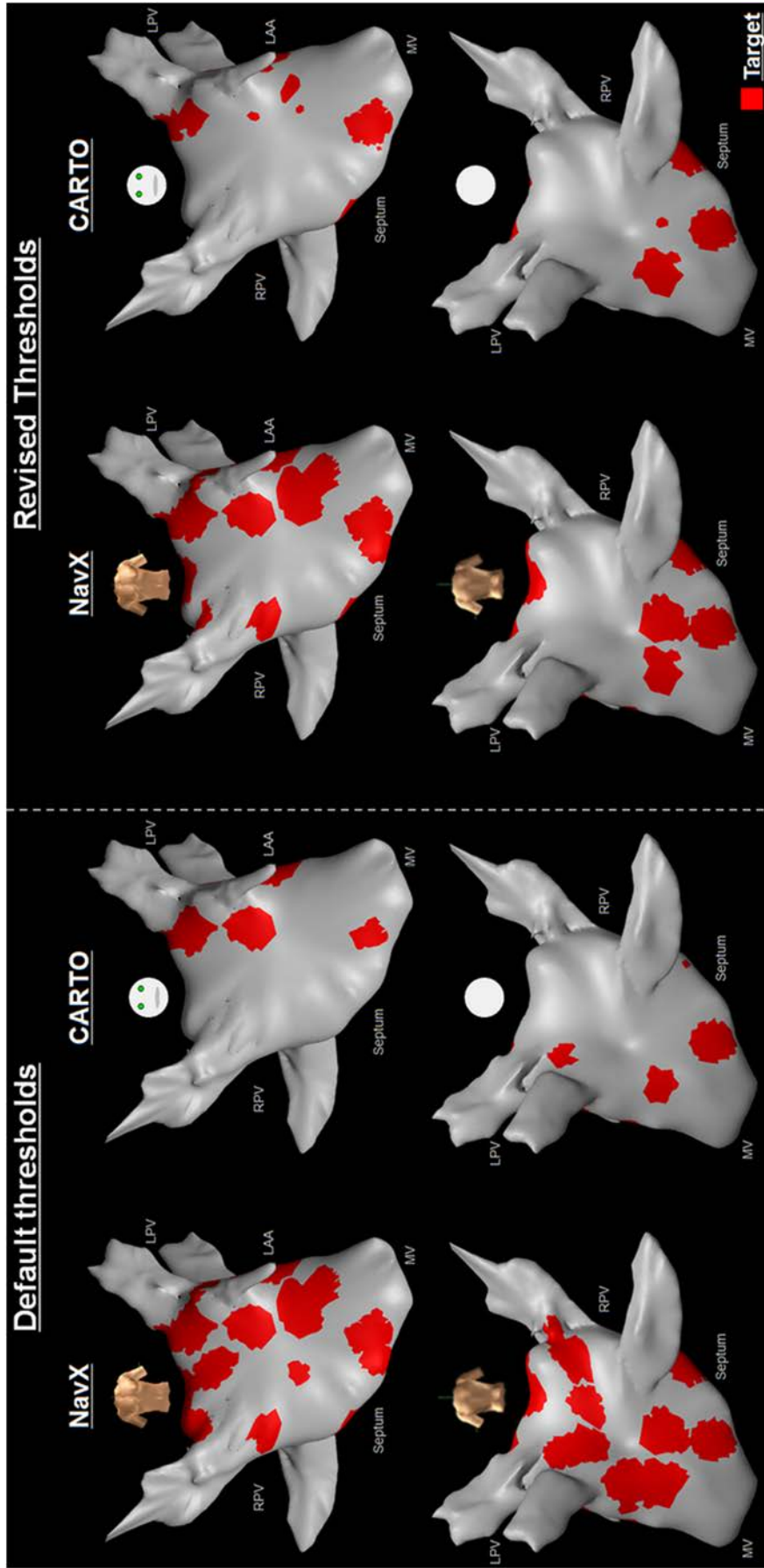


Figure 4-7 Illustration of CFAE classification performed by NavX and CARTO in the LA from one patient using their default (left) and revised (right) thresholds. Explanations are provided in the text.

## 4.4 Discussion

This is the first study that uses the same bipolar AEG data collected during persAF ablation to compare CFAE detection performed by the algorithms embedded in NavX and CARTO systems. Additionally, the thresholds for the indices used by both systems were adjusted to minimize the differences between them. The results presented here highlight the discordances in CFAE classification between both systems, which could produce potential disparities in CFAE-guided ablation. The proposed revised thresholds counterbalance the differences of automated CFAE classification performed by the algorithms embedded in each system and reduce the discordances between them. Unifying methods of CFAE classification would allow comparable CFAE maps to be generated which could then act as a standard for future clinical studies.

### 4.4.1 Atrial substrate characterized by CFAE

The true significance of CFAE in the pathophysiology of AF remains to be determined. Although it is believed that CFAEs represent atrial substrate during persAF (Ashihara *et al.*, 2012, Calkins *et al.*, 2012b, Nademanee *et al.*, 2004, Rostock *et al.*, 2006, Zlochiver *et al.*, 2008), recent investigations have shown that fractionated AEGs during AF may characterize remote atrial far-field activity (Atienza *et al.*, 2011, Narayan *et al.*, 2011), and passive wave front collision within the atrial anatomy (Roux *et al.*, 2009). Recent work has reported no benefit when ablation of CFAEs was performed in addition to PVI in persAF patients (Verma *et al.*, 2015). However, this work has been openly criticized for: (i) not considering the combination of PVI, anatomical lines creation and CFAE ablation and; (ii) the CFAE mapping algorithm used (Sohal *et al.*, 2015). Discordances in CFAE mapping algorithms create significant difficulty in comparing CFAE-ablation studies. Minimizing the differences in CFAE classification between NavX and CARTO may help to clarify the significance of CFAE as a driver of persAF. Therefore, prudence is needed when comparing the outcomes in AF ablation incorporating CFAE-targeted approaches in different electrophysiological studies using different mapping systems (Elayi *et al.*, 2008, Lin *et al.*, 2009a, Nademanee *et al.*, 2004, Oral *et al.*, 2007, Oral *et al.*, 2009, Porter *et al.*, 2008, Verma *et al.*, 2010, Verma *et al.*, 2011, Verma *et al.*, 2015).

#### **4.4.2 The lack of a gold standard for CFAE definition**

There is currently no gold standard for CFAE classification in human persAF. This remains one of the biggest challenges for CFAE-based ablation. Visual assessment performed by experts could help on arbitration of fractionation, but would also introduce subjectivity to the method as each specialist has his/her own perception of what defines fractionation (Aizer *et al.*, 2008, Hunter *et al.*, 2009, Ng *et al.*, 2010). Additionally, even if the experts were able to visually identify if an AEG is fractionated, still this would not be sufficient to effectively conclude that the AEG is a true representation of atrial substrate (these would correspond to atrial regions that organize AF when ablated). This ultimate conclusion is only possible by assessing if AF becomes more organized after ablating this particular atrial region by assessing if there is an appreciable change in the rhythm – either AF termination or increase in AF CL. Any ‘external reference’ other than ‘AEGs that organized AF after ablation’ would only introduce subjectivity to the method, and would contribute little to objectively identifying LA regions as a surrogate of pro-arrhythmogenic sites. Therefore, visual assessment of fractionation for the recorded signals performed by clinicians was not included in this study. The present study focused on the classification performed automatically by both systems as currently performed in CFAE-guided ablation therapy, without the interference and subjectivity induced by operators. This allowed for an objective investigation of CFAE detection by investigating each system – one at a time – as being the ‘gold’ standard for CFAE classification.

#### **4.4.3 CFAE detection performed by NavX and CARTO algorithms**

We have shown that CFAE target identification is dependent on the system used and settings applied during the procedure. Different CFAE mapping algorithms are based on different premises to measure fractionation. For instance, NavX identifies AEGs with a very short cycle length with or without multiple potentials. CARTO, on the other hand, mostly measures AEGs that are composed of two deflections or more and/or have a perturbation of the baseline with continuous deflections (Nademanee *et al.*, 2004).

The comparison between both mapping systems using their default settings produced a low correlation ( $\rho=-0.563$ ,  $P<0.0001$ ), which supports recently published data (Lau *et al.*, 2015). However, the Spearman's correlation does not consider the thresholds for CFAE classification. The values – and correlation – of CFE-Mean and ICL only have a full

electrophysiological meaning when linked with the thresholds used. This information is provided by the Kappa score.

It is known that both systems are not used simultaneously during atrial substrate mapping and that physicians frequently vary the settings for CFAE mapping in a patient-specific manner (Elayi *et al.*, 2008, Lin *et al.*, 2009a, Nademane *et al.*, 2004, Oral *et al.*, 2007, Oral *et al.*, 2009, Porter *et al.*, 2008, Verma *et al.*, 2010, Verma *et al.*, 2011, Verma *et al.*, 2015). Our results propose revised thresholds for CFAE detection to be used independently by NavX and CARTO to even out the discordances between them. Therefore, a CFAE map created with NavX utilizing the revised NavX's thresholds will look more similar to the one that would have been created with CARTO utilizing CARTO's revised thresholds proposed in this work, as illustrated in Figure 4-7.

The use of both primary and complementary indices is an additional way to even out differences in CFAE classification performed by each system. There is little data available about the complementary indices measured by automated algorithms being used to either target or support CFAE identification during atrial substrate mapping (Redfearn *et al.*, 2009, Scherr *et al.*, 2009, Tsai *et al.*, 2012). However, the ROC curves generated using the agreement between CFE-Mean and ICL as the reference for classification for CFE-StdDev, ACI and SCI (Figure 4-6C to 4-6E) provide evidence that these complementary indices can help to distinguish CFAE from non-CFAE effectively. This would further improve the agreement of CFAE classification performed by both systems.

#### **4.4.4 Study limitations**

The current study was limited to retrospective data. Further understanding of the underlying cardio-electrophysiological mechanisms behind CFAEs would be helpful for the validation of the suggested revised thresholds, such as in (i) computational intracardiac models that simulate both atrial electrical activity and ablation procedures during AF (Krueger *et al.*, 2013) and; (ii) prospective studies using the revised thresholds in the identification of ablation targets during substrate mapping.

#### **4.5 Conclusions**

In this chapter, we provide a direct quantitative comparison of CFAE detection during persAF, applying the automated algorithms embedded in NavX and CARTO systems to

the same bipolar AEG data. We have demonstrated that CFAE mapping (and thus ablation target identification) varies significantly for the same individual, depending on the system and its settings. Our work takes a first step to understanding and minimizing the discordance between NavX and CARTO. We propose revised thresholds that adjust sensitivity and specificity of CFAE detection as independently performed by NavX (CFE-Mean  $\leq$  84 ms; CFE-StdDev  $\leq$  47 ms) and CARTO (ICL  $\geq$  4; ACI  $\leq$  82 ms; SCI  $\leq$  58 ms). These thresholds counterbalance the intrinsic differences between the CFAE algorithms embedded in each system, allowing comparable CFAE maps to be generated which would facilitate the direct comparison of CFAE-guided ablation outcomes in future studies.

## Chapter 5

# Characterization of atrial electrogram fractionation before and after pulmonary vein isolation in human persistent atrial fibrillation

### 5.1 Introduction

Catheter ablation has become a consolidated therapy for patients with AF (Calkins *et al.*, 2012b). PVI has been proved effective in the treatment of pAF (Haissaguerre *et al.*, 1998), but insufficient for persAF due to patient specific structural and electrical changes in the LA (Brooks *et al.*, 2010). AEGs with low amplitude and multiple deflections / activations were thought to represent cardiac tissue with structural and electric remodelling induced by sustained AF. CFAEs have been introduced as markers of such atrial sites and, therefore, potential targets for ablation (Nademanee *et al.*, 2004). CFAE-guided ablation has been accepted by many as a useful adjunctive therapy to PVI for persAF (Calkins *et al.*, 2012a), but the results have been inconsistent, with some studies concluding that CFAE-guided ablation is beneficial (Deisenhofer *et al.*, 2009, Elayi *et al.*, 2008, Lin *et al.*, 2009a, Verma *et al.*, 2007, Verma *et al.*, 2008a, Verma *et al.*, 2010), while others reported it as ineffective (Dixit *et al.*, 2012, Oral *et al.*, 2009, Verma *et al.*, 2015). This low reproducibility of outcomes in persAF ablation targeting CFAEs motivated the investigation of the accuracy of current methods for atrial substrate identification (Almeida *et al.*, 2016, Lau *et al.*, 2015). Additionally, previous work has shown that a large proportion of CFAEs are a result of remote AF drivers and, therefore, a passive phenomenon not important to the maintenance of AF (Jadidi *et al.*, 2012a, Rostock *et al.*, 2006, Roux *et al.*, 2009, Tuan *et al.*, 2011). Conversely, other studies have suggested that

some CFAEs represent active sources responsible for the perpetuation of AF (Takahashi *et al.*, 2008, Verma *et al.*, 2014, Yamabe *et al.*, 2009).

In this chapter, we investigate the effect that PVI and roof line ablation (PVI+RL) has on the presence of AEG fractionation. Multiple indices of fractionation have been used to investigate different features of atrial regions that have been either changed or unchanged by PVI+RL.

## **5.2 Methods**

### **5.2.1 Study population**

The study population consisted of 18 persAF patients (16 male; mean age  $56.1 \pm 9.3$  years; history of AF  $67.2 \pm 45.6$  months) referred to our institution for first time catheter ablation. Details of the clinical characteristics of the study subjects have been provided elsewhere (Tuan *et al.*, 2011). Study approval was obtained from the local ethics committee and all procedures were performed with full informed consent. Table 5-1 summarizes the clinical characteristics of the study subjects. All patients were treated in the Glenfield Hospital by doctors from the Cardiovascular Department led by Prof. G. André Ng.

### **5.2.2 Electrophysiological study**

Details of the electrophysiologic study, mapping procedure, and the clinical characteristics of the study subjects have been described previously (Tuan *et al.*, 2011). 18 persAF patients (16 male; mean age  $56.1 \pm 9.3$  years; history of AF  $67.2 \pm 45.6$  months) referred to our institution for first time catheter ablation were included in this study. Study approval was obtained from the local ethics committee and all procedures were performed with full informed consent.

3D LA geometry was created within NavX (Verma *et al.*, 2010) using a deflectable, variable loop circular PV mapping catheter (Inquiry Optima, St. Jude Medical). PVI was performed with a point-by-point wide area circumferential ablation approach, followed by the creation of a single roof line (Cool Path Duo irrigated RF catheter, St. Jude Medical). No additional ablation targeting CFAE was performed in this study. Sequential point-by-point bipolar AEGs were collected from 15 pre-determined atrial regions before

and after LA ablation (Tuan *et al.*, 2011). All patients were in AF before and after ablation during signal collection.

Table 5-1 Clinical characteristics of study population (N = 18).

Age, yrs	56.1 ± 9.3
Male/Female	16/2
History of AF, months	67.2 ± 45.6
Ejection Fraction,%	48 ± 1
Left Atrial Diameter, mm	47 ± 1
History of coronary artery disease	4
Medication* (number of patients on)	
ACE inhibitor / ARB	11
Amiodarone	10
Beta-blockers	8
Calcium channel blockers	2
Digoxin	1
Sotalol	5

\* All anti-arrhythmic and rate-controlling drugs were stopped for at least five half-lives before the procedure, with the exception of amiodarone. ACE = angiotensin-converting-enzyme; AF = atrial fibrillation; ARB = angiotensin receptor blockers. Values are in mean ± SD or n.

### 5.2.3 Signal analysis

A total of 797 bipolar AEGs were recorded from the LA, 455 before and 342 after ablation, with a sampling frequency of 1200 Hz, and band-pass filtered within 30–300 Hz. When an improvement of signal-to-noise ratio was necessary, a 50 Hz Notch filter was applied.

From those AEGs, 207 pairs were identified as collected in the same atrial location, before and after ablation. Points were considered to be from similar atrial locations if they were collected 5 mm or less from each other. Only points remote from ablation lesions were considered. Each pair of AEG (207 before and 207 after ablation), their corresponding CFE-Mean, CFE-StdDev and PP values were exported from NavX with a fixed time

window length of 2.5 s. A validated offline MATLAB algorithm was used to compute the ICL, the ACI and the SCI, as defined by CARTO – see *Appendix A, Validation of an Offline Algorithm to reproduce CARTO CFAE definition for CFAE identification* (Almeida *et al.*, 2016). CFAE criteria as defined by both systems were considered in the current study in an attempt to minimize the inconsistencies between the two methods, with CFAEs defined as AEGs with both  $CFE\text{-Mean} \leq 120$  ms and  $ICL \geq 4$  (Figure 5-1). The indices of fractionation computed by NavX and CARTO that are usually used in EP studies to guide AF ablation are described in detail on *Chapter 4, Minimizing discordances in automated classification of fractionated electrograms in human persistent atrial fibrillation*. The LA maps of the 18 patients were segmented by an experienced clinician into 6 regions – PVs; Roof; Posterior; Anterior; Septum and Lateral.

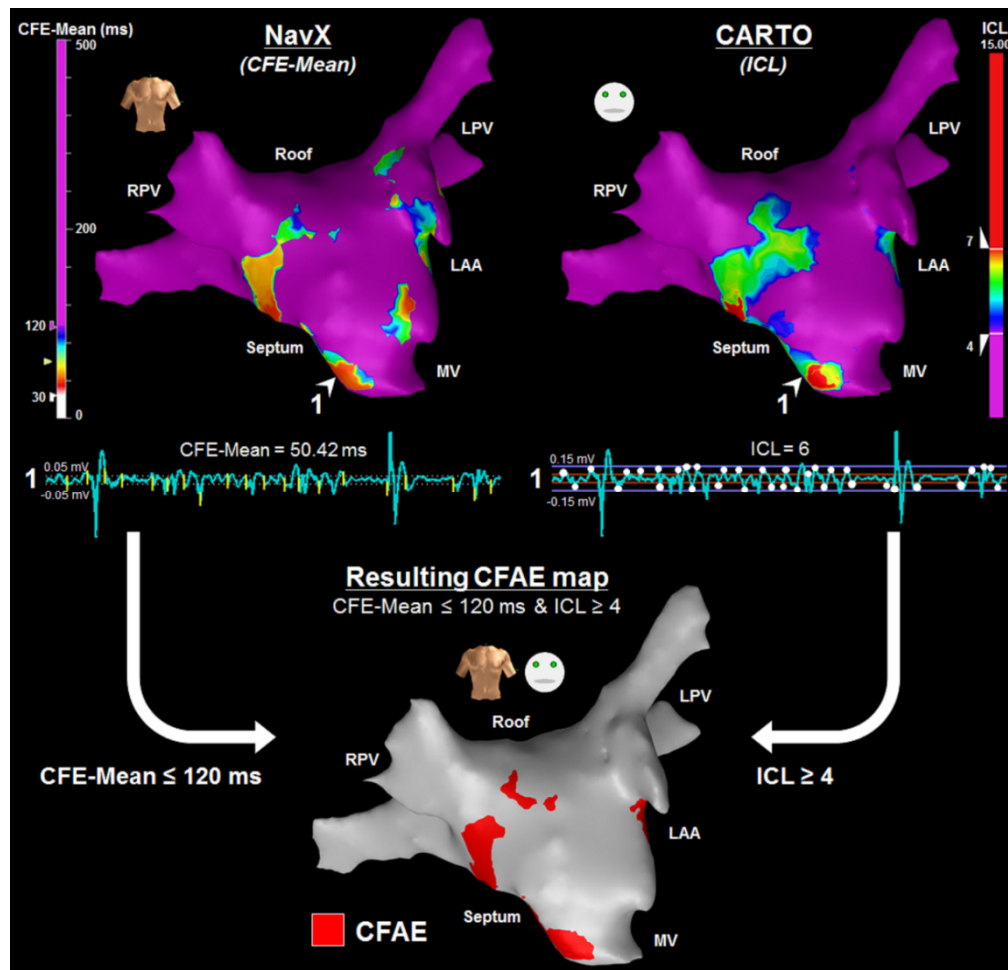


Figure 5-1 NavX (upper left) and CARTO (upper right) 3D LA geometry representation for the same patient, with their respective automated CFAE detection algorithms (Almeida *et al.*, 2016). The illustrated AEG has  $CFE\text{-Mean} = 50.42$  ms and  $ICL = 6$ . LA regions hosting AEGs with both  $CFE\text{-Mean} \leq 120$  ms and  $ICL \geq 4$  were considered CFAEs (bottom map).

## 5.2.4 Indices of fractionation

Twelve indices were computed from the 207 pairs of AEGs, accordingly:

- *Indices of fractionation computed by commercial mapping systems:* CFE-Mean and CFE-StdDev, as defined by NavX. AEGs with CFE-Mean within 30 – 120 ms are considered fractionated and CFE-Mean > 120 ms represents low fractionation; ICL, ACI and SCI, as defined by CARTO; Typically, ICL < 4 represents low fractionation,  $4 \leq \text{ICL} < 7$  refers to moderate fractionation and ICL  $\geq 7$  indicates high fractionation (Almeida *et al.*, 2016);
- *Information theory indices:* ShEn, SampEn, and K-L divergence. Both ShEn and SampEn assume high values for CFAEs, while K-L assumes small values for CFAEs (Cover and Thomas, 1991, Lake *et al.*, 2002, Shannon, 1948);
- *Amplitude based indices:* PP and amplitude root mean square (RMS). Small values of PP has been shown to correlate with fibrotic atrial tissue (Oakes *et al.*, 2009);
- *Frequency based indices:* DF and OI. OI is bounded between 0 and 1, and smaller values indicate more fractionated AEGs (Everett *et al.*, 2001, Sanders *et al.*, 2005).

Details about all these descriptors can be found on *Chapter 3, Mathematical & Signal Processing Tools*.

## 5.2.5 Statistical analysis

All non-normally distributed variables are expressed as median  $\pm$  interquartile interval. Nonparametric paired multiple data were analysed using the Friedman test with Dunn's correction, while nonparametric unpaired data were analysed using the Mann–Whitney test. Spearman's correlation was computed to quantify the correlation between indices of fractionation. Robust MANOVA using Munzel and Brunner's method (Munzel and Brunner, 2000), and LDA were used to test the differences between groups across the twelve indices of fractionation. The discriminant scores for the LDA were calculated with the entire database, and the model was validated considering the leave-one-out cross-validation (LOOCV) method. Both MANOVA and LDA were implemented in R version

3.2.0 (2015). These multivariate tests were performed on two sets of data, separately: before and after PVI+RL. P-values less than 0.05 were considered statistically significant.

## **5.3 Results**

### **5.3.1 Effect of PVI+RL on the distribution of CFAEs**

AEGs that were collected in corresponding atrial regions before and after PVI+RL were identified (Figure 5-2), and their CFAE classification compared. Four groups of AEGs were identified in terms of the presence of fractionation before and after PVI+RL (Figure 5-2A): Group 1 represents AEGs classified as CFAEs at baseline that remained CFAEs after ablation; Group 2 represents CFAEs at baseline that converted to non-CFAEs after ablation; Group 3 represents non-CFAEs at baseline that became CFAEs after ablation; Group 4 represents non-CFAEs at baseline that remained non-CFAEs after ablation. Figure 5-2B illustrates the different types of AEGs found in the four groups.

Our results show PVI+RL reduced the overall number of CFAEs. 70% of 207 AEGs were classified as CFAEs at baseline. After PVI+RL, the number of AEGs classified as CFAEs decreased to 40% ( $P < 0.0001$ ). As illustrated in Figure 5-3A, 45% of the AEGs that were CFAEs before ablation remained fractionated after ablation (group 1), while 55% converted to non-CFAE (group 2); 29% of the AEGs not fractionated prior ablation became fractionated (group 3), while 71% remained not fractionated (group 4).

Figure 5-3B illustrates the occurrence of the different types of AEGs (group 1, 2, 3, and 4) per LA region. CFAEs unchanged by PVI+RL (group 1) were observed in all regions, with the LA roof showing the highest incidence of remaining CFAEs, followed by the anterior wall, septum, PVs, posterior wall and lateral. AEGs converting to non-CFAE after PVI+RL (group 2) were observed in all regions, with the lateral LA showing the highest incidence of CFAEs responsive to PVI+RL. The PVs and lateral LA were the only regions where no AEGs became CFAEs after PVI+RL (group 3). AEGs remaining non-CFAEs (group 4) were observed in all regions.

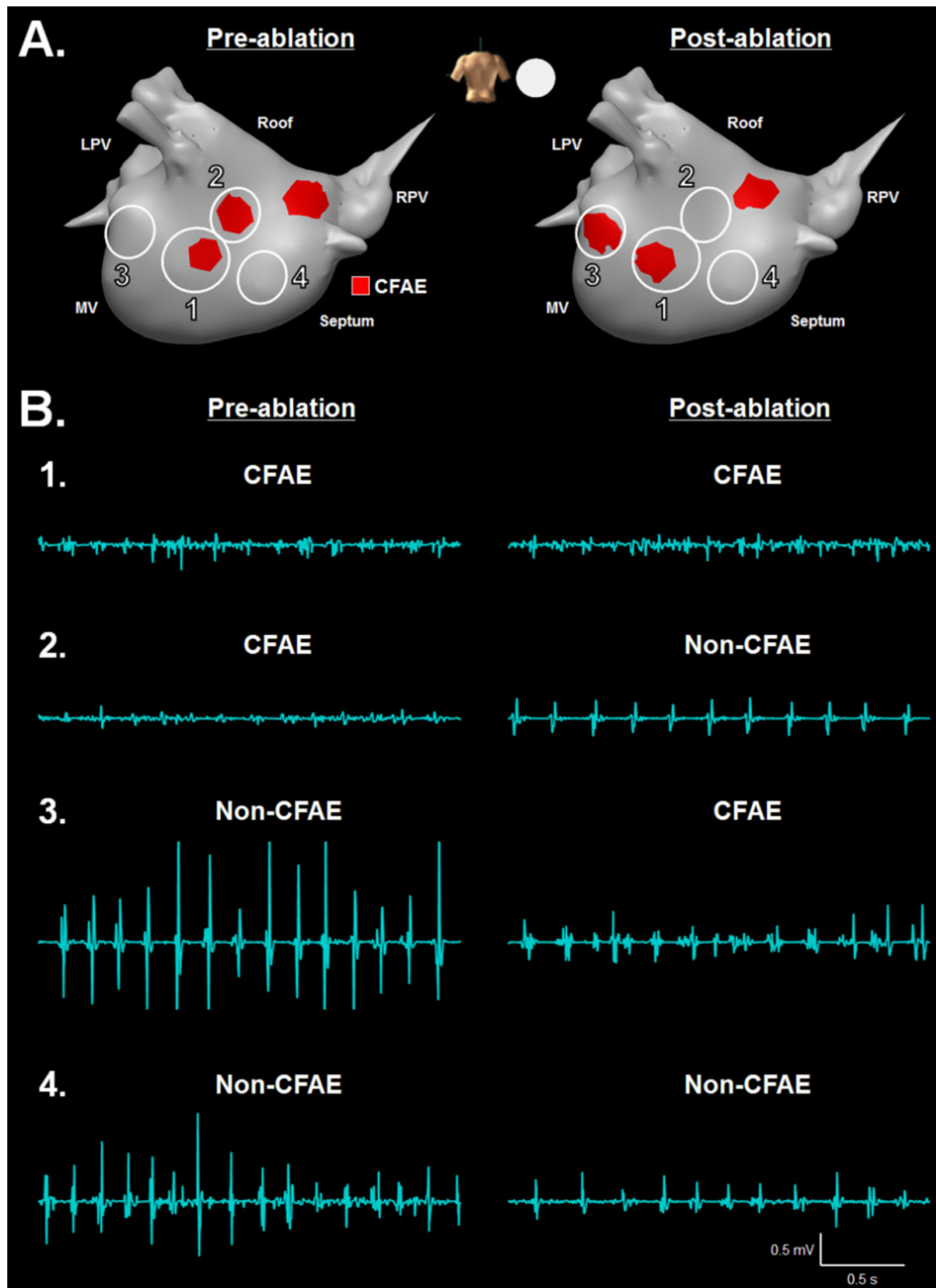


Figure 5-2 Illustration of the different types of AEGs found in this study. A. 207 AEGs before ablation were compared with 207 AEGs after ablation, collected in corresponding LA region. Four groups of AEGs were identified in terms of CFAE, before and after ablation: CFAE before and after ablation (group 1); CFAE before, non-CFAE after ablation (group 2); non-CFAE before, CFAE after ablation (group 3); and non-CFAE before and after ablation (group 4). B. Illustration of AEGs found in each group. Highly fractionated AEGs were found in group 1 before and after ablation; fractionated AEGs before ablation with increased organization after ablation in group 2; organized activation before ablation with increased fractionation after ablation in group 3; organized activation before and after ablation in group 4.

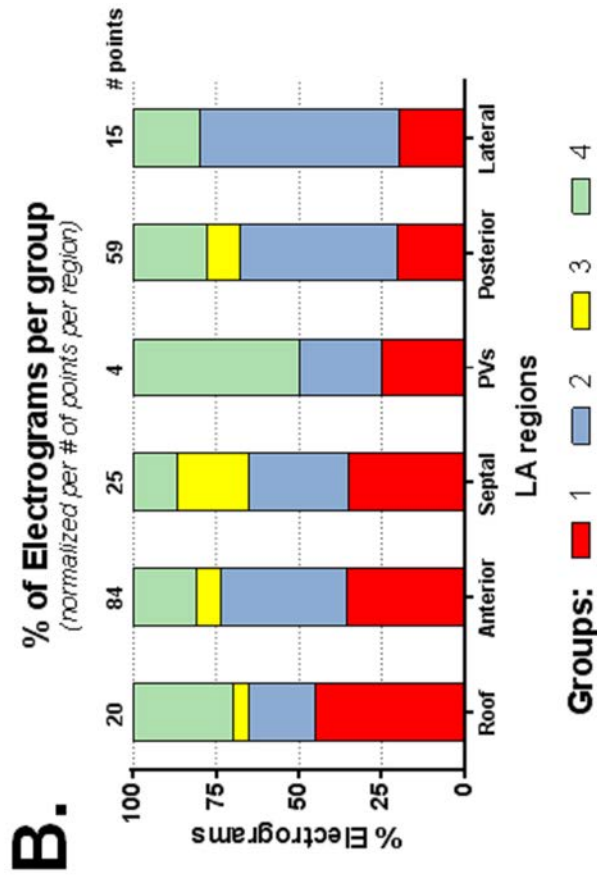
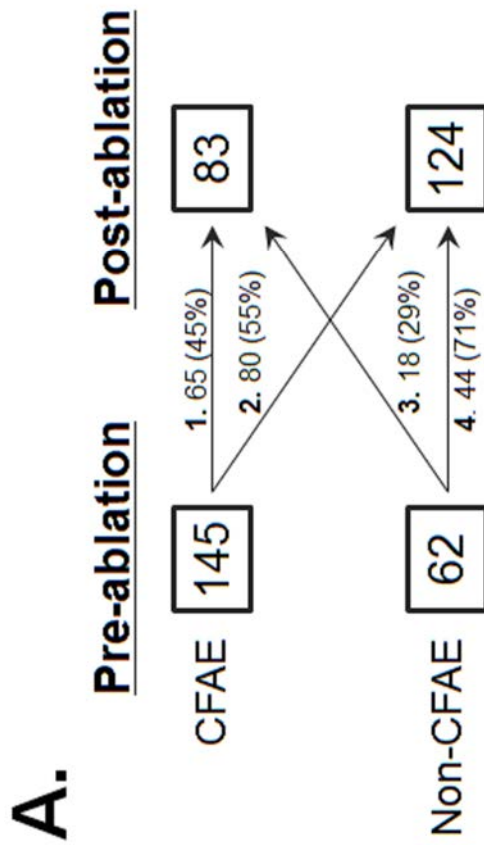


Figure 5-3 Effect of PVI on the AF behaviour. A. 45% of the AEGs classified as CFAEs before ablation remained fractionated after ablation, while the remainder became non-CFAE. 71% of the AEGs classified as non-CFAEs before ablation remained not fractionated after ablation, while the remainder became CFAE. B. Incidence of different types of AEGs (group 1, 2, 3 and 4) in the different LA regions, namely: roof, anterior wall, septum, PVs, posterior wall and lateral. The number of paired points – before and after ablation – collected per regions is also provided.

### **5.3.2 Correlation between indices of fractionation**

Each fractionation index has been compared to all remaining indices. Figure 5-4 provides the comparison and Spearman's correlation coefficients between them. Considering conventional fractionation indices, CFE-Mean was most highly correlated with CFE-StdDev ( $\rho=0.891$ ,  $P<0.0001$ ), but these indices are biased by a scaling effect. RMS showed the second highest correlation with CFE-Mean ( $\rho=-0.611$ ,  $P<0.0001$ ). All other indices correlated moderately or worse with CFE-Mean. Meanwhile ICL was most highly correlated with SCI ( $\rho=-0.744$ ,  $P<0.0001$ ), with all other indices correlating only moderately or worse, including ACI ( $\rho=-0.498$ ,  $P<0.0001$ ).

Confounding indices presented high correlation amongst each other as expected: ACI vs SCI ( $\rho=0.766$ ,  $P<0.0001$ ); ShEn vs SampEn ( $\rho=0.621$ ,  $P<0.0001$ ); ShEn vs K-L ( $\rho=-0.827$ ,  $P<0.0001$ ); SampEn vs K-L ( $\rho=-0.847$ ,  $P<0.0001$ ); PP vs RMS ( $\rho=0.813$ ,  $P<0.0001$ ). The remaining indices had moderate or poor correlation with each other.

### **5.3.3 Effect of PVI+RL on the indices of fractionation**

Although most indices correlated poorly with each other, ablation had a significant effect on all indices of fractionation, except for the OI (Figure 5-5). CFE-Mean, CFE-StdDev, ACI, SCI and K-L significantly increased after PVI+RL, suggesting less fractionated AEGs (all  $P<0.0001$ ). Similarly, ICL, ShEn, SampEn, PP, RMS and DF significantly decreased after ablation (all  $P<0.0001$ ).

### **5.3.4 Characterization of AEGs before and after PVI+RL**

As expected, CFE-Mean ( $P<0.0001$ ), CFE-StdDev ( $P<0.0001$ ), ACI ( $P<0.0001$ ), SCI ( $P<0.0001$ ) and K-L ( $P=0.0004$ ) were all lower for AEGs classified as CFAEs when compared to non-CFAEs. Similarly, ICL ( $P<0.0001$ ), ShEn ( $P=0.06$ ), SampEn ( $P<0.0001$ ), PP ( $P<0.0001$ ), RMS ( $P<0.0001$ ), DF ( $P=0.0044$ ) and OI ( $P=0.0086$ ) demonstrated higher values for fractionated AEGs.

No single index on its own was able to discriminate the different groups of AEGs, whether measured before (Figure 5-6) or after (Figure 5-7) PVI+RL. However, the multiple linear combinations conducted on MANOVA suggest a significant main effect of the groups of AEGs (1, 2, 3 and 4) on the indices of fractionation on both before (F-ratio  $F = 9.41$ ,

P<0.0001) and after ablation ( $F = 14.74$ ,  $P<0.0001$ ) datasets. MANOVA was followed up with LDA, which revealed three discriminant functions both before and after ablation. The LOOCV revealed that the LDA successfully discriminated, prior to any ablation, 40% of the AEGs in group 1; 73% of group 2; 39% of group 3 and; 59% of group 4. After PVI+RL, LDA correctly identified 86% of the AEGs in group 1; 76% of group 2; 5.6% of group 3 and; 27% of group 4. The ranked results from MANOVA and the discriminant scores from the LDA can be seen in the *Appendix E, Ranked results from the MANOVA and The coefficients from the LDA.*

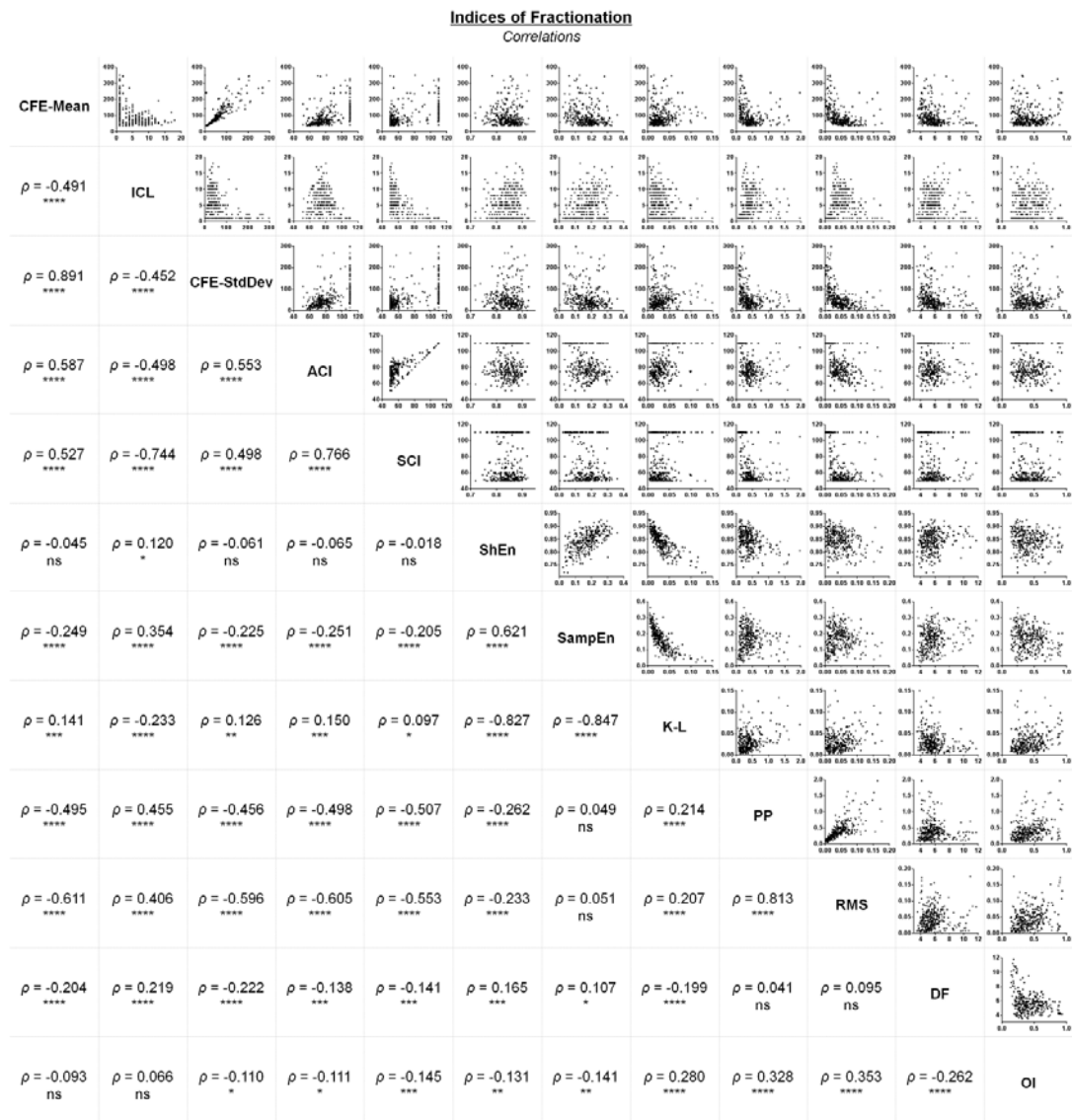


Figure 5-4 Correlations between different indices of fractionation measured from the same AEG database. Confounding indices had high correlation among each other: CFE-Mean vs. CFE-StdDev, ACI vs. SCI, ShEn vs. SampEn, ShEn vs. K-L, SampEn vs. K-L and PP vs. RMS. The remaining indices had moderate or poor correlation with each other. \*\*\*\* P<0.0001; \*\*\* P<0.001; \*\* P<0.01; \* P<0.05; ns = not significant.

## Indices of Fractionation *Effect of AF ablation*

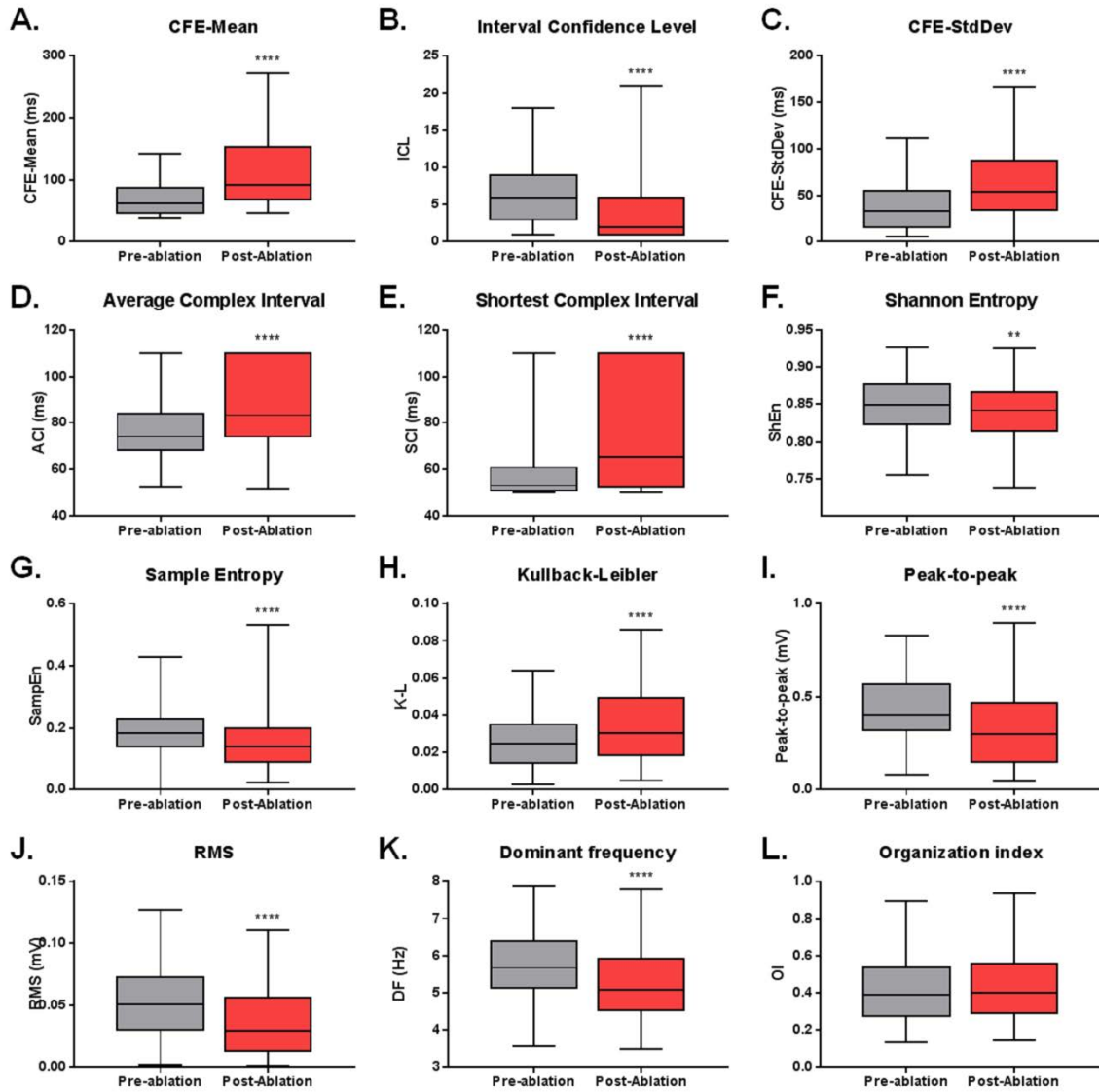


Figure 5-5 Effect of PVI and roof line creation on the indices of fractionation. Effect of PVI and roof line creation on: A. CFE-Mean; B. ICL; C. CFE-StdDev; D. ACI; E. SCI; F. ShEn; G. SampEn; H. K-L; I. PP; J. RMS; K. DF; L. OI. All indices, except OI, were significantly affected by ablation. \*\*\*\*  $P < 0.0001$ ; \*\*\*  $P < 0.001$ ; \*\*  $P < 0.01$ .

### Indices of Fractionation

Per AEG group before PVI + RL

■ CFAEs ■ Non-CFAEs

Group	Pre-ablation	→	Post-ablation
1.	CFAE	→	CFAE
2.	CFAE	→	Non-CFAE
3.	Non-CFAE	→	CFAE
4.	Non-CFAE	→	Non-CFAE

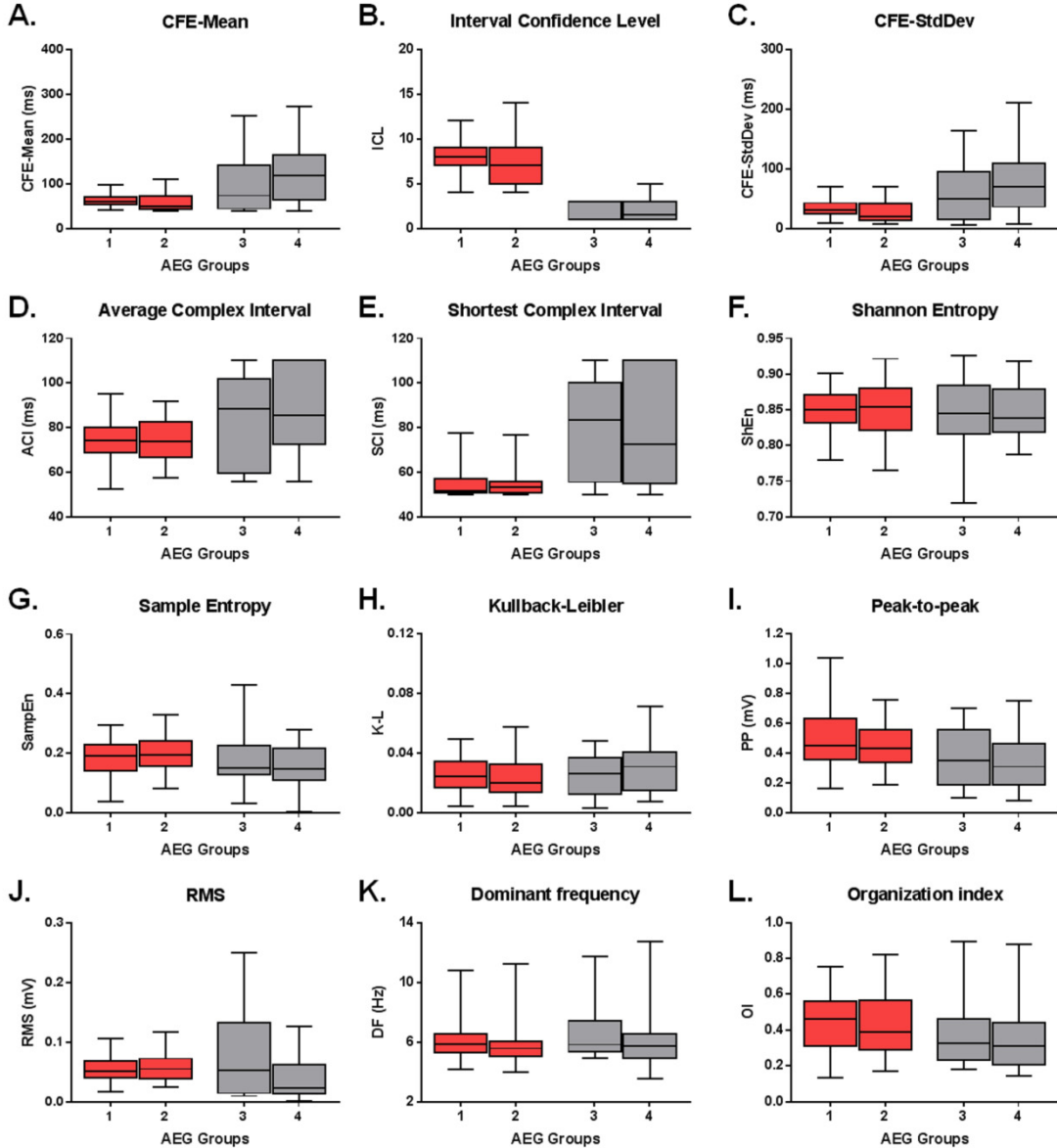


Figure 5-6 The characterization of AEGs in the different groups (1, 2, 3 and 4) at baseline according different indices of fractionation: A. CFE-Mean; B. ICL; C. CFE-StdDev; D. ACI; E. SCI; F. ShEn; G. SampEn; H. K-L; I. PP; J. RMS; K. DF; L. OI.

## Indices of Fractionation

Per AEG group after PVI + RL

■ CFAEs ■ Non-CFAEs

Group	Pre-ablation	→	Post-ablation
1.	CFAE	→	CFAE
2.	CFAE	→	Non-CFAE
3.	Non-CFAE	→	CFAE
4.	Non-CFAE	→	Non-CFAE

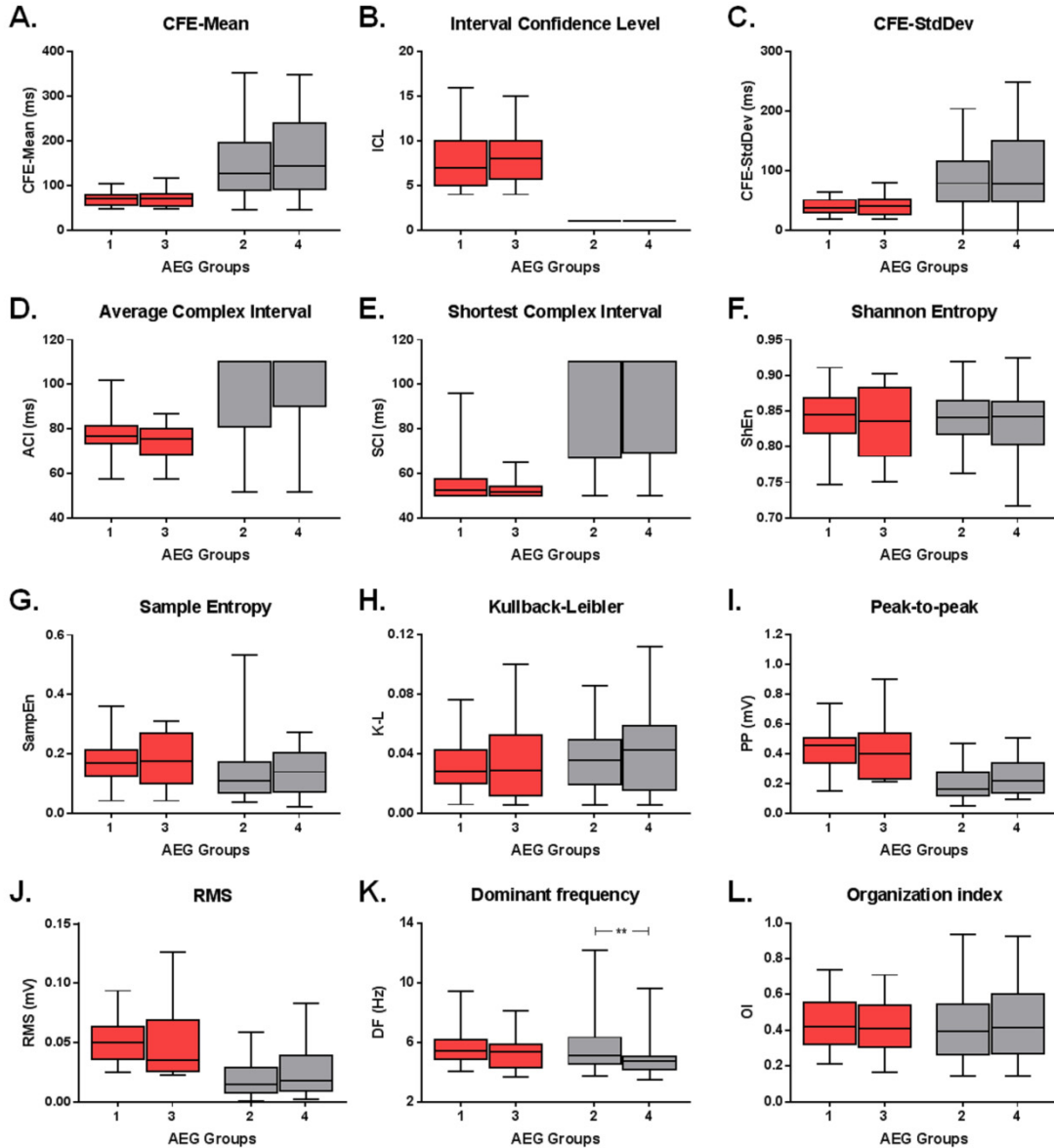


Figure 5-7 The characterization of AEGs in the different groups (1, 2, 3 and 4) at baseline according different indices of fractionation: A. CFE-Mean; B. ICL; C. CFE-StdDev; D. ACI; E. SCI; F. ShEn; G. SampEn; H. K-L; I. PP; J. RMS; K. DF; L. OI.

## 5.4 Discussion

The present work investigated the incidence of AEG fractionation in corresponding atrial regions before and after PVI+RL in persAF patients. This is the first work to analyse the changes in fractionated signals in pre-specified atrial regions following PVI+RL at sites distant to lesions using multiple features measured from the signals, suggesting the co-existence of AEGs that are affected and AEGs that are unaffected by PVI+RL (Lin *et al.*, 2009b). Little correlation was found between the different features, suggesting that the quantification of AEG fractionation remains a great challenge.

### 5.4.1 AEG fractionation as surrogate for AF drivers

CFAEs have been introduced as markers for atrial regions responsible for triggering and perpetuating atrial arrhythmias and as targets for ablation (Nademanee *et al.*, 2004), but failed to provide a definite solution for persAF therapy, as shown by the low reproducibility of ablation outcomes (Deisenhofer *et al.*, 2009, Dixit *et al.*, 2012, Elayi *et al.*, 2008, Lin *et al.*, 2009a, Oral *et al.*, 2009, Verma *et al.*, 2007, Verma *et al.*, 2008a, Verma *et al.*, 2010, Verma *et al.*, 2015). Conceptually, CFAEs are thought to represent the fractionated electric activity resultant from slow or inhomogeneous conduction in atrial regions that underwent structural and electrical remodelling due to sustained AF. These regions could be anchored in the atrium and would be important in triggering and perpetuating atrial arrhythmias (de Bakker and Wittkampf, 2010).

Previous work has reported that some CFAEs are able to identify drivers responsible for AF perpetuation, and the ablation of those regions organizes the arrhythmia (Deisenhofer *et al.*, 2009, Elayi *et al.*, 2008, Lin *et al.*, 2009a, Verma *et al.*, 2007, Verma *et al.*, 2008a, Verma *et al.*, 2010). In other cases, however, CFAEs fail to identify the AF drivers, and ablation of those CFAEs does not organize the arrhythmia (Dixit *et al.*, 2012, Oral *et al.*, 2009, Verma *et al.*, 2015). Consequently, there is intense debate on whether CFAEs represent true AF drivers responsible for AF perpetuation (Takahashi *et al.*, 2008, Verma *et al.*, 2014, Yamabe *et al.*, 2009), or if CFAEs represent a passive phenomenon not important to the maintenance of AF – such as local cycle length (Rostock *et al.*, 2006), distal PV firing (Roux *et al.*, 2009, Tuan *et al.*, 2011), or wave collision in otherwise normal unscarred atrial tissue (Jadidi *et al.*, 2012a).

The present results illustrate the complexity of patient-specific ablation target identification and the challenges to discriminate which CFAEs are surrogates of AF drivers. PVI+RL changed AF behaviour, and distinct atrial regions responded differently to ablation. PVI+RL organized fractionation in large regions of the LA that were fractionated prior to PVI+RL, supporting the perception that CFAE-guided ablation should be performed after PVI and anatomical lines (Lin *et al.*, 2009b).

Nearly half of the AEGs classified as CFAEs at baseline remained fractionated after PVI. Previous work has suggested that PVI+RL would eliminate passive CFAEs created by the existence of PV firing whilst highlighting AEGs unchanged by PVI+RL that might therefore represent non-PV persAF drivers (Lin *et al.*, 2009b). Another interpretation could be that PVI would eliminate some active CFAEs since the purpose of PVI is to isolate active AF drivers.

Similarly, some regions classified as non-CFAE at baseline became CFAE after ablation. While it seems unlikely that these AEGs represent structural scar or anchored atrial substrate as they were not fractionated prior to PVI, they could also represent underlying AF drivers that have moved or have been modulated by ablation.

Finally, even if active AF drivers within the PVs are eliminated by PVI but AF perpetuates secondary to multiple wavelet re-entries in the remodelled atrium, the observed CFAEs collected after PVI would all be a passive phenomenon. This is especially true in persAF in which the atria have undergone significant remodelling.

Nevertheless, the discrimination of the different types of AEGs – i.e., either responsive or unresponsive to PVI+RL – might help in the characterization of atrial substrate in persAF studies.

#### **5.4.2 Multivariate analysis for atrial substrate characterization**

Previous investigations have identified CFAEs using either a single index or visual inspection (Jadidi *et al.*, 2012a, Rostock *et al.*, 2006, Roux *et al.*, 2009, Takahashi *et al.*, 2008, Tuan *et al.*, 2011, Verma *et al.*, 2014, Yamabe *et al.*, 2009). Visual classification of CFAEs introduces subjectivity to the method as each specialist has his/her own perception of what defines significant fractionation, while previous works have shown

that classification performed by distinct methodologies might lead to conflicting results (Almeida *et al.*, 2016, Lau *et al.*, 2015).

A recent study has suggested that different indices of fractionation are not true representations of atrial substrate after showing poor correlation between them (Lau *et al.*, 2015). However, assuming that atrial substrate corresponds to atrial regions that organize AF when ablated, this conclusion can only be validated by assessing the effect of ablation on these indices. In the present study, indices of fractionation also correlated poorly with each other. However, most of those indices were affected by AF ablation. Additionally, both MANOVA and LDA indicate that it is possible to discriminate AEGs that were either changed or unchanged by PVI+RL. This suggests that, individually, the indices of fractionation are insufficient for proper atrial substrate characterization, which may contribute to the inconclusive ablation outcomes targeting CFAEs in persAF therapy. However, despite their low correlation with each other, different indices measure complementary electrophysiological characteristics of the AEG and using these indices in combination provides a more complete characterization of the underlying atrial tissue. For instance, CFE-Mean and CFE-StdDev measure the overall fractionation interval of AEGs based on negative deflections, while ICL, ACI and SCI help to characterize complex intervals considering peaks and troughs. These indices computed by commercial mapping systems have been extensively used to guide persAF ablation with varying outcomes (Deisenhofer *et al.*, 2009, Dixit *et al.*, 2012, Elayi *et al.*, 2008, Lin *et al.*, 2009a, Oral *et al.*, 2009, Verma *et al.*, 2007, Verma *et al.*, 2008a, Verma *et al.*, 2010, Verma *et al.*, 2015). Entropy indices provide a direct estimation of the amplitude distribution of a signal and, therefore, its complexity. Entropy has been reported to effectively identify the core of rotors during AF mapping (Ganesan *et al.*, 2013), which could contribute to investigations using the focal impulse and rotor modulation (FIRM) ablation strategy (Narayan *et al.*, 2012). PP and RMS might help to characterize low amplitude values related with scar cardiac tissue, which have also been proposed as targets for AF ablation (Oakes *et al.*, 2009). DF helps to characterize the main activation wave front in an AEG and might represent atrial regions hosting either rapid ectopic activities or small re-entry circuits that are driving the arrhythmia. It has been suggested that ablation at these sites could be an effective way to organize AF (Sanders *et al.*, 2005).

### 5.4.3 Substrate-based ablation for persAF

Whilst recent studies in persAF ablation suggest that linear ablation in addition to PVI did not improve ablation outcome, the results highlighted the fact that PVI alone is still not adequate (Verma *et al.*, 2015, Wong *et al.*, 2015). Substrate-based atrial ablation had been proposed to be required and early data had suggested positive effects in selected patients (Deisenhofer *et al.*, 2009, Elayi *et al.*, 2008, Lin *et al.*, 2009a, Verma *et al.*, 2007, Verma *et al.*, 2008a, Verma *et al.*, 2010). On the one hand, a stepwise approach was proposed which required iterative extensive ablation at certain anatomical locations including linear lesions (O'Neill *et al.*, 2006). On the other hand, the approach proposed by Nademanee and colleagues aiming at CFAE often involved extensive scattered atrial ablation (Nademanee *et al.*, 2004). With either approach, extensive ablation often caused little or no change, whilst effects can be seen at a certain point of the iterative process that could lead to either AF organization or, more specifically, AF termination. Although the effect of ablating at this final terminating site could be the result of cumulative effects from some or all of the preceding locations, there is increasing interest to identify this 'last' ablation site so it could be targeted 'first'. Further work to improve the understanding of AEG characteristics related with atrial substrate could contribute towards this goal – which would allow us to ablate the *last* lesion *first*.

### 5.4.4 Study limitations

The current study was limited to retrospective data with low resolution CFAE maps. More AEG points would help to consolidate the present results. The linear methods MANOVA and LDA have been used in this study as an initial attempt to discriminate the AEG groups. Non-linear classification methods might be useful to improve the multivariate classification of atrial substrate, but such analysis is beyond the scope of the present work (Schilling *et al.*, 2015).

## 5.5 Conclusions

In this chapter we investigated multiple characteristics of AEGs collected in corresponding atrial regions, before and after PVI+RL. Our results suggest the co-existence of AEGs that are responsive and AEGs that are unresponsive to PVI+RL. Different indices of fractionation have been measured from the AEGs. Individually, these

indices are insufficient for AEG classification. The combination of those indices, however, is effective in identifying complementary characteristics of the AEGs. Multivariate AEG classification should be considered in future studies for better AEG characterization in order to verify if the different types of AEGs relate to AF drivers after persAF ablation.

## Chapter 6

# The spatio-temporal consistency of atrial electrograms in persistent atrial fibrillation

### 6.1 Introduction

PVI has been proved effective in the treatment of pAF (Haissaguerre *et al.*, 1998), but it is less effective for persAF therapy due to structural and electrical changes in the LA (Brooks *et al.*, 2010). Patient-specific ablation targeting atrial substrate has become accepted in addition to PVI in persAF (Calkins *et al.*, 2012c). During AF, AEGs with low amplitude and multiple activations are thought to represent atrial substrate, with structural and electric remodelling (Nademanee *et al.*, 2004).

CFAEs have been introduced as markers of such atrial sites and, therefore, targets for ablation (Nademanee *et al.*, 2004). CFAE-guided ablation has become broadly used as an adjunctive therapy to PVI for persAF (Calkins *et al.*, 2012c). However, the low reproducibility of outcomes (Verma *et al.*, 2008a, Deisenhofer *et al.*, 2009, Lin *et al.*, 2009a, Verma *et al.*, 2010, Oral *et al.*, 2009, Dixit *et al.*, 2012, Elayi *et al.*, 2008) and recent evidences that CFAE ablation additional to PVI does not improve the ablation outcome (Verma *et al.*, 2015, Wong *et al.*, 2015) motivated intense debate on the meaning of the atrial substrate represented by CFAEs. Moreover, there is no consensus about the spatio-temporal dynamics of the underlying mechanisms of AF (Salinet *et al.*, 2013), which might be one of the reasons for the inconsistency in CFAE-guided ablation outcomes in persAF patients.

Some methods for automated CFAE classification consider recording duration segments as short as 2.5 s to measure AEG fractionation (Monir and Pollak, 2008). This is supported by previous works suggesting that AEG fractionation has a high degree of spatial and temporal stability (Redfean *et al.*, 2009, Roux *et al.*, 2008, Scherr *et al.*, 2009, Verma *et al.*, 2008b). However, other works have shown that the assessment of AEG

fractionation requires a recording duration of 5 s at each site to obtain a consistent fractionation (Lin *et al.*, 2008, Stiles *et al.*, 2008, Tsai *et al.*, 2012). In this chapter we sought to investigate the spatio-temporal behaviour of AEGs considering consecutive AEGs with 2.5 s, and also to investigate AEG fractionation using AEGs with 2.5 s, 5 s and 8 s.

## 6.2 Methods

### 6.2.1 Study population

The population consisted of 18 patients (16 male; mean age  $56.1 \pm 9.3$  years; history of AF  $67.2 \pm 45.6$  months) referred to our institution for first time catheter ablation of persAF. Table 6-1 summarizes the clinical characteristics of the study subjects. All patients were in AF at the start of the procedure. Study approval was obtained from the local ethics committee and all procedures were performed with full informed consent.

Table 6-1 Clinical characteristics of study population (N = 18).

Age, yrs	$56.1 \pm 9.3$
Male/Female	16/2
History of AF, months	$67.2 \pm 45.6$
Ejection Fraction,%	$48 \pm 1$
Left Atrial Diameter, mm	$47 \pm 1$
History of coronary artery disease	4
Medication* (number of patients on)	
ACE inhibitor / ARB	11
Amiodarone	10
Beta-blockers	8
Calcium channel blockers	2
Digoxin	1
Sotalol	5

\* All anti-arrhythmic and rate-controlling drugs were stopped for at least five half-lives before the procedure, with the exception of amiodarone. ACE = angiotensin-converting-enzyme; AF = atrial fibrillation; ARB = angiotensin receptor blockers. Values are in mean  $\pm$  SD or n.

## 6.2.2 Electrophysiological study

All antiarrhythmic drugs, except amiodarone, were discontinued for at least 5 half-lives before the start of the procedure. Details of the mapping procedure have been described previously (Tuan *et al.*, 2011). Briefly, 3D LA geometry was created within NavX using a deflectable, variable loop circular PV mapping catheter (Inquiry Optima, St. Jude Medical). PVI was performed with a point-by-point wide area circumferential ablation approach, followed by the creation of a single roof line (Cool Path Duo irrigated RF catheter, St. Jude Medical). No additional ablation targeting CFAE was performed in this study. Sequential point-by-point bipolar AEGs were collected from 15 pre-determined atrial regions before and after LA ablation (Tuan *et al.*, 2011). All patients were in AF before and after ablation during signal collection.

## 6.2.3 Signal analysis

A total of 797 AEGs were recorded from the LA, 455 before and 342 after PVI, with a sampling frequency of 1200 Hz, and band-pass filtered within 30–300 Hz. When an improvement of signal-to-noise ratio was necessary, a 50 Hz Notch filter was applied.

Each AEG was exported from NavX with three segment lengths (2.5 s, 5 s and 8 s). A validated offline MATLAB algorithm was used to compute the ICL, ACI and SCI as defined by the CARTO criteria for CFAE classification – see *Appendix A, Validation of an Offline Algorithm to reproduce CARTO CFAE definition for CFAE identification* (Almeida *et al.*, 2016).  $ICL \geq 4$  was considered for CFAE classification.

The LA maps of the 18 patients were segmented by an experienced clinician into 6 regions – PVs; roof; posterior; anterior; septum and; lateral. The analyses described below consider the combined data before and after PVI+RL (total 797 AEGs). Detailed analyses before (455 AEGs) and after (342 AEGs) PVI+RL are provided in the *Appendix F, the spatio-temporal consistency of atrial electrograms in persistent atrial fibrillation before and after PVI+RL*.

## 6.2.4 Temporal consistency of AEG fractionation with different segment lengths

CFAE classifications performed in AEGs with different segment lengths have been analysed to investigate the temporal consistency of AEG fractionation. The configuration

of the different segment lengths as exported from NavX is illustrated on Figure 6-1A. The maximum AEG length that can be exported from NavX is 8 s, and smaller segments are exported as portions of the original 8 s. The 2.5 s segment of data corresponds to the interval from 5-s to 7.5-s of the entire segment, while the 5 s segment corresponds to the interval between 3 s and 8 s.

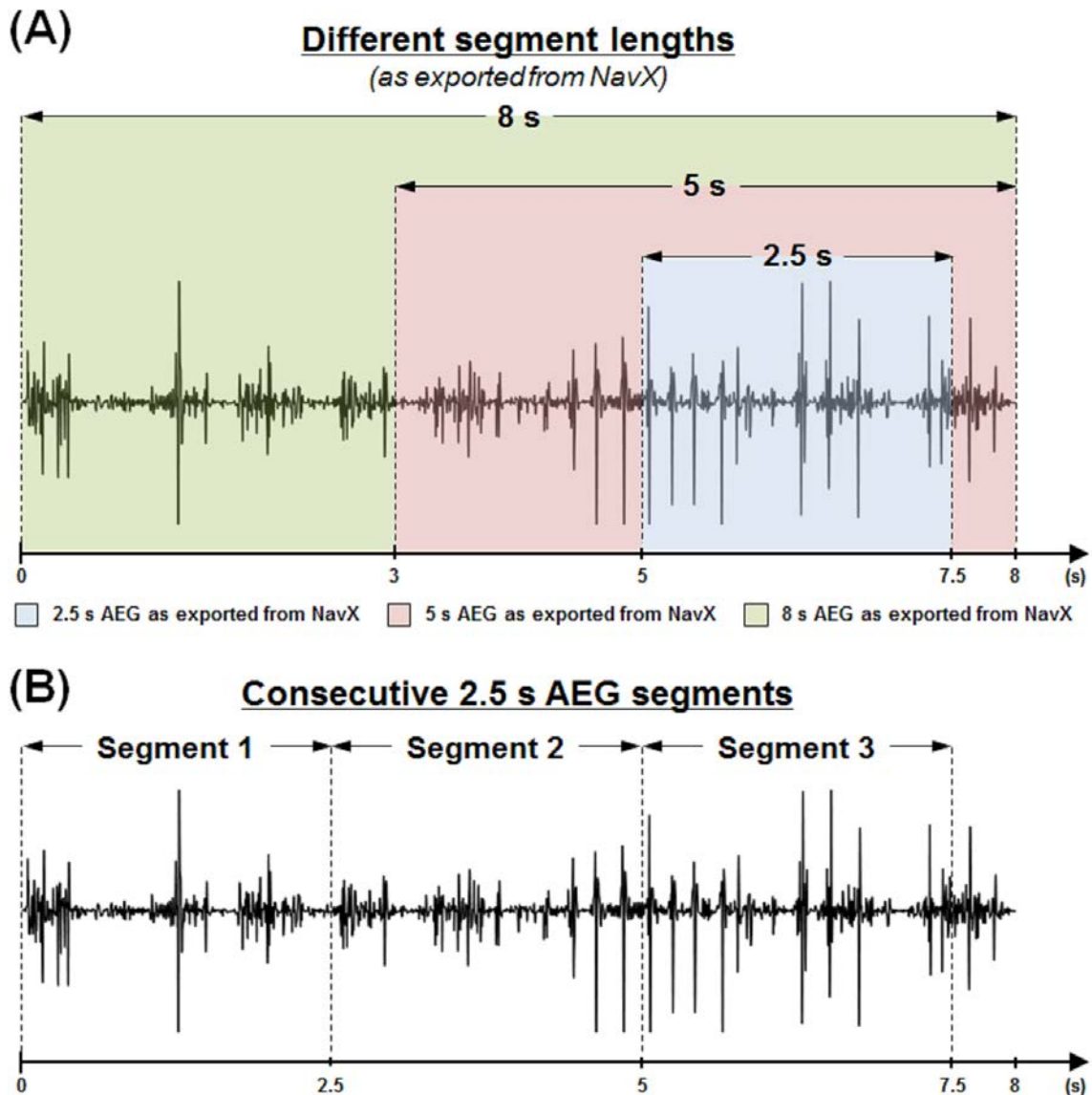


Figure 6-1 A. Different segment lengths exported from NavX to investigate the temporal consistency of AEG fractionation. The maximum AEG length that can be exported from NavX is 8 s, and smaller segments are exported as portions of the original 8 s. B. The 8 s segments were divided in three consecutive 2.5 s segments, as illustrated in Figure 1B, accordingly: 0 to 2.5 s; 2.5 s to 5 s; 5 s to 7.5 s.

The ICL for 2.5 s, 5 s and 8 s segments were measured. Currently, ICL thresholding for CFAE classification as defined by CARTO is referred to a default 2.5 s segment length ( $ICL \geq 4$ ). Hence, there is no validated ICL threshold for CFAE classification using segment lengths longer than 2.5-s. Therefore, the ICL calculated for the 5 s segment lengths was normalized by a factor of 2, while the ICL calculated for the 8 s segment lengths was normalized by 3.2. For instance, if  $ICL = 8$  inside a 5 s segment, the normalized ICL is 4 for a corresponding 2.5 s segment. Similarly, if  $ICL = 12$  inside an 8 s segment, the normalized ICL is also 4, approximately. That allowed a head-to-head comparison between ICL as measured with 2.5 s, 5 s and 8 s. Bland-Altman plots were created to assess the average difference (bias) from the ICL, ACI and SCI measured with the different segment lengths.

### **6.2.5 Temporal behaviour of consecutive AEGs**

Consecutive AEG segments were assessed to infer about AEG temporal behaviour. For each AEG, the 8 s segments were divided in three consecutive 2.5 s segments, as illustrated in Figure 6-1B, accordingly: 0 to 2.5 s; 2.5 s to 5 s; 5 s to 7.5 s. Therefore, three consecutive segments with 2.5 s length were created for each one of the 797 AEGs, allowing the investigation of the temporal behaviour in the same points. The ICL was measured for each segment, and each segment was compared to the other. A best fit exponential was computed to estimate the time constant of stable AEGs according to Graphpad Prism 6's (©2014 GraphPad Software, La Jolla, California) One Phase Decay best fit.

### **6.2.6 Statistical analysis**

All continuous non-normally distributed variables are expressed as median  $\pm$  interquartile interval. Nonparametric paired multiple data were analysed using the Friedman test with Dunn's correction. Spearman's correlation ( $\rho$ ) was calculated to quantify the correlation between AEG classifications measured with different segment lengths (2.5 s, 5 s and 8 s), and the correlation between AEG classifications measured within the three consecutive segments.

The agreement of CFAE classification performed by ICL – either measured with different segment lengths (2.5 s, 5 s and 8 s) or within the three consecutive segments – was

assessed by the Cohen's kappa ( $\kappa$ ) score (Cohen, 1968). A Kappa score within range  $0 \leq \kappa < 0.4$  suggests marginal agreement between two indices;  $0.4 \leq \kappa \leq 0.75$  good agreement and;  $\kappa > 0.75$  excellent agreement (Landis and Koch, 1977). P-values of less than 0.05 were considered statistically significant.

## 6.3 Results

### 6.3.1 Temporal behaviour of consecutive AEGs

Three types of AEGs have been identified when investigating the consecutive segments, as illustrated in Figure 6-2: 'stable CFAEs' (upper trace) as AEGs with  $ICL \geq 4$  in all assessed segments; 'stable non-CFAEs' (middle trace) as AEGs with  $ICL < 4$  in all assessed segments and; 'unstable AEG' (lower trace) as AEGs with  $ICL$  varying to and from  $ICL \geq 4$  to  $ICL < 4$  within the assessed segments. Each AEG segment also affected the resulting CFAE map as generated by ICL, ACI and SCI (Figure 6-3). The location of the AEGs classified as stable CFAE, stable non-CFAE and unstable shown in Figure 6-2 are also marked in the ICL map in Figure 6-3.

Moderate correlation was found in the AEG classification performed by ICL, ACI and SCI, measured in each consecutive segment, as shown in Table 6-2. The average correlation for ICL within the three segments was  $\rho = 0.74 \pm 0.01$  (mean  $\pm$  SD), while ACI was  $\rho = 0.44 \pm 0.02$ , and SCI was  $\rho = 0.55 \pm 0.03$ . The average agreement of CFAE classification performed by ICL between segments was  $\kappa = 0.64 \pm 0.04$ .

The temporal behaviour of the three consecutive segments for each collected point is shown on Figure 6-4. 85% of the AEGs initially classified as fractionated in segment 1 remained fractionated in segment 2, while 15% changed from fractionated to non-fractionated. Similarly, 77% of the AEGs classified as non-fractionated in segment 1 remained non-fractionated in segment 2, while 23% changed from non-fractionated to fractionated. In the following segments, 87% of AEGs classified as fractionated in segment 2 remained fractionated in segment 3, while 13% changed from fractionated to non-fractionated. 80% of the AEGs classified as non-fractionated in segment 2 remained non-fractionated in segment 3, while 20% changed from non-fractionated to fractionated.

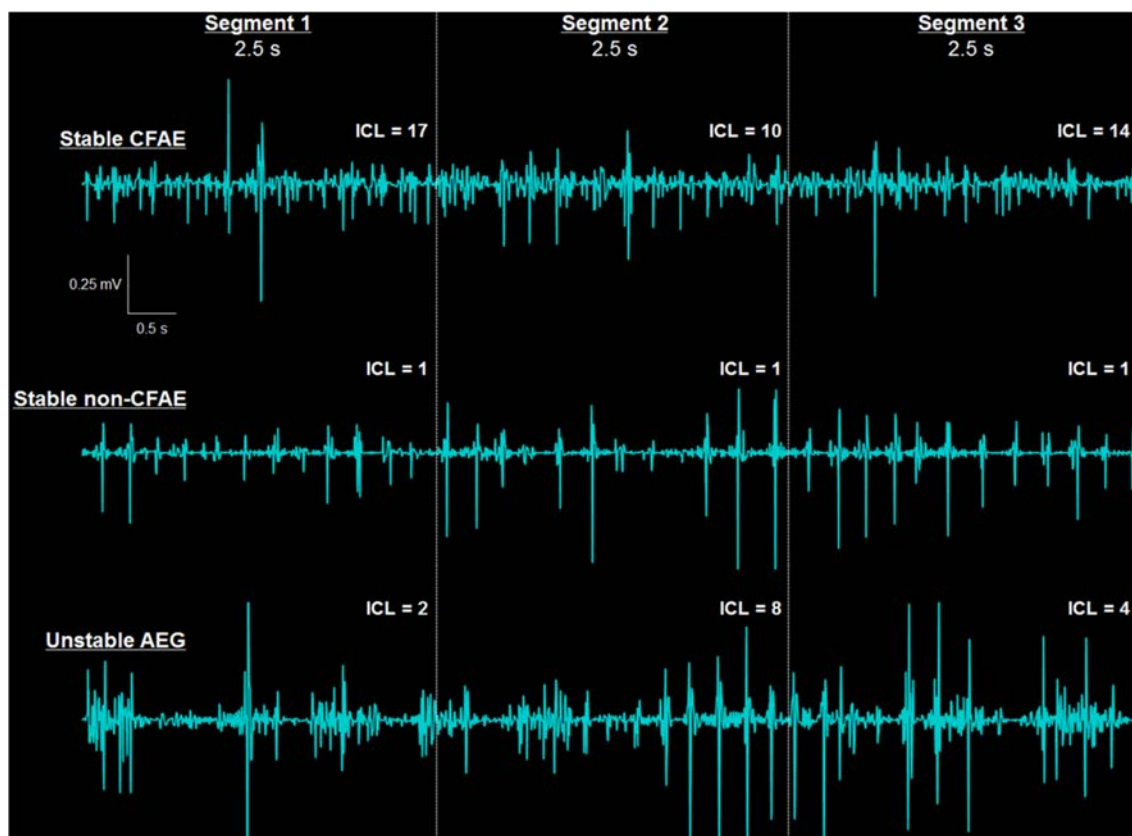


Figure 6-2 Illustration of the different types of AEGs found when analysing the consecutive AEG segments. Stable CFAEs (upper trace) are AEGs with  $ICL \geq 4$  in all assessed segments (upper trace). Stable non-CFAEs (middle trace) are AEGs with  $ICL < 4$  in all assessed segments. Unstable AEG (lower trace) are AEGs with ICL varying from  $ICL \geq 4$  to  $ICL < 4$  within the assessed segments.

Table 6-2 Spearman's correlation and Kappa score for ICL, ACI and SCI measured from the consecutive 2.5 s AEG segments.

2.5 s AEG segment	1 vs 2	1 vs 3	2 v 3	P value*	
Spearman's correlation ( $\rho$ )	ICL	0.735	0.726	0.748	<0.0001
	ACI	0.455	0.430	0.421	<0.0001
	SCI	0.554	0.521	0.569	<0.0001
Kappa score ( $\kappa$ )	0.616	0.620	0.676	<0.0001	

\* P-values for all cases.

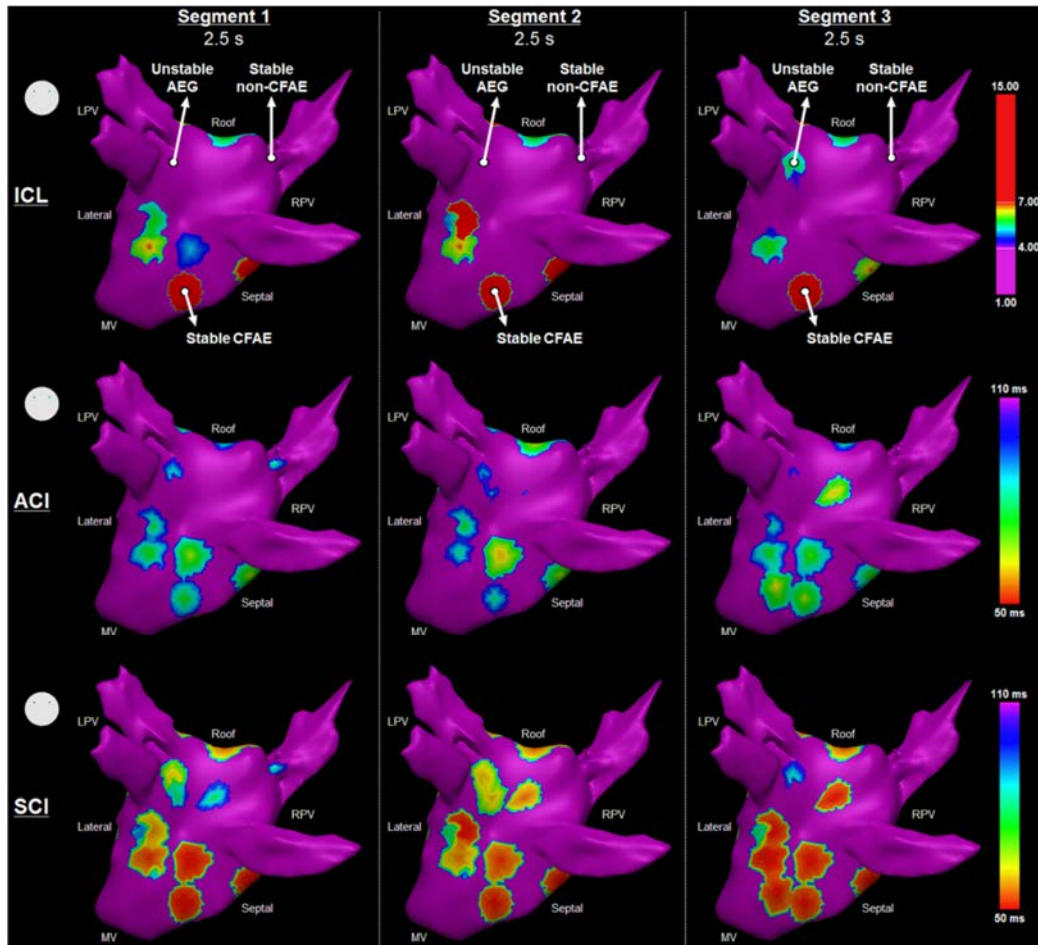


Figure 6-3 The resultant LA maps based on the three consecutive AEG segments with 2.5 s duration each for one patient as measured by ICL (upper), ACI (middle) and SCI (bottom). The location of the AEGs classified as stable CFAE, stable non-CFAE and unstable shown in Figure 6-2 are marked in the ICL map.

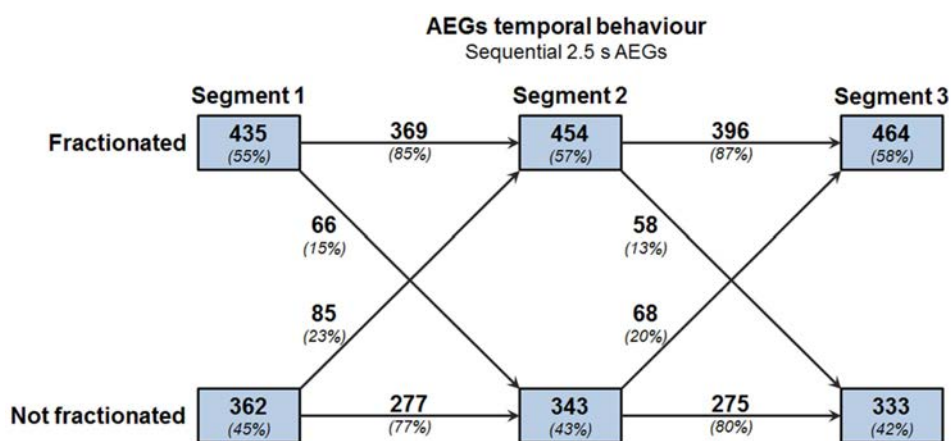


Figure 6-4 The temporal behaviour of three consecutive AEG segments with 2.5 s duration each. The 8 s segments were divided in three consecutive 2.5 s length segments. The ICL was measured in each segment and classified whether as fractionated or non-fractionated. The AEGs that remained fractionated, remained non-fractionated and changed classification were assessed between segments.

When comparing segment 1 versus 2, 47% of the total AEGs were labelled as stable CFAEs, while 35% were stable non-CFAEs, and 18% AEGs were unstable (Figure 6-5A). When comparing segment 2 versus 3, 49% of the total AEGs were labelled as stable CFAEs, 35% were stable non-CFAEs, and 16% AEGs were unstable. A total of 43% AEGs were stable CFAEs within the three segments, 31% were stable non-CFAEs and 26% were unstable.

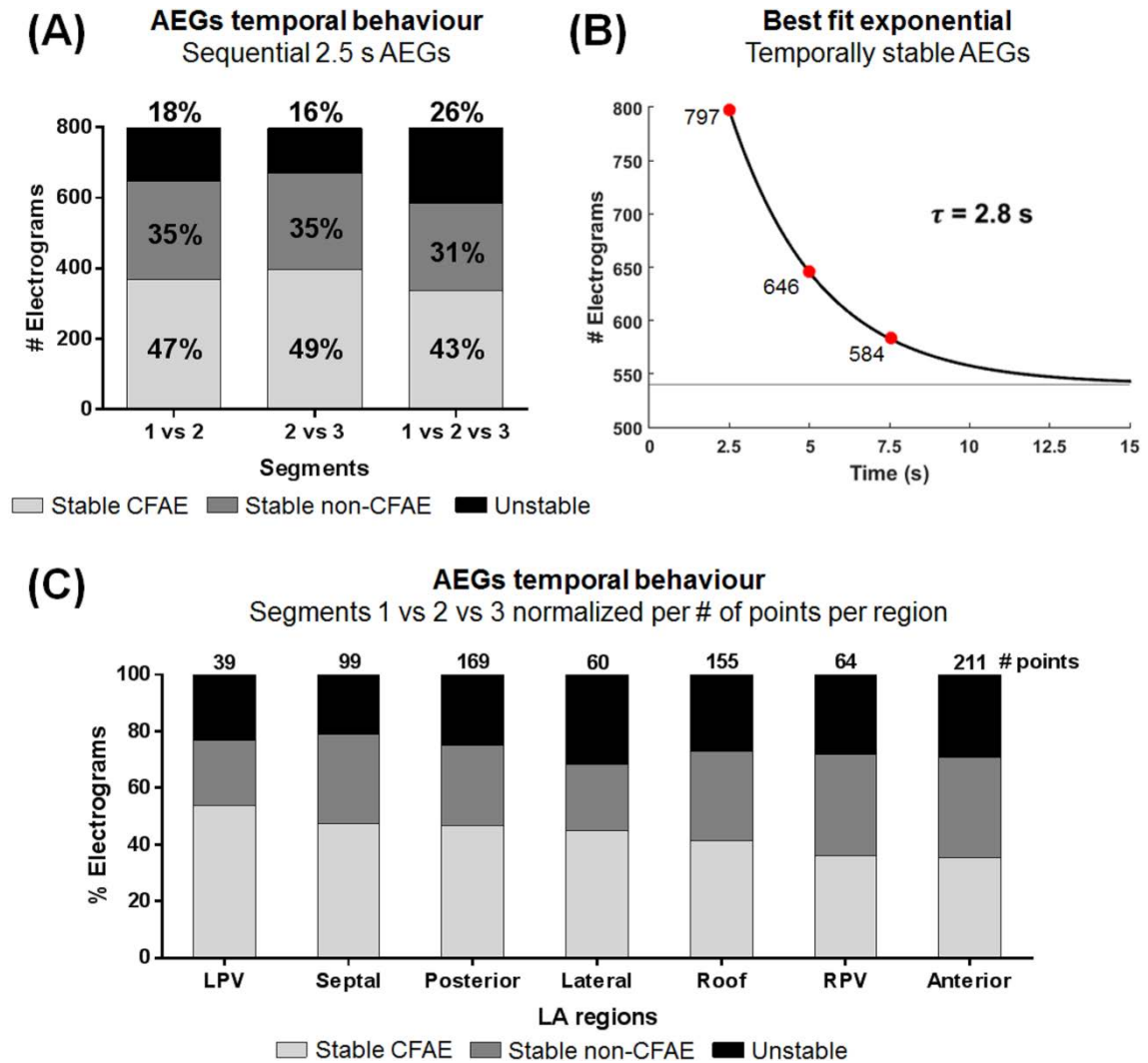


Figure 6-5 A. All AEG segments were mutually compared. The percentage of ‘stable CFAE’, ‘stable non CFAE’ and ‘unstable AEG’ in each segment was calculated. B. The temporal decay of stable AEGs was assessed. In the first 2.5 s segment, all AEGs were considered stable. On segment 2, a total of 151 AEGs were classified as unstable. On the last segment, additional 62 AEGs changed their classification. The exponential best fit with a temporal decay with time constant ( $\tau$ ) of 2.8 s. C. The regional occurrence of the different types of AEGs normalized by the number of collected points per region.

Figure 6-5B illustrates the temporal decay of stable AEGs (CFAEs and non-CAFE). In the first 2.5 s segment, all AEGs were considered stable since it was the first classification (797 AEGs). On segment 2, a total of 151 AEGs were classified as unstable, remaining 646 stable AEGs. On the last segment, additional 62 AEGs changed their classification, remaining 584 stable AEGs. The exponential best fit suggests a temporal decay with time constant ( $\tau$ ) of 2.8 s, in which 540 AEGs (68% of 797 AEGs) would be temporally stable.

The occurrence of the different types of AEGs (stable CFAE, stable non-CFAE and unstable AEG) per LA region, considering the three AEG segments, is shown in Figure 6-5C. Stable CFAEs were observed in all regions, with the anterior wall showing the highest incidence, followed by the septum, lateral, posterior wall, roof and PVs. Unstable AEGs were also observed in all regions, with the LPV showing the highest incidence.

Although PVI+RL reduced AEG fractionation in all regions, unstable AEGs were still present at baseline and after ablation (see *Appendix F, The spatio-temporal consistency of atrial electrograms in persistent atrial fibrillation before and after PVI+RL*). In particular, the reduction in AEG fractionation after ablation was more evident in the AEGs collected in the PVs, as well as fewer unstable AEGs were identified in these regions after PVI+RL. The exponential best fit indicated similar AEG temporal behaviour before and after PVI+RL ( $\tau = 2.7$  s and 3 s, respectively).

### **6.3.2 Temporal consistency of AEG fractionation with different segment lengths**

There was no significant difference between ICL measured with 5 s versus 2.5 s and 8 s, as illustrated by Figure 6-6A. However, ICL measured with 2.5 s was significantly different than with 8 s. The bias calculated from the Bland-Altman plots suggests a smaller average difference between ICL calculated with 5 s and 8 s when compared with the other segment lengths (2.5 s vs 5 s and 2.5 s vs 8 s, Figure 6-6B).

Different segment lengths had little influence on ACI, but significantly affected SCI (Figure 6-6A). From the Bland-Altman plots, it is possible to infer that SCI calculated with longer segment lengths will assume smaller values. A longer AEG segment length increases the probability of a shorter complex interval to occur when compared to shorter AEG segments, which would explain the high influence of the segment lengths on the

SCI. Nevertheless, the Bland-Altman plots also suggest smaller average difference between 5 s and 8 s for both ACI and SCI. Similar results have been found when looking into the data separately before and after PVI+RL (please see *Appendix F, The spatio-temporal consistency of atrial electrograms in persistent atrial fibrillation before and after PVI+RL*).

The AEGs with 5 s generated more similar AEG classification compared to 8 s, as shown in Table 6-3. The Spearman's correlation was higher for 5 s vs 8 s for ICL, ACI and SCI, than 2.5 s vs 5 s and 2.5 s vs 8 s. The Kappa score also suggests higher agreement in the CFAE classification performed by 5 s and 8 s segments. Figure 6-7 illustrates graphically an example of the resulting AEG classification map for ICL, ACI and SCI measured with 2.5 s, 5 s and 8 s segment lengths. AEG classification maps for the other patients are provided in the *Appendix F, The spatio-temporal consistency of atrial electrograms in persistent atrial fibrillation before and after PVI+RL*.

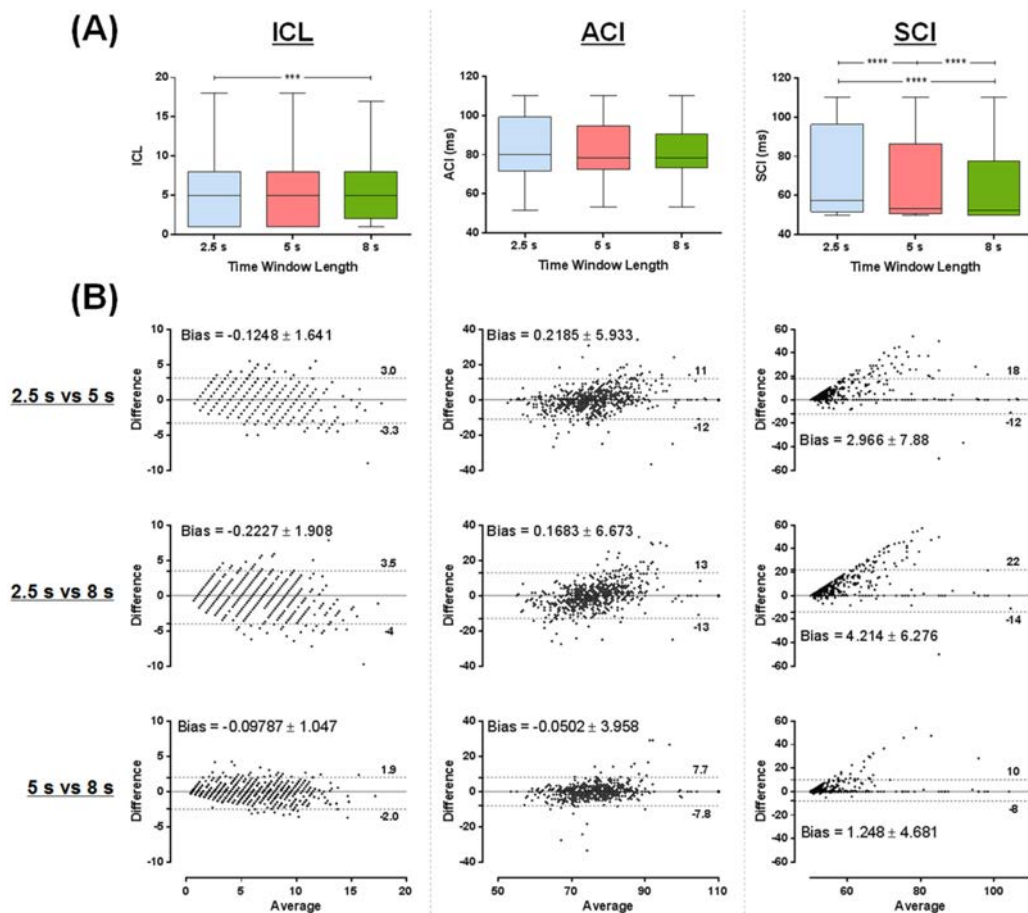


Figure 6-6 A. The ICL, ACI and SCI measured with 2.5 s, 5 s and 8 s. B. Bland-Altman plots for ICL, ACI and SCI measured with 2.5 s, 5 s and 8-s. \*\*\*\* P<0.0001; \*\*\* P<0.001.

Table 6-3 Spearman’s correlation and Kappa score for ICL, ACI and SCI measured from the different segment lengths (2.5 s, 5 s and 8 s).

AEG segment lengths		2.5 s v 5 s	2.5 s v 8 s	5 s v 8 s	P value*
Spearman’s correlation ( $\rho$ )	ICL	0.925	0.897	0.960	<0.0001
	ACI	0.885	0.851	0.932	<0.0001
	SCI	0.872	0.818	0.921	<0.0001
Kappa score ( $\kappa$ )		0.836	0.780	0.874	<0.0001

\* P-values for all cases.

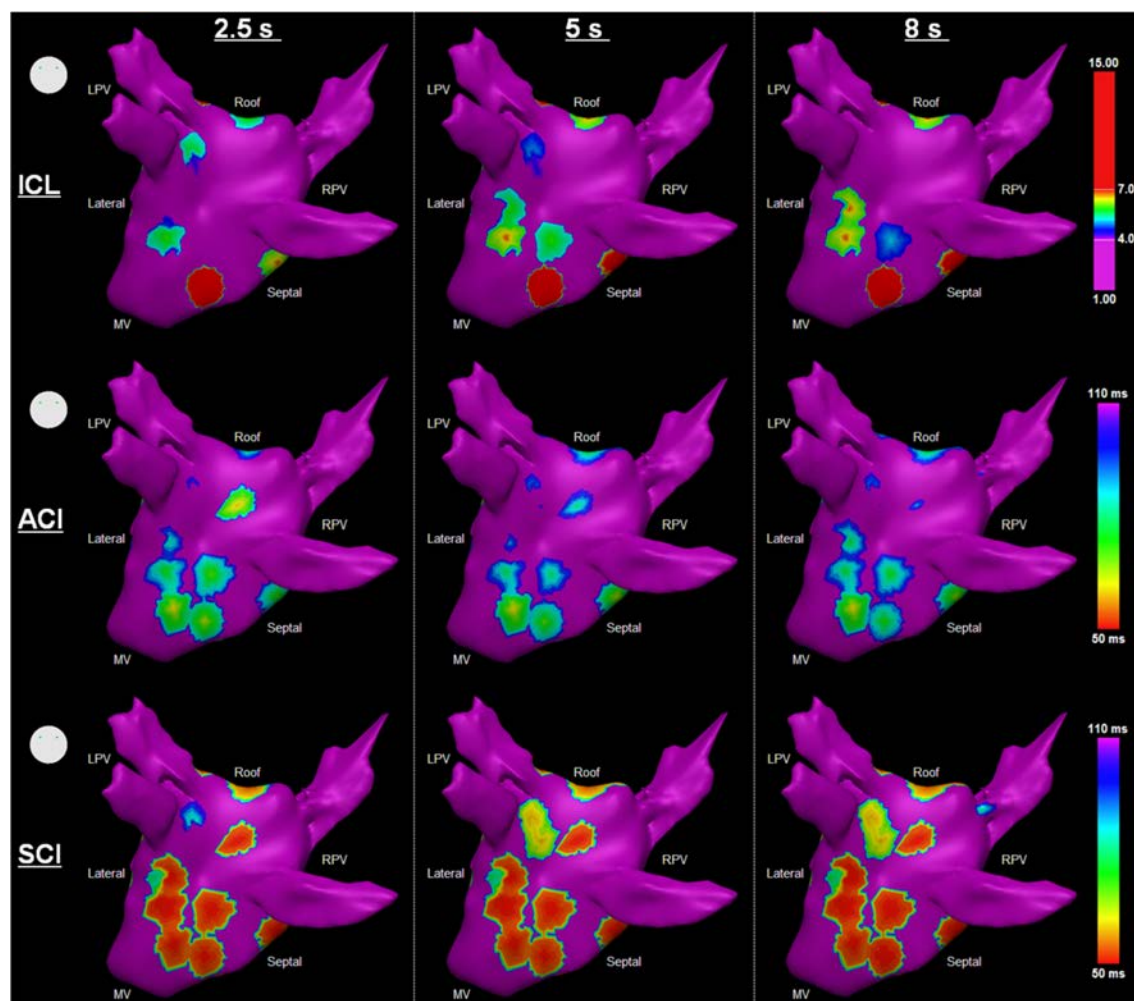


Figure 6-7 The resultant LA maps based on the different segment lengths (2.5 s, 5 s and 8 s) for one patient as measured by ICL (upper), ACI (middle) and SCI (bottom).

## **6.4 Discussion**

This is the first work to assess the spatio-temporal behaviour of AEGs in the same collected points using consecutive segments, while different AEG durations have been analysed for fractionation consistency along time. The results suggest that the ablation target identification performed with the CARTO criterion using 2.5 s AEGs is dependent on the time instant that the AEGs are collected. AEGs with 2.5 s might be insufficient to detect stable fractionation and 5 s or longer should be preferred for consistent AEG classification.

### **6.4.1 Patient-specific atrial substrate in persAF**

AF sustained for long periods of time may induce structural and electrical remodelling in the atrial tissue (de Bakker and Wittkamp, 2010). These regions are believed to be anchored in the atrium, representing areas of remodelled atrial substrate, important in triggering and perpetuating atrial arrhythmias. AEGs acquired from such regions demonstrate low amplitude, multiple deflection activations that characterize fractionated activity due to slow or inhomogeneous conduction. The ablation of atrial regions hosting fractionated AEGs had been accepted by many as a useful additional therapy for persAF treatment (Calkins *et al.*, 2012b).

With this premise, atrial regions hosting fractionated AEGs could be surrogates for atrial substrate (Nademanee *et al.*, 2004). As a consequence, targeting those regions during ablation could organize or terminate the arrhythmia. However, CFAE-guided ablation has produced conflicting outcomes in previous electrophysiological studies, suggesting that not all fractionated AEG is a surrogate for atrial substrate and, therefore, not all CFAEs should be targets for ablation (Deisenhofer *et al.*, 2009, Dixit *et al.*, 2012, Elayi *et al.*, 2008, Lin *et al.*, 2009a, Oral *et al.*, 2009, Verma *et al.*, 2008a, Verma *et al.*, 2010, Verma *et al.*, 2015, Wong *et al.*, 2015).

### **6.4.2 The temporal behaviour of AEGs during persAF**

Despite much effort to understand atrial substrate properties during persAF (Lin *et al.*, 2008, Roux *et al.*, 2008, Scherr *et al.*, 2009, Stiles *et al.*, 2008, Tsai *et al.*, 2012, Verma *et al.*, 2008b), the dynamic nature of some AEGs continues to pose challenge for electrophysiologists in search of critical sites for ablation (Salinet *et al.*, 2013, Redfearn

*et al.*, 2009, Roux *et al.*, 2008, Scherr *et al.*, 2009, Verma *et al.*, 2008b, Lin *et al.*, 2008, Stiles *et al.*, 2008, Tsai *et al.*, 2012).

Previous works have suggested that CFAEs demonstrate a high degree of spatial and temporal stability by analysing consecutive CFAE maps where the AEGs for each map are collected in different time instants (Redfearn *et al.*, 2009, Roux *et al.*, 2008, Scherr *et al.*, 2009, Verma *et al.*, 2008b). Our results, however, suggest that ablation target identification using the CARTO criterion is dependent on the time instant that the AEGs are collected. Some AEGs have unstable temporal behaviour, switching from fractionated to non-fractionated depending on the moment it is collected. This would affect the resulting CFAE map and, therefore, both ablation strategy and outcomes. Considering that the atrial substrate is anchored and should host “stable” fractionated activity, atrial regions represented by unstable AEGs should not be targeted during ablation as they might be a result of passive wave collision from remote AF drivers and, therefore, not a true representation of atrial substrate (Jadidi *et al.*, 2012a, Rostock *et al.*, 2006, Roux *et al.*, 2009, Tuan *et al.*, 2011). Ablation of those regions might create areas of slow or anisotropic conduction, thereby creating more pro-arrhythmogenic areas which would perpetuate the arrhythmia instead of organizing or terminating it (Zaman and Narayan, 2015).

The results also suggest that ablation is effective in reducing both AEG fractionation and unstable AEGs, as illustrated in the *Appendix F, The spatio-temporal consistency of atrial electrograms in persistent atrial fibrillation before and after PVI+RL*. Considering that, in the present study, ablation targeted the PVs and the roof, the ablation effect was more evident in those regions, in particular the PVs. As a consequence, PVI+RL resulted in more organized atrial activations in those areas when compared to the others.

#### **6.4.3 The AEG duration for atrial substrate assessment**

Previous work has investigated different segment lengths to consistently characterize CFAEs using NavX, since this system allows for different AEG duration recordings (1 s to 8 s). Published data suggest AEG duration of 5 s or longer to consistently measure CFAEs using NavX algorithm (Lin *et al.*, 2008, Stiles *et al.*, 2008). As CARTO inherently limits the AEG collection to 2.5 s, few studies accomplished an investigation for the ‘best’

segment length to assess fractionation, also suggesting that 5 s should be considered for proper AEG classification (Tsai *et al.*, 2012).

Our results suggest that AEG duration of 2.5 s might not be sufficient to measure CFAEs consistently using CARTO criterion. If CFAEs were temporally consistent, it would be expected for the recording duration to have little influence in the CFAE classification and, ultimately, the CFAE map created with CARTO criterion measured with 2.5 s should not differ from maps created using 5 s or 8 s. Our results, however, suggest that longer segment lengths produce more consistent CFAE maps. Therefore, CARTO criterion should be revisited to consider recording durations of 5 s or longer to measure AEG fractionation.

#### **6.4.4 Limitations**

The present chapter represents a retrospective investigation of the spatio-temporal behaviour of AEGs during persAF. Prospective studies using AEGs with 5 s or longer in the identification of ablation targets using the CARTO criteria would be helpful for further understand the underlying spatio-temporal behaviour of the atrial substrate in persAF. Additional points to calculate the one phase decay best fit could improve the estimation of the temporal constant for AEGs.

#### **6.5 Conclusions**

This chapter investigated the temporal behaviour of AEGs collected during persAF and the temporal consistency of fractionation considering different AEG segment lengths. Three types of AEGs have been described by investigating consecutive AEGs: stable CFAEs, stable non-CFAEs and unstable AEGs. Different segment lengths produced different AEG classifications as performed by the CARTO criterion. Longer time windows provide a more consistent measure of fractionation than 2.5 s, as limited by the CARTO system.

## Chapter 7

# Main findings and future investigations

Multiple mechanisms are likely to co-exist during the initiation and perpetuation of AF, including multiple rapid ectopic activities, multiple wavelets meandering and multiple circuit re-entries, especially in persAF. As a consequence of this underlying complexity, the identification of targets for persAF ablation remains challenging. Although CFAE-guided ablation became a consolidated therapy for persAF complementary to PVI, conflicting ablation outcomes have cast doubt on the efficacy of this approach, and CFAEs have been openly criticized for AF therapy.

Indeed not all AEG fractionation might be a CFAE – considering the concept that a CFAE is a representation of AF drivers – but some fractionated AEGs are surrogates of critical sites for AF maintenance, and better characterization of these may result in better outcomes in persAF ablation. CFAE-guided ablation is, and will continue to be, an important procedure in the treatment of AF. But a thorough re-evaluation of the definition of CFAE is necessary in order to refine the identification of atrial regions responsible for the perpetuation of the arrhythmia in patients with persAF.

In the present thesis, we investigated current methods for AEG fractionation classification during persAF and their relationship with the underlying mechanisms for AF maintenance and perpetuation. In particular, potential contributing factors concerning the low reproducibility of CFAE-guided ablation outcomes in persAF therapy have been explored, such as inconsistencies in automated CFAE classification, the co-existence of different types of CFAEs, and insufficient AEG duration for CFAE detection.

### 7.1 Main Findings

The results presented in this thesis allowed for the following findings and contributions to the field:

- CFAE mapping and ablation target identification may vary for the same individual, depending on the system being used and settings being applied. This is direct evidence that there is currently no consensus on CFAE definition and that different EAM systems are assessing different aspects of the AEGs during substrate mapping in AF (Almeida *et al.*, 2013a, Almeida *et al.*, 2014, Almeida *et al.*, 2015a, Almeida *et al.*, 2015b, Almeida *et al.*, 2015c, Almeida *et al.*, 2016).
- Revised thresholds have been found for both primary and complementary indices – as measured by NavX and CARTO – to minimize the differences in CFAE classification performed independently by either system. This is the first work to propose defined thresholds and guidelines for the complementary indices to characterize CFAE based on the agreement between the two EAM systems, NavX and CARTO. These thresholds would help to counterbalance the differences of automated CFAE classification performed by each system and facilitate comparisons of CFAE ablation outcomes guided by either NavX or CARTO in future works (Almeida *et al.*, 2014, Almeida *et al.*, 2015a, Almeida *et al.*, 2015b, Almeida *et al.*, 2015c, Almeida *et al.*, 2016).
- We have shown that AEGs that are either affected or unaffected by PVI+RL co-exist during persAF. These different types of AEGs – i.e., either responsive or unresponsive to PVI+RL – might represent different types of AF drivers. Although single descriptors measured from the AEGs were not able to discriminate the different types of AEGs individually, we showed that multivariate analysis using multiple descriptors measured from the AEGs can be used to effectively discriminate the different types of AEGs and might help in the characterization of atrial substrate in persAF studies. This work represents an initial step towards multivariate AEG classification for atrial substrate characterization (Almeida *et al.*, 2013b, Almeida *et al.*, 2013c).
- The identification of ablation targets with CARTO criterion using 2.5 s segment lengths is dependent on the time instant when the AEGs are collected. The results also suggest that AEG duration of 2.5 s might not be sufficient to measure CFAEs consistently using CARTO criterion. AEGs with 5 s generated more similar AEG classification compared to 8 s than AEGs with 2.5 s. Therefore, CARTO criterion

should be revisited to consider recording durations of 5 s or longer to measure AEG fractionation.

## **7.2 Future Investigations**

The results reported in this thesis helped to identify and define future investigations. Some of the suggestions below are already being conducted by the current researchers from the Bioengineering group in collaboration with the Cardiovascular Science group, both from the University of Leicester, and other opportunities might be considered for future PhD students.

### **7.2.1 CFAE EStimation imPRovement based on the agreement between EnSite NavX and BioSense CARTO (CFAE ESPRESSO)**

The definition of CFAE for ablation of persAF is currently vague. The two major commercial systems available are not always concordant in their classification of CFAEs for ablation of persAF. We hypothesize that the definition of CFAE can be consistently constrained by the concurrent application of CFAE-classification algorithms from the two major commercial systems currently available, and that this constrained definition will be useful in guiding persAF ablation after PVI+RL.

The revised thresholds found for both primary and complementary indices as measured by each EAM system investigated on Chapter 4 were estimated from retrospective data. These thresholds will be used prospectively in the identification of ablation targets during substrate mapping for further validation. The pilot study, entitled the CFAE EStimation imPRovement based on the agreement between EnSite NavX and BioSense CARTO (CFAE ESPRESSO), is being currently conducted in Glenfield Hospital led by Prof. G. André Ng. Two protocols for CFAE ESPRESSO have been proposed, one for NavX (Figure 7-1) and other for CARTO (Figure 7-2). The CFAE map in NavX will be created with the following settings: deflection duration 10 ms, refractory period 30 ms, peak-peak sensitivity 0.05 mV, 2.5 s window lengths (8 s data for retrospective analysis only). The colour bar for CFE-Mean will be set at  $\leq 84$  ms, and the colour bar for CFE-StdDev will be set at  $\leq 47$  ms. The overlapping regions between the CFE-mean and CFE-StdDev maps – as illustrated by Figure 7-1 – will be targeted for ablation.

# CFAE ESPRESSO – Pilot Study

CFAE Estimation imProvement based on the agreement between  
EnSite NavX and BioSense CARTO

## Protocol for EnSite NavX

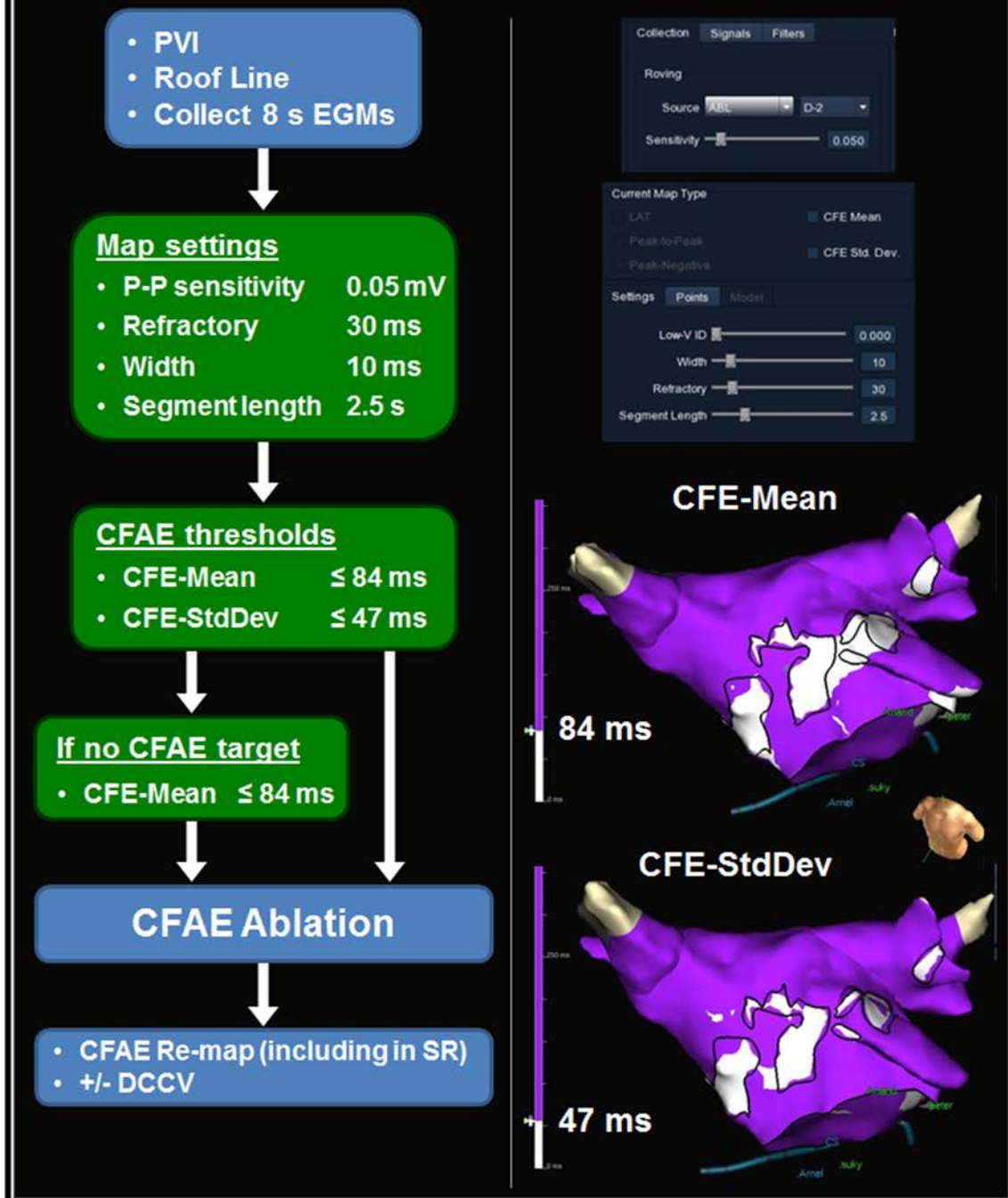


Figure 7-1 The CFAE ESPRESSO protocol for NavX.

Similarly, the CFAE map in CARTO will be created with the following settings: thresholds values set at 0.05–0.15 mV; duration times 50–110 ms; confidence level low = 3 and high = 4. The colour bar for ICL will be set at  $\geq 4$ , the colour bar for ACI  $\leq 82$  ms, and for SCI  $\leq 58$  ms. The overlapping regions between the ICL, ACI and SCI maps – as illustrated by Figure 7-2 – will be targeted for ablation.

The CFAE ESPRESSO pilot study will recruit a total of twenty patients undergoing persAF ablation: ten patients will have CFAE ablation guided by NavX and ten by CARTO. Only persAF patients in AF at the moment of the procedure will be included. PVI+RL will be performed followed by CFAE-guided ablation. Patients will be excluded from the ESPRESSO cohort if PVI+RL results in SR. AEGs will be collected for CFAE classification after PVI+RL. The AEGs will be pre-processed with notch filter at 50 Hz, and band-pass filtered in 30–300 Hz.

### **7.2.2 Multivariate characterization of atrial substrate in persAF patients**

Identifying AEGs that represent critical atrial regions to the maintenance of AF remains challenging. The characteristics of AEGs correlating with AF organization and/or termination have been investigated previously (Haissaguerre *et al.*, 2005b, Heist *et al.*, 2012, Lin *et al.*, 2013, Porter *et al.*, 2008, Schmitt *et al.*, 2007, Takahashi *et al.*, 2008). These AEGs would represent the ground truth for AF ablation and, therefore, the true representation of the atrial substrate in persAF. However, most of those works have relied on few, if not only one, AEG descriptors, which can be a limiting factor when describing a complex phenomenon such as persAF. Additionally, none of those works have performed an integrated multivariate analysis using different indices of fractionation to characterise the AEGs related with AF termination. Combined multiple indices of fractionation and multivariate analysis is, therefore, crucial for investigating different features of the AEGs.

Indices of fractionation as those proposed in Chapter 5 – but not limited to them – will be calculated from the AEGs. Four groups of AEGs will be defined regarding the effect of ablation in each point: CL decrease, CL without change, CL increase, AF termination. Preferential sites for AF organisation and termination will be identified, and the multiple indices of fractionation will be used to measure different features of the AEGs.

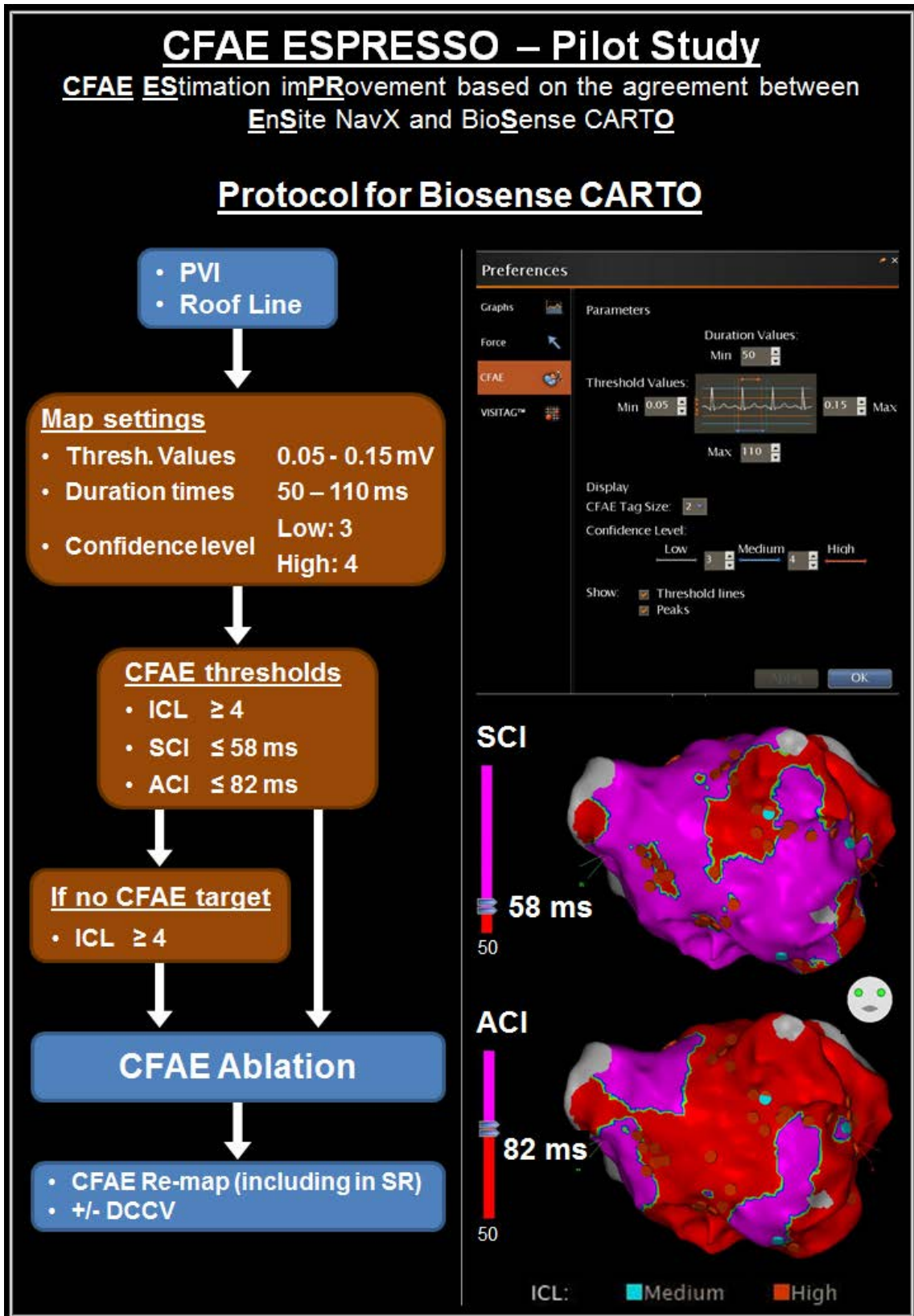


Figure 7-2 The CFAE ESPRESSO protocol for CARTO.

There is increasing interest in multivariate analysis techniques because they incorporate information into the statistical analysis about the relationships between all the available variables, which is a clear advantage upon separate univariate analyses of each variable in a study (Schilling *et al.*, 2015). This increasing interest is also related to continuous improvements in computational power. There are many techniques that could be considered for multivariate classification of AEGs, both linear and nonlinear methods, such as LDA, MANOVA, nonparametric density estimation, projection pursuit, neural networks, fuzzy logic, reduced-rank regression, nonlinear manifold learning, principal and independent component analyses, kernel methods and support vector machines, decision trees, and random forests (Izenman, 2008). A thorough investigation would help to identify the best descriptors and technique for AEG classification and, ultimately, atrial substrate characterisation.

### **7.2.3 DF-guided persAF ablation**

AEGs with high DF are believed to represent atrial substrates with periodic activation responsible for the maintenance of persAF. Previous work has shown inter-atrial DF gradient reduction followed by DF-guided ablation, prolonging patient's SR.

Our group has been investigating the characteristics of DF using non-contact high density mapping, which allowed for the simultaneous collection of up to 2048 virtual AEGs. DF was calculated from those AEGs from spectral analysis, and the spatio-temporal behaviour of DF has been assessed (Chu *et al.*, 2015, Dastagir *et al.*, 2014, Dastagir *et al.*, 2015b, Li *et al.*, 2015, Salinet *et al.*, 2013). DF was defined within the physiological range of 4 – 10 Hz. Recent works have suggested that DF regions are temporally unstable and may exhibit cyclic behaviour (Salinet *et al.*, 2013). Identifying atrial regions that are more prone to host DF might contribute to the identification of AF drivers in persAF.

In order to identify such regions, highest DF (HDF) regions for each individual window were defined as any LA geometry node where the calculated DF was within  $\pm 0.25$  Hz of the maximum DF measured for that window. This region is considered to represent regions maintaining the persAF arrhythmia and the area of HDF bounded by  $\pm 0.25$  Hz forms a cloud which is assumed to represent the HDF activity for that region. Our group recently published the initial results of persAF ablation outcomes targeting the centre of gravity of the HDF clouds with cyclical behaviour (Chu *et al.*, 2015).

The next step of the research is to create cumulative HDF clouds stacked on the 3D LA as illustrated in Figure 7-3. The number of times HDF occurring at each node of LA can be counted for in order to find the HDF density. Atrial regions with highest occurrence of HDF would represent regions with highest incidence of periodic activation that could be responsible for AF perpetuation, and are potential targets for ablation.

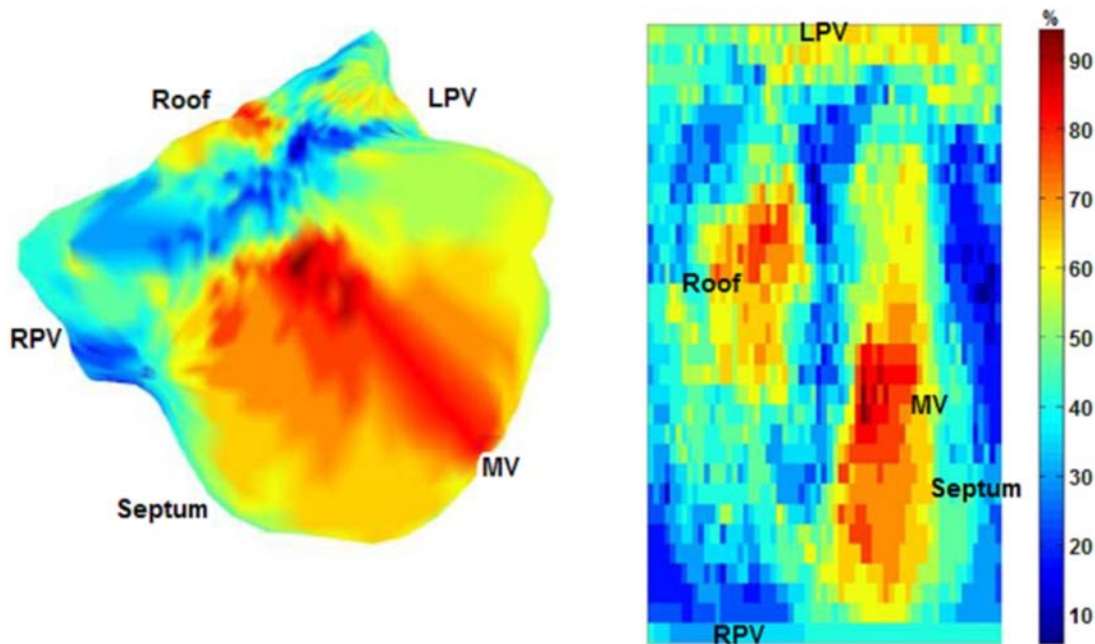


Figure 7-3 Representation of the cumulative HDF clouds stacked on the 3D LA (left-hand side) and 2D spatial map of LA (right-hand side). Modified from (Dastagir *et al.*, 2014).

Additionally, our group has recently identified dominant patterns, defined as the HDF pattern with the highest recurrence, as illustrated in Figure 7-4 (Li *et al.*, 2015). The proposed method identifies and quantifies the spatiotemporal regularity of the HDFs. The investigation of recurrent HDF regions might offer a more comprehensive dynamic overview of persAF behaviour, and the ablation targeting such regions could be considered in future works.

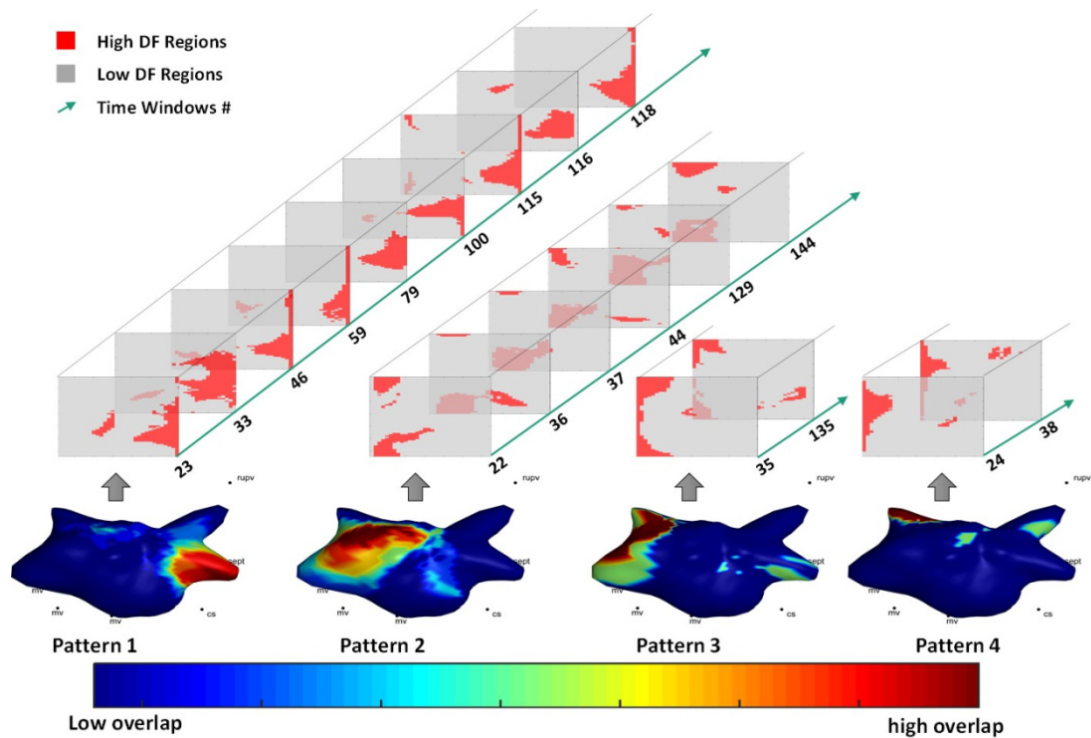


Figure 7-4 Illustration of recurrent patterns with the 2D HDF maps involved in each pattern and the corresponding time windows numbers. Color-coded 3D geometry shows the overlap of all the pattern windows. Modified from (Li *et al.*, 2015).

#### 7.2.4 Phase analysis and rotor-guided persAF ablation

Ablation targeting PS and rotors has gained increasing interest in the past few years with early data suggesting high termination rate for persAF ablation (Haissaguerre *et al.*, 2014, Narayan *et al.*, 2012). However, there is intense debate on the best ablation strategy targeting rotors and that rotor-guided ablation might not be as effective in treating persAF as initially reported (Benharash *et al.*, 2015, Spector *et al.*, 2012).

Similar to DF, the spatio-temporal stability of the rotors in the atria during AF has been questioned, and recent works have suggested that rotors might not be anchored in the atrium during AF, as illustrated in Figure 7-5 (Salinet *et al.*, 2015). This would have direct influence in rotor-guided ablation strategy using current methods (Narayan *et al.*, 2012).

As also proposed for investigating the spatio-temporal behaviour of HDF, the cumulative rotor occurrences at each node of LA can be counted for in order to find the rotor density. Atrial regions with highest occurrence of rotors would represent regions with highest incidence of re-entries that could be responsible for AF perpetuation, and are potential targets for ablation (Figure 7-6).

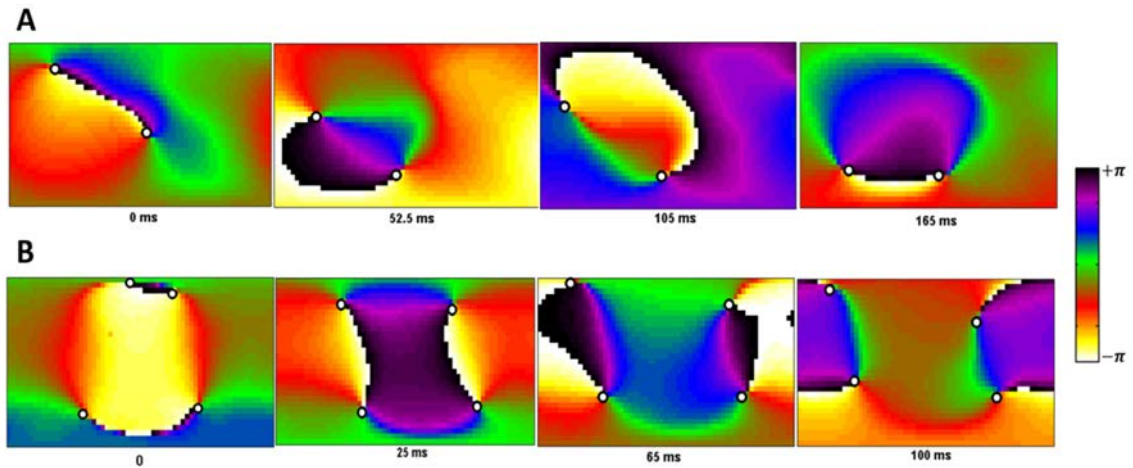


Figure 7-5 Consecutive 2D phase mapping with PS drifting point dislocating across the LA area at different short time steps. The paired PS point had their trajectory starting near the roof (left-hand side) and move through the LA endocardium area (A); (B) an analogous lack of spatio-temporal PS stability behaviour is observed now with a set of two paired PS points.

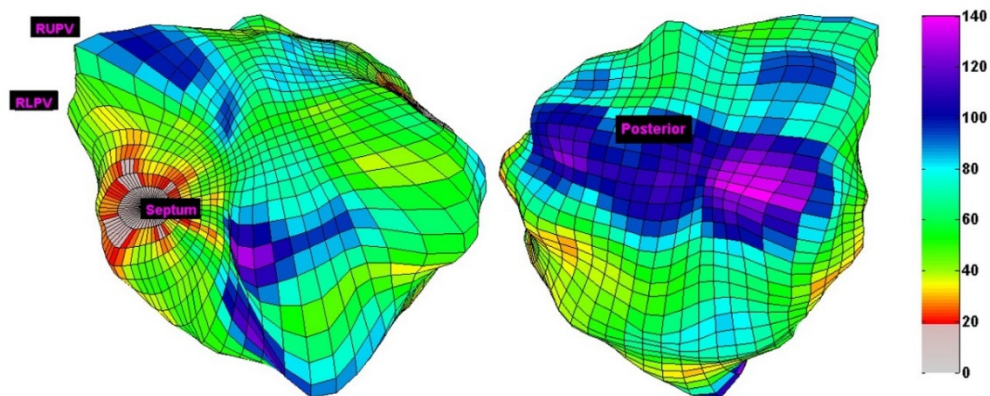


Figure 7-6 Representation of the cumulative rotor occurrence stacked on the 3D LA.

Additionally, different groups have developed different methods for PS detection and rotor identification. These methods are based on different premises and solutions, which could result in distinct PS detection (Dastagir *et al.*, 2015a, Salinet *et al.*, 2015), leading to inconsistent ablation target identification. Ultimately, this could influence ablation outcomes. Therefore, minimizing differences in PS detection as performed by different methods might help to improve the identification of re-entry activity during AF.

### 7.2.5 Multi-mechanism integrative tool for online AF mapping

Catheter ablation has become an established therapy for patients with AF. However, the outcomes remain suboptimal in persAF patients, which motivated the investigation of varying techniques to identify AF drivers, such as CFAEs, DF and rotors (Atienza *et al.*,

2009, Nademanee *et al.*, 2004, Narayan *et al.*, 2012). Understanding the relationship between the different theories might help to improve AF driver identification (Dastagir *et al.*, 2015a). Current methods for atrial substrate mapping have hampered data access in clinical systems, which affected the development of novel algorithms for the automated analysis of AEGs. The development of software platforms that allow rapid implementation of new algorithms is therefore important for the verification of their functionality and suitable visualization for discussion in the clinical environment (Li *et al.*, 2014, Oesterlein *et al.*, 2015). Our research group has recently developed a platform to guide catheter ablation of persAF using DF mapping (Li *et al.*, 2014). This platform (Figure 7-7) – developed on MATLAB – has an automated graphical user interface to process non-contact unipolar AEGs recorded simultaneously by St. Jude Ensite Velocity System and provides 3D representation of the LA with DF behaviours and phase analysis. This platform is a flexible tool that allows for the integration of additional features from AEGs that could be used in future works in the investigation of new methods for mapping and ablation of atrial substrate.

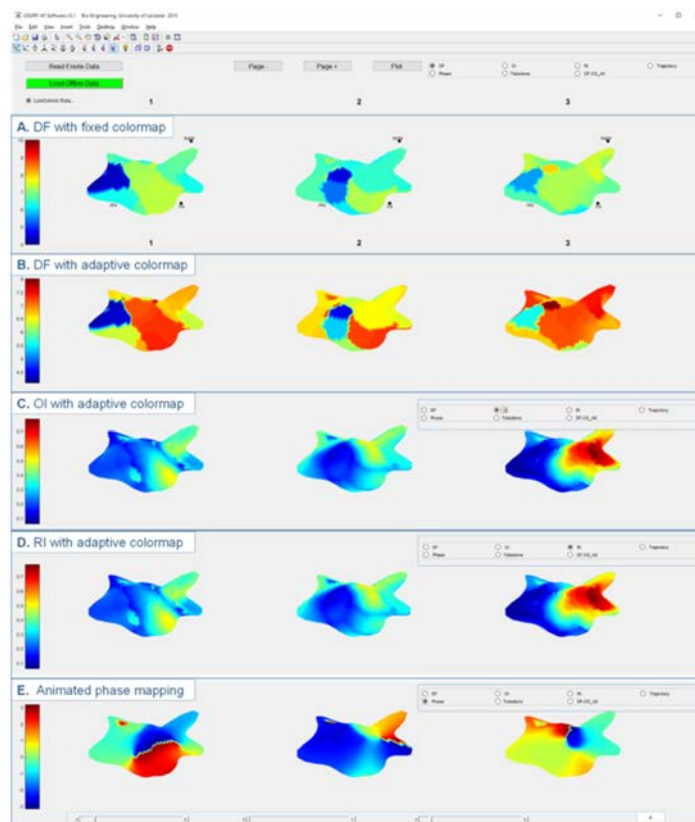


Figure 7-7 A. DF with fixed colour map B.DF with adaptive colour map. C. OI with adaptive colour map D. RI with adaptive colour map E. Phase maps with slider to play, pause, forward and backward.

## 7.3 Publications, conferences and supervisions

### 7.3.1 Journal publications

1. **Almeida TP**, Chu GS, Salinet, JL, Vanheusden FJ, Li X, Tuan JH, Stafford, PJ, Ng GA, Schlindwein FS. Minimizing discordances in automated classification of fractionated electrograms in human persistent atrial fibrillation. Medical & Biological Engineering & Computing, published online 25 February 2016, 1-12.

### 7.3.2 Journal publications in submission

1. **Almeida TP**, Chu GS, Li X, Dastagir N, Tuan JH, Stafford PJ, Schlindwein FS, Ng GA. Characterization of atrial electrogram fractionation before and after pulmonary vein isolation in human persistent atrial fibrillation. Submitted to Journal of Cardiovascular Electrophysiology in April 2016.
2. **Almeida TP**, Chu GS, Bell MJ, Li X, Salinet JL, Dastagir N, Tuan JH, Stafford PJ, Schlindwein FS, Ng GA. The spatio-temporal consistency of atrial electrogram fractionation in persistent atrial fibrillation. Submitted to Circulation: Arrhythmia and Electrophysiology in May 2016.

### 7.3.3 Journal publications in preparation

1. Dastagir N, **Almeida TP**, Vanheusden FJ, Li X, Salinet JL, Chu GS, Stafford PJ, Schlindwein FS, Ng GA. Using high dominant frequency density maps to understand spatiotemporal behaviour of atrial electrograms in persistent atrial fibrillation.
2. Li X, Chu GS, **Almeida TP**, Dastagir N, Vanheusden FJ, Salinet JL, Stafford PJ, Schlindwein FS, Ng AG. Analysis on Recurrent High Dominant Frequency Patterns in Left Atrium during Human Persistent Atrial Fibrillation.
3. Li X, Dastagir N, Guillem MS, **Almeida TP**, Salinet JL, Chu GS, Stafford PJ, Ng AG, Schlindwein FS. Techniques for automated detection of phase singularities using high density non-contact mapping in atrial fibrillation.
4. Li X, Salinet JL, **Almeida TP**, Vanheusden FJ, Chu GS, Ng GA, Schlindwein FS. An interactive platform to guide catheter ablation in human persistent atrial fibrillation using dominant frequency, organization and phase mapping.

5. Salinet JL, Guillem MS, **Almeida TP**, Li X, Chu GS, Dastagir N, Vanheusden FJ, Stafford PJ, Schlindwein FS, Ng GA. Drifting rotors propagation surrounded by high dominant frequency areas in persistent atrial fibrillation.
6. Vanheusden FJ, Salinet JL, Chu GS, Li X, **Almeida TP**, Dastagir N, Stafford PJ, Schlindwein FS, Ng GA. Analysis of the electrophysiological relevance of non-invasive dominant frequency analysis in atrial fibrillation.

#### **7.3.4 Conference papers**

1. **Almeida TP**, Chu GS, Salinet JL, Vanheusden FJ, Li X, Tuan JH, Stafford, PJ, Ng GA, Schlindwein FS. Unifying automated fractionated atrial electrograms classification using electroanatomical mapping systems in persistent atrial fibrillation studies. Oral Presentation, Computing in Cardiology, Nice, France, 06-09/09/2015.
2. Dastagir N, Li X, Vanheusden FJ, **Almeida TP**, Salinet JL, Chu GS, Stafford PJ, Ng GA, Schlindwein FS. Combination of Frequency and Phase to Characterise the Spatiotemporal Behaviour of Cardiac Waves during Persistent Atrial Fibrillation in Humans. Oral Presentation, Computing in Cardiology, Nice, France, 06-09/09/2015.
3. Freitas EB, Salinet JL, **Almeida TP**, Oliveira HJQ. A Novel Method for Automatic Standardization of Digital Electrocardiographs. Poster Presentation, Computing in Cardiology, Nice, France, 06-09/09/2015.
4. Li X, Chu GS, **Almeida TP**, Vanheusden FJ, Dastagir N, Salinet JL, Stafford PJ, Ng GA, Schlindwein FS. Investigation on Recurrent High Dominant Frequency Spatiotemporal Patterns during Persistent Atrial Fibrillation. Oral Presentation, Computing in Cardiology, Nice, France, 06-09/09/2015.
5. Salinet JL, Guillem MS, **Almeida TP**, Li X, Goroso, G, Chu GS, Ng GA, Schlindwein FS. Drifting rotors prevalence is associated with dominant frequency reduction after persistent atrial fibrillation ablation. Oral Presentation, Computing in Cardiology, Nice, France, 06-09/09/2015.
6. Dastagir N, Vanheusden FJ, **Almeida TP**, Li X, Salinet JL, Chu GS, Ng GA, Schlindwein FS. Spatiotemporal Behaviour of High Dominant Frequency during Persistent Atrial Fibrillation. Oral Presentation, Computing in Cardiology, Boston, USA, 07/09/2014.

7. Li X, Salinet JL, **Almeida TP**, Vanheusden FJ, Chu GS, Ng GA, Schlindwein FS. A Platform to guide Catheter Ablation of Persistent Atrial Fibrillation using Dominant Frequency Mapping. Oral Presentation, Computing in Cardiology, Boston, USA, 07/09/2014.
8. **Almeida TP**, Salinet JL, Chu GS, Ng GA, Schlindwein FS. Different Definitions of Complex Fractionated Atrial EGMs do not concur with Clinical Perspective. Poster Presentation, Computing in Cardiology, Zaragoza, Spain, 25/09/2013.
9. Vanheusden FJ, Li X, Chu GS, **Almeida TP**, Ng GA, Schlindwein FS. Analysis of Spatial Variability for the Development of Reduced-Lead Body Surface Maps. Poster Presentation, Computing in Cardiology, Zaragoza, Spain, 24/09/2013.

### **7.3.5 Conference abstracts**

1. Man SH, Dastagir N, Burridge JA, **Almeida TP**, Schlindwein FS, Hodson T, Siddiqui S, Chu GS, Varanasi SS, Chin D, Ng GA. Externally Recorded Cardiac Acoustic Signals to Assess Response to Cardiac Resynchronization Devices. Heart Rhythm 37<sup>th</sup> Annual Scientific Sessions. Oral Presentation, AB01, Allied Professionals, Clinical Research Abstract Presentations, San Francisco, CA, USA, 05/05/2016.
2. Dastagir N, Vanheusden FJ, Chu GS, Salinet JL, Li X, **Almeida TP**, Stafford PJ, Schlindwein FS, Ng GA. Spatiotemporal Analysis of Phase and Frequency Dynamics in Human Persistent Atrial Fibrillation. Poster Presentation, American Heart Association Scientific Sessions 2015, Orlando, USA, 07-11/11/2015.
3. **Almeida TP**, Chu GS, Salinet JL, Vanheusden FJ, Li X, Dastagir N, Tuan JH, Stafford PJ, Ng GA, Schlindwein FS. Targeting complex fractionated atrial electrograms during persistent atrial fibrillation ablation: quid faciat? Poster Presentation, Atrial Signals 2015, Karlsruhe, Germany, 22-24/10/2015.
4. Dastagir N, Li X, **Almeida TP**, Vanheusden FJ, Chu GS, Stafford PJ, Ng GA, Schlindwein FS. Effects of Filtering Atrial electrograms on the relationship of Phase and Dominant Frequency. Poster Presentation, Atrial Signals 2015, Karlsruhe, Germany, 22-24/10/2015.
5. Li X, Chu GS, **Almeida TP**, Vanheusden FJ, Dastagir N, Salinet JL, Stafford PJ, Ng GA, Schlindwein FS. Recurrent High Dominant Frequency Spatial Patterns in Atrial

- Fibrillation. Poster Presentation, Atrial Signals 2015, Karlsruhe, Germany, 22-24/10/2015.
6. Salinet JL, Guillem MS, **Almeida TP**, Li X, Chu GS, Vanheusden FJ, Dastagir N, Ng GA, Schlindwein FS. Co-localised drifting rotors and frequency activity followed by activity reduction after persistent Atrial Fibrillation ablation. Poster Presentation, Atrial Signals 2015, Karlsruhe, Germany, 22-24/10/2015.
  7. Schlindwein FS, Chu GS, **Almeida TP**, Li X, Dastagir N, Vanheusden FJ, Salinet JL, Stafford PJ, Ng GA. Frequency, phase and fractionation of atrial electrograms help guide AF ablation. Poster Presentation, Atrial Signals 2015, Karlsruhe, Germany, 22-24/10/2015.
  8. **Almeida TP**, Chu GS, Salinet JL, Vanheusden FJ, Li X, Tuan JH, Stafford PJ, Schlindwein FS, Ng GA. Differences in fractionated electrogram detection: a direct quantitative comparison between NavX and CARTO. Poster presentation, Heart Rhythm Congress, Birmingham, UK, 04-07/09/2015.
  9. Dastagir N, Salinet JL, Li X, Vanheusden FJ, **Almeida TP**, Chu GS, Stafford PJ, Schlindwein FS, Ng GA. Relationship of Phase Singularities and High Dominant Frequency Regions During Persistent Atrial Fibrillation in Humans. Poster presentation, Heart Rhythm Congress, Birmingham, UK, 04-07/09/2015.
  10. Chu GS, Vanheusden FJ, Li X, **Almeida TP**, Salinet JL, Dastagir N, Varanasi SS, Chi SH, Siddiqui S, Man SH, Stafford PJ, Sandilands AJ, Schlindwein FS, Ng GA. Targeting cyclical highest dominant frequency in the ablation of persistent atrial fibrillation. Young Investigator Competition Finalist, Heart Rhythm Congress, Birmingham, UK, 04-07/09/2015.
  11. Li X, Chu GS, **Almeida TP**, Vanheusden FJ, Dastagir N, Salinet JL, Stafford PJ, Schlindwein FS, Ng GA. Recurrent High Dominant Frequency Patterns in Persistent Atrial Fibrillation. Oral presentation, Heart Rhythm Congress, Birmingham, UK, 04-07/09/2015.
  12. Chu GS, **Almeida TP**, Masca N, Chin SH, Varanasi SS, Siddiqui S, Man SH, Brown PD, Stafford PJ, Sandilands AJ, Schlindwein FS, Ng GA. A mechanistic analysis of human versus robotically-assisted paroxysmal AF ablation. Heart Rhythm 36<sup>th</sup> Annual Scientific Sessions. Poster Presentation, Boston, USA, 13-16/05/2016.

13. **Almeida TP**, Chu GS, Salinet JL, Vanheusden FJ, Li X, Tuan JH, Stafford PJ, Schlindwein FS, Ng GA. Investigating differences in complex fractionated atrial EGM discrimination as performed by CARTO and NavX algorithms. Poster Presentation, Heart Rhythm Congress 2014, Birmingham, UK, 05-08/10/2014.
14. Chu GS, **Almeida TP**, Chin SH, Varanasi SS, Siddiqui S, Man SH, Brown PD, Stafford PJ, Sandilands AJ, Schlindwein FS, Ng GA. Characterising the relationship between force and catheter stability during manual and robotic paroxysmal AF ablation. Oral Presentation, Heart Rhythm Congress 2014, Birmingham, UK, 05-08/10/2014.
15. Dastagir N, Chu GS, Vanheusden FJ, Salinet JL, **Almeida TP**, Li X, Stafford PJ, Sandilands AJ, Schlindwein FS, Ng GA. Ablation for Persistent Atrial Fibrillation Shrinks Left Atrial High Dominant Frequency Areas. Poster Presentation, Heart Rhythm Congress 2014, Birmingham, UK, 05-08/10/2014.
16. Chu GS, Masca, N., **Almeida TP**, Chin SH., Varanasi SS, Brown PD, Stafford PJ, Sandilands AJ, Schlindwein FS, Ng GA. Catheter stability during manual paroxysmal AF ablation can match a robotically-assisted procedure. Heart Rhythm 35<sup>th</sup> Annual Scientific Sessions. Oral Presentation, AB01, Allied Professionals, Clinical Research Abstract Presentations, San Francisco, USA, 09/05/2014.
17. **Almeida TP**, Salinet JL, Chu GS, Schlindwein FS, Ng GA. Atrial EGM Complexity as a Clinical Instrument for Measuring Temporal Fractionation Variability during Atrial Fibrillation. Poster Presentation, Heart Rhythm Congress 2013, Birmingham, UK, 20-23/10/2013.
18. Chu GS, Chin SH, Winter J, Armstrong S, Masca N, **Almeida TP**, Brown PD, Sandilands AJ, Schlindwein FS, Ng GA. Manual and Amigo robotic-assisted AF ablation show similar clinical outcomes: the early results of MAST-AF. Oral Presentation, Heart Rhythm Congress 2013, Birmingham, UK, 20-23/10/2013.
19. Vanheusden FJ, Li X, Chu GS, **Almeida TP**, Schlindwein FS, Ng GA. Development of Reduced-lead Body Surface Mapping System Using Spatial Frequency Analysis. Poster Presentation, Heart Rhythm Congress 2013, Birmingham, UK, 20-23/10/2013.
20. Chu GS, Chin SH, Winter J, Armstrong S, Masca N, **Almeida TP**, Brown PD, Schlindwein FS, Ng GA. Exploring the relationship between contact force and

clinical outcomes between Human and Robot-assisted AF ablation: early results of MAST-AF. 6<sup>th</sup> APHRS & CardioRhythm 2013, Hong Kong, 3-6/10/2013.

21. Chu GS, Masca N, **Almeida TP**, Brown PD, Schlindwein FS, Ng GA. Human vs Robot: a comparison of catheter contact force application for AF ablation (a MAST-AF substudy). Poster Presentation, EHRA EUROPACE, Athens, Greece, 23-16/06/2013.
22. Chu GS, Masca N, **Almeida TP**, Brown PD, Schlindwein FS, Ng GA. Human vs Robot: a comparison of catheter contact force application for AF ablation (a MAST-AF substudy). Poster Presentation, British Cardiovascular Society Annual Conference, London, UK, 5-6/06/2013. doi:10.1136/heartjnl-2013-304019.74
23. **Almeida TP**, Salinet JL, Chu GS, Tuan JH, Schlindwein FS, Ng GA. Atrial EGMs Complexity as an Objective Measurement of Fractionation during Atrial Fibrillation. Heart Rhythm 34<sup>th</sup> Annual Scientific Sessions. Oral Presentation, AB01, Allied Professionals, Clinical Research Abstract Presentations, Denver, CO, USA, 09/05/2013.

### **7.3.6 Supervisions and Co-supervisions**

#### *7.3.6.1 Master's degree*

1. Xiong CA. Descriptive Comparison of Complex Fractionated Atrial Fibrillation Electrogram Classification between two Commercial Mapping Systems. 2014, M.Sc. Final Year Project. Engineering Department, University of Leicester. Supervisor: Schlindwein FS, Co-supervisor: **Almeida TP**.

#### *7.3.6.2 B.Eng. Final Year Project*

1. Bell MJ. Temporal assessment of electrogram fractionation in human persistent atrial fibrillation. 2016, B.Eng. Final Year Project. Engineering Department, University of Leicester. Supervisor: Schlindwein FS, Co-supervisor: **Almeida TP**.
2. Kusimo H. Digital Signal Processing of Atrial Fibrillation: Finding Complex Fractionated Activities. 2013, B.Eng. Final Year Project. Engineering Department, University of Leicester. Supervisor: Schlindwein FS, Co-supervisor: **Almeida TP**.

## Appendices

### **Appendix A : Validation of an Offline Algorithm to reproduce CARTO CFAE definition for CFAE Identification**

#### **Introduction**

CARTO software provides 3D EAM and online automated CFAE detection based on selected voltage peaks and troughs inside a 2.5 s window of sequentially recorded bipolar AEGs. The algorithm subsequently identifies voltage peaks and troughs of bipolar AEGs that exceed a user defined programmable lower voltage threshold to exclude noise, but that do not exceed an upper voltage threshold. The time intervals between successive peaks and/or troughs falling within the voltage window are measured. Complex intervals that fall within a user defined programmable duration are identified during the entire 2.5 s time window. The number of identified complex intervals is referred to as Interval Confidence Level (ICL), and characterizes the repetitiveness of the CFAE complexes. The shortest identified interval is referred to as Shortest Complex Interval (SCI), while the average is referred to as Average Complex Interval (ACI). The default CARTO EGM settings consider a voltage window of 0.05-0.15 mV and a programmable time interval of 50-110 ms. Typically,  $ICL < 4$  represents low fractionation,  $4 \leq ICL < 7$  refers to moderate fractionation and  $ICL \geq 7$  indicates high fractionation.

The objective of this part of the study was to validate a MATLAB algorithm that reproduces CARTO CFAE definition and computes ICL, SCI and ACI.

#### **Methods**

587 sequentially recorded AEGs were exported from 3 patients referred to our institution for catheter ablation of persAF guided by CARTO. All AEGs were recorded with sampling frequency of 1 kHz, and filtered with a 30–300 Hz band-pass filter. Signals were exported with 2.5 s recording duration using CARTO EGM settings (0.05-0.15 mV; 50-110 ms). The peaks and troughs of an AEG were identified. Those that exceeded a user defined programmable lower voltage threshold to exclude noise, but that did not exceed an upper voltage threshold, were marked. The time intervals between successive marked peaks and/or troughs falling within the voltage window were measured. ICL, SCI

and ACI were identified within the recorded 2.5 s AEG. The ICL, SCI and ACI computed by the MATLAB script were compared directly with CARTO system output.

### **Statistical Analysis**

All continuous non-normally distributed variables are expressed as median  $\pm$  interquartile interval. Nonparametric unpaired data were analysed by Mann–Whitney test. The level of statistical significance was set at a  $P < 0.05$ .

### **Results**

Figure S1 illustrates the comparison between the metrics measured by CARTO and the ones measured by MATLAB. Figure S1 A.i refers to the ICL distribution as measured by CARTO and MATLAB ( $p > 0.9999$  when comparing ICL as measured by CARTO and MATLAB). Figure S1 A.ii shows the correlation between ICL measured by CARTO and MATLAB. Figure S1 B.i refers to the SCI distribution as measured by CARTO and MATLAB ( $p > 0.9999$  when comparing SCI as measured by CARTO and MATLAB). Figure S1 B.ii shows the correlation between SCI as measured by CARTO and MATLAB. Figure S1 C.i refers to ACI distribution as measured by CARTO and MATLAB ( $p > 0.9999$  when comparing ACI as measured by CARTO and MATLAB). Figure S1 C.ii shows the correlation between ACI as measured by CARTO and MATLAB.

Agreement between CARTO and MATLAB was 100% for ICL, SCI and ACI.

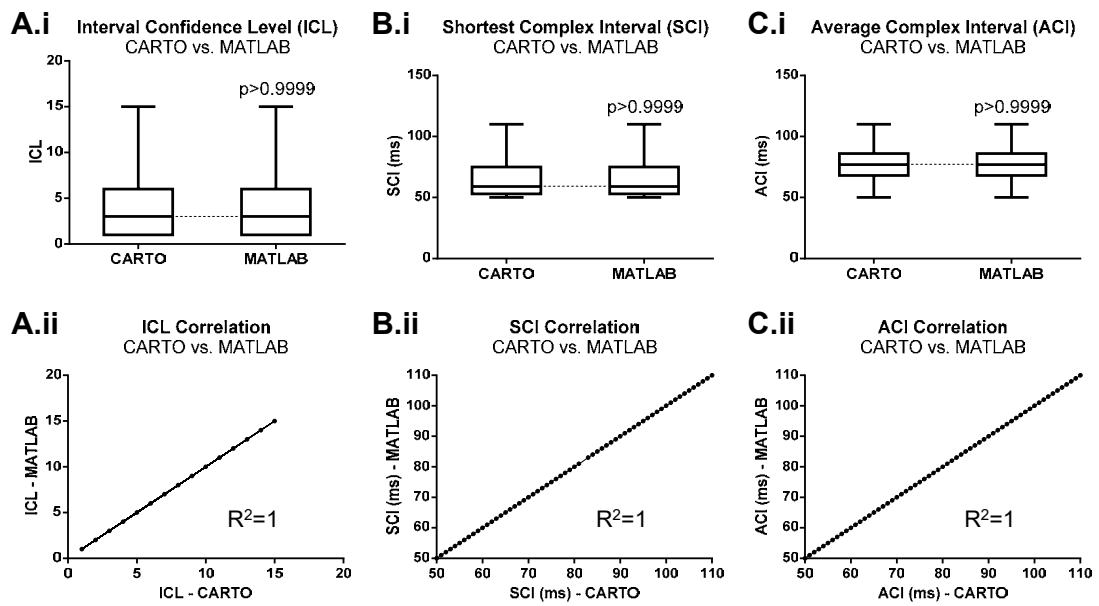


Figure S1. Comparison between ICL, SCI and ACI as computed by CARTO system and MATLAB. A.i ICL. A.ii ICL correlation between CARTO and MATLAB. B.i SCI. B.ii SCI correlation between CARTO and MATLAB. C.i ACI. C.ii ACI correlation between CARTO and MATLAB. Overall, agreement between CARTO and MATLAB was 100% for ICL, SCI and ACI.

## **Appendix B : Influence of AEG duration on ICL and CFE-Mean**

### **Introduction**

Currently, the CARTO system considers only AEGs with 2.5 s duration for CFAE detection using ICL. Hence, there is no validated fractionation threshold for ICL using time windows longer than 2.5 s. Nevertheless, the effects of different time windows – 2.5 s, 5 s, 8 s – were assessed on overall ICL and CFE-Mean for the completeness of the investigation.

### **Methods**

797 AEGs were and its corresponding CFE-Mean was exported from NavX with three time window lengths (2.5 s, 5 s and 8 s). The default threshold for fractionation detection was 30-120 ms if CFE-Mean was measured using NavX EGM settings and 50-110 ms for CARTO EGM settings. The validated offline algorithm was used to compute the ICL of each exported AEG for CFAE identification as defined by CARTO.  $ICL \geq 7$  was used as the default threshold for ICL CFAE categorization.

### **Results**

The results suggest that there was no significant difference between CFE-Mean measured within 2.5 s vs. 5 s vs. 8 s AEGs segments, using either NavX EGM settings or CARTO EGM settings ( $P \approx 1.00$  for 2.5 s vs. 5 s vs. 8 s using NavX EGM settings;  $P \approx 1.00$  for 2.5 s vs. 5 s and 5 s vs. 8 s, and  $P = 0.2443$  for 2.5 s vs. 8 s using CARTO EGM settings). On the other hand, longer AEG duration increased ICL irrespective of EGM settings ( $P < 0.0001$  for all cases).

We observed that different time windows had little influence on overall CFE-Mean. In contrast, longer time windows significantly increased ICL, as expected. As ICL is the count of complex intervals within a time interval, it can be expected that longer time window lengths would have higher ICL. There is currently no validated fractionation threshold for ICL using time windows longer than 2.5 s. The default settings for ICL in CARTO considers windows of 2.5 s. On the other hand, NavX allows for different time window lengths during CFAE analysis (from 1 s to 8 s). As CFE-Mean is the average of

the FIs within a given time window, it can be inferred that longer time window lengths would not affect CFE-Mean significantly.

Since our data showed that different AEG durations had little influence on CFE-Mean, NavX and CARTO algorithms could be compared using the same AEG data with a fixed AEG duration of 2.5 s, following the default settings for ICL in CARTO.

## **Appendix C : CFAE detection thresholds for CFE-Mean and ICL**

### **Methods**

Receiver operating characteristic (ROC) curves were created to find optimum thresholds for ICL and CFE-Mean according to the CFAE classifications performed by each opposite metric. Firstly, CFAE classification (CFAE / non-CFAE) was performed on all 797 AEGs by a fixed CFE-Mean threshold. Eight CFE-Mean thresholds were considered (CFE-Mean  $\leq$  120; 110; 100; 90; 80; 70; 60; 50 ms). Each classification was then used to create ROC curves by varying ICL. Individual optimal values for ICL were found based on the optimum sensitivity and specificity of each ROC curve. Similarly, CFAE classification (CFAE / non-CFAE) was performed on all 797 AEGs by a fixed ICL threshold. Four ICL thresholds were considered (ICL  $\geq$  4; 5; 6; 7). Each classification was then used to create ROC curves by varying CFE-Mean. Individual optimal values for CFE-Mean were found based on the optimum sensitivity and specificity of each ROC curve.

Additionally, approximately 90% (697) of the total AEGs were randomly selected to create ROC curves using only the default thresholds for CFE-Mean and ICL. The remaining 10% (100) AEGs were used to validate and compare the CFAE classification performed by CFE-Mean and ICL using both default and optimum thresholds found in the ROC curves. This process was repeated thirty times, each time with a different set of 90%/10% randomly selected AEGs. Therefore, thirty ROC curves were created for ICL and thirty for CFE-Mean.

This part of the study considered AEGs with 2.5 s, ICL measured with CARTO EGM settings and CFE-Mean measured with NavX EGM settings. The area under the ROC curve (AUROC) and optimum sensitivity and specificity were calculated for each measure.

### **Results**

Figure S2A shows the ROC curve according to the CFAE classification performed by CFE-Mean (CFE-Mean  $\leq$  120; 110; 100; 90; 80; 70; 60; 50 ms) and varying ICL. Table

S1 shows the AUROC, the default and optimum threshold for ICL, alongside the sensitivity and specificity found on the ROC curves for both thresholds. The results from the ROC curve suggest that the default threshold for CARTO ( $ICL \geq 7$ ) provided a high specificity, but poor sensitivity for CFAE detection in all cases. The proposed threshold ( $ICL \geq 4$ ) provides the optimum sensitivity and specificity for CFAE detection in accordance to the CFAE classification performed by NavX.

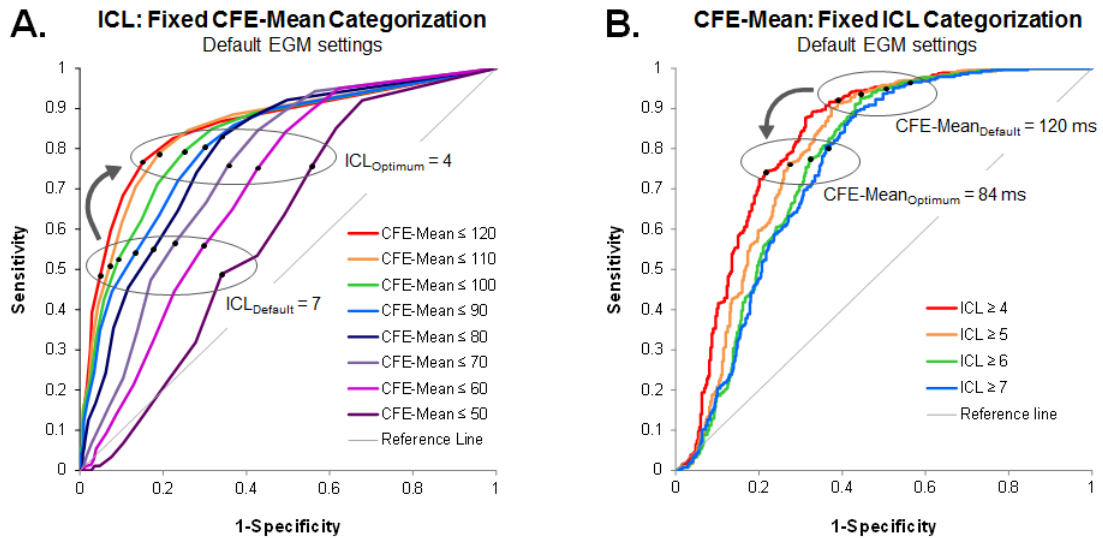


Figure S2. Receiver operating characteristic (ROC) curves based on ICL or CFE-Mean categorization. ROC curves of A. ICL according to CFAE classification using fixed CFE-Mean thresholds (CFE-Mean  $\leq$  120; 110; 100; 90; 80; 70; 60; 50 ms) and; B. CFE-Mean according to CFAE classification using fixed ICL thresholds ( $ICL \geq$  4; 5; 6; 7).

Figure S2B shows the ROC curve according to CFAE classification performed by ICL ( $ICL \geq$  4; 5; 6; 7) and varying CFE-Mean. Table S2 shows the AUROC, the default and optimum threshold for CFE-Mean, alongside the sensitivity and specificity, for each curve. The default threshold for NavX (CFE-Mean  $\leq$  120 ms) always provided a high sensitivity, but poor specificity for CFAE detection. The proposed threshold (CFE-Mean  $\leq$  84 ms) provides the optimum sensitivity and specificity for CFAE detection in accordance to the CFAE classification performed by CARTO in all the cases.

The details of the ROC curves according to the CFAE classification performed by ICL ( $ICL \geq$  7) from the thirty set of 90% randomly selected AEGs are shown on Table S3. The details of the ROC curves according to the CFAE classification performed by CFE-Mean (CFE-Mean  $\leq$  120 ms) from the thirty set of 90% randomly selected AEGs are shown on Table S4.

Tables:

Table S1. Sensitivity and specificity for default and optimized ICL thresholds according CFE-Mean categorization.

	ICL threshold		Sensitivity	1-Specificity	AUROC	P-value
CFE-Mean $\leq$ 120	Default	7	0.492	0.05	0.854	< 0.0001
	Optimum	4	0.769	0.153		
CFE-Mean $\leq$ 110	Default	7	0.510	0.072	0.849	< 0.0001
	Optimum	4	0.790	0.191		
CFE-Mean $\leq$ 100	Default	7	0.527	0.093	0.829	< 0.0001
	Optimum	4	0.794	0.251		
CFE-Mean $\leq$ 90	Default	7	0.537	0.131	0.812	< 0.0001
	Optimum	4	0.804	0.301		
CFE-Mean $\leq$ 80	Default	7	0.547	0.175	0.793	< 0.0001
	Optimum	4	0.831	0.342		
CFE-Mean $\leq$ 70	Default	7	0.571	0.232	0.752	< 0.0001
	Optimum	5	0.760	0.357		
CFE-Mean $\leq$ 60	Default	7	0.550	0.292	0.701	< 0.0001
	Optimum	5	0.748	0.425		
CFE-Mean $\leq$ 50	Default	7	0.489	0.341	0.600	0.002
	Optimum	4	0.761	0.560		

AUROC = Area under receiver operating characteristic curve; ICL = Interval confidence level.

Table S2. Sensitivity and specificity for default and optimized CFE-Mean thresholds according ICL categorization.

	CFE-Mean threshold (ms)		Sensitivity	1-Specificity	AUROC	P-value
ICL $\geq$ 4	Default	120	0.920	0.387	0.823	< 0.0001
	Optimum	84.63	0.744	0.216		
ICL $\geq$ 5	Default	120	0.938	0.450	0.793	< 0.0001
	Optimum	84.18	0.765	0.270		
ICL $\geq$ 6	Default	120	0.948	0.502	0.765	< 0.0001
	Optimum	84.18	0.777	0.321		
ICL $\geq$ 7	Default	120	0.958	0.553	0.756	< 0.0001
	Optimum	84.18	0.807	0.361		

AUROC = Area under receiver operating characteristic curve.

Table S3. Sensitivity and specificity for default and optimized ICL thresholds according CFE-Mean categorization from the thirty set of 90% randomly selected AEGs.

	ICL threshold (ms)		Sensitivity	1-Specificity	AUROC	P-value																																																																																																																																																																																																														
Test 1	Default	7	0.495	0.060	0.859	P<0.0001																																																																																																																																																																																																														
	Revised	3	0.835	0.200			Test 2	Default	7	0.499	0.043	0.858	P<0.0001	Revised	3	0.830	0.216	Test 3	Default	7	0.496	0.046	0.844	P<0.0001	Revised	4	0.756	0.161	Test 4	Default	7	0.506	0.047	0.855	P<0.0001	Revised	4	0.772	0.156	Test 5	Default	7	0.489	0.057	0.848	P<0.0001	Revised	4	0.766	0.167	Test 6	Default	7	0.485	0.052	0.851	P<0.0001	Revised	4	0.761	0.146	Test 7	Default	7	0.496	0.051	0.855	P<0.0001	Revised	4	0.775	0.152	Test 8	Default	7	0.497	0.048	0.861	P<0.0001	Revised	4	0.768	0.138	Test 9	Default	7	0.481	0.056	0.848	P<0.0001	Revised	4	0.766	0.158	Test 10	Default	7	0.491	0.046	0.853	P<0.0001	Revised	4	0.765	0.144	Test 11	Default	7	0.481	0.047	0.850	P<0.0001	Revised	4	0.764	0.160	Test 12	Default	7	0.490	0.048	0.848	P<0.0001	Revised	4	0.769	0.159	Test 13	Default	7	0.499	0.049	0.858	P<0.0001	Revised	3	0.828	0.211	Test 14	Default	7	0.491	0.050	0.855	P<0.0001	Revised	4	0.779	0.158	Test 15	Default	7	0.501	0.052	0.851	P<0.0001	Revised	4	0.767	0.151	Test 16	Default	7	0.482	0.051	0.849	P<0.0001	Revised	4	0.762	0.164	Test 17	Default	7	0.499	0.053	0.849	P<0.0001	Revised	4	0.768	0.170	Test 18	Default	7	0.495	0.043	0.855	P<0.0001	Revised	4	0.769	0.154	Test 19	Default	7	0.479	0.044	0.852	P<0.0001	Revised	3	0.817	0.206	Test 20	Default	7	0.504	0.049	0.856	P<0.0001	Revised
Test 2	Default	7	0.499	0.043	0.858	P<0.0001																																																																																																																																																																																																														
	Revised	3	0.830	0.216			Test 3	Default	7	0.496	0.046	0.844	P<0.0001	Revised	4	0.756	0.161	Test 4	Default	7	0.506	0.047	0.855	P<0.0001	Revised	4	0.772	0.156	Test 5	Default	7	0.489	0.057	0.848	P<0.0001	Revised	4	0.766	0.167	Test 6	Default	7	0.485	0.052	0.851	P<0.0001	Revised	4	0.761	0.146	Test 7	Default	7	0.496	0.051	0.855	P<0.0001	Revised	4	0.775	0.152	Test 8	Default	7	0.497	0.048	0.861	P<0.0001	Revised	4	0.768	0.138	Test 9	Default	7	0.481	0.056	0.848	P<0.0001	Revised	4	0.766	0.158	Test 10	Default	7	0.491	0.046	0.853	P<0.0001	Revised	4	0.765	0.144	Test 11	Default	7	0.481	0.047	0.850	P<0.0001	Revised	4	0.764	0.160	Test 12	Default	7	0.490	0.048	0.848	P<0.0001	Revised	4	0.769	0.159	Test 13	Default	7	0.499	0.049	0.858	P<0.0001	Revised	3	0.828	0.211	Test 14	Default	7	0.491	0.050	0.855	P<0.0001	Revised	4	0.779	0.158	Test 15	Default	7	0.501	0.052	0.851	P<0.0001	Revised	4	0.767	0.151	Test 16	Default	7	0.482	0.051	0.849	P<0.0001	Revised	4	0.762	0.164	Test 17	Default	7	0.499	0.053	0.849	P<0.0001	Revised	4	0.768	0.170	Test 18	Default	7	0.495	0.043	0.855	P<0.0001	Revised	4	0.769	0.154	Test 19	Default	7	0.479	0.044	0.852	P<0.0001	Revised	3	0.817	0.206	Test 20	Default	7	0.504	0.049	0.856	P<0.0001	Revised	4	0.773	0.153								
Test 3	Default	7	0.496	0.046	0.844	P<0.0001																																																																																																																																																																																																														
	Revised	4	0.756	0.161			Test 4	Default	7	0.506	0.047	0.855	P<0.0001	Revised	4	0.772	0.156	Test 5	Default	7	0.489	0.057	0.848	P<0.0001	Revised	4	0.766	0.167	Test 6	Default	7	0.485	0.052	0.851	P<0.0001	Revised	4	0.761	0.146	Test 7	Default	7	0.496	0.051	0.855	P<0.0001	Revised	4	0.775	0.152	Test 8	Default	7	0.497	0.048	0.861	P<0.0001	Revised	4	0.768	0.138	Test 9	Default	7	0.481	0.056	0.848	P<0.0001	Revised	4	0.766	0.158	Test 10	Default	7	0.491	0.046	0.853	P<0.0001	Revised	4	0.765	0.144	Test 11	Default	7	0.481	0.047	0.850	P<0.0001	Revised	4	0.764	0.160	Test 12	Default	7	0.490	0.048	0.848	P<0.0001	Revised	4	0.769	0.159	Test 13	Default	7	0.499	0.049	0.858	P<0.0001	Revised	3	0.828	0.211	Test 14	Default	7	0.491	0.050	0.855	P<0.0001	Revised	4	0.779	0.158	Test 15	Default	7	0.501	0.052	0.851	P<0.0001	Revised	4	0.767	0.151	Test 16	Default	7	0.482	0.051	0.849	P<0.0001	Revised	4	0.762	0.164	Test 17	Default	7	0.499	0.053	0.849	P<0.0001	Revised	4	0.768	0.170	Test 18	Default	7	0.495	0.043	0.855	P<0.0001	Revised	4	0.769	0.154	Test 19	Default	7	0.479	0.044	0.852	P<0.0001	Revised	3	0.817	0.206	Test 20	Default	7	0.504	0.049	0.856	P<0.0001	Revised	4	0.773	0.153																			
Test 4	Default	7	0.506	0.047	0.855	P<0.0001																																																																																																																																																																																																														
	Revised	4	0.772	0.156			Test 5	Default	7	0.489	0.057	0.848	P<0.0001	Revised	4	0.766	0.167	Test 6	Default	7	0.485	0.052	0.851	P<0.0001	Revised	4	0.761	0.146	Test 7	Default	7	0.496	0.051	0.855	P<0.0001	Revised	4	0.775	0.152	Test 8	Default	7	0.497	0.048	0.861	P<0.0001	Revised	4	0.768	0.138	Test 9	Default	7	0.481	0.056	0.848	P<0.0001	Revised	4	0.766	0.158	Test 10	Default	7	0.491	0.046	0.853	P<0.0001	Revised	4	0.765	0.144	Test 11	Default	7	0.481	0.047	0.850	P<0.0001	Revised	4	0.764	0.160	Test 12	Default	7	0.490	0.048	0.848	P<0.0001	Revised	4	0.769	0.159	Test 13	Default	7	0.499	0.049	0.858	P<0.0001	Revised	3	0.828	0.211	Test 14	Default	7	0.491	0.050	0.855	P<0.0001	Revised	4	0.779	0.158	Test 15	Default	7	0.501	0.052	0.851	P<0.0001	Revised	4	0.767	0.151	Test 16	Default	7	0.482	0.051	0.849	P<0.0001	Revised	4	0.762	0.164	Test 17	Default	7	0.499	0.053	0.849	P<0.0001	Revised	4	0.768	0.170	Test 18	Default	7	0.495	0.043	0.855	P<0.0001	Revised	4	0.769	0.154	Test 19	Default	7	0.479	0.044	0.852	P<0.0001	Revised	3	0.817	0.206	Test 20	Default	7	0.504	0.049	0.856	P<0.0001	Revised	4	0.773	0.153																														
Test 5	Default	7	0.489	0.057	0.848	P<0.0001																																																																																																																																																																																																														
	Revised	4	0.766	0.167			Test 6	Default	7	0.485	0.052	0.851	P<0.0001	Revised	4	0.761	0.146	Test 7	Default	7	0.496	0.051	0.855	P<0.0001	Revised	4	0.775	0.152	Test 8	Default	7	0.497	0.048	0.861	P<0.0001	Revised	4	0.768	0.138	Test 9	Default	7	0.481	0.056	0.848	P<0.0001	Revised	4	0.766	0.158	Test 10	Default	7	0.491	0.046	0.853	P<0.0001	Revised	4	0.765	0.144	Test 11	Default	7	0.481	0.047	0.850	P<0.0001	Revised	4	0.764	0.160	Test 12	Default	7	0.490	0.048	0.848	P<0.0001	Revised	4	0.769	0.159	Test 13	Default	7	0.499	0.049	0.858	P<0.0001	Revised	3	0.828	0.211	Test 14	Default	7	0.491	0.050	0.855	P<0.0001	Revised	4	0.779	0.158	Test 15	Default	7	0.501	0.052	0.851	P<0.0001	Revised	4	0.767	0.151	Test 16	Default	7	0.482	0.051	0.849	P<0.0001	Revised	4	0.762	0.164	Test 17	Default	7	0.499	0.053	0.849	P<0.0001	Revised	4	0.768	0.170	Test 18	Default	7	0.495	0.043	0.855	P<0.0001	Revised	4	0.769	0.154	Test 19	Default	7	0.479	0.044	0.852	P<0.0001	Revised	3	0.817	0.206	Test 20	Default	7	0.504	0.049	0.856	P<0.0001	Revised	4	0.773	0.153																																									
Test 6	Default	7	0.485	0.052	0.851	P<0.0001																																																																																																																																																																																																														
	Revised	4	0.761	0.146			Test 7	Default	7	0.496	0.051	0.855	P<0.0001	Revised	4	0.775	0.152	Test 8	Default	7	0.497	0.048	0.861	P<0.0001	Revised	4	0.768	0.138	Test 9	Default	7	0.481	0.056	0.848	P<0.0001	Revised	4	0.766	0.158	Test 10	Default	7	0.491	0.046	0.853	P<0.0001	Revised	4	0.765	0.144	Test 11	Default	7	0.481	0.047	0.850	P<0.0001	Revised	4	0.764	0.160	Test 12	Default	7	0.490	0.048	0.848	P<0.0001	Revised	4	0.769	0.159	Test 13	Default	7	0.499	0.049	0.858	P<0.0001	Revised	3	0.828	0.211	Test 14	Default	7	0.491	0.050	0.855	P<0.0001	Revised	4	0.779	0.158	Test 15	Default	7	0.501	0.052	0.851	P<0.0001	Revised	4	0.767	0.151	Test 16	Default	7	0.482	0.051	0.849	P<0.0001	Revised	4	0.762	0.164	Test 17	Default	7	0.499	0.053	0.849	P<0.0001	Revised	4	0.768	0.170	Test 18	Default	7	0.495	0.043	0.855	P<0.0001	Revised	4	0.769	0.154	Test 19	Default	7	0.479	0.044	0.852	P<0.0001	Revised	3	0.817	0.206	Test 20	Default	7	0.504	0.049	0.856	P<0.0001	Revised	4	0.773	0.153																																																				
Test 7	Default	7	0.496	0.051	0.855	P<0.0001																																																																																																																																																																																																														
	Revised	4	0.775	0.152			Test 8	Default	7	0.497	0.048	0.861	P<0.0001	Revised	4	0.768	0.138	Test 9	Default	7	0.481	0.056	0.848	P<0.0001	Revised	4	0.766	0.158	Test 10	Default	7	0.491	0.046	0.853	P<0.0001	Revised	4	0.765	0.144	Test 11	Default	7	0.481	0.047	0.850	P<0.0001	Revised	4	0.764	0.160	Test 12	Default	7	0.490	0.048	0.848	P<0.0001	Revised	4	0.769	0.159	Test 13	Default	7	0.499	0.049	0.858	P<0.0001	Revised	3	0.828	0.211	Test 14	Default	7	0.491	0.050	0.855	P<0.0001	Revised	4	0.779	0.158	Test 15	Default	7	0.501	0.052	0.851	P<0.0001	Revised	4	0.767	0.151	Test 16	Default	7	0.482	0.051	0.849	P<0.0001	Revised	4	0.762	0.164	Test 17	Default	7	0.499	0.053	0.849	P<0.0001	Revised	4	0.768	0.170	Test 18	Default	7	0.495	0.043	0.855	P<0.0001	Revised	4	0.769	0.154	Test 19	Default	7	0.479	0.044	0.852	P<0.0001	Revised	3	0.817	0.206	Test 20	Default	7	0.504	0.049	0.856	P<0.0001	Revised	4	0.773	0.153																																																															
Test 8	Default	7	0.497	0.048	0.861	P<0.0001																																																																																																																																																																																																														
	Revised	4	0.768	0.138			Test 9	Default	7	0.481	0.056	0.848	P<0.0001	Revised	4	0.766	0.158	Test 10	Default	7	0.491	0.046	0.853	P<0.0001	Revised	4	0.765	0.144	Test 11	Default	7	0.481	0.047	0.850	P<0.0001	Revised	4	0.764	0.160	Test 12	Default	7	0.490	0.048	0.848	P<0.0001	Revised	4	0.769	0.159	Test 13	Default	7	0.499	0.049	0.858	P<0.0001	Revised	3	0.828	0.211	Test 14	Default	7	0.491	0.050	0.855	P<0.0001	Revised	4	0.779	0.158	Test 15	Default	7	0.501	0.052	0.851	P<0.0001	Revised	4	0.767	0.151	Test 16	Default	7	0.482	0.051	0.849	P<0.0001	Revised	4	0.762	0.164	Test 17	Default	7	0.499	0.053	0.849	P<0.0001	Revised	4	0.768	0.170	Test 18	Default	7	0.495	0.043	0.855	P<0.0001	Revised	4	0.769	0.154	Test 19	Default	7	0.479	0.044	0.852	P<0.0001	Revised	3	0.817	0.206	Test 20	Default	7	0.504	0.049	0.856	P<0.0001	Revised	4	0.773	0.153																																																																										
Test 9	Default	7	0.481	0.056	0.848	P<0.0001																																																																																																																																																																																																														
	Revised	4	0.766	0.158			Test 10	Default	7	0.491	0.046	0.853	P<0.0001	Revised	4	0.765	0.144	Test 11	Default	7	0.481	0.047	0.850	P<0.0001	Revised	4	0.764	0.160	Test 12	Default	7	0.490	0.048	0.848	P<0.0001	Revised	4	0.769	0.159	Test 13	Default	7	0.499	0.049	0.858	P<0.0001	Revised	3	0.828	0.211	Test 14	Default	7	0.491	0.050	0.855	P<0.0001	Revised	4	0.779	0.158	Test 15	Default	7	0.501	0.052	0.851	P<0.0001	Revised	4	0.767	0.151	Test 16	Default	7	0.482	0.051	0.849	P<0.0001	Revised	4	0.762	0.164	Test 17	Default	7	0.499	0.053	0.849	P<0.0001	Revised	4	0.768	0.170	Test 18	Default	7	0.495	0.043	0.855	P<0.0001	Revised	4	0.769	0.154	Test 19	Default	7	0.479	0.044	0.852	P<0.0001	Revised	3	0.817	0.206	Test 20	Default	7	0.504	0.049	0.856	P<0.0001	Revised	4	0.773	0.153																																																																																					
Test 10	Default	7	0.491	0.046	0.853	P<0.0001																																																																																																																																																																																																														
	Revised	4	0.765	0.144			Test 11	Default	7	0.481	0.047	0.850	P<0.0001	Revised	4	0.764	0.160	Test 12	Default	7	0.490	0.048	0.848	P<0.0001	Revised	4	0.769	0.159	Test 13	Default	7	0.499	0.049	0.858	P<0.0001	Revised	3	0.828	0.211	Test 14	Default	7	0.491	0.050	0.855	P<0.0001	Revised	4	0.779	0.158	Test 15	Default	7	0.501	0.052	0.851	P<0.0001	Revised	4	0.767	0.151	Test 16	Default	7	0.482	0.051	0.849	P<0.0001	Revised	4	0.762	0.164	Test 17	Default	7	0.499	0.053	0.849	P<0.0001	Revised	4	0.768	0.170	Test 18	Default	7	0.495	0.043	0.855	P<0.0001	Revised	4	0.769	0.154	Test 19	Default	7	0.479	0.044	0.852	P<0.0001	Revised	3	0.817	0.206	Test 20	Default	7	0.504	0.049	0.856	P<0.0001	Revised	4	0.773	0.153																																																																																																
Test 11	Default	7	0.481	0.047	0.850	P<0.0001																																																																																																																																																																																																														
	Revised	4	0.764	0.160			Test 12	Default	7	0.490	0.048	0.848	P<0.0001	Revised	4	0.769	0.159	Test 13	Default	7	0.499	0.049	0.858	P<0.0001	Revised	3	0.828	0.211	Test 14	Default	7	0.491	0.050	0.855	P<0.0001	Revised	4	0.779	0.158	Test 15	Default	7	0.501	0.052	0.851	P<0.0001	Revised	4	0.767	0.151	Test 16	Default	7	0.482	0.051	0.849	P<0.0001	Revised	4	0.762	0.164	Test 17	Default	7	0.499	0.053	0.849	P<0.0001	Revised	4	0.768	0.170	Test 18	Default	7	0.495	0.043	0.855	P<0.0001	Revised	4	0.769	0.154	Test 19	Default	7	0.479	0.044	0.852	P<0.0001	Revised	3	0.817	0.206	Test 20	Default	7	0.504	0.049	0.856	P<0.0001	Revised	4	0.773	0.153																																																																																																											
Test 12	Default	7	0.490	0.048	0.848	P<0.0001																																																																																																																																																																																																														
	Revised	4	0.769	0.159			Test 13	Default	7	0.499	0.049	0.858	P<0.0001	Revised	3	0.828	0.211	Test 14	Default	7	0.491	0.050	0.855	P<0.0001	Revised	4	0.779	0.158	Test 15	Default	7	0.501	0.052	0.851	P<0.0001	Revised	4	0.767	0.151	Test 16	Default	7	0.482	0.051	0.849	P<0.0001	Revised	4	0.762	0.164	Test 17	Default	7	0.499	0.053	0.849	P<0.0001	Revised	4	0.768	0.170	Test 18	Default	7	0.495	0.043	0.855	P<0.0001	Revised	4	0.769	0.154	Test 19	Default	7	0.479	0.044	0.852	P<0.0001	Revised	3	0.817	0.206	Test 20	Default	7	0.504	0.049	0.856	P<0.0001	Revised	4	0.773	0.153																																																																																																																						
Test 13	Default	7	0.499	0.049	0.858	P<0.0001																																																																																																																																																																																																														
	Revised	3	0.828	0.211			Test 14	Default	7	0.491	0.050	0.855	P<0.0001	Revised	4	0.779	0.158	Test 15	Default	7	0.501	0.052	0.851	P<0.0001	Revised	4	0.767	0.151	Test 16	Default	7	0.482	0.051	0.849	P<0.0001	Revised	4	0.762	0.164	Test 17	Default	7	0.499	0.053	0.849	P<0.0001	Revised	4	0.768	0.170	Test 18	Default	7	0.495	0.043	0.855	P<0.0001	Revised	4	0.769	0.154	Test 19	Default	7	0.479	0.044	0.852	P<0.0001	Revised	3	0.817	0.206	Test 20	Default	7	0.504	0.049	0.856	P<0.0001	Revised	4	0.773	0.153																																																																																																																																	
Test 14	Default	7	0.491	0.050	0.855	P<0.0001																																																																																																																																																																																																														
	Revised	4	0.779	0.158			Test 15	Default	7	0.501	0.052	0.851	P<0.0001	Revised	4	0.767	0.151	Test 16	Default	7	0.482	0.051	0.849	P<0.0001	Revised	4	0.762	0.164	Test 17	Default	7	0.499	0.053	0.849	P<0.0001	Revised	4	0.768	0.170	Test 18	Default	7	0.495	0.043	0.855	P<0.0001	Revised	4	0.769	0.154	Test 19	Default	7	0.479	0.044	0.852	P<0.0001	Revised	3	0.817	0.206	Test 20	Default	7	0.504	0.049	0.856	P<0.0001	Revised	4	0.773	0.153																																																																																																																																												
Test 15	Default	7	0.501	0.052	0.851	P<0.0001																																																																																																																																																																																																														
	Revised	4	0.767	0.151			Test 16	Default	7	0.482	0.051	0.849	P<0.0001	Revised	4	0.762	0.164	Test 17	Default	7	0.499	0.053	0.849	P<0.0001	Revised	4	0.768	0.170	Test 18	Default	7	0.495	0.043	0.855	P<0.0001	Revised	4	0.769	0.154	Test 19	Default	7	0.479	0.044	0.852	P<0.0001	Revised	3	0.817	0.206	Test 20	Default	7	0.504	0.049	0.856	P<0.0001	Revised	4	0.773	0.153																																																																																																																																																							
Test 16	Default	7	0.482	0.051	0.849	P<0.0001																																																																																																																																																																																																														
	Revised	4	0.762	0.164			Test 17	Default	7	0.499	0.053	0.849	P<0.0001	Revised	4	0.768	0.170	Test 18	Default	7	0.495	0.043	0.855	P<0.0001	Revised	4	0.769	0.154	Test 19	Default	7	0.479	0.044	0.852	P<0.0001	Revised	3	0.817	0.206	Test 20	Default	7	0.504	0.049	0.856	P<0.0001	Revised	4	0.773	0.153																																																																																																																																																																		
Test 17	Default	7	0.499	0.053	0.849	P<0.0001																																																																																																																																																																																																														
	Revised	4	0.768	0.170			Test 18	Default	7	0.495	0.043	0.855	P<0.0001	Revised	4	0.769	0.154	Test 19	Default	7	0.479	0.044	0.852	P<0.0001	Revised	3	0.817	0.206	Test 20	Default	7	0.504	0.049	0.856	P<0.0001	Revised	4	0.773	0.153																																																																																																																																																																													
Test 18	Default	7	0.495	0.043	0.855	P<0.0001																																																																																																																																																																																																														
	Revised	4	0.769	0.154			Test 19	Default	7	0.479	0.044	0.852	P<0.0001	Revised	3	0.817	0.206	Test 20	Default	7	0.504	0.049	0.856	P<0.0001	Revised	4	0.773	0.153																																																																																																																																																																																								
Test 19	Default	7	0.479	0.044	0.852	P<0.0001																																																																																																																																																																																																														
	Revised	3	0.817	0.206			Test 20	Default	7	0.504	0.049	0.856	P<0.0001	Revised	4	0.773	0.153																																																																																																																																																																																																			
Test 20	Default	7	0.504	0.049	0.856	P<0.0001																																																																																																																																																																																																														
	Revised	4	0.773	0.153																																																																																																																																																																																																																

Table S3. Cont.

	ICL threshold (ms)	Sensitivity	1-Specificity	AUROC	P-value	
Test 21	Default	7	0.475	0.049	0.849	P<0.0001
	Revised	4	0.759	0.147		
Test 22	Default	7	0.503	0.043	0.856	P<0.0001
	Revised	4	0.771	0.159		
Test 23	Default	7	0.499	0.051	0.856	P<0.0001
	Revised	4	0.782	0.162		
Test 24	Default	7	0.499	0.046	0.852	P<0.0001
	Revised	4	0.762	0.147		
Test 25	Default	7	0.491	0.047	0.854	P<0.0001
	Revised	4	0.766	0.150		
Test 26	Default	7	0.493	0.051	0.850	P<0.0001
	Revised	4	0.770	0.164		
Test 27	Default	7	0.492	0.056	0.841	P<0.0001
	Revised	4	0.756	0.160		
Test 28	Default	7	0.478	0.057	0.844	P<0.0001
	Revised	3	0.812	0.217		
Test 29	Default	7	0.483	0.056	0.851	P<0.0001
	Revised	4	0.763	0.149		
Test 30	Default	7	0.500	0.038	0.863	P<0.0001
	Revised	4	0.768	0.139		

Table S4. Sensitivity and specificity for default and optimized ICL thresholds according CFE-Mean categorization from the thirty set of 90% randomly selected AEGs.

	CFE-Mean threshold (ms)		Sensitivity	1-Specificity	AUROC	P-value
Test 1	Default	120	0.957	0.572	0.752	P<0.0001
	Revised	84.4	0.806	0.371		
Test 2	Default	120	0.964	0.552	0.753	P<0.0001
	Revised	84.4	0.822	0.374		
Test 3	Default	120	0.960	0.541	0.757	P<0.0001
	Revised	84.2	0.798	0.359		
Test 4	Default	120	0.961	0.546	0.757	P<0.0001
	Revised	84.4	0.813	0.351		
Test 5	Default	120	0.952	0.559	0.742	P<0.0001
	Revised	84.2	0.804	0.374		
Test 6	Default	120	0.955	0.557	0.747	P<0.0001
	Revised	84.2	0.801	0.359		
Test 7	Default	120	0.956	0.542	0.762	P<0.0001
	Revised	84.2	0.815	0.355		
Test 8	Default	120	0.960	0.553	0.750	P<0.0001
	Revised	84.2	0.806	0.366		
Test 9	Default	120	0.951	0.554	0.751	P<0.0001
	Revised	84.2	0.795	0.360		
Test 10	Default	120	0.959	0.545	0.752	P<0.0001
	Revised	82.1	0.780	0.361		
Test 11	Default	120	0.959	0.555	0.755	P<0.0001
	Revised	84.2	0.807	0.363		
Test 12	Default	120	0.952	0.564	0.758	P<0.0001
	Revised	84.2	0.806	0.366		
Test 13	Default	120	0.961	0.526	0.750	P<0.0001
	Revised	84.2	0.801	0.367		
Test 14	Default	120	0.955	0.536	0.763	P<0.0001
	Revised	84.0	0.824	0.362		
Test 15	Default	120	0.957	0.549	0.760	P<0.0001
	Revised	84.2	0.815	0.354		
Test 16	Default	120	0.955	0.554	0.754	P<0.0001
	Revised	84.2	0.799	0.362		
Test 17	Default	120	0.961	0.558	0.753	P<0.0001
	Revised	84.2	0.805	0.365		
Test 18	Default	120	0.964	0.554	0.757	P<0.0001
	Revised	84.4	0.805	0.361		
Test 19	Default	120	0.963	0.571	0.748	P<0.0001
	Revised	84.2	0.800	0.372		
Test 20	Default	120	0.961	0.562	0.752	P<0.0001
	Revised	84.2	0.807	0.365		

Table S4. Cont.

	CFE-Mean threshold (ms)		Sensitivity	1-Specificity	AUROC	P-value
Test 21	Default	120	0.959	0.574	0.748	P<0.0001
	Revised	84.2	0.803	0.373		
Test 22	Default	120	0.965	0.552	0.758	P<0.0001
	Revised	84.2	0.812	0.357		
Test 23	Default	120	0.956	0.543	0.762	P<0.0001
	Revised	84.4	0.825	0.365		
Test 24	Default	120	0.960	0.538	0.756	P<0.0001
	Revised	84.2	0.815	0.350		
Test 25	Default	120	0.960	0.549	0.762	P<0.0001
	Revised	84.2	0.810	0.356		
Test 26	Default	120	0.956	0.549	0.754	P<0.0001
	Revised	84.2	0.807	0.364		
Test 27	Default	120	0.952	0.553	0.757	P<0.0001
	Revised	84.2	0.808	0.356		
Test 28	Default	120	0.951	0.561	0.753	P<0.0001
	Revised	84.2	0.799	0.362		
Test 29	Default	120	0.951	0.553	0.750	P<0.0001
	Revised	84.2	0.792	0.361		
Test 30	Default	120	0.968	0.551	0.762	P<0.0001
	Revised	84.2	0.825	0.360		

## **Appendix D : CFAE detection thresholds for CFE-StdDev, ACI and SCI**

### **Methods**

The revised thresholds for both CFE-Mean and ICL found in the ROC curves were used concurrently to perform a new CFAE classification on the thirty sets of 697 randomly sampled AEGs. In this new classification, an AEG was classified as CFAE only if both CFE-Mean and ICL agreed with the classification using their revised thresholds. These new classifications were used to create ROC curves and hence obtain the optimum sensitivity and specificity thresholds for the complementary metrics – CFE-StdDev, ACI and SCI.

Therefore, the complementary metrics were used to identify AEGs that were classified as CFAEs by both CFE-Mean and ICL, using the revised thresholds.

### **Results**

Table S5 shows the AUROC, the default and optimum threshold for CFE-StdDev, ACI and SCI, alongside the sensitivity and specificity, for each curve. The details of the Chi-square test and Cohen's kappa for from the thirty set of 10% randomly selected AEGs for validation are shown on Table S6.

Table S5. Sensitivity and specificity for CFE-StdDev, ACI and SCI ROC curves according to the CFAE classification in agreement between CFE-Mean and ICL.

	Threshold (ms)		Sensitivity	1-Specificity	AUROC	P-value
Test 1	CFE-StdDev	47.06	0.900	0.189	0.878	P<0.0001
	ACI	82.08	0.826	0.363	0.757	
	SCI	58.75	0.817	0.293	0.808	
Test 2	CFE-StdDev	47.73	0.922	0.202	0.873	P<0.0001
	ACI	82.92	0.846	0.366	0.757	
	SCI	58.75	0.814	0.304	0.810	
Test 3	CFE-StdDev	46.31	0.898	0.181	0.877	P<0.0001
	ACI	82.08	0.819	0.361	0.756	
	SCI	57.92	0.795	0.287	0.812	
Test 4	CFE-StdDev	45.73	0.896	0.183	0.876	P<0.0001
	ACI	82.92	0.853	0.379	0.753	
	SCI	58.75	0.833	0.307	0.812	
Test 5	CFE-StdDev	45.52	0.890	0.186	0.876	P<0.0001
	ACI	82.08	0.813	0.359	0.754	
	SCI	58.75	0.813	0.304	0.806	
Test 6	CFE-StdDev	45.73	0.891	0.181	0.876	P<0.0001
	ACI	82.08	0.827	0.372	0.747	
	SCI	58.75	0.823	0.313	0.805	
Test 7	CFE-StdDev	46.55	0.900	0.176	0.886	P<0.0001
	ACI	82.08	0.820	0.348	0.767	
	SCI	58.75	0.817	0.282	0.819	
Test 8	CFE-StdDev	46.55	0.903	0.191	0.876	P<0.0001
	ACI	82.08	0.829	0.357	0.759	
	SCI	57.92	0.803	0.291	0.814	
Test 9	CFE-StdDev	45.71	0.891	0.178	0.877	P<0.0001
	ACI	82.08	0.819	0.354	0.757	
	SCI	58.75	0.805	0.304	0.805	
Test 10	CFE-StdDev	47.73	0.918	0.208	0.868	P<0.0001
	ACI	82.08	0.830	0.360	0.760	
	SCI	58.75	0.833	0.298	0.813	
Test 11	CFE-StdDev	46.55	0.902	0.187	0.875	P<0.0001
	ACI	82.08	0.821	0.364	0.756	
	SCI	58.75	0.828	0.314	0.804	
Test 12	CFE-StdDev	45.73	0.894	0.172	0.887	P<0.0001
	ACI	82.08	0.825	0.344	0.771	
	SCI	57.92	0.798	0.273	0.824	
Test 13	CFE-StdDev	47.73	0.921	0.199	0.879	P<0.0001
	ACI	82.08	0.823	0.362	0.759	
	SCI	57.92	0.797	0.298	0.808	
Test 14	CFE-StdDev	47.73	0.927	0.190	0.880	P<0.0001
	ACI	82.08	0.832	0.338	0.774	
	SCI	58.75	0.815	0.287	0.818	

Table S5. Cont.

	Threshold (ms)		Sensitivity	1-Specificity	AUROC	P-value
Test 15	CFE-StdDev	46.55	0.907	0.176	0.884	P<0.0001
	ACI	82.08	0.827	0.355	0.764	
	SCI	58.75	0.823	0.302	0.810	
Test 16	CFE-StdDev	47.73	0.922	0.184	0.890	P<0.0001
	ACI	82.08	0.823	0.360	0.761	
	SCI	58.75	0.823	0.305	0.810	
Test 17	CFE-StdDev	45.73	0.893	0.186	0.875	P<0.0001
	ACI	82.08	0.830	0.365	0.759	
	SCI	57.92	0.807	0.297	0.811	
Test 18	CFE-StdDev	47.73	0.930	0.186	0.883	P<0.0001
	ACI	82.92	0.850	0.370	0.765	
	SCI	58.75	0.823	0.302	0.813	
Test 19	CFE-StdDev	45.52	0.892	0.180	0.878	P<0.0001
	ACI	82.92	0.842	0.370	0.756	
	SCI	58.75	0.815	0.305	0.810	
Test 20	CFE-StdDev	45.71	0.898	0.170	0.882	P<0.0001
	ACI	82.08	0.832	0.353	0.762	
	SCI	58.75	0.815	0.315	0.810	
Test 21	CFE-StdDev	46.09	0.896	0.185	0.878	P<0.0001
	ACI	82.08	0.818	0.358	0.754	
	SCI	58.75	0.815	0.303	0.810	
Test 22	CFE-StdDev	45.73	0.897	0.176	0.880	P<0.0001
	ACI	82.08	0.830	0.363	0.759	
	SCI	57.92	0.807	0.292	0.814	
Test 23	CFE-StdDev	47.85	0.925	0.192	0.882	P<0.0001
	ACI	82.08	0.818	0.344	0.766	
	SCI	58.75	0.821	0.305	0.817	
Test 24	CFE-StdDev	46.55	0.902	0.185	0.875	P<0.0001
	ACI	82.08	0.818	0.345	0.762	
	SCI	59.58	0.842	0.305	0.824	
Test 25	CFE-StdDev	46.09	0.899	0.182	0.879	P<0.0001
	ACI	82.92	0.845	0.367	0.758	
	SCI	58.75	0.814	0.302	0.810	
Test 26	CFE-StdDev	47.20	0.913	0.186	0.877	P<0.0001
	ACI	82.08	0.820	0.358	0.757	
	SCI	58.75	0.823	0.310	0.807	
Test 27	CFE-StdDev	47.06	0.902	0.179	0.889	P<0.0001
	ACI	82.08	0.824	0.366	0.763	
	SCI	58.75	0.837	0.299	0.819	
Test 28	CFE-StdDev	47.20	0.911	0.186	0.880	P<0.0001
	ACI	82.08	0.819	0.364	0.753	
	SCI	58.75	0.826	0.304	0.808	

Table S5. Cont.

	Threshold (ms)		Sensitivity	1-Specificity	AUROC	P-value
Test 29	CFE-StdDev	45.52	0.883	0.177	0.874	P<0.0001
	ACI	82.08	0.811	0.365	0.751	
	SCI	58.75	0.801	0.296	0.811	
Test 30	CFE-StdDev	46.55	0.914	0.192	0.808	P<0.0001
	ACI	82.08	0.825	0.367	0.749	
	SCI	57.92	0.801	0.291	0.808	

Table S6. Chi-square test and Cohen’s kappa CFAE classification performed by default and optimized thresholds for NavX and CARTO from the validation dataset.

	Thresholds	$\chi^2$	P-values	Kappa	P-values
Test 1	Default	24.5	<0.0001	0.423	<0.0001
	Revised	13.9		0.387	
Test 2	Default	11.2	0.001	0.283	0.001
	Revised	21.1	<0.0001	0.473	<0.0001
Test 3	Default	10.4	0.001	0.257	0.001
	Revised	14.8	<0.0001	0.402	<0.0001
Test 4	Default	9.6	0.002	0.241	0.001
	Revised	21.7	<0.0001	0.486	<0.0001
Test 5	Default	23.1	<0.0001	0.404	<0.0001
	Revised	34.8		0.609	
Test 6	Default	20.8	<0.0001	0.393	<0.0001
	Revised	28.9		0.556	
Test 7	Default	13.0	<0.0001	0.281	<0.0001
	Revised	15.9		0.419	
Test 8	Default	13.5	<0.0001	0.305	<0.0001
	Revised	15.2		0.408	
Test 9	Default	23.4	<0.0001	0.409	<0.0001
	Revised	21.2		0.480	
Test 10	Default	12.8	<0.0001	0.295	<0.0001
	Revised	19.6		0.458	
Test 11	Default	18.7	<0.0001	0.382	<0.0001
	Revised	25.8		0.518	
Test 12	Default	24.3	<0.0001	0.419	<0.0001
	Revised	9.1	0.003	0.321	0.001
Test 13	Default	15.0	<0.0001	0.328	<0.0001
	Revised	21.1		0.475	
Test 14	Default	11.6	0.001	0.260	<0.0001
	Revised	11.9		0.366	
Test 15	Default	13.5	<0.0001	0.288	<0.0001
	Revised	18.5		0.451	
Test 16	Default	20.4	<0.0001	0.388	<0.0001
	Revised	10.7	0.001	0.343	0.001
Test 17	Default	16.8	<0.0001	0.338	<0.0001
	Revised	29.1		0.554	
Test 18	Default	12.9	<0.0001	0.311	<0.0001
	Revised	9.7	0.002	0.330	0.001
Test 19	Default	24.2	<0.0001	0.466	<0.0001
	Revised	43.0		0.674	
Test 20	Default	12.8	<0.0001	0.295	<0.0001
	Revised	18.7		0.454	

Table S6. Cont.

	Thresholds	$\chi^2$	P-values	Kappa	P-values
Test 21	Default	30.0	<0.0001	0.521	<0.0001
	Revised	17.4		0.437	
Test 22	Default	9.5	0.002	0.255	0.001
	Revised	19.7	<0.0001	0.463	<0.0001
Test 23	Default	12.5	<0.0001	0.272	<0.0001
	Revised	18.9		0.454	
Test 24	Default	9.0	0.003	0.232	0.001
	Revised	5.8	0.016	0.261	0.009
Test 25	Default	14.0	<0.0001	0.313	<0.0001
	Revised	21.1		0.480	
Test 26	Default	15.8	<0.0001	0.323	<0.0001
	Revised	16.9		0.430	
Test 27	Default	19.9	<0.0001	0.361	<0.0001
	Revised	16.7		0.422	
Test 28	Default	27.4	<0.0001	0.459	<0.0001
	Revised	25.0		0.519	
Test 29	Default	22.4	<0.0001	0.396	<0.0001
	Revised	43.8		0.680	
Test 30	Default	8.4	0.004	0.247	0.002
	Revised	9.9	0.002	0.334	0.001

## Appendix E : Ranked results from the MANOVA and The coefficients from the LDA

Table S7. Ranked results of effect of the group of AEGs (1, 2, 3 and 4) on the indices of fractionation before and after ablation from the MANOVA.

AEG group	Pre-ablation				Post-ablation			
	1	2	3	4	1	2	3	4
CFE-Mean	0.476	0.336	0.395	0.667	0.279	0.622	0.481	0.559
ICL	0.685	0.563	0.449	0.218	0.790	0.293	0.451	0.452
CFE-StdDev	0.478	0.330	0.398	0.673	0.310	0.635	0.490	0.539
ACI	0.446	0.428	0.494	0.605	0.327	0.646	0.524	0.527
SCI	0.398	0.404	0.500	0.685	0.266	0.678	0.533	0.526
ShEn	0.497	0.505	0.482	0.486	0.523	0.487	0.482	0.487
SampEn	0.524	0.528	0.506	0.414	0.600	0.382	0.468	0.509
KL	0.505	0.480	0.502	0.536	0.454	0.542	0.532	0.514
PP	0.582	0.552	0.516	0.368	0.708	0.327	0.453	0.489
RMS	0.551	0.587	0.566	0.383	0.702	0.342	0.468	0.480
DF	0.537	0.459	0.497	0.542	0.582	0.534	0.514	0.394
OI	0.573	0.513	0.472	0.396	0.536	0.439	0.478	0.500

At baseline, the first discriminant function explained 89.1% of the variance, followed by 6.6% and 4.3%, successfully identifying 65% of the AEG classifications. After PVI+RL, the first discriminant function explained 97% of the variance, followed by 2.5% and 0.5%, and the correct identification of the AEG groups improved to 72%. The coefficients from the LDA can be seen in Table S8.

Table S8. Coefficients from the LDA to discriminate the AEG groups (1, 2, 3 and 4) across the twelve indices of fractionation. Both SCI and ShEn were the indices with the highest importance in identifying the discriminant functions before and after ablation.

Linear discriminants	Pre-ablation			Post-ablation		
	LD1	LD2	LD3	LD1	LD2	LD3
CFE-Mean	1.854	0.072	3.084	0.257	0.701	-0.223
ICL	-1.862	0.584	-0.918	-3.230	0.162	-0.803
CFE-StdDev	-0.296	0.773	-2.407	0.052	0.028	0.107
ACI	-1.910	-0.197	5.006	2.987	1.667	7.101
SCI	0.076	-1.444	<b>-6.722</b>	<b>-3.888</b>	0.380	-3.091
ShEn	<b>-2.716</b>	<b>-3.444</b>	-2.201	-3.849	<b>-8.194</b>	<b>16.263</b>
SampEn	-0.414	0.3712	0.107	-0.269	-0.180	-0.295
KL	-0.096	0.925	-0.015	-0.624	-0.997	0.231
PP	0.290	0.759	0.516	-0.100	0.500	0.452
RMS	-0.388	-1.412	-1.192	0.133	0.515	0.945
DF	1.160	0.949	-2.019	0.141	-3.500	0.861
OI	-0.106	-0.168	-0.913	-0.140	-0.339	0.125

## **Appendix F : the spatio-temporal consistency of atrial electrograms in persistent atrial fibrillation before and after PVI+RL**

### **Temporal behaviour of consecutive AEGs before PVI+RL**

The temporal behaviour of the three consecutive segments for each collected point prior PVI+RL is shown on Figure S3. Figure S3A shows that 86% of the AEGs initially classified as fractionated in segment 1 remained fractionated in segment 2, while 14% changed from fractionated to non-fractionated. Similarly, 67% of the AEGs classified as non-fractionated in segment 1 remained non-fractionated in segment 2, while 33% changed from non-fractionated to fractionated. In the following segments, 88% of AEGs classified as fractionated in segment 2 remained fractionated in segment 3, while 12% changed from fractionated to non-fractionated. 74% of the AEGs classified as non-fractionated in segment 2 remained non-fractionated in segment 3, while 26% changed from non-fractionated to fractionated. When comparing segment 1 versus 2, 57% of the total AEGs before any ablation were labelled as stable CFAEs, while 23% were stable non-CFAEs, and 20% AEGs were unstable (Figure S3B). When comparing segment 2 versus 3, 60% of the total AEGs were labelled as stable CFAEs, 24% were stable non-CFAEs, and 16% AEGs were unstable. A total of 52% AEGs were stable CFAEs within the three segments, 20% were stable non-CFAEs and 26% were unstable.

Figure S3C illustrates the temporal decay of stable AEGs (CFAEs and non-CFAE) before PVI+RL. In the first 2.5 s segment, all AEGs were considered stable since it was the first classification (455 AEGs). On segment 2, a total of 92 AEGs were classified as unstable, remaining 363 stable AEGs. On the last segment, additional 36 AEGs changed their classification, remaining 327 stable AEGs. The exponential best fit suggests a temporal decay ( $\tau$ ) of 2.7 s, in which 304 AEGs (67% of 455 AEGs) would be temporally stable prior PVI+RL.

The occurrence of the different types of AEGs (stable CFAE, stable non-CFAE and unstable AEG) per LA region before ablation, considering the three AEG segments, is shown in Figure S3D. Stable CFAEs were observed in all regions, with the anterior wall showing the highest incidence, followed by the septum, posterior wall, lateral, roof and

PVs. Unstable AEGs were also observed in all regions, with the lateral showing the highest incidence.

### **Temporal behaviour of consecutive AEGs after PVI+RL**

The temporal behaviour of the three consecutive segments for each collected point after PVI+RL is shown on Figure S4. Figure S4A shows that 81% of the AEGs initially classified as fractionated in segment 1 remained fractionated in segment 2, while 19% changed from fractionated to non-fractionated. Similarly, 84% of the AEGs classified as non-fractionated in segment 1 remained non-fractionated in segment 2, while 16% changed from non-fractionated to fractionated. In the following segments, 83% of AEGs classified as fractionated in segment 2 remained fractionated in segment 3, while 17% changed from fractionated to non-fractionated. 87% of the AEGs classified as non-fractionated in segment 2 remained non-fractionated in segment 3, while 13% changed from non-fractionated to fractionated. When comparing segment 1 versus 2, 32% of the total AEGs after ablation were labelled as stable CFAEs, while 51% were stable non-CFAEs, and 17% AEGs were unstable (Figure S4B). When comparing segment 2 versus 3, 35% of the total AEGs were labelled as stable CFAEs, 50% were stable non-CFAEs, and 15% AEGs were unstable. A total of 28% AEGs were stable CFAEs within the three segments, 47% were stable non-CFAEs and 25% were unstable.

Figure S4C illustrates the temporal decay of stable AEGs (CFAEs and non-CFAEs) after PVI+RL. In the first 2.5 s segment, all AEGs were considered stable since it was the first classification (342 AEGs). On segment 2, a total of 59 AEGs were classified as unstable, remaining 283 stable AEGs. On the last segment, additional 26 AEGs changed their classification, remaining 257 stable AEGs. The exponential best fit suggests a temporal decay ( $\tau$ ) of 3 s, in which 236 AEGs (69% of 342 AEGs) would be temporally stable after PVI+RL.

The occurrence of the different types of AEGs (stable CFAE, stable non-CFAE and unstable AEG) per LA region after ablation, considering the three AEG segments, is shown in Figure S4D. Stable CFAEs were observed in all regions, with the anterior wall showing the highest incidence, followed by the septum, posterior wall, lateral, roof and

PVs. Unstable AEGs were also observed in all regions, with the anterior wall showing the highest incidence.

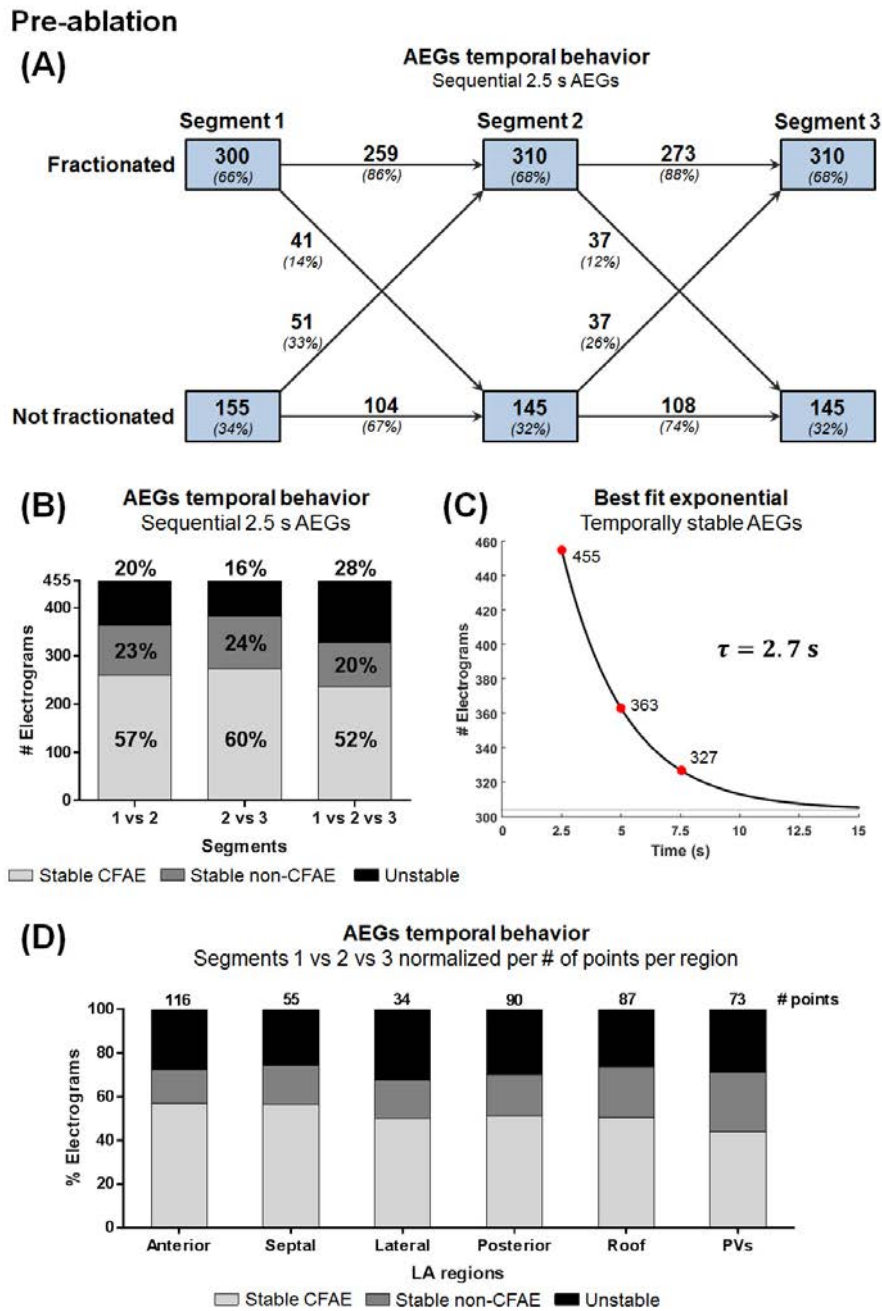
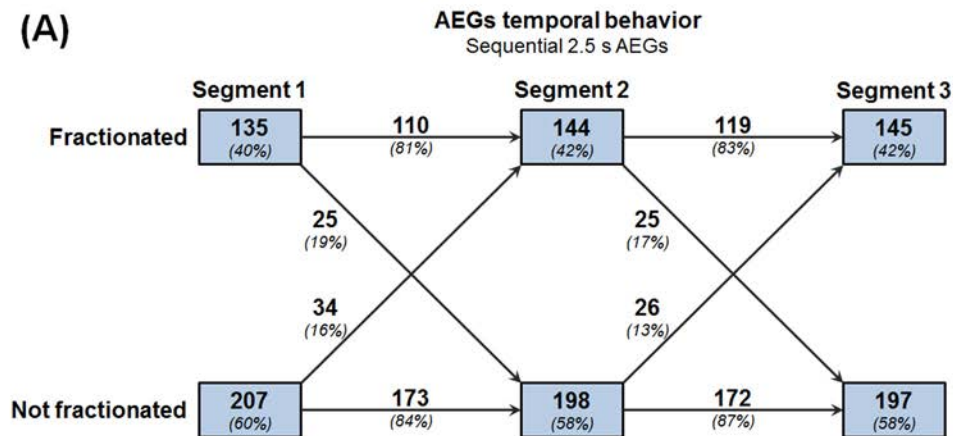


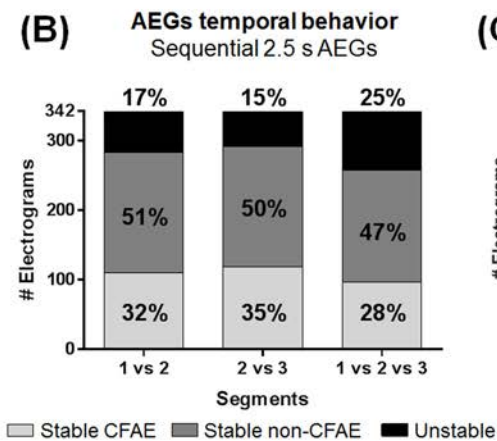
Figure S3. The temporal behaviour of three consecutive AEG segments with 2.5 s duration each prior PVI+RL. A. The 8 s segments were divided in three consecutive 2.5 s length segments. The ICL was measured in each segment and classified whether as fractionated or non-fractionated. The AEGs that remained fractionated, remained non-fractionated and changed classification were assessed between segments. B. The percentage of ‘stable CFAE’; ‘stable non CFAE’ and ‘unstable AEG’ calculated in each segment. C. The temporal decay of stable AEGs assessed within 7.5 s. D. The regional occurrence of the different types of AEGs normalized by the number of collected points per region.

Post-ablation

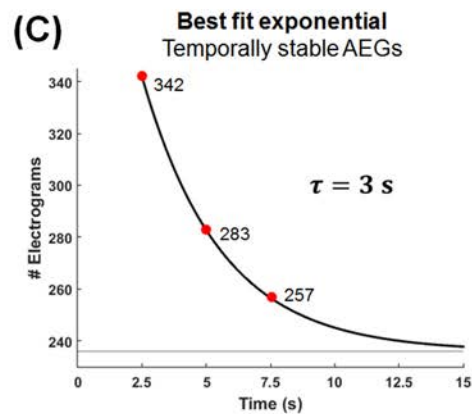
(A)



(B)



(C)



(D)

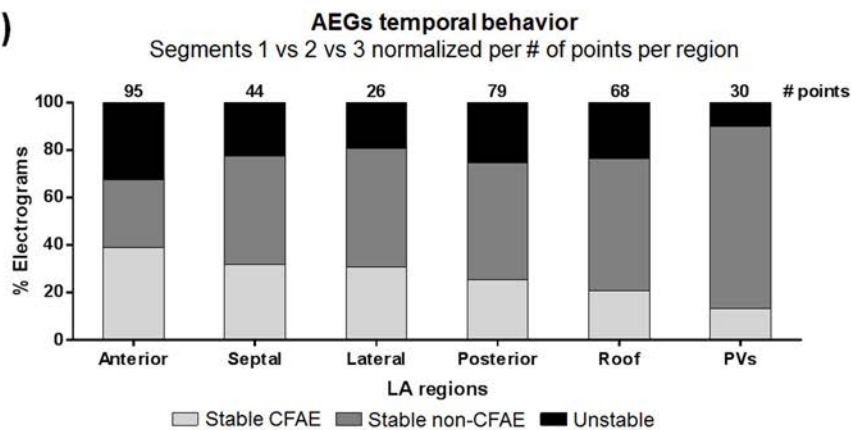


Figure S4. The temporal behaviour of three consecutive AEG segments with 2.5 s duration each after PVI+RL. A. The 8 s segments were divided in three consecutive 2.5 s length segments. The ICL was measured in each segment and classified whether as fractionated or non-fractionated. The AEGs that remained fractionated, remained non-fractionated and changed classification were assessed between segments. B. The percentage of ‘stable CFAE’; ‘stable non CFAE’ and ‘unstable AEG’ calculated in each segment. C. The temporal decay of stable AEGs assessed within 7.5 s. D. The regional occurrence of the different types of AEGs normalized by the number of collected points per region.

## Temporal consistency of AEG fractionation with different segment lengths before PVI+RL

ICL measured with 2.5 s, 5 s and 8 s before ablation is illustrated in Figure S5A. ICL measured with 2.5 s was significantly different than with 5 s and 8 s. The bias calculated from the Bland-Altman plots suggests a smaller average difference between ICL calculated with 5 s and 8 s when compared with the other segment lengths (2.5 s vs 5 s and 2.5 s vs 8 s, Figure S5B).

### Pre-ablation

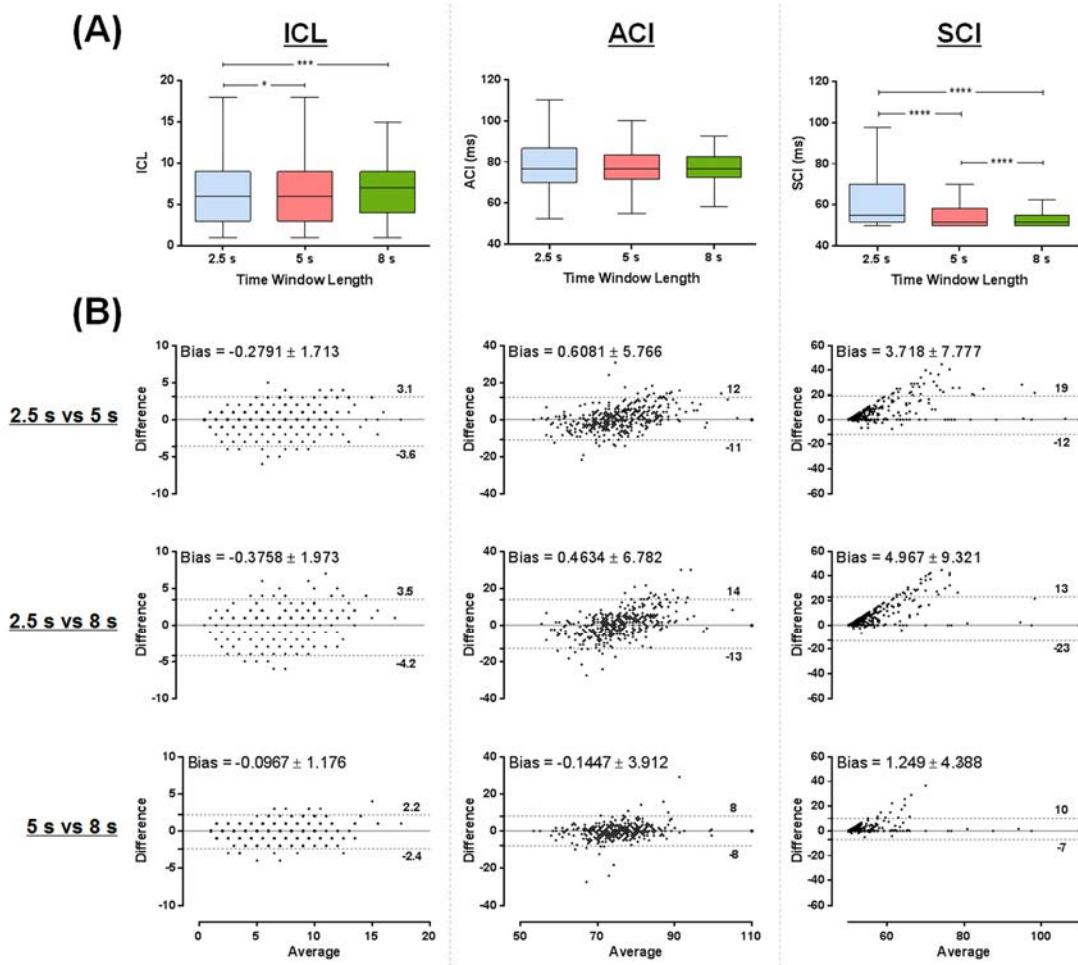


Figure S5. The ICL, ACI and SCI measured with 2.5 s, 5 s and 8 s prior ablation. B. Bland-Altman plots for ICL, ACI and SCI measured with 2.5 s, 5 s and 8 s. \*\*\*\* P<0.0001; \*\*\* P<0.001; \* P<0.05.

Different segment lengths had little influence on ACI prior ablation, but significantly affected SCI (Figure S5A). Nevertheless, the Bland-Altman plots also suggest smaller average difference between 5 s and 8 s for both ACI and SCI (Figure S5B).

## **Temporal consistency of AEG fractionation with different segment lengths after PVI+RL**

Different segment lengths had little influence on ICL measured with 2.5 s, 5 s and 8 s after ablation is illustrated in Figure S6A. The bias calculated from the Bland-Altman plots suggests a smaller average difference between ICL calculated with 5 s and 8 s when compared with the other segment lengths (2.5 s vs 5 s and 2.5 s vs 8 s, Figure S6B).

Different segment lengths also had little influence on ACI after ablation, but significantly affected SCI (Figure S6A). Nevertheless, the Bland-Altman plots also suggest smaller average difference between 5 s and 8 s for both ACI and SCI (Figure S4B).

## **LA maps based on the consecutive AEG segments and different segment lengths**

The LA maps based on the three consecutive AEG segments with 2.5 s duration each for all patients as measured by ICL, ACI and SCI are shown on Figures S7, S8 and S9, respectively. The LA maps based on the on the different segment lengths (2.5 s, 5 s and 8 s) for all patients as measured by ICL, ACI and SCI are shown on Figures S10, S11 and S12, respectively.

Post-ablation

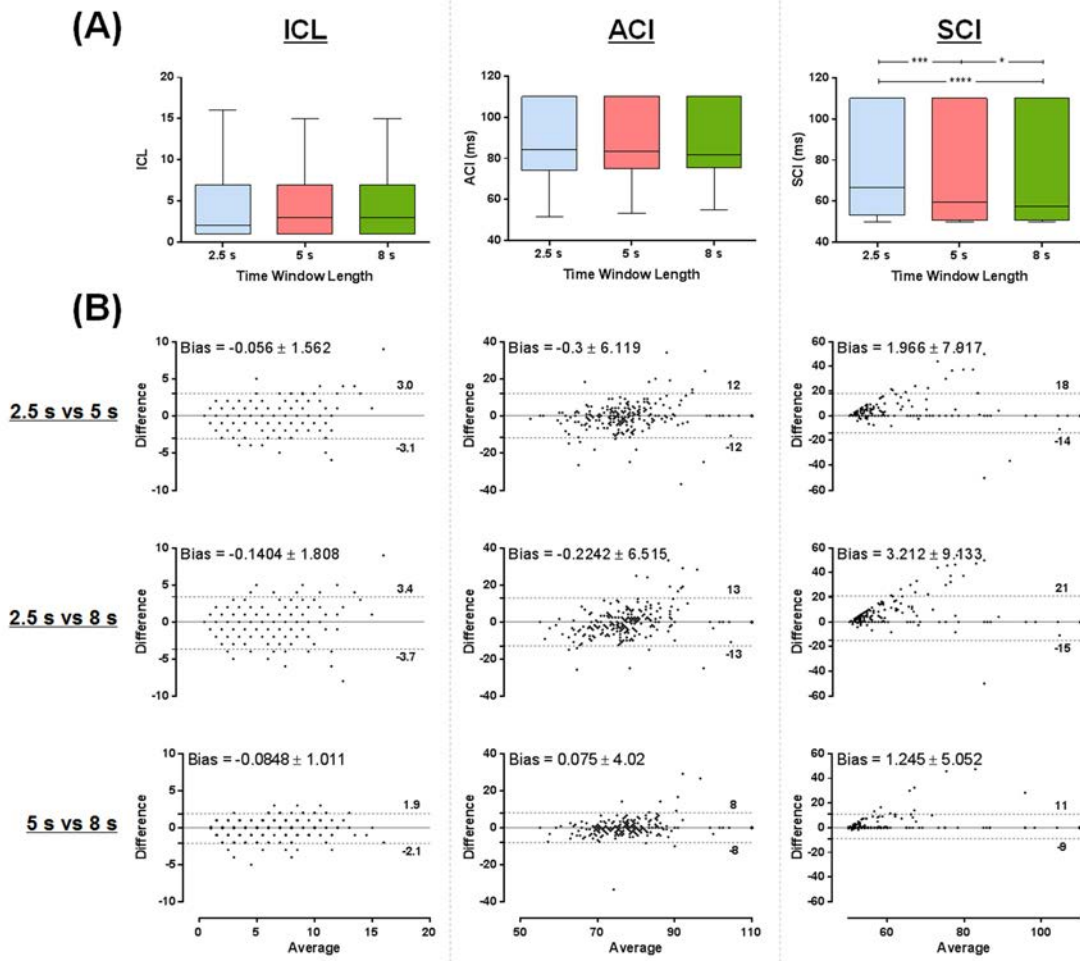


Figure S6. The ICL, ACI and SCI measured with 2.5 s, 5 s and 8 s after ablation. B. Bland-Altman plots for ICL, ACI and SCI measured with 2.5 s, 5 s and 8 s. \*\*\*\* P<0.0001; \*\*\* P<0.001; \* P<0.05.

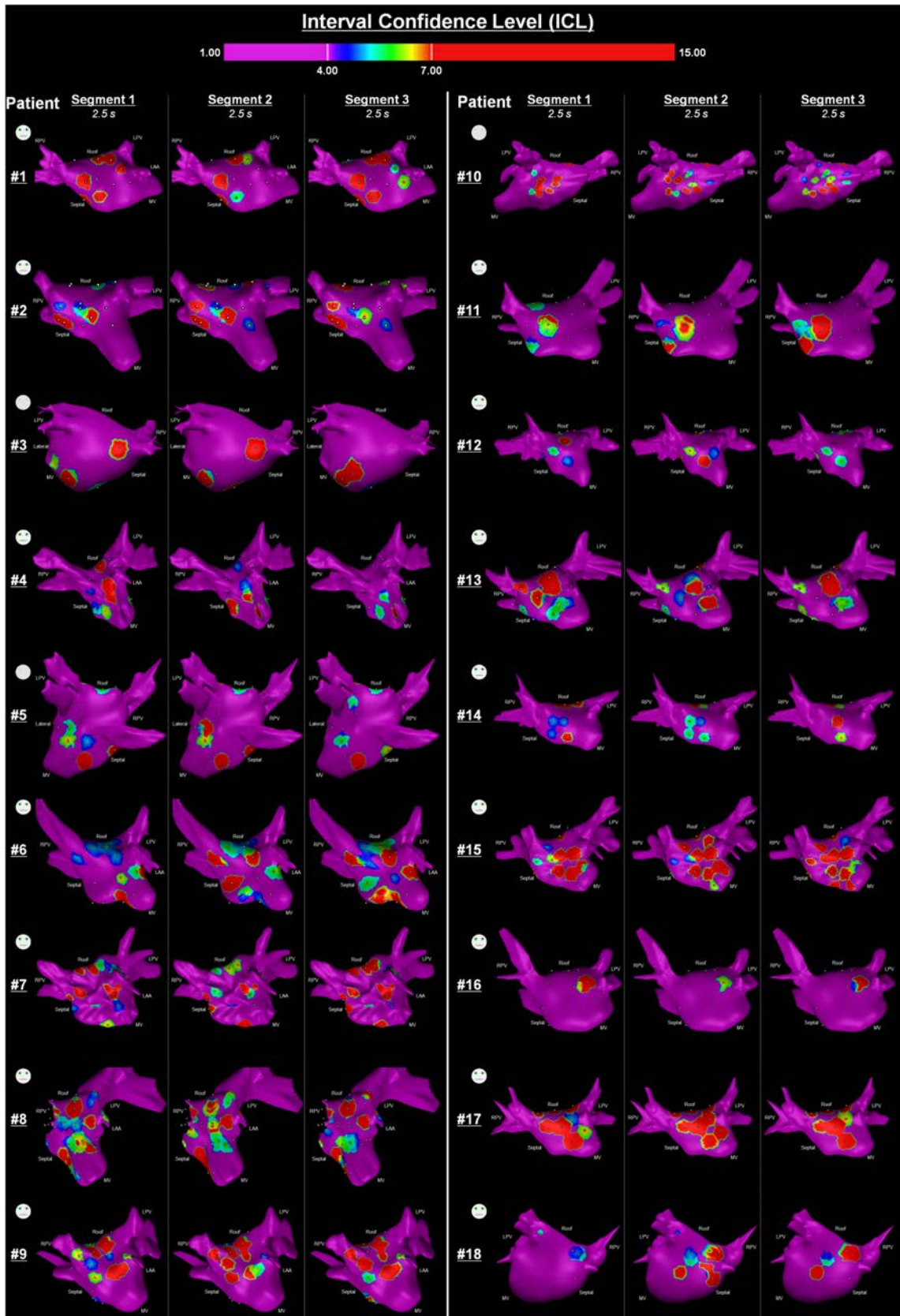


Figure S7. The three consecutive AEG segments with 2.5 s duration measured by ICL.

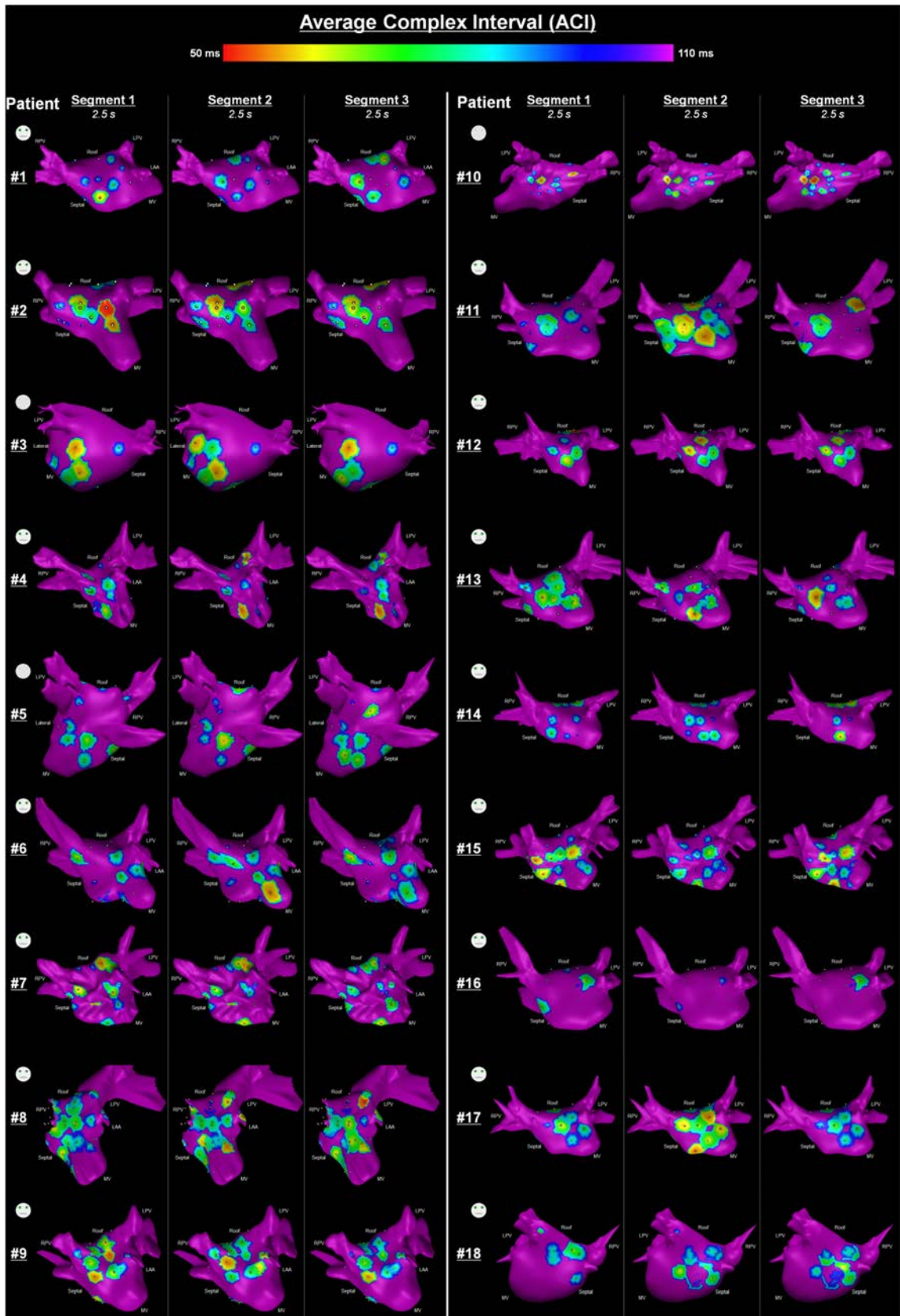


Figure S8. The three consecutive AEG segments with 2.5 s duration measured by ACI.

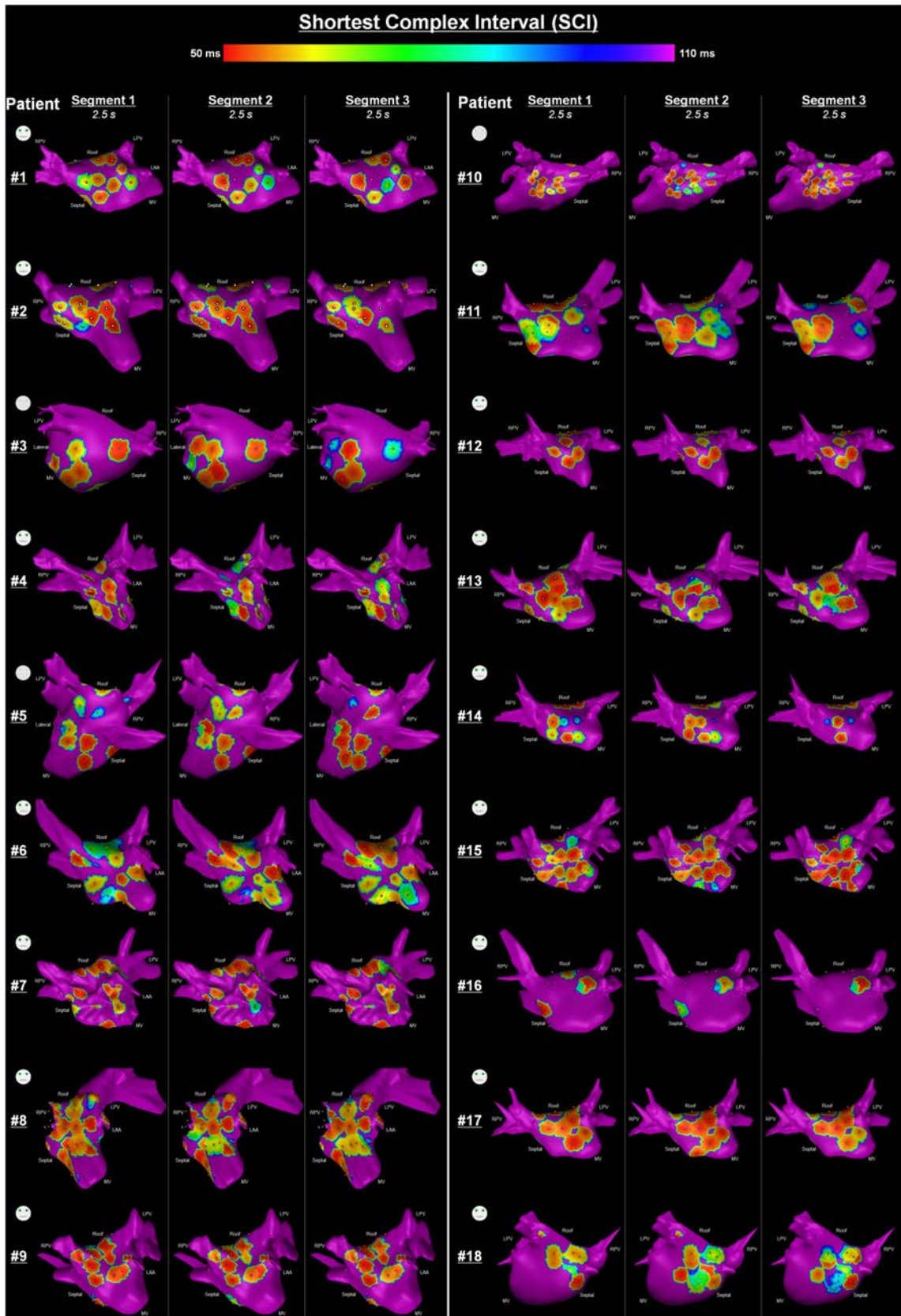


Figure S9. The three consecutive AEG segments with 2.5 s duration measured by SCI.

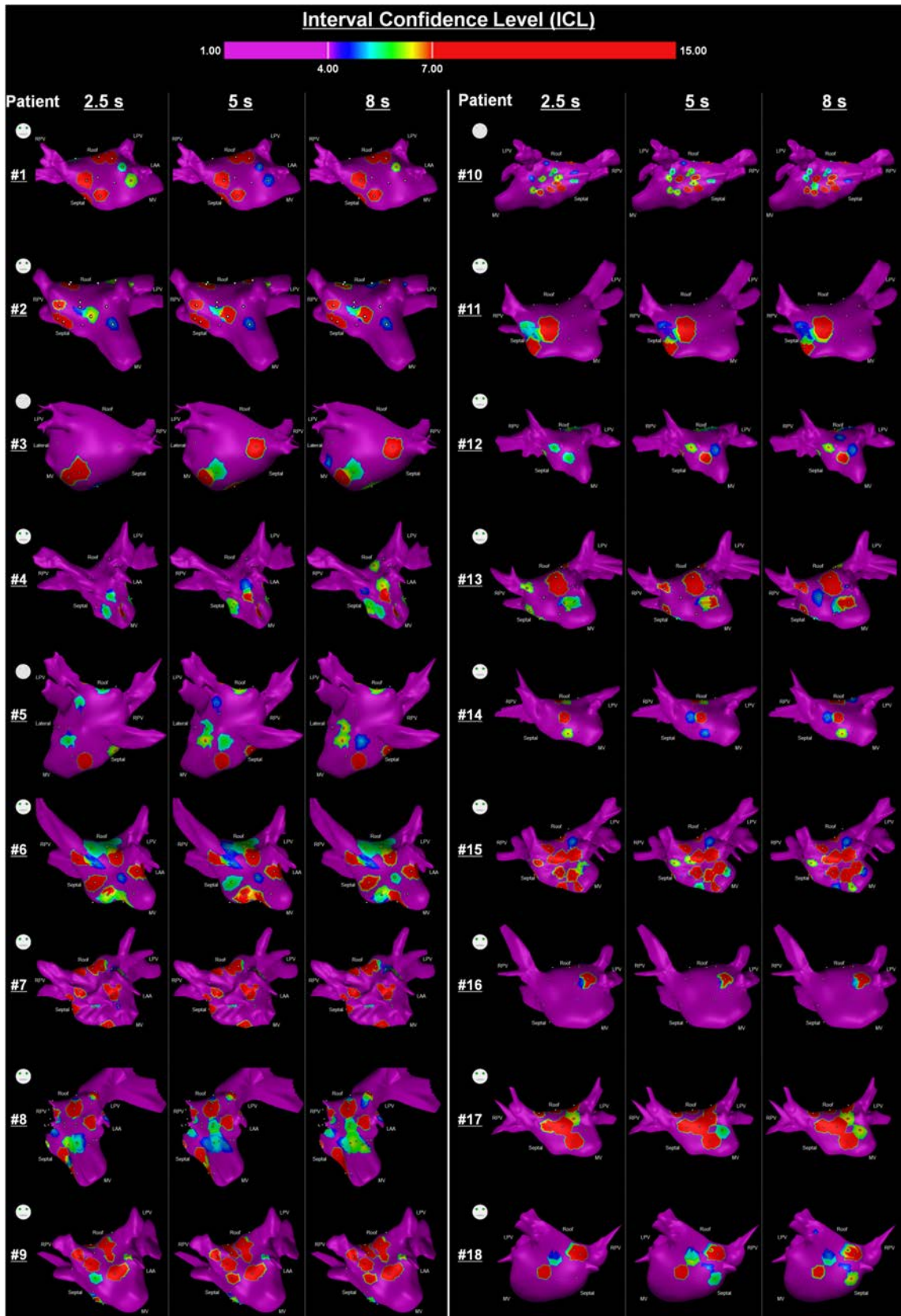


Figure S10. The different segment lengths (2.5 s, 5 s and 8 s) measured by ICL.

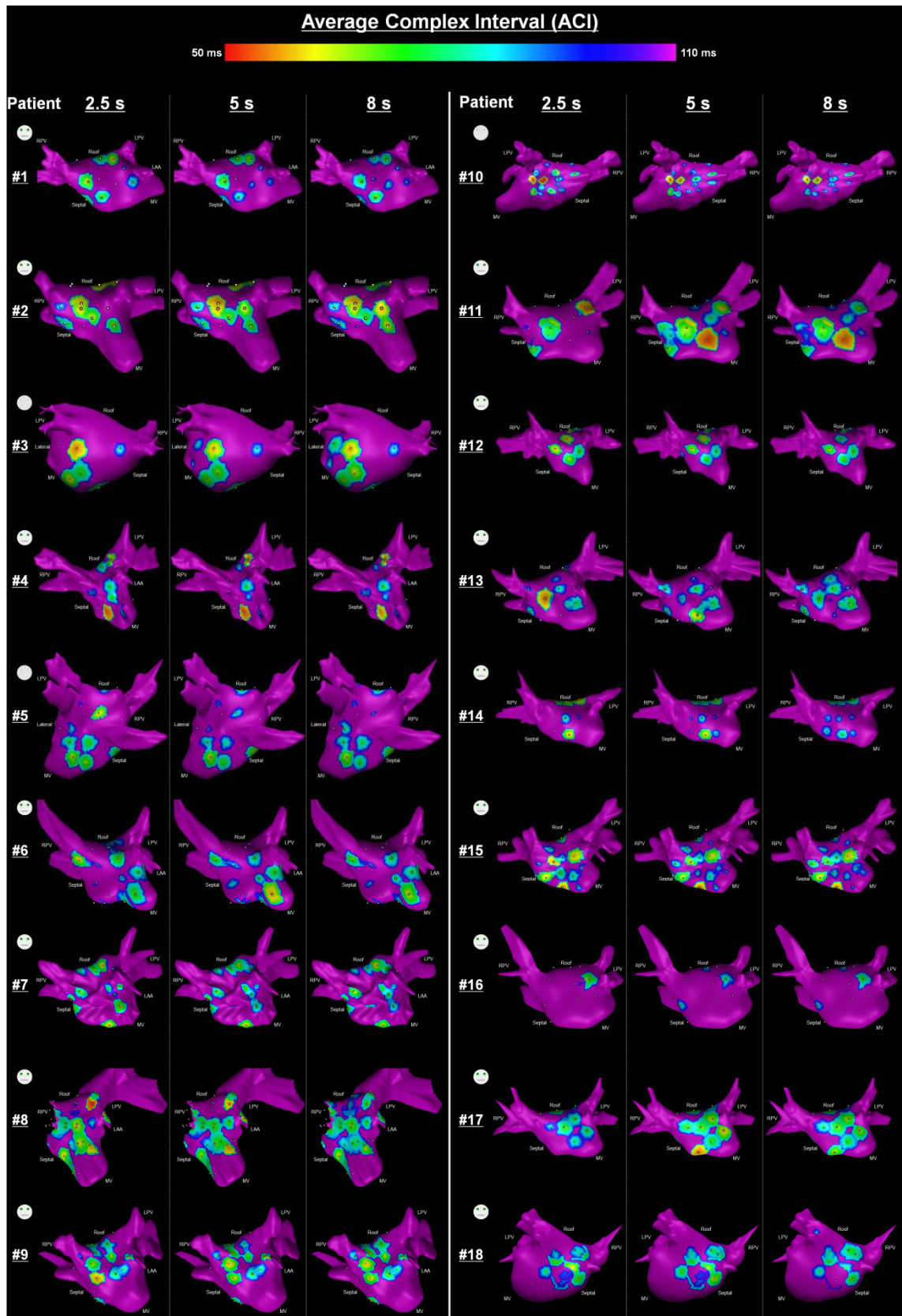


Figure S11. The different segment lengths (2.5 s, 5 s and 8 s) measured by ACI.



## References

- AIZER, A., HOLMES, D. S., GARITSKI, A. C., BERNSTEIN, N. E., SMYTH-MELSKY, J. M., FERRICK, A. M. & CHINITZ, L. A. 2008. Standardization and validation of an automated algorithm to identify fractionation as a guide for atrial fibrillation ablation. *Heart Rhythm*, 5, 1134-1141.
- ALCARAZ, R., ABASOLO, D., HORNERO, R. & RIETA, J. J. 2010. Optimal parameters study for sample entropy-based atrial fibrillation organization analysis. *Comput Methods Programs Biomed*, 99, 124-32.
- ALLESSIE, M., AUSMA, J. & SCHOTTEN, U. 2002. Electrical, contractile and structural remodeling during atrial fibrillation. *Cardiovasc Res*, 54, 230-46.
- ALLESSIE, M. & DE GROOT, N. 2014. CrossTalk opposing view: Rotors have not been demonstrated to be the drivers of atrial fibrillation. *The Journal of Physiology*, 592, 3167-3170.
- ALLESSIE, M. A., BONKE, F. I. M. & SCHOPMAN, F. J. 1973. Circus Movement in Rabbit Atrial Muscle as a Mechanism of Tachycardia. *Circ Res*, 33, 54-62.
- ALLESSIE, M. A., DE GROOT, N. M., HOUBEN, R. P., SCHOTTEN, U., BOERSMA, E., SMEETS, J. L. & CRIJNS, H. J. 2010. Electropathological substrate of long-standing persistent atrial fibrillation in patients with structural heart disease: longitudinal dissociation. *Circ Arrhythm Electrophysiol*, 3, 606-15.
- ALLESSIE, M. A., LAMMERS, W. J. E. P., BONKE, F. I. M. & HOLLEN, J. 1985. Experimental evaluation of Moe's multiple wavelet hypothesis of atrial fibrillation. In: ZIPES, D. & JALIFE, J. (eds.) *In Cardiac Electrophysiology and Arrhythmias (1985)*, pp. 265-276 Key: citeulike:10380603. Orlando, FL: Grune & Stratton.
- ALMEIDA, T. P., CHU, G. S., SALINET, J. L., VANHEUSDEN, F. J., LI, X., DASTAGIR, N., TUAN, J. H., STAFFORD, P. J., NG, G. A. & SCHLINDWEIN, F. S. Targeting complex fractionated atrial electrograms during persistent atrial fibrillation ablation: quid faciat? Atrial Signals 2015, 2015a Karlsruhe.

- ALMEIDA, T. P., CHU, G. S., SALINET, J. L., VANHEUSDEN, F. J., LI, X., TUAN, J. H., STAFFORD, P. J., NG, G. A. & SCHLINDWEIN, F. S. 2016. Minimizing discordances in automated classification of fractionated electrograms in human persistent atrial fibrillation. *Medical & Biological Engineering & Computing*, published online 25 February 2016, 1-12.
- ALMEIDA, T. P., CHU, G. S., SALINET, J. L., VANHEUSDEN, F. J., LI, X., TUAN, J. H., STAFFORD, P. J., SCHILINDWEIN, F. S. & NG, G. A. 2015b. Differences in fractionated electrogram detection: a direct quantitative comparison between NavX and CARTO. *Europace*, 17, v18-v21.
- ALMEIDA, T. P., CHU, G. S., SALINET, J. L., VANHEUSDEN, F. J., LI, X., TUAN, J. H., STAFFORD, P. J., SCHILINDWEIN, F. S. & NG, G. A. 2015c. Unifying Automated Fractionated Atrial Electrogram Classification using Electroanatomical Mapping Systems in Persistent Atrial Fibrillation Studies *Computing in Cardiology Conference (CinC), 2015*, 53-56.
- ALMEIDA, T. P., CHU, G. S., VANHEUSDEN, F. J., LI, X., SALINET, J. L., TUAN, J. H., STAFFORD, P. J., SCHLINDWEIN, F. S. & NG, G. A. 2014. Investigating differences in complex fractionated atrial electrogram discrimination as performed by CARTO and NavX algorithms. *Europace*, 16, iii25-iii25.
- ALMEIDA, T. P., SALINET, J. L., CHU, G. S., NG, G. A. & SCHLINDWEIN, F. S. 2013a. Different definitions of complex fractionated atrial electrograms do not concur with the clinical perspective. *Computing in Cardiology Conference (CinC), 2013*, 1055-1058.
- ALMEIDA, T. P., SALINET, J. L., CHU, G. S., SCHLINDWEIN, F. S. & NG, G. A. 2013b. Atrial Electrogram Complexity as a Clinical Instrument for Measuring Temporal Fractionation Variability during Atrial Fibrillation. *Europace*, 15, iv31-iv35.
- ALMEIDA, T. P., SALINET, J. L., CHU, G. S., TUAN, J. H., SCHLINDWEIN, F. S. & NG, G. A. 2013c. Atrial Electrogram Complexity as an Objective Measurement of Fractionation during Atrial Fibrillation. *Heart Rhythm*, 10, S1-S40.

- ASHIHARA, T., HARAGUCHI, R., NAKAZAWA, K., NAMBA, T., IKEDA, T., NAKAZAWA, Y., OZAWA, T., ITO, M., HORIE, M. & TRAYANOVA, N. A. 2012. The role of fibroblasts in complex fractionated electrograms during persistent/permanent atrial fibrillation: implications for electrogram-based catheter ablation. *Circ Res*, 110, 275-84.
- ATIENZA, F., ALMENDRAL, J., JALIFE, J., ZLOCHIVER, S., PLOUTZ-SNYDER, R., TORRECILLA, E. G., ARENAL, A., KALIFA, J., FERNANDEZ-AVILES, F. & BERENFELD, O. 2009. Real-time dominant frequency mapping and ablation of dominant frequency sites in atrial fibrillation with left-to-right frequency gradients predicts long-term maintenance of sinus rhythm. *Heart Rhythm*, 6, 33-40.
- ATIENZA, F., CALVO, D., ALMENDRAL, J., ZLOCHIVER, S., GRZEDA, K. R., MARTINEZ-ALZAMORA, N., GONZALEZ-TORRECILLA, E., ARENAL, A., FERNANDEZ-AVILES, F. & BERENFELD, O. 2011. Mechanisms of fractionated electrograms formation in the posterior left atrium during paroxysmal atrial fibrillation in humans. *J Am Coll Cardiol*, 57, 1081-92.
- AUSMA, J., WIJFFELS, M., THONÉ, F., WOUTERS, L., ALLESSIE, M. & BORGERS, M. 1997. Structural Changes of Atrial Myocardium due to Sustained Atrial Fibrillation in the Goat. *Circulation*, 96, 3157-3163.
- BARBARO, V., BARTOLINI, P., CALCAGNINI, G., MORELLI, S., MICHELUCCI, A. & GENSINI, G. 2000. Automated classification of human atrial fibrillation from intraatrial electrograms. *Pace-Pacing and Clinical Electrophysiology*, 23, 192-202.
- BARBARO, V., BARTOLINI, P., CALGAGNINI, G., CENSI, F., MORELLI, S. & MICHELUCCI, A. 2001. Mapping the organization of atrial fibrillation with basket catheters part I: Validation of a real-time algorithm. *Pace-Pacing and Clinical Electrophysiology*, 24, 1082-1088.
- BENHARASH, P., BUCH, E., FRANK, P., SHARE, M., TUNG, R., SHIVKUMAR, K. & MANDAPATI, R. 2015. Quantitative analysis of localized sources identified

by focal impulse and rotor modulation mapping in atrial fibrillation. *Circ Arrhythm Electrophysiol*, 8, 554-61.

BISHOP, C. M. 2006. *Pattern recognition and machine learning*, New York, Springer.

BOLLMANN, A. & LOMBARDI, F. 2006. Electrocardiology of atrial fibrillation - Current knowledge and future challenges. *Ieee Engineering in Medicine and Biology Magazine*, 25, 15-23.

BORGGREFE, M., HINDRICKS, G., HAVERKAMP, W. & BREITHARDT, G. 1990. Catheter ablation using radiofrequency energy. *Clinical Cardiology*, 13, 127-131.

BRAY, J. H. & MAXWELL, S. E. 1985. *Multivariate analysis of variance*, Newbury Park, CA, Sage.

BROOKS, A. G., STILES, M. K., LABORDERIE, J., LAU, D. H., KUKLIK, P., SHIPP, N. J., HSU, L. F. & SANDERS, P. 2010. Outcomes of long-standing persistent atrial fibrillation ablation: A systematic review. *Heart Rhythm*, 7, 835-846.

BUCH, E., SHARE, M., TUNG, R., BENHARASH, P., SHARMA, P., KONERU, J., MANDAPATI, R., ELLENBOGEN, K. A. & SHIVKUMAR, K. 2016. Long-term clinical outcomes of focal impulse and rotor modulation for treatment of atrial fibrillation: A multicenter experience. *Heart Rhythm*, 13, 636-41.

CALKINS, H., KUCK, K. H., CAPPATO, R., BRUGADA, J., CAMM, A. J., CHEN, S.-A., CRIJNS, H. J. G., DAMIANO, R. J., JR., DAVIES, D. W., DIMARCO, J., EDGERTON, J., ELLENBOGEN, K., EZEKOWITZ, M. D., HAINES, D. E., HAISSAGUERRE, M., HINDRICKS, G., IESAKA, Y., JACKMAN, W., JALIFE, J., JAIS, P., KALMAN, J., KEANE, D., KIM, Y.-H., KIRCHHOF, P., KLEIN, G., KOTTKAMP, H., KUMAGAI, K., LINDSAY, B. D., MANSOUR, M., MARCHLINSKI, F. E., MCCARTHY, P. M., MONT, J. L., MORADY, F., NADEMANEE, K., NAKAGAWA, H., NATALE, A., NATTEL, S., PACKER, D. L., PAPPONE, C., PRYSTOWSKY, E., RAVIELE, A., REDDY, V., RUSKIN, J. N., SHEMIN, R. J., TSAO, H.-M. & WILBER, D. 2012a. 2012 HRS/EHRA/ECAS Expert Consensus Statement on Catheter and Surgical Ablation of Atrial Fibrillation: Recommendations for Patient Selection,

Procedural Techniques, Patient Management and Follow-up, Definitions, Endpoints, and Research Trial Design. *Heart Rhythm*, 9, 632-696.e21.

CALKINS, H., KUCK, K. H., CAPPATO, R., BRUGADA, J., CAMM, A. J., CHEN, S. A., CRIJNS, H. J., DAMIANO, R. J., JR., DAVIES, D. W., DIMARCO, J., EDGERTON, J., ELLENBOGEN, K., EZEKOWITZ, M. D., HAINES, D. E., HAISSAGUERRE, M., HINDRICKS, G., IESAKA, Y., JACKMAN, W., JALIFE, J., JAIS, P., KALMAN, J., KEANE, D., KIM, Y. H., KIRCHHOF, P., KLEIN, G., KOTTKAMP, H., KUMAGAI, K., LINDSAY, B. D., MANSOUR, M., MARCHLINSKI, F. E., MCCARTHY, P. M., MONT, J. L., MORADY, F., NADEMANEE, K., NAKAGAWA, H., NATALE, A., NATTEL, S., PACKER, D. L., PAPPONE, C., PRYSTOWSKY, E., RAVIELE, A., REDDY, V., RUSKIN, J. N., SHEMIN, R. J., TSAO, H. M. & WILBER, D. 2012b. 2012 HRS/EHRA/ECAS Expert Consensus Statement on Catheter and Surgical Ablation of Atrial Fibrillation: recommendations for patient selection, procedural techniques, patient management and follow-up, definitions, endpoints, and research trial design. *Europace*, 14, 528-606.

CALKINS, H., KUCK, K. H., CAPPATO, R., BRUGADA, J., CAMM, A. J., CHEN, S. A., CRIJNS, H. J. G., DAMIANO, R. J., DAVIES, D. W., DIMARCO, J., EDGERTON, J., ELLENBOGEN, K., EZEKOWITZ, M. D., HAINES, D. E., HAISSAGUERRE, M., HINDRICKS, G., IESAKA, Y., JACKMAN, W., JALIFE, J., JAIS, P., KALMAN, J., KEANE, D., KIM, Y. H., KIRCHHOF, P., KLEIN, G., KOTTKAMP, H., KUMAGAI, K., LINDSAY, B. D., MANSOUR, M., MARCHLINSKI, F. E., MCCARTHY, P. M., MONT, J. L., MORADY, F., NADEMANEE, K., NAKAGAWA, H., NATALE, A., NATTEL, S., PACKER, D. L., PAPPONE, C., PRYSTOWSKY, E., RAVIELE, A., REDDY, V., RUSKIN, J. N., SHEMIN, R. J., TSAO, H. M. & WILBER, D. 2012c. 2012 HRS/EHRA/ECAS Expert Consensus Statement on Catheter and Surgical Ablation of Atrial Fibrillation: Recommendations for Patient Selection, Procedural Techniques, Patient Management and Follow-up, Definitions, Endpoints, and Research Trial Design A report of the Heart Rhythm Society (HRS) Task Force on Catheter and Surgical Ablation of Atrial Fibrillation.

Developed in partnership with the European Heart Rhythm Association (EHRA), a registered branch of the European Society of Cardiology (ESC) and the European Cardiac Arrhythmia Society (ECAS); and in collaboration with the American College of Cardiology (ACC), American Heart Association (AHA), the Asia Pacific Heart Rhythm Society (APHRS), and the Society of Thoracic Surgeons (STS). Endorsed by the governing bodies of the American College of Cardiology Foundation, the American Heart Association, the European Cardiac Arrhythmia Society, the European Heart Rhythm Association, the Society of Thoracic Surgeons, the Asia Pacific Heart Rhythm Society, and the Heart Rhythm Society. *Heart Rhythm*, 9, 632-+.

CALKINS, H., REYNOLDS, M. R., SPECTOR, P., SONDHI, M., XU, Y., MARTIN, A., WILLIAMS, C. J. & SLEDGE, I. 2009. Treatment of atrial fibrillation with antiarrhythmic drugs or radiofrequency ablation: two systematic literature reviews and meta-analyses. *Circ Arrhythm Electrophysiol*, 2, 349-61.

CALO, L., DE RUVO, E., SCIARRA, L., GRICIA, R., NAVONE, G., DE LUCA, L., NUCCIO, F., SETTE, A., PRISTIPINO, C., DULIO, A., GAITA, F. & LIOY, E. 2008. Diagnostic accuracy of a new software for complex fractionated electrograms identification in patients with persistent and permanent atrial fibrillation. *J Cardiovasc Electrophysiol*, 19, 1024-1030.

CAMM, A. J., KIRCHHOF, P., LIP, G. Y. H., SCHOTTEN, U., SVELIEVA, I., ERNST, S., VAN GELDER, I. C., AL-ATTAR, N., HINDRICKS, G., PRENDERGAST, B., HEIDBUCHEL, H., ALFIERI, O., ANGELINI, A., ATAR, D., COLONNA, P., DE CATERINA, R., DE SUTTER, J., GOETTE, A., GORENEK, B., HELDAL, M., HOHLÖSER, S. H., KOLH, P., LE HEUZEY, J. Y., PONIKOWSKI, P., RUTTEN, F. H. & CARDIOL, E. S. 2010. Guidelines for the management of atrial fibrillation The Task Force for the Management of Atrial Fibrillation of the European Society of Cardiology (ESC). *Europace*, 12, 1360-1420.

CHEN, P. S., CHOU, C. C., TAN, A. Y., ZHOU, S., FISHBEIN, M. C., HWANG, C., KARAGUEUZIAN, H. S. & LIN, S. F. 2006. The mechanisms of atrial fibrillation. *J Cardiovasc Electrophysiol*, 17 Suppl 3, S2-7.

- CHEN, W., ZHUANG, J., YU, W. & WANG, Z. 2009. Measuring complexity using FuzzyEn, ApEn, and SampEn. *Medical Engineering & Physics*, 31, 61-68.
- CHU, G. S., LI, X., VANHEUSDEN, F. J., ALMEIDA, T. P., SALINET, J. L., DASTAGIR, N., VARANASI, S. S., CHIN, S. H., SIDDIQUI, S., MAN, S. H., STAFFORD, P. J., SANDILANDS, A. J., SCHLINDWEIN, F. S. & NG, G. A. 2015. Targeting cyclical highest dominant frequency in the ablation of persistent atrial fibrillation. *Europace*, 17, v1-v2.
- CHU, G. S., MASCA, N., ALMEIDA, T. P., CHIN, S. H., VARANASI, S. S., SIDDIQUI, S., BROWN, P. D., STAFFORD, P. J., SANDILANDS, A. J., SCHLINDWEIN, F. S. & NG, G. A. 2014. Catheter stability during manual paroxysmal AF ablation can match a robotically-assisted procedure. *Heart Rhythm*, 11, S281.
- CHUGH, S. S., HAVMOELLER, R., NARAYANAN, K., SINGH, D., RIENSTRA, M., BENJAMIN, E. J., GILLUM, R. F., KIM, Y. H., MCANULTY, J. H., JR., ZHENG, Z. J., FOROUZANFAR, M. H., NAGHAVI, M., MENSAH, G. A., EZZATI, M. & MURRAY, C. J. 2014. Worldwide epidemiology of atrial fibrillation: a Global Burden of Disease 2010 Study. *Circulation*, 129, 837-47.
- COHEN, J. 1968. Weighted kappa: nominal scale agreement with provision for scaled disagreement or partial credit. *Psychol Bull*, 70, 213-20.
- COOLEY, J. W., LEWIS, P. A. W. & WELCH, P. D. 1969. The Fast Fourier Transform and Its Applications. *Education, IEEE Transactions on*, 12, 27-34.
- CORREA DE SA, D. D., THOMPSON, N., STINNETT-DONNELLY, J., ZNOJKIEWICZ, P., HABEL, N., MULLER, J. G., BATES, J. H., BUZAS, J. S. & SPECTOR, P. S. 2011. Electrogram fractionation: the relationship between spatiotemporal variation of tissue excitation and electrode spatial resolution. *Circ Arrhythm Electrophysiol*, 4, 909-16.
- COSIO, F. G., PALACIOS, J., VIDAL, J. M., COCINA, E. G., GOMEZ-SANCHEZ, M. A. & TAMARGO, L. 1983. Electrophysiologic studies in atrial fibrillation. Slow

conduction of premature impulses: a possible manifestation of the background for reentry. *Am J Cardiol*, 51, 122-30.

COVER, T. M. & THOMAS, J. A. 1991. *Elements of information theory*, New York, Wiley.

COX, J. L., CANAVAN, T. E., SCHUESSLER, R. B., CAIN, M. E., LINDSAY, B. D., STONE, C., SMITH, P. K., CORR, P. B. & BOINEAU, J. P. 1991. The surgical treatment of atrial fibrillation. II. Intraoperative electrophysiologic mapping and description of the electrophysiologic basis of atrial flutter and atrial fibrillation. *J Thorac Cardiovasc Surg*, 101, 406-26.

COX, J. L., SCHUESSLER, R. B., LAPPAS, D. G. & BOINEAU, J. P. 1996. An 8 1/2-year clinical experience with surgery for atrial fibrillation. *Ann Surg*, 224, 267-73; discussion 273-5.

DASTAGIR, N., LI, X., VANHEUSDEN, F. J., ALMEIDA, T. P., SALINET, J. L., CHU, G. S., STAFFORD, P. J., NG, G. A. & SCHLINDWEIN, F. S. Combination of frequency and phase to characterise the spatiotemporal behaviour of cardiac waves during persistent atrial fibrillation in humans. Computing in Cardiology Conference (CinC), 2015, 6-9 Sept. 2015 2015a. 57-60.

DASTAGIR, N., SALINET, J., VANHEUSDEN, F. J., ALMEIDA, T. P., XIN, L., CHU, G. S., NG, G. A. & SCHLINDWEIN, F. S. Spatiotemporal behaviour of high dominant frequency during persistent atrial fibrillation. Computing in Cardiology Conference (CinC), 2014, 7-10 Sept. 2014 2014. 653-656.

DASTAGIR, N., VANHEUSDEN, F. J., CHU, G. S., SALINET, J. L., LI, X., ALMEIDA, T. P., STAFFORD, P. J., SCHLINDWEIN, F. S. & NG, G. A. 2015b. Spatiotemporal Analysis of Phase and Frequency Dynamics in Human Persistent Atrial Fibrillation. *Circulation*, 132, A15890.

DAUBECHIES, I. 1992. *Ten lectures on Wavelets*, Philadelphia, PA, USA, Society for Industrial and Applied Mathematics.

DE BAKKER, J. M., VAN CAPELLE, F. J., JANSE, M. J., TASSERON, S., VERMEULEN, J. T., DE JONGE, N. & LAHPOR, J. R. 1993. Slow conduction

in the infarcted human heart. 'Zigzag' course of activation. *Circulation*, 88, 915-26.

DE BAKKER, J. M. T. & WITTKAMPF, F. H. M. 2010. The Pathophysiologic Basis of Fractionated and Complex Electrograms and the Impact of Recording Techniques on Their Detection and Interpretation. *Circ Arrhythm Electrophysiol*, 3, 204-213.

DE GROOT, N. M., HOUBEN, R. P., SMEETS, J. L., BOERSMA, E., SCHOTTEN, U., SCHALIJ, M. J., CRIJNS, H. & ALLESSIE, M. A. 2010. Electropathological substrate of longstanding persistent atrial fibrillation in patients with structural heart disease: epicardial breakthrough. *Circulation*, 122, 1674-82.

DEISENHOFER, I., ESTNER, H., REENTS, T., FICHTNER, S., BAUER, A., WU, J. J., KOLB, C., ZRENNER, B., SCHMITT, C. & HESSLING, G. 2009. Does Electrogram Guided Substrate Ablation Add to the Success of Pulmonary Vein Isolation in Patients with Paroxysmal Atrial Fibrillation ? A Prospective, Randomized Study. *J Cardiovasc Electrophysiol*, 20, 514-521.

DIXIT, S., MARCHLINSKI, F. E., LIN, D., CALLANS, D. J., BALA, R., RILEY, M. P., GARCIA, F. C., HUTCHINSON, M. D., RATCLIFFE, S. J., COOPER, J. M., VERDINO, R. J., PATEL, V. V., ZADO, E. S., CASH, N. R., KILLIAN, T., TOMSON, T. T. & GERSTENFELD, E. P. 2012. Randomized ablation strategies for the treatment of persistent atrial fibrillation: RASTA study. *Circ Arrhythm Electrophysiol*, 5, 287-94.

DOWNEY, J. M. & HEUSCH, G. 2001. Sequence of Cardiac Activation and Ventricular Mechanics. In: SPERELAKIS, N., KURACHI, Y., TERZIC, A. & COHEN, M. V. (eds.) *Heart Physiology and Pathophysiology*. 4th ed. San Diego, California: Academic Press.

DURRER, D., FORMIJNE, P., VAN, D. R., VAN, L. A., BULLER, J. & MEYLER, F. L. 1961. The electrocardiogram in normal and some abnormal conditions; in revived human fetal heart and in acute and chronic coronary occlusion. *Am Heart J*, 61, 303-16.

- ECKARDT, L. & BREITHARDT, G. 2009. Construction and Interpretation of Endocardial Maps: From Basic Electrophysiology to 3D Mapping. *In*: SHENASA, M. (ed.) *Cardiac mapping*. 3rd ed. Oxford ; Hoboken, NJ: Wiley-Blackwell.
- EINTHOVEN, W. 1906. Le telecardiogramme. *Archives Internationales de Physiologie* 4, 132.
- ELAYI, C. S., VERMA, A., DI BIASE, L., CHING, C. K., PATEL, D., BARRETT, C., MARTIN, D., RONG, B., FAHMY, T. S., KHAYKIN, Y., HONGO, R., HAO, S., PELARGONIO, G., DELLO RUSSO, A., CASELLA, M., SANTARELLI, P., POTENZA, D., FANELLI, R., MASSARO, R., ARRUDA, M., SCHWEIKERT, R. A. & NATALE, A. 2008. Ablation for longstanding permanent atrial fibrillation: results from a randomized study comparing three different strategies. *Heart Rhythm*, 5, 1658-64.
- EVERETT, T. H. T., MOORMAN, J. R., KOK, L. C., AKAR, J. G. & HAINES, D. E. 2001. Assessment of global atrial fibrillation organization to optimize timing of atrial defibrillation. *Circulation*, 103, 2857-61.
- FAES, L., NOLLO, G., ANTOLINI, R., GAITA, F. & RAVELLI, F. 2002. A method for quantifying atrial fibrillation organization based on wave-morphology similarity. *IEEE Trans Biomed Eng*, 49, 1504-13.
- FAWCETT, T. 2006. An introduction to ROC analysis. *Pattern Recognition Letters*, 27, 861-874.
- FENELON, G. & DE PAOLA, A. A. V. 2000. Novas Idéias Sobre os Mecanismos Eletrofisiológicos da Fibrilação Atrial suas Implicações Terapêuticas. *Reblampa*, 13, 5-12.
- FIELD, A., MILES, J. & FIELD, Z. 2012. *Discovering Statistics using R*, London, SAGE Publications Ltd.
- FUSTER, V., RYDEN, L. E., CANNOM, D. S., CRIJNS, H. J., CURTIS, A. B., ELLENBOGEN, K. A., HALPERIN, J. L., LE HEUZEY, J. Y., KAY, G. N., LOWE, J. E., OLSSON, S. B., PRYSTOWSKY, E. N., TAMARGO, J. L.,

WANN, S., PRIORI, S. G., BLANC, J. J., BUDAJ, A., CAMM, A. J., DEAN, V., DECKERS, J. W., DESPRES, C., DICKSTEIN, K., LEKAKIS, J., MCGREGOR, K., METRA, M., MORAIS, J., OSTERSPEY, A., TAMARGO, J. L., ZAMORANO, J. L., SMITH, S. C., JACOBS, A. K., ADAMS, C. D., ANDERSON, J. L., ANTMAN, E. M., HALPERIN, J. L., HUNT, S. A., NISHIMURA, R., ORNATO, J. P., PAGE, R. L., RIEGEL, B. & GUIDELINES, E. C. P. 2006. ACC/AHA/ESC 2006 guidelines for the management of patients with atrial fibrillation - executive summary - A report of the American College of Cardiology/American Heart Association Task Force on practice guidelines and the European Society of Cardiology Committee for Practice Guidelines (Writing Committee to Revise the 2001 Guidelines for the Management of Patients with Atrial Fibrillation) Developed in collaboration with the European Heart Rhythm Association and the Heart Rhythm Society. *Eur Heart J*, 27, 1799-2030.

GALLAGHER, J. J., KASELL, J. H., COX, J. L., SMITH, W. M., IDEKER, R. E. & SMITH, W. M. 1982. Techniques of intraoperative electrophysiologic mapping. *Am J Cardiol*, 49, 221-40.

GALLAGHER, M. M. & CAMM, J. 1998. Classification of atrial fibrillation. *Am J Cardiol*, 82, 18N-28N.

GANESAN, A. N., KUKLIK, P., LAU, D. H., BROOKS, A. G., BAUMERT, M., LIM, W. W., THANIGAIMANI, S., NAYYAR, S., MAHAJAN, R., KALMAN, J. M., ROBERTS-THOMSON, K. C. & SANDERS, P. 2013. Bipolar electrogram shannon entropy at sites of rotational activation: implications for ablation of atrial fibrillation. *Circ Arrhythm Electrophysiol*, 6, 48-57.

GARDNER, P. I., URSELL, P. C., FENOGLIO, J. J., JR. & WIT, A. L. 1985. Electrophysiologic and anatomic basis for fractionated electrograms recorded from healed myocardial infarcts. *Circulation*, 72, 596-611.

GARREY, W. E. 1914. The nature of fibrillatory contraction of the heart. Its relation to tissue mass and form. *American Journal of Physiology*, 33, 397-414.

- GASPO, R., BOSCH, R. F., TALAJIC, M. & NATTEL, S. 1997. Functional mechanisms underlying tachycardia-induced sustained atrial fibrillation in a chronic dog model. *Circulation*, 96, 4027-35.
- GEPSTEIN, L., HAYAM, G. & BENHAIM, S. A. 1997. A novel method for nonfluoroscopic catheter-based electroanatomical mapping of the heart - In vitro and in vivo accuracy results. *Circulation*, 95, 1611-1622.
- GESELOWITZ, D. B. 1989. On the Theory of the Electrocardiogram. *Proceedings of the Ieee*, 77, 857-876.
- GRAY, R. A., PERTSOV, A. M. & JALIFE, J. 1998. Spatial and temporal organization during cardiac fibrillation. *Nature*, 392, 75-8.
- GUYTON, A. C. & HALL, J. E. 2006. *Textbook of medical physiology*, Philadelphia, Elsevier Saunders.
- HABEL, N., ZNOJKIEWICZ, P., THOMPSON, N., MULLER, J. G., MASON, B., CALAME, J., CALAME, S., SHARMA, S., MIRCHANDANI, G., JANKS, D., BATES, J., NOORI, A., KARNBACH, A., LUSTGARTEN, D. L., SOBEL, B. E. & SPECTOR, P. 2010. The temporal variability of dominant frequency and complex fractionated atrial electrograms constrains the validity of sequential mapping in human atrial fibrillation. *Heart Rhythm*, 7, 586-593.
- HAISSAGUERRE, M., HOCINI, M., DENIS, A., SHAH, A. J., KOMATSU, Y., YAMASHITA, S., DALY, M., AMRAOUI, S., ZELLERHOFF, S., PICAT, M. Q., QUOTB, A., JESEL, L., LIM, H., PLOUX, S., BORDACHAR, P., ATTUEL, G., MEILLET, V., RITTER, P., DERVAL, N., SACHER, F., BERNUS, O., COCHET, H., JAIS, P. & DUBOIS, R. 2014. Driver Domains in Persistent Atrial Fibrillation. *Circulation*.
- HAISSAGUERRE, M., HOCINI, M., SANDERS, P., SACHER, F., ROTTER, M., TAKAHASHI, Y., ROSTOCK, T., HSU, L. F., BORDACHAR, P., REUTER, S., ROUDAUT, R., CLEMENTY, J. & JAIS, P. 2005a. Catheter ablation of long-lasting persistent atrial fibrillation: clinical outcome and mechanisms of subsequent arrhythmias. *J Cardiovasc Electrophysiol*, 16, 1138-47.

- HAISSAGUERRE, M., JAIS, P., SHAH, D. C., TAKAHASHI, A., HOCINI, M., QUINIOU, G., GARRIGUE, S., LE MOUROUX, A., LE METAYER, P. & CLEMENTY, J. 1998. Spontaneous initiation of atrial fibrillation by ectopic beats originating in the pulmonary veins. *N Engl J Med*, 339, 659-66.
- HAISSAGUERRE, M., MARCUS, F. I., FISCHER, B. & CLEMENTY, J. 1994. Radiofrequency catheter ablation in unusual mechanisms of atrial fibrillation: report of three cases. *J Cardiovasc Electrophysiol*, 5, 743-51.
- HAISSAGUERRE, M., SANDERS, P., HOCINI, M., TAKAHASHI, Y., ROTTER, M., SACHER, F., ROSTOCK, T., HSU, L. F., BORDACHAR, P., REUTER, S., ROUDAUT, R., CLEMENTY, J. & JAIS, P. 2005b. Catheter ablation of long-lasting persistent atrial fibrillation: critical structures for termination. *J Cardiovasc Electrophysiol*, 16, 1125-37.
- HARRIS, F. J. 1978. On the use of windows for harmonic analysis with the discrete Fourier transform. *Proceedings of the IEEE*, 66, 51-83.
- HAYTER, A. J. 2012. *Probability and statistics for engineers and scientists*, Boston, MA, Brooks/Cole, Cengage Learning.
- HEIJMAN, J., ALGALARRONDO, V., VOIGT, N., MELKA, J., WEHRENS, X. H., DOBREV, D. & NATTEL, S. 2015. The value of basic research insights into atrial fibrillation mechanisms as a guide to therapeutic innovation: A critical analysis. *Cardiovasc Res*.
- HEIST, E. K., CHALHOUB, F., BARRETT, C., DANIK, S., RUSKIN, J. N. & MANSOUR, M. 2012. Predictors of atrial fibrillation termination and clinical success of catheter ablation of persistent atrial fibrillation. *Am J Cardiol*, 110, 545-51.
- HOEKSTRA, B. P. T., DIKS, C. G. H., ALLESSIE, M. A. & DEGOEDE, J. 1995. Nonlinear-Analysis of Epicardial Atrial Electrograms of Electrically-Induced Atrial-Fibrillation in Man. *Journal of Cardiovascular Electrophysiology*, 6, 419-440.

- HUNTER, R. J., DIAB, I., THOMAS, G., DUNCAN, E., ABRAMS, D., DHINOJA, M., SPORTON, S., EARLEY, M. J. & SCHILLING, R. J. 2009. Validation of a classification system to grade fractionation in atrial fibrillation and correlation with automated detection systems. *Europace*, 11, 1587-1596.
- HYVARINEN, A. & OJA, E. 2000. Independent component analysis: algorithms and applications. *Neural Networks*, 13, 411-430.
- IZENMAN, A. J. 2008. *Modern multivariate statistical techniques : regression, classification, and manifold learning*, New York ; London, Springer.
- JADIDI, A. S., COCHET, H., SHAH, A. J., KIM, S. J., DUNCAN, E., MIYAZAKI, S., SERMESANT, M., LEHRMANN, H., LEDERLIN, M., LINTON, N., FORCLAZ, A., NAULT, I., RIVARD, L., WRIGHT, M., LIU, X. P., SCHERR, D., WILTON, S. B., ROTEN, L., PASCALE, P., DERVAL, N., SACHER, F., KNECHT, S., KEYL, C., HOCINI, M., MONTAUDON, M., LAURENT, F., HAISSAGUERRE, M. & JAIS, P. 2013. Inverse Relationship Between Fractionated Electrograms and Atrial Fibrosis in Persistent Atrial Fibrillation Combined Magnetic Resonance Imaging and High-Density Mapping. *J Am Coll Cardiol*, 62, 802-812.
- JADIDI, A. S., DUNCAN, E., MIYAZAKI, S., LELLOUCHE, N., SHAH, A. J., FORCLAZ, A., NAULT, I., WRIGHT, M., RIVARD, L., LIU, X., SCHERR, D., WILTON, S. B., SACHER, F., DERVAL, N., KNECHT, S., KIM, S. J., HOCINI, M., NARAYAN, S., HAISSAGUERRE, M. & JAIS, P. 2012a. Functional nature of electrogram fractionation demonstrated by left atrial high-density mapping. *Circ Arrhythm Electrophysiol*, 5, 32-42.
- JADIDI, A. S., DUNCAN, E., MIYAZAKI, S., LELLOUCHE, N., SHAH, A. J., FORCLAZ, A., NAULT, I., WRIGHT, M., RIVARD, L., LIU, X. P., SCHERR, D., WILTON, S. B., SACHER, F., DERVAL, N., KNECHT, S., KIM, S. J., HOCINI, M., NARAYAN, S., HAISSAGUERRE, M. & JAIS, P. 2012b. Functional Nature of Electrogram Fractionation Demonstrated by Left Atrial High-Density Mapping. *Circ Arrhythm Electrophysiol*, 5, 32-U104.

- JAIS, P., HAISSAGUERRE, M., SHAH, D. C., CHOUAIRI, S., GENCEL, L., HOCINI, M. & CLEMENTY, J. 1997. A focal source of atrial fibrillation treated by discrete radiofrequency ablation. *Circulation*, 95, 572-6.
- JALIFE, J., BERENFELD, O. & MANSOUR, M. 2002. Mother rotors and fibrillatory conduction: a mechanism of atrial fibrillation. *Cardiovascular Research*, 54, 204-216.
- KALIFA, J. M., TANAKA, K., ZAITSEV, A. V., WARREN, M., VAIDYANATHAN, R., AUERBACH, D., PANDIT, S., VIKSTROM, K. L., PLOUTZ-SNYDER, R., TALKACHOU, A., ATIENZA, F., GUIRAUDON, G., JALIFE, J. & BERENFELD, O. 2006. Mechanisms of wave fractionation at boundaries of high-frequency excitation in the posterior left atrium of the isolated sheep heart during atrial fibrillation. *Circulation*, 113, 626-633.
- KIM, I. B., RODEFELD, M. D., SCHUESSLER, R. B., COX, J. L. & BOINEAU, J. P. 1996. Relationship between local atrial fibrillation interval and refractory period in the isolated canine atrium. *Circulation*, 94, 2961-2967.
- KIMBER, S., DOWNAR, E., MASSE, S., SEVAPTSIDIS, E., CHEN, T., MICKLEBOROUGH, L. & PARSONS, I. 1996. A comparison of unipolar and bipolar electrodes during cardiac mapping studies. *Pacing Clin Electrophysiol*, 19, 1196-204.
- KIRCHHOF, C., CHORRO, F., SCHEFFER, G. J., BRUGADA, J., KONINGS, K., ZETELAKI, Z. & ALLESSIE, M. 1993. Regional entrainment of atrial fibrillation studied by high-resolution mapping in open-chest dogs. *Circulation*, 88, 736-49.
- KNECHT, S., SUBBIAH, R., HOCINI, M., JAÏS, P., LIM, K., MATSUO, A., ARANTES, L., O'NEILL, M. D., DERVAL, N., SACHER, F., DEPLAGNE, A., BORDACHAR, P., CLÉMENTY, J. & HAISSAGUERRE, M. 2009. Interpretation of Atrial Electrograms During Atrial Fibrillation. In: SHENASA, M. (ed.) *Cardiac mapping*. 3rd ed. Oxford ; Hoboken, NJ: Wiley-Blackwell.

- KONINGS, K. T., KIRCHHOF, C. J., SMEETS, J. R., WELLENS, H. J., PENN, O. C. & ALLESSIE, M. A. 1994. High-density mapping of electrically induced atrial fibrillation in humans. *Circulation*, 89, 1665-80.
- KONINGS, K. T. S., SMEETS, L. R. M., PENN, O. C., WELLENS, H. J. J. & ALLESSIE, M. A. 1997. Configuration of unipolar atrial electrograms during electrically induced atrial fibrillation in humans. *Circulation*, 95, 1231-1241.
- KRUEGER, M. W., SCHULZE, W. H., RHODE, K. S., RAZAVI, R., SEEMANN, G. & DOSSEL, O. 2013. Towards personalized clinical in-silico modeling of atrial anatomy and electrophysiology. *Med Biol Eng Comput*, 51, 1251-60.
- KUSUMOTO, F. M. 1999. Unipolar recording in cardiac electrophysiologic studies. *J Interv Card Electrophysiol*, 3, 121-7.
- LAKE, D. E. 2009. Nonparametric Entropy Estimation Using Kernel Densities. *Methods in Enzymology*. Academic Press.
- LAKE, D. E., RICHMAN, J. S., GRIFFIN, M. P. & MOORMAN, J. R. 2002. Sample entropy analysis of neonatal heart rate variability. *Am J Physiol Regul Integr Comp Physiol*, 283, R789-97.
- LANDIS, J. R. & KOCH, G. G. 1977. The measurement of observer agreement for categorical data. *Biometrics*, 33, 159-74.
- LAU, D. H., MAESEN, B., ZEEMERING, S., KUKLIK, P., VAN HUNNIK, A., LANKVELD, T. A. R., BIDAR, E., VERHEULE, S., NIJS, J., MAESSEN, J., CRIJNS, H., SANDERS, P. & SCHOTTEN, U. 2015. Indices of Bipolar Complex Fractionated Atrial Electrograms Correlate Poorly with Each Other and Atrial Fibrillation Substrate Complexity. *Heart Rhythm*, 15, 1415–1423.
- LAU, D. H., MAESEN, B., ZEEMERING, S., VERHEULE, S., CRIJNS, H. J. & SCHOTTEN, U. 2012. Stability of Complex Fractionated Atrial Electrograms: A Systematic Review. *J Cardiovasc Electrophysiol*, 23, 980-987.
- LEE, G., KUMAR, S., TEH, A., MADRY, A., SPENCE, S., LAROBINA, M., GOLDBLATT, J., BROWN, R., ATKINSON, V., MOTEN, S., MORTON, J. B.,

- SANDERS, P., KISTLER, P. M. & KALMAN, J. M. 2014. Epicardial wave mapping in human long-lasting persistent atrial fibrillation: transient rotational circuits, complex wavefronts, and disorganized activity. *Eur Heart J*, 35, 86-97.
- LEWIS, T. 1925. *The mechanism and graphic registration of the heart beat*, London, Shaw & Sons.
- LI, X., CHU, G. S., ALMEIDA, T. P., VANHEUSDEN, F. J., DASTAGIR, N., SALINET, J. L., STAFFORD, P. J., NG, G. A. & SCHLINDWEIN, F. S. Investigation on recurrent high dominant frequency spatiotemporal patterns during persistent atrial fibrillation. Computing in Cardiology Conference (CinC), 2015, 6-9 Sept. 2015 2015. 61-64.
- LI, X., SALINET, J. L., ALMEIDA, T. P., VANHEUSDEN, F. J., CHU, G. S., NG, G. A. & SCHLINDWEIN, F. S. A platform to guide catheter ablation of persistent atrial fibrillation using dominant frequency mapping. Computing in Cardiology Conference (CinC), 2014, 7-10 Sept. 2014 2014. 649-652.
- LIM, H. S., DERVAL, N., KOMATSU, Y., ZELLERHOFF, S., DENIS, A., SHAH, A. J., SACHER, F., HOCINI, M., JAĚS, P. & HAĚSSAGUERRE, M. 2015. Is Ablation to Termination the Best Strategy for Ablation of Persistent Atrial Fibrillation?: Persistent Atrial Fibrillation Is Best Ablated by a Strategy That Terminates the Arrhythmia: Procedural Termination Is Associated With Improved Long-Term Outcomes. *Circulation: Arrhythmia and Electrophysiology*, 8, 963-971.
- LIN, Y. J., LO, M. T., LIN, C., CHANG, S. L., LO, L. W., HU, Y. F., CHAO, T. F., LI, C. H., CHANG, Y. C., HSIEH, W. H., CHUNG, F. P., TSAO, H. M., CHANG, H. Y., HUANG, N. E. & CHEN, S. A. 2013. Nonlinear Analysis of Fibrillatory Electrogram Similarity to Optimize the Detection of Complex Fractionated Electrograms During Persistent Atrial Fibrillation. *Journal of Cardiovascular Electrophysiology*, 24, 280-289.
- LIN, Y. J., TAI, C. T., CHANG, S. L., LO, L. W., TUAN, T. C., WONGCHAROEN, W., UDYAVAR, A. R., HU, Y. F., CHANG, C. J., TSAI, W. C., KAO, T., HIGA, S. & CHEN, S. A. 2009a. Efficacy of additional ablation of complex fractionated

- atrial electrograms for catheter ablation of nonparoxysmal atrial fibrillation. *J Cardiovasc Electrophysiol*, 20, 607-15.
- LIN, Y. J., TAI, C. T., KAO, T., CHANG, S. L., LO, L. W., TUAN, T. C., UDYAVAR, A. R., WONGCHAROEN, W., HU, Y. F., TSO, H. W., TSAI, W. C., CHANG, C. J., UENG, K. C., HIGA, S. & CHEN, S. A. 2009b. Spatiotemporal Organization of the Left Atrial Substrate After Circumferential Pulmonary Vein Isolation of Atrial Fibrillation. *Circ Arrhythm Electrophysiol*, 2, 233-241.
- LIN, Y. J., TAI, C. T., KAO, T., CHANG, S. L., WONGCHAROEN, W., LO, L. W., TUAN, T. C., UDYAVAR, A. R., CHEN, Y. J., HIGA, S., UENG, K. C. & CHEN, S. A. 2008. Consistency of complex fractionated atrial electrograms during atrial fibrillation. *Heart Rhythm*, 5, 406-412.
- MAHNKOPF, C., BADGER, T. J., BURGON, N. S., DACCARETT, M., HASLAM, T. S., BADGER, C. T., MCGANN, C. J., AKOUM, N., KHOLMOVSKI, E., MACLEOD, R. S. & MARROUCHE, N. F. 2010. Evaluation of the left atrial substrate in patients with lone atrial fibrillation using delayed-enhanced MRI: implications for disease progression and response to catheter ablation. *Heart Rhythm*, 7, 1475-81.
- MAINARDI, L. T., PORTA, A., CALCAGNINI, G., BARTOLINI, P., MICHELUCCI, A. & CERUTTI, S. 2001. Linear and non-linear analysis of atrial signals and local activation period series during atrial-fibrillation episodes. *Medical & Biological Engineering & Computing*, 39, 249-254.
- MALMIVUO, J. & PLONSEY, R. 1995. *Bioelectromagnetism - Principles and Applications of Bioelectric and Biomagnetic Fields*, New York, Oxford University Press.
- MANDAPATI, R., SKANES, A., CHEN, J., BERENFELD, O. & JALIFE, J. 2000. Stable microreentrant sources as a mechanism of atrial fibrillation in the isolated sheep heart. *Circulation*, 101, 194-199.
- MINES, G. R. 1913. On dynamic equilibrium in the heart. *J Physiol*, 46, 349-83.

- MOE, G. K. & ABILDSKOV, J. A. 1959. Atrial fibrillation as a self-sustaining arrhythmia independent of focal discharge. *Am Heart J*, 58, 59-70.
- MOE, G. K., RHEINBOLDT, W. C. & ABILDSKOV, J. A. 1964. A Computer Model of Atrial Fibrillation. *Am Heart J*, 67, 200-20.
- MOHANTY, S., GIANNI, C., MOHANTY, P., HALBFASS, P., METZ, T., TRIVEDI, C., DENEKE, T., TOMASSONI, G., BAI, R., AL-AHMAD, A., BAILEY, S., BURKHARDT, J. D., GALLINGHOUSE, G. J., HORTON, R., HRANITZKY, P. M., SANCHEZ, J. E., DI BIASE, L. & NATALE, A. 2016. Impact of Rotor Ablation in Non-Paroxysmal AF Patients: Results from a Randomized Trial (OASIS). *Journal of the American College of Cardiology*.
- MONIR, G. & POLLAK, S. J. 2008. Consistency of the CFAE phenomena using custom software for automated detection of complex fractionated atrial electrograms (CFAEs) in the left atrium during atrial fibrillation. *J Cardiovasc Electrophysiol*, 19, 915-919.
- MUNZEL, U. & BRUNNER, E. 2000. Nonparametric Tests in the Unbalanced Multivariate One-Way Design. *Biometrical Journal*, 42, 837-854.
- NADEMANEE, K. 2011. Mapping of Complex Fractionated Atrial Electrograms as Target Sites for AF Ablation. *2011 Annual International Conference of the Ieee Engineering in Medicine and Biology Society (Embc)*, 5539-5542.
- NADEMANEE, K., MCKENZIE, J., KOSAR, E., SCHWAB, M., SUNSANEEWITAYAKUL, B., VASAVAKUL, T., KHUNNAWAT, C. & NGARMUKOS, T. 2004. A new approach for catheter ablation of atrial fibrillation: Mapping of the electrophysiologic substrate. *J Am Coll Cardiol*, 43, 2044-2053.
- NADEMANEE, K., SCHWAB, M., PORATH, J. & ABBO, A. 2006. How to perform electrogram-guided atrial fibrillation ablation. *Heart Rhythm*, 3, 981-984.
- NARAYAN, S. M., KRUMMEN, D. E., SHIVKUMAR, K., CLOPTON, P., RAPPEL, W. J. & MILLER, J. M. 2012. Treatment of atrial fibrillation by the ablation of localized sources: CONFIRM (Conventional Ablation for Atrial Fibrillation With

or Without Focal Impulse and Rotor Modulation) trial. *J Am Coll Cardiol*, 60, 628-36.

- NARAYAN, S. M., WRIGHT, M., DERVAL, N., JADIDI, A., FORCLAZ, A., NAULT, I., MIYAZAKI, S., SACHER, F., BORDACHAR, P., CLEMENTY, J., JAIS, P., HAISSAGUERRE, M. & HOCINI, M. 2011. Classifying fractionated electrograms in human atrial fibrillation using monophasic action potentials and activation mapping: Evidence for localized drivers, rate acceleration, and nonlocal signal etiologies. *Heart Rhythm*, 8, 244-253.
- NATALE, A., RAVIELE, A., ARENTZ, T., CALKINS, H., CHEN, S. A., HAISSAGUERRE, M., HINDRICKS, G., HO, Y., KUCK, K. H., MARCHLINSKI, F., NAPOLITANO, C., PACKER, D., PAPPONE, C., PRYSTOWSKY, E. N., SCHILLING, R., SHAH, D., THEMISTOCLAKIS, S. & VERMA, A. 2007. Venice Chart international consensus document on atrial fibrillation ablation. *J Cardiovasc Electrophysiol*, 18, 560-80.
- NATTEL, S. 2002. New ideas about atrial fibrillation 50 years on. *Nature*, 415, 219-26.
- NATTEL, S., BURSTEIN, B. & DOBREV, D. 2009. Molecular Remodelling and Chronic Atrial Fibrillation. In: ZIPES, D. P. & JALIFE, J. (eds.) *Cardiac electrophysiology : from cell to bedside*. 5th ed. ed. Philadelphia, Pa.: Saunders.
- NG, J., BORODYANSKIY, A. I., CHANG, E. T., VILLUENDAS, R., DIBS, S., KADISH, A. H. & GOLDBERGER, J. J. 2010. Measuring the Complexity of Atrial Fibrillation Electrograms. *J Cardiovasc Electrophysiol*, 21, 649-655.
- NG, J., KADISH, A. H. & GOLDBERGER, J. J. 2006. Effect of electrogram characteristics on the relationship of dominant frequency to atrial activation rate in atrial fibrillation. *Heart Rhythm*, 3, 1295-305.
- O'NEILL, M. D., JAIS, P., TAKAHASHI, Y., JONSSON, A., SACHER, F., HOCINI, M., SANDERS, P., ROSTOCK, T., ROTTER, M., PERNAT, A., CLEMENTY, J. & HAISSAGUERRE, M. 2006. The stepwise ablation approach for chronic atrial fibrillation--evidence for a cumulative effect. *J Interv Card Electrophysiol*, 16, 153-67.

- OAKES, R. S., BADGER, T. J., KHOLMOVSKI, E. G., AKOUM, N., BURGON, N. S., FISH, E. N., BLAUER, J. J., RAO, S. N., DIBELLA, E. V., SEGERSON, N. M., DACCARETT, M., WINDFELDER, J., MCGANN, C. J., PARKER, D., MACLEOD, R. S. & MARROUCHE, N. F. 2009. Detection and quantification of left atrial structural remodeling with delayed-enhancement magnetic resonance imaging in patients with atrial fibrillation. *Circulation*, 119, 1758-67.
- OESTERLEIN, T. G., SCHMID, J., BAUER, S., JADIDI, A., SCHMITT, C., DÖSSEL, O. & LUIK, A. 2015. Analysis and visualization of intracardiac electrograms in diagnosis and research: Concept and application of KaPAVIE. *Computer Methods and Programs in Biomedicine*.
- ORAL, H. 2009. Atrial Fibrillation: Mechanisms , Features , and Management Pathophysiology. In: ZIPES, D. P. & JALIFE, J. (eds.) *Cardiac electrophysiology : from cell to bedside*. 5th ed. ed. Philadelphia, Pa.: Saunders.
- ORAL, H., CHUGH, A., GOOD, E., WIMMER, A., DEY, S., GADEELA, N., SANKARAN, S., CRAWFORD, T., SARRAZIN, J. F., KUHNE, M., CHALFOUN, N., WELLS, D., FREDERICK, M., FORTINO, J., BENLOUCIF-MOORE, S., JONGNARANGSIN, K., PELOSI, F., BOGUN, F. & MORADY, F. 2007. Radiofrequency catheter ablation of chronic atrial fibrillation guided by complex electrograms. *Circulation*, 115, 2606-2612.
- ORAL, H., CHUGH, A., YOSHIDA, K., SARRAZIN, J. F., KUHNE, M., CRAWFORD, T., CHALFOUN, N., WELLS, D., BOONYAPISIT, W., VEERAREDDY, S., BILLAKANTY, S., WONG, W. S., GOOD, E., JONGNARANGSIN, K., PELOSI, F., JR., BOGUN, F. & MORADY, F. 2009. A randomized assessment of the incremental role of ablation of complex fractionated atrial electrograms after antral pulmonary vein isolation for long-lasting persistent atrial fibrillation. *J Am Coll Cardiol*, 53, 782-9.
- ORAL, H., KNIGHT, B. P., TADA, H., OZAYDIN, M., CHUGH, A., HASSAN, S., SCHARF, C., LAI, S. W., GREENSTEIN, R., PELOSI, F., JR., STRICKBERGER, S. A. & MORADY, F. 2002. Pulmonary vein isolation for paroxysmal and persistent atrial fibrillation. *Circulation*, 105, 1077-81.

- OROZCO-DUQUE, A., NOVAK, D., KREMEN, V. & BUSTAMANTE, J. 2015. Multifractal analysis for grading complex fractionated electrograms in atrial fibrillation. *Physiol Meas*, 36, 2269-84.
- PERTSOV, A. M., DAVIDENKO, J. M., SALOMONSZ, R., BAXTER, W. T. & JALIFE, J. 1993. Spiral waves of excitation underlie reentrant activity in isolated cardiac muscle. *Circ Res*, 72, 631-50.
- PINCUS, S. M. 1991. Approximate Entropy as a Measure of System-Complexity. *Proceedings of the National Academy of Sciences of the United States of America*, 88, 2297-2301.
- PLONSEY, R. & BARR, R. C. 2007. *Bioelectricity : a quantitative approach*, New York, NY, Springer.
- PORTER, M., SPEAR, W., AKAR, J. G., HELMS, R., BRYSEWICZ, N., SANTUCCI, P. & WILBER, D. J. 2008. Prospective study of atrial fibrillation termination during ablation guided by automated detection of fractionated electrograms. *J Cardiovasc Electrophysiol*, 19, 613-620.
- PROVIDÊNCIA, R., LAMBIASE, P. D., SRINIVASAN, N., GANESHA BABU, G., BRONIS, K., AHSAN, S., KHAN, F. Z., CHOW, A. W. C., ROWLAND, E., LOWE, M. & SEGAL, O. R. 2015. Is There Still a Role for CFAE Ablation in Addition to Pulmonary Vein Isolation in Patients with Paroxysmal and Persistent Atrial Fibrillation? A Meta-Analysis of 1,415 Patients. *Circulation: Arrhythmia and Electrophysiology*.
- REDFEARN, D. P., SIMPSON, C. S., ABDOLLAH, H. & BARANCHUK, A. M. 2009. Temporo-spatial stability of complex fractionated atrial electrograms in two distinct and separate episodes of paroxysmal atrial fibrillation. *Europace*, 11, 1440-1444.
- RICHMAN, J. S. & MOORMAN, J. R. 2000. Physiological time-series analysis using approximate entropy and sample entropy. *American Journal of Physiology-Heart and Circulatory Physiology*, 278, H2039-H2049.

- RODRIGO, M., GUILLEM, M. S., CLIMENT, A. M., PEDRÓN-TORRECILLA, J., LIBEROS, A., MILLET, J., FERNÁNDEZ-AVILÉS, F., ATIENZA, F. & BERENFELD, O. 2014. Body surface localization of left and right atrial high-frequency rotors in atrial fibrillation patients: A clinical-computational study. *Heart Rhythm*, 11, 1584-1591.
- ROLF, S., HINDRICKS, G., SOMMER, P., RICHTER, S., ARYA, A., BOLLMANN, A., KOSIUK, J. & KOUTALAS, E. 2015. Electroanatomical mapping of atrial fibrillation: Review of the current techniques and advances. *J Atrial Fibrillation*, 7, 57-68.
- ROLF, S., KIRCHER, S., ARYA, A., EITEL, C., SOMMER, P., RICHTER, S., GASPAR, T., BOLLMANN, A., ALTMANN, D., PIEDRA, C., HINDRICKS, G. & PIORKOWSKI, C. 2014. Tailored atrial substrate modification based on low-voltage areas in catheter ablation of atrial fibrillation. *Circ Arrhythm Electrophysiol*, 7, 825-33.
- ROSTOCK, T., ROTTER, M., SANDERS, P., TAKAHASHI, Y., JAIS, P., HOCINI, M., HSU, L. F., SACHER, F., CLEMENTY, J. & HAISSAGUERRE, M. 2006. High-density activation mapping of fractionated electrograms in the atria of patients with paroxysmal atrial fibrillation. *Heart Rhythm*, 3, 27-34.
- ROUX, J. F., GOJRATY, S., BALA, R., LIU, C. F., DIXIT, S., HUTCHINSON, M. D., GARCIA, F., LIN, D., CALLANS, D. J., RILEY, M., MARCHLINSKI, F. & GERSTENFELD, E. P. 2009. Effect of pulmonary vein isolation on the distribution of complex fractionated electrograms in humans. *Heart Rhythm*, 6, 156-160.
- ROUX, J. F., GOJRATY, S., BALA, R., LIU, C. F., HUTCHINSON, M. D., DIXIT, S., CALLANS, D. J., MARCHLINSKI, F. & GERSTENFELD, E. P. 2008. Complex fractionated electrogram distribution and temporal stability in patients undergoing atrial fibrillation ablation. *J Cardiovasc Electrophysiol*, 19, 815-820.
- SALINET, J. L., GUILLEM, M. S., ALMEIDA, T. P., LI, X., GOROSO, G., CHU, G. S., NG, G. A. & SCHLINDWEIN, F. S. Drifting rotor prevalence is associated with dominant frequency reduction after persistent atrial fibrillation ablation.

2015 Computing in Cardiology Conference (CinC), 6-9 Sept. 2015 2015. 269-272.

SALINET, J. L., TUAN, J. H., SANDILANDS, A. J., STAFFORD, P. J., SCHLINDWEIN, F. S. & ANDRÉ NG, G. 2013. Distinctive Patterns of Dominant Frequency Trajectory Behavior in Drug-Refractory Persistent Atrial Fibrillation. *J Cardiovasc Electrophysiol*, 25, 371-379.

SANDERS, P., BERENFELD, O., HOCINI, M., JAIS, P., VAIDYANATHAN, R., HSU, L. F., GARRIGUE, S., TAKAHASHI, Y., ROTTER, M., SACHER, F., SCAVEE, C., PLOUTZ-SNYDER, R., JALIFE, J. & HAISSAGUERRE, M. 2005. Spectral analysis identifies sites of high-frequency activity maintaining atrial fibrillation in humans. *Circulation*, 112, 789-97.

SCHEINMAN, M. M., MORADY, F., HESS, D. S. & GONZALEZ, R. 1982. Catheter-induced ablation of the atrioventricular junction to control refractory supraventricular arrhythmias. *JAMA*, 248, 851-5.

SCHERF, D. 1947. Studies on auricular tachycardia caused by aconitine administration. *Proc Soc Exp Biol Med*, 64, 233-9.

SCHERR, D., DALAL, D., CHEEMA, A., CHENG, A., HENRIKSON, C. A., SPRAGG, D., MARINE, J. E., BERGER, R. D., CALKINS, H. & DONG, J. 2007. Automated detection and characterization of complex fractionated atrial electrograms in human left atrium during atrial fibrillation. *Heart Rhythm*, 4, 1013-1020.

SCHERR, D., DALAL, D., CHEEMA, A., NAZARIAN, S., ALMASRY, I., BILCHICK, K., CHENG, A., HENRIKSON, C. A., SPRAGG, D., MARINE, J. E., BERGER, R. D., CALKINS, H. & DONG, J. 2009. Long- and Short-Term Temporal Stability of Complex Fractionated Atrial Electrograms in Human Left Atrium During Atrial Fibrillation. *J Cardiovasc Electrophysiol*, 20, 13-21.

SCHILLING, C. 2012. *Analysis of Atrial Electrograms*. PhD, Karlsruhe Institute of Technology.

- SCHILLING, C., KELLER, M., SCHERR, D., OESTERLEIN, T., HAISSAGUERRE, M., SCHMITT, C., DOSSEL, O. & LUIK, A. 2015. Fuzzy decision tree to classify complex fractionated atrial electrograms. *Biomed Tech (Berl)*, 60, 245-55.
- SCHILLING, R. J., PETERS, N. S. & DAVIES, W. 1998. Simultaneous endocardial mapping in the human left ventricle using a noncontact catheter - Comparison of contact and reconstructed electrograms during sinus rhythm. *Circulation*, 98, 887-898.
- SCHMITT, C., ESTNER, H., HECHER, B., LUIK, A., KOLB, C., KARCH, M., NDREPEPA, G., ZRENNER, B., HESSLING, G. & DEISENHOFER, I. 2007. Radiofrequency ablation of complex fractionated atrial electrograms (CFAE): Preferential sites of acute termination and regularization in paroxysmal and persistent atrial fibrillation. *Journal of Cardiovascular Electrophysiology*, 18, 1039-1046.
- SCHNECK, D. J. 2000. An Outline of Cardiovascular Structure and Function. In: BRONZINO, J. D. (ed.) *The biomedical engineering handbook*. 2nd ed ed. Boca Raton Berlin: CRC Press Springer.
- SCHOTTEN, U., VERHEULE, S., KIRCHHOF, P. & GOETTE, A. 2011. Pathophysiological mechanisms of atrial fibrillation: a translational appraisal. *Physiol Rev*, 91, 265-325.
- SCHUESSLER, R. B., GRAYSON, T. M., BROMBERG, B. I., COX, J. L. & BOINEAU, J. P. 1992. Cholinergically mediated tachyarrhythmias induced by a single extrastimulus in the isolated canine right atrium. *Circ Res*, 71, 1254-67.
- SEGAL, O. R., KOA-WING, M., JARMAN, J., PETERS, N., MARKIDES, V. & DAVIES, D. W. 2011. Intracardiac Mapping. In: MACFARLANE, P. W., VAN OOSTEROM, A., PAHLM, O., KLIGFIELD, P., JANSE, M. & CAMM, J. (eds.) *Comprehensive Electrocardiology*. 2nd ed. London: Springer.
- SEMMLOW, J. L. 2009. *Biosignal and medical image processing*, Boca Raton, CRC Press.

- SHANNON, C. E. 1948. The mathematical theory of communication. *The Bell System Technical Journal*, 27, 379-423.
- SHOUCRI, R. M. 1991. The pressure-volume relation in the left ventricle and the pump function of the heart. *Ann Biomed Eng*, 19, 699-721.
- SKANES, A. C., MANDAPATI, R., BERENFELD, O., DAVIDENKO, J. M. & JALIFE, J. 1998. Spatiotemporal periodicity during atrial fibrillation in the isolated sheep heart. *Circulation*, 98, 1236-1248.
- SOHAL, M., CHOUDHURY, R., TAGHJI, P., LOUW, R., WOLF, M., FEDIDA, J., VANDEKERCKHOVE, Y., TAVERNIER, R., DUYTSCHAEVER, M. & KNECHT, S. 2015. Is Mapping of Complex Fractionated Electrograms Obsolete? *Arrhythmia & Electrophysiology Review*, 4, 109–15.
- SPACH, M. S., MILLER, W. T., 3RD, MILLER-JONES, E., WARREN, R. B. & BARR, R. C. 1979. Extracellular potentials related to intracellular action potentials during impulse conduction in anisotropic canine cardiac muscle. *Circ Res*, 45, 188-204.
- SPECTOR, P. S., CORREA DE SA, D. D., TISCHLER, E. S., THOMPSON, N. C., HABEL, N., STINNETT-DONNELLY, J., BENSON, B. E., BIELAU, P. & BATES, J. H. 2012. Ablation of multi-wavelet re-entry: general principles and in silico analyses. *Europace*, 14 Suppl 5, v106-v111.
- STEINHAUS, B. M. 1989. Estimating cardiac transmembrane activation and recovery times from unipolar and bipolar extracellular electrograms: a simulation study. *Circ Res*, 64, 449-62.
- STEVENSON, W. G. & ALBERT, C. M. 2012. Catheter ablation for paroxysmal atrial fibrillation. *N Engl J Med*, 367, 1648-9.
- STEVENSON, W. G. & SOEJIMA, K. 2005. Recording techniques for clinical electrophysiology. *J Cardiovasc Electrophysiol*, 16, 1017-22.
- STEWART, S., MURPHY, N., WALKER, A., MCGUIRE, A. & MCMURRAY, J. J. V. 2004. Cost of an emerging epidemic: an economic analysis of atrial fibrillation in the UK. *Heart*, 90, 286-292.

- STILES, M. K., BROOKS, A. G., JOHN, B., SHASHIDHAR, WILSON, L., KUKLIK, P., DIMITRI, H., LAU, D. H., ROBERTS-THOMSON, R. L., MACKENZIE, L., WILLOUGHBY, S., YOUNG, G. D. & SANDERS, P. 2008. The effect of electrogram duration on quantification of complex fractionated atrial electrograms and dominant frequency. *J Cardiovasc Electrophysiol*, 19, 252-258.
- TAKAHASHI, Y., O'NEILL, M. D., HOCINI, M., DUBOIS, R., MATSUO, S., KNECHT, S., MAHAPATRA, S., LIM, K. T., JAIS, P., JONSSON, A., SACHER, F., SANDERS, P., ROSTOCK, T., BORDACHAR, P., CLEMENTY, J., KLEIN, G. J. & HAISSAGUERRE, M. 2008. Characterization of electrograms associated with termination of chronic atrial fibrillation by catheter ablation. *J Am Coll Cardiol*, 51, 1003-10.
- TAKAHASHI, Y., SANDERS, P., JAIS, P., HOCINI, M., DUBOIS, R., ROTTER, M., ROSTOCK, T., NALLIAH, C. J., SACHER, F., CLEMENTY, J. & HAISSAGUERRE, M. 2006. Organization of frequency spectra of atrial fibrillation: relevance to radiofrequency catheter ablation. *J Cardiovasc Electrophysiol*, 17, 382-8.
- TERASAWA, T., BALK, E. M., CHUNG, M., GARLITSKI, A. C., ALSHEIKH-ALI, A. A., LAU, J. & IP, S. 2009. Systematic review: comparative effectiveness of radiofrequency catheter ablation for atrial fibrillation. *Ann Intern Med*, 151, 191-202.
- TSAI, W. C., WANG, J. H., LIN, Y. J., TSAO, H. M., CHANG, S. L., LO, L. W., HU, Y. F., CHANG, C. J., TANG, W. H., HUANG, S. Y., SUENARI, K., TUAN, T. C. & CHEN, S. A. 2012. Consistency of the Automatic Algorithm in Detecting Complex Fractionated Electrograms using an Electroanatomical Navigation System. *Pacing Clin Electrophysiol*, 35, 980-989.
- TUAN, J., JEILAN, M., KUNDU, S., NICOLSON, W., CHUNG, I., STAFFORD, P. J. & NG, G. A. 2011. Regional fractionation and dominant frequency in persistent atrial fibrillation: effects of left atrial ablation and evidence of spatial relationship. *Europace*, 13, 1550-1556.

- VAN DER VELDEN, H. M. W., VAN DER ZEE, L., WIJFFELS, M. C., VAN LEUVEN, C., DORLAND, R., VOS, M. A., JONGSMA, H. J. & ALLESSIE, M. A. 2000. Atrial fibrillation in the goat induces changes in monophasic action potential and mRNA expression of ion channels involved in repolarization. *J Cardiovasc Electrophysiol*, 11, 1262-9.
- VERMA, A., JIANG, C. Y., BETTS, T. R., CHEN, J., DEISENHOFER, I., MANTOVAN, R., MACLE, L., MORILLO, C. A., HAVERKAMP, W., WEERASOORIYA, R., ALBENQUE, J. P., NARDI, S., MENARDI, E., NOVAK, P., SANDERS, P. & INVESTIGATORS, S. A. I. 2015. Approaches to catheter ablation for persistent atrial fibrillation. *N Engl J Med*, 372, 1812-22.
- VERMA, A., LAKKIREDDY, D., WULFFHART, Z., PILLARISETTI, J., FARINA, D., BEARDSALL, M., WHALEY, B., GIEWERCER, D., TSANG, B. & KHAYKIN, Y. 2011. Relationship Between Complex Fractionated Electrograms (CFE) and Dominant Frequency (DF) Sites and Prospective Assessment of Adding DF-Guided Ablation to Pulmonary Vein Isolation in Persistent Atrial Fibrillation (AF). *J Cardiovasc Electrophysiol*, 22, 1309-1316.
- VERMA, A., MANTOVAN, R., MACLE, L., DE MARTINO, G., CHEN, J., MORILLO, C. A., NOVAK, P., CALZOLARI, V., GUERRA, P. G., NAIR, G., TORRECILLA, E. G. & KHAYKIN, Y. 2010. Substrate and Trigger Ablation for Reduction of Atrial Fibrillation (STAR AF): a randomized, multicentre, international trial. *Eur Heart J*, 31, 1344-56.
- VERMA, A., NOVAK, P., MACLE, L., WHALEY, B., BEARDSALL, M., WULFFHART, Z. & KHAYKIN, Y. 2008a. A prospective, multicenter evaluation of ablating complex fractionated electrograms (CFEs) during atrial fibrillation (AF) identified by an automated mapping algorithm: Acute effects on AF and efficacy as an adjuvant strategy. *Heart Rhythm*, 5, 198-205.
- VERMA, A., PATEL, D., FAMY, T., MARTIN, D. O., BURKHARDT, J. D., ELAYI, S. C., LAKKIREDDY, D., WAZNI, O., CUMMINGS, J., SCHWEIKERT, R. A., SALIBA, W., TCHOU, P. J. & NATALE, A. 2007. Efficacy of adjuvant anterior

left atrial ablation during intracardiac echocardiography-guided pulmonary vein antrum isolation for atrial fibrillation. *J Cardiovasc Electrophysiol*, 18, 151-6.

VERMA, A., SANDERS, P., CHAMPAGNE, J., MACLE, L., NAIR, G. M., CALKINS, H. & WILBER, D. J. 2014. Selective complex fractionated atrial electrograms targeting for atrial fibrillation study (SELECT AF): a multicenter, randomized trial. *Circ Arrhythm Electrophysiol*, 7, 55-62.

VERMA, A., WULFFHART, Z., BEARDSALL, M., WHALEY, B., HILL, C. & KHAYKIN, Y. 2008b. Spatial and temporal stability of complex fractionated electrograms in patients with persistent atrial fibrillation over longer time periods: relationship to local electrogram cycle length. *Heart Rhythm*, 5, 1127-33.

WALTERS, T. E. & KALMAN, J. M. 2015. Human Persistent Atrial Fibrillation Is Maintained by Rotors: The Jury Is Still Out. *Circulation: Arrhythmia and Electrophysiology*, 8, 517-519.

WANG, J., BOURNE, G. W., WANG, Z., VILLEMAIRE, C., TALAJIC, M. & NATTEL, S. 1993. Comparative mechanisms of antiarrhythmic drug action in experimental atrial fibrillation. Importance of use-dependent effects on refractoriness. *Circulation*, 88, 1030-44.

WANG, Z., PAGE, P. & NATTEL, S. 1992. Mechanism of flecainide's antiarrhythmic action in experimental atrial fibrillation. *Circ Res*, 71, 271-87.

WELLS, J. L., KARP, R. B., KOUCHOUKOS, N. T., MACLEAN, W. A. H., JAMES, T. N. & WALDO, A. L. 1978. Characterization of Atrial-Fibrillation in Man - Studies Following Open-Heart Surgery. *Pace-Pacing and Clinical Electrophysiology*, 1, 426-438.

WIJFFELS, M. C. E. F., KIRCHHOF, C. J. H. J., DORLAND, R. & ALLESSIE, M. A. 1995. Atrial-Fibrillation Begets Atrial-Fibrillation - a Study in Awake Chronically Instrumented Goats. *Circulation*, 92, 1954-1968.

WINTERBERG, H. 1907. Studien über Herzflimmern. *Archiv für die gesamte Physiologie des Menschen und der Tiere*, 117, 223-256.

- WITTKAMPF, F. H., WEVER, E. F., DERKSEN, R., WILDE, A. A., RAMANNA, H., HAUER, R. N. & ROBLES DE MEDINA, E. O. 1999. Localisa: new technique for real-time 3-dimensional localization of regular intracardiac electrodes. *Circulation*, 99, 1312-7.
- WONG, K. C., PAISEY, J. R., SOPHER, M., BALASUBRAMANIAM, R., JONES, M., QURESHI, N., HAYES, C. R., GINKS, M. R., RAJAPPAN, K., BASHIR, Y. & BETTS, T. R. 2015. No Benefit of Complex Fractionated Atrial Electrogram Ablation in Addition to Circumferential Pulmonary Vein Ablation and Linear Ablation: Benefit of Complex Ablation Study. *Circ Arrhythm Electrophysiol*, 8, 1316-24.
- WRIGHT, M., HAISSAGUERRE, M., KNECHT, S., MATSUO, S., O'NEILL, M. D., NAULT, I., LELLOUCHE, N., HOCINI, M., SACHER, F. & JAIS, P. 2008. State of the art: catheter ablation of atrial fibrillation. *J Cardiovasc Electrophysiol*, 19, 583-92.
- WU, J., ESTNER, H., LUIK, A., UCER, E., REENTS, T., PFLAUMER, A., ZRENNER, B., HESSLING, G. & DEISENHOFER, I. 2008. Automatic 3D mapping of complex fractionated atrial electrograms (CFAE) in patients with paroxysmal and persistent atrial fibrillation. *J Cardiovasc Electrophysiol*, 19, 897-903.
- YAMABE, H., MORIHISA, K., TANAKA, Y., UEMURA, T., ENOMOTO, K., KAWANO, H. & OGAWA, H. 2009. Mechanisms of the maintenance of atrial fibrillation: role of the complex fractionated atrial electrogram assessed by noncontact mapping. *Heart Rhythm*, 6, 1120-8.
- YAMAZAKI, M. & JALIFE, J. 2012. Pathophysiology of atrial fibrillation: From initiation to maintenance. *Journal of Arrhythmia*, 28, 129-139.
- YUE, L., FENG, J., GASPO, R., LI, G. R., WANG, Z. & NATTEL, S. 1997. Ionic remodeling underlying action potential changes in a canine model of atrial fibrillation. *Circ Res*, 81, 512-25.
- ZAMAN, J. A. & NARAYAN, S. M. 2015. Ablation of Atrial Fibrillation: How Can Less Be More? *Circ Arrhythm Electrophysiol*, 8, 1303-5.

- ZHOU, G., CHEN, S., CHEN, G., ZHANG, F., MENG, W., YAN, Y., LU, X., WEI, Y. & LIU, S. 2013. Procedural arrhythmia termination and long-term single-procedure clinical outcome in patients with non-paroxysmal atrial fibrillation. *J Cardiovasc Electrophysiol*, 24, 1092-100.
- ZHOU, X., ZHOU, C. & STEWART, B. G. Comparisons of discrete wavelet transform, wavelet packet transform and stationary wavelet transform in denoising PD measurement data. *Electrical Insulation*, 2006. Conference Record of the 2006 IEEE International Symposium on, 11-14 June 2006 2006. 237-240.
- ZIAD, I., MILLER, J. M. & ZIPES, D. P. 2013. Atrial Fibrillation. *In*: ZIAD, I., MILLER, J. M. & ZIPES, D. P. (eds.) *Clinical Arrhythmology and Electrophysiology*. 2nd ed. Philadelphia, Pa.: Saunders.
- ZLOCHIVER, S., YAMAZAKI, M., KALIFA, J. & BERENFELD, O. 2008. Rotor meandering contributes to irregularity in electrograms during atrial fibrillation. *Heart Rhythm*, 5, 846-54.